[redacted]

MARTIN MARIETTA ENERGY SYSTEMS LIBRARIES
3 4456 0360755 9

CENTRAL RESEARCH LIBRARY
DOCUMENT COLLECTION

ORNL-1895
Progress

HOMOGENEOUS REACTOR PROJECT

QUARTERLY PROGRESS REPORT

FOR PERIOD ENDING APRIL 30, 1955

OAK RIDGE NATIONAL LABORATORY
CENTRAL RESEARCH LIBRARY
DOCUMENT COLLECTION
LIBRARY LOAN COPY
DO NOT TRANSFER TO ANOTHER PERSON
If you wish someone else to see this document, send in name with document and the library will arrange a loan.

OAK RIDGE NATIONAL LABORATORY
OPERATED BY
CARBIDE AND CARBON CHEMICALS COMPANY
A DIVISION OF UNION CARBIDE AND CARBON CORPORATION
UCC
POST OFFICE BOX P
OAK RIDGE, TENNESSEE

[redacted]

[redacted]

[redacted]

DECLASSIFIED

CLASSIFICATION CHANGED

BY AUTHORITY TID-1148

BY: E. Morrison 7/24/57

Contract No. W-7405-eng-26

ORNL-1895

This document consists of 220 pages.

Copy 7 of 310 copies. Series A.

HOMOGENEOUS REACTOR PROJECT

QUARTERLY PROGRESS REPORT

For Period Ending April 30, 1955

Project Director – J. A. Swartout
Associate Director – C. E. Winters

Experimental Reactors – S. E. Beall
Thorium Breeder Reactor – J. A. Lane and R. B. Briggs
Corrosion – E. G. Bohlmann
Engineering Development – J. A. Lane
Chemical Engineering Development – F. R. Bruce
Supporting Chemical Research – E. H. Taylor

Compiled by

H. F. McDuffie
D. C. Kelly

DATE RECEIVED BY INFORMATION AND REPORTS DIVISION

(MAY 13, 1955)

DATE ISSUED

JUN 30 1955

OAK RIDGE NATIONAL LABORATORY
Operated by
CARBIDE AND CARBON CHEMICALS COMPANY
A Division of Union Carbide and Carbon Corporation
Post Office Box P
Oak Ridge, Tennessee

[redacted]

3 4456 0360755 9

[redacted]

INTERNAL DISTRIBUTION

1. E. Center
2. gy Library
3. Physics Library
4. y Library
5-6. xperimental Engine g Library
7-9. Central R rch Library
10-18. Laboratory ords Dept.
19. Laboratory R rds, ORNL R.C.
20. R. E. Aven
21. S. E. Beall
22. D. S. Billington
23. E. P. Blizard
24. E. G. Bohlmann
25. C. J. Borkowski
26. G. E. Boyd
27. R. B. Briggs
28. F. R. Bruce
29. A. D. Callihan
30. D. W. Cardwell
31. W. L. Carter
32. G. H. Cartledge
33. R. A. Charpie
34. W. E. Clark
35. G. H. Clewett
36. T. E. Cole
37. E. L. Compere
38. D. D. Cowen
39. S. Cromer
40. F. L. Culler
41. J. S. Culver
42. J. S. Drury
43. W. K. Eister
44. L. B. Emlet (K-25)
45. D. E. Ferguson
46. W. J. Fretague
47. J. H. Frye, Jr.
48. J. L. Gabbard
49. W. R. Gall
50. H. E. Goeller
51. C. B. Graham
52. J. L. Gregg
53. J. C. Griess
54. W. O. Harms
55. P. N. Haubenreich
56. C. J. Hochanadel
57. A. Hollaender
58. A. S. Householder
59. H. K. Jackson
60. G. R. Jenkins (C&CCC, South Charleston)
61. G. H. Jenks
62. W. H. Jordan
63. P. R. Kasten
64. C. P. Keim
65. M. T. Kelley
66. R. B. Korsmeyer
67. A. S. Kitzes
68. J. A. Lane
69. C. E. Larson
70. R. E. Leuze
71. S. C. Lind
72. R. B. Lindauer
73. R. S. Livingston
74. M. I. Lundin
75. R. N. Lyon
76. W. L. Marshall
77. H. F. McDuffie
78. J. P. McBride
79. R. A. McNees
80. J. R. McWherter
81. O. Menis
82. E. C. Miller
83. K. Z. Morgan
84. E. J. Murphy
85. E. O. Nurmi
86. J. P. Murray (Y-12)
87. L. F. Parsly
88. H. F. Poppendiek
89. L. R. Quarles
90. P. M. Reyling
91. A. M. Rom
92. W. L. Ross
H. C. Savage
9 C. H. Secoy
95 . L. Segaser
96. D. Shipley
97. Skinner
98. R. Stoughton
99. A. nell
100. I. Sp k
101. C. D. no
102. J. A. S out
103. E. H. Ta
104. D. G. Thom
105. P. F. Thom
106. M. Tobias

[redacted]

[redacted]

107. W. E. Unger
108. W. P. Walker
109. B. Weaver
110. A. M. Weinberg
111. T. A. Welton
112. E. P. Wigner (consultant)
113. G. C. Williams
114. J. C. Wilson
115. C. E. Winters
116. F. C. VonderLage
117. F. C. Zapp
118. P. C. Zmola
119. ORNL Document Reference Library, Y-12 Branch

EXTERNAL DISTRIBUTION

[redacted]

AF Plant Representative, Burbank
AF Plant Representative, Seattle
F Plant Representative, Wood-Ridge
erican Locomotive Company
rican Machine and Foundry Company
Project Office, Fort Worth
e National Laboratory
orces Special Weapons Project (Sandia)
rces Special Weapons Project, Washington
ergy Commission, Washington
Wilcox
rial Institute
Corporation
Company
D)
Laboratory
Bureau of Ships
cks
e
Chicago Patent Group
Chief of Naval Research
Combustion Engineering,
y
ct
Department of the Navy – Op
Detroit Edison Company
Division of Research and Medic AEC, ORO
duPont Company, Augusta
duPont Company, Wilmington
Duquesne Light Company
East Hartford Area
Engineer Research and Development oratories
Foster Wheeler Corporation
General Electric Company (ANPD)
General Electric Company (APS)
General Electric Company, Richland
Hanford Operations Office
Headquarters, Air Force Special Weapons Center
Iowa State College

[redacted]

[redacted]

196. Kaiser Engineers
197-[redacted]0. Knolls Atomic Power Laboratory
201-[redacted] Los Alamos Scientific Laboratory
2[redacted] Massachusetts Institute of Technology (Benedict)
204[redacted]aterials Laboratory (WADC)
205. [redacted]nsanto Chemical Company
206. [redacted]nd Laboratory
207. N[redacted]nal Advisory Committee for Aeronautics, Cleveland
208. Na[redacted]al Advisory Committee for Aeronautics, Washington
209-210. Nav[redacted]esearch Laboratory
211. Newp[redacted]News Shipbuilding and Dry Dock Company
212. New Y[redacted]Operations Office
213. New Yo[redacted]niversity
214-215. North Am[redacted]an Aviation, Inc.
216. Nuclear D[redacted]opment Associates, Inc.
217. Nuclear Me[redacted] Inc.
218. Pacific-Nort[redacted]st Power Group
219. Patent Branch[redacted]ashington
220. Pennsylvania P[redacted]er and Light Company
221-227. Phillips Petrole[redacted]Company (NRTS)
228. Powerplant Labor[redacted]ry (WADC)
229. Pratt and Whitney [redacted]craft Division (Fox Project)
230. San Francisco Oper[redacted]ns Office
231. Seminole Electric Co[redacted]erative, Inc.
232. Sylvania Electric Prod[redacted], Inc.
233. Tennessee Valley Autho[redacted] (Dean)
234. USAF Headquarters
235. USAF Project Rand
236. U.S. Naval Postgraduate Sc[redacted]
237. U.S. Naval Radiological Defe[redacted] Laboratory
238-239. University of California Radia[redacted] Laboratory, Berkeley
240-241. University of California Radiati[redacted]aboratory, Livermore
242. Vitro Engineering Division
243. Vitro Laboratories
244. Walter Kidde Nuclear Laboratories, [redacted]
245. Westinghouse Electric Corporation (I[redacted])
246-310. Technical Information Service, Oak Ri[redacted]

[redacted]

[redacted]

Reports previously issued in this series are as follows:

ORNL-527	Date issued, December 28, 1949
ORNL-630	Period Ending February 28, 1950
ORNL-730	Feasibility Report – Date Issued, July 6, 1950
ORNL-826	Period Ending August 31, 1950
ORNL-925	Period Ending November 30, 1950
ORNL-990	Period Ending February 28, 1951
ORNL-1057	Period Ending May 15, 1951
ORNL-1121	Period Ending August 15, 1951
ORNL-1221	Period Ending November 15, 1951
ORNL-1280	Period Ending March 15, 1952
ORNL-1318	Period Ending July 1, 1952
ORNL-1424	Period Ending October 1, 1952
ORNL-1478	Period Ending January 1, 1953
ORNL-1554	Period Ending March 31, 1953
ORNL-1605	Period Ending July 31, 1953
ORNL-1658	Period Ending October 31, 1953
ORNL-1678	Period Ending January 31, 1954
ORNL-1753	Period Ending April 30, 1954
ORNL-1772	Period Ending July 31, 1954
ORNL-1813	Period Ending October 31, 1954
ORNL-1853	Period Ending ~~April~~ Jan. 30, 1955

[redacted]

[redacted]

HRP QUARTERLY PROGRESS REPORT

SUMMARY

PART I. EXPERIMENTAL REACTORS

1. Homogeneous Reactor Test

1.1 Project Status. – Construction of the steel container cell and shield structure by the contractor was completed in February. Additional work by the contractor to increase the design strength of the cell by installing anchor bolts around the bases of the columns is in progress. Arrangements are being made for the contractor to perform additional construction work within the main bay of the building.

ORNL forces have occupied the four-level control area. Installation of reactor instrumentation is ahead of schedule.

Ninety-nine purchase orders for HRT components and materials ($312,000), two development contracts ($160,000), and 70 purchase orders for instrumentation ($131,000) make a total present commitment of $603,000 for the HRT.

1.2 Design. – During this quarter, flowsheets for all the reactor systems were completed and issued. Drawings of all cell-wall penetrations and their locations were approved and issued for construction, and designs of valve pits at the east and west sides of the cell were completed. Design of a blast shield for the reactor pressure vessel was completed, and the unit is now under construction. A subassembly of the main components of the low-pressure fuel system has been designed and issued, including weighing systems for dump tanks and condensate tanks.

Detail drawings of high-pressure piping are ready for final checking and approval. Drawings of low-pressure process piping and service piping are being made.

1.3 Reactor Analysis. – The effect of prompt-neutron lifetime upon reactor safety was investigated for the HRT. It was found that for a given pressure rise the allowable rate of reactivity addition was relatively insensitive to the average prompt-neutron lifetime, although the rate decreased somewhat with decreasing lifetime for the higher pressure rises. With only source neutrons present and the reactor initially subcritical, the allowable rate was practically independent of the initial value of k_e. For a core-pressure rise of 400 psi, the corresponding rate of reactivity addition was about 0.8% per second; for a pressure rise of 4000 psi, the rate was 2.5 to 3.0% per second.

The effects of changing the water temperature on the shell side of the core heat exchanger were studied. The rate at which the temperature of the fuel solution leaving the heat exchanger varies with time was found to be approximately the same as that of the shell-side temperature under a wide variety of operating conditions. If it is assumed that the heat-exchanger water temperature is in equilibrium with the existing pressure, a limit on rates of pressure decrease can be specified, based on allowable rates of reactivity addition. For a reactivity addition of $0.005\Delta k_e$ per second, the allowable rate of steam pressure decrease should not exceed 20 psi/sec at all operating pressures when the 400A pump is in normal operation. If the average rate of pressure decrease is greater than this, the 400A pump should be stopped. A time constant of 1 sec should be adequate for the instrumental device stopping the pump.

The effects of overpressure and temperature upon the stability of the HRT against "walk-away" are reported. The degree of stability for a particular operating condition is only mildly dependent upon temperature but is quite dependent upon overpressure.

1.4 Component Development. – All HRT-size development pumps have been received. The 300A pump was assembled with the 230-gpm impeller and installed in a loop with a vertical pressurizer. The first 400A pump has operated since January 19, 1955, with a UO_2SO_4 solution containing approximately 30 g of uranium per kilogram of solution, 0.005 *m* $CuSO_4$, and 10 mole % excess H_2SO_4. The pump casing for the second 400A pump was shipped to the manufacturer for repair. The HRT fuel mockup pump was assembled with the 300-gpm impeller.

Final fabrication, inspection, and testing of the HRT fuel and blanket pumps were delayed by a change in the design of the thermal barrier. Delivery is now expected in June.

Fabrication of the HRT fuel and blanket heat exchangers at Foster Wheeler is nearing completion. Both units were tubed, and all primary nozzle

[redacted]

welds were completed satisfactorily. Several difficulties arose in the tube-joint welding of the first unit, and similar welding of the second exchanger is being deferred until these difficulties have been resolved.

The first phase of the HRT dump test, which was carried out to obtain fundamental information on the pressure-time curves of the pressure vessel, pressure drops through the discharge line and dump valve, and mass flow rates, is nearing completion.

The HRT mockup loop completed the water phase of its operation. The performance of the system and of the HRT-type components was excellent. After completion of the water operation, the loop was modified to include water injection to the circulating pump and the pressurizer and oxygen addition at the suction line of the injection pump. Operation with uranyl sulfate solution is planned for May.

The HRT feed pump system on the mockup was tested to determine the capabilities and limitations of this feed pump under all HRT operating conditions. The system operated satisfactorily for over 1200 hr; only minor difficulties occurred.

1.5 Controls and Instruments. – Design was completed for the HRT subcontract electrical work extension including the installation of all conduits, ducts, and electrical equipment outside the control-room area. A pneumatic weigh system for high-accuracy inventory of the dump tanks and condensate tanks was selected and procured. Design of the low-pressure valve was approved for construction after thermal-cycle tests failed to reveal any leakage. A cylinder-type operator featuring nylon O-ring seals has been selected as the HRT valve actuator. Redesign and improvement of the HRE liquid-level transmitter are aimed toward an improved coil and suspension system.

PART II. THORIUM BREEDER REACTOR

2. Conceptual Design

2.1 Reactor Analysis. – An economic study of one-region thorium breeder reactors was completed. Where possible, the process characteristics and cost factors were the same as those used previously in studies of two-region-type reactors. The minimum-cost reactor is about 12 ft in diameter, operating with 260 g of thorium per liter on a chemical processing cycle of about 450 days. The ratio of U^{232} to U^{233} produced is approximately 2×10^{-4} in the minimum-cost one-region system, compared with 4×10^{-5} in the two-region system. The unit cost of power is 0.9 mill/kwhr higher than for the optimum two-region reactor if it is assumed that the fixed costs for both reactor types are equal and that each reactor delivers 125 Mw of electrical power.

2.2 Engineering Studies. – With the results of the optimization studies as a basis, preliminary design of the major plant components was undertaken during the last quarter, along with a study of a plant layout. The process flow diagram of the reactor plant was completed and is presented.

A possible station layout based on underwater maintenance in the operating areas is presented. Three turbogenerator sets, each of 100 Mw electrical capability, are located in a room 360 ft long by 114 ft wide. Auxiliary items are located in the basement. A control area 26 ft wide by 300 ft long is located between the turbogenerator plant and the reactor plant. Each reactor and its turbogenerator are individually controlled. The reactor plant consists of a space 80 ft wide by 300 ft long and 45½ ft above ground level. Three cylindrical shield tanks 66 ft in diameter and 116 ft high contain the reactors, the steam generator, and most radioactive components.

In the event of equipment rupture, the contamination is confined to the shield tank, which is kept closed at all times during operation. The tank normally is operated at ½ atm absolute pressure but will withstand an internal pressure of 50 psig. Equipment which may require rather frequent maintenance is grouped under an access hatch in the tank dome through which remote maintenance may be possible.

To minimize both pipe stresses and fissionable material inventory, the core circulation loop is anchored at a single point (the pump), and the rest of the equipment is free to move with thermal expansion, being supported either on rollers or springs.

The heat balance for the turbine cycle was completed and is presented. In the event of a leak in the steam generator, the turbine can be isolated from the reactor in a fraction of a second by actuation of the standard throttle valves supplied with the turbine. In addition, to back up the throttle valves, motor-operated isolation valves are provided next to the reactor to cut off the flow leaving the reactor tank.

[redacted]

Preliminary designs of several major reactor components are presented; included are: (1) the reactor vessel and core pressurizer combination, (2) the core and blanket circulating pumps, (3) the core and blanket steam generators, (4) the recombiners, (5) the core and blanket system dump tanks, and (6) the fission-gas disposal system.

PART III. CORROSION

3. Pump-Loop Corrosion Tests

3.1 Pump-Loop Operation and Maintenance. – Three of the type 347 stainless steel dynamic-corrosion test loops containing uranyl sulfate solution (0.04 *m* uranyl sulfate, 0.006 *m* sulfuric acid, 0.005 *m* copper sulfate), equivalent to that presently planned for use in the HRT, are on long-term operation. These loops are operating at 200, 250, and 300°C and contain corrosion samples made of a variety of materials.

The new 100A pump loop designed for corrosion studies of thorium oxide slurries is operating with a thorium oxide slurry containing 280 g of thorium per kilogram of H_2O at 250°C.

3.2 Results of Loop Tests. – The corrosion resistance of a number of alloys to uranyl sulfate solutions ranging in concentration from 0.02 to 0.17 *m* and at temperatures from 100 to 300°C has been determined. Generally, only the austenitic stainless steels and a few ferritic stainless steels showed a high degree of resistance at all concentrations and temperatures.

A series of tests was completed with 0.04 *m* uranyl sulfate containing 0.006 *m* sulfuric acid at 175°C. The observed corrosion rate of type 347 stainless steel specimens was 6 mpy at all flow rates.

It was demonstrated that the introduction of relatively large amounts of a salt of sulfuric acid into a uranyl sulfate solution reduced the corrosion of stainless steel substantially at all flow rates. Magnesium sulfate showed the most favorable solubility characteristics.

A survey of the corrosion of stainless steel by various mineral acids at high temperatures was completed. The type and extent of corrosion were dependent on the nature of the anion of the acid, the acid concentration, the temperature, and the presence or absence of oxygen. Generally, acids which contained a strongly oxidizing anion caused the formation of the more stable films.

3.3 Sedimentation Rates of Thorium Oxide Slurries at Elevated Temperatures. – Elevated-temperature sedimentation studies have shown rates severalfold greater than would be expected from calculations based on particle size.

4. Radiation Corrosion

4.1 In-Pile Loop. – In-pile loop GG was installed in beam hole HB-4 in the LITR for radiation corrosion studies. Loop EE is now under test in the mockup. The number of coupons was increased in loop EE, and stressed and coupled specimens were added in the core position in order to obtain more data from each loop.

An in-pile loop, for operation at 300°C and 2000 psi in beam hole HB-2, is now being designed.

Preliminary work is under way for the study of the feasibility of circulating thorium oxide slurries in an in-pile loop. One run with thorium oxide slurry was made in a modified in-pile loop.

A second in-pile loop run was completed in the LITR beam hole HB-4 installation. The composition of the solution charged to the loop for the in-pile operation was as follows: 0.17 *m* UO_2SO_4 (88.8% U^{235}), 0.031 *m* $CuSO_4$, and 0.04 *m* H_2SO_4. The loop contained Zircaloy-2 coupon corrosion specimens in Zircaloy-2 holders in both the in-line and core positions. The total in-pile circulating time was 661.5 hr, of which approximately 460 hr was with the LITR at 3 Mw. The fission power released in the loop, with the LITR at 3 Mw, was approximately 600 w, as determined by cesium analysis. The generalized corrosion rate, indicated by oxygen consumption and the increase in nickel concentration, decreased from 6 to 2.2 mpy during the course of the run. The in-line Zircaloy-2 coupons showed no attack; this is consistent with out-of-pile experience. The core coupons were attacked appreciably, with the extent of attack essentially proportional to the power density. The highest corrosion rate measured was 3.36 mpy at a power density of 3.66 kw/liter.

A third in-pile loop test was completed in the LITR installation in beam hole HB-4.

4.2 LITR Bomb Tests. – The addition of 195 ppm Cr(VI) to a solution 0.17 *m* in UO_2SO_4 (93% U^{235}), 0.02 *m* in $CuSO_4$, and 0.04 *m* in H_2SO_4 resulted in a corrosion rate of 5.7 mpy for Zircaloy-2 at 250°C and 5 w/ml, compared with a rate of 6.4 mpy for a bomb experiment (H-60) which was

[redacted]

identical, except for the absence of chromium.

A solution 0.17 *m* in UO_2SO_4 (44% U^{235}) and 0.02 *m* in $CuSO_4$ gave a rate of 4.5 mpy for Zircaloy-2 at 250°C and 2.5 w/ml, compared with a rate of 9 to 10 mpy for experiments (H-57, H-58) which were identical, except that they employed 93% U^{235}, which gave a power density of 5 w/ml.

A solution 0.17 *m* in UO_2SO_4 (20% U^{235}), 0.02 *m* in $CuSO_4$, and 0.45 *m* in H_2SO_4 gave a corrosion rate of 2.2 mpy for Zircaloy-2 at 250°C and 2.5 w/ml. This high-acid experiment was run in the LITR beam hole HB-5, where the flux is slightly less than twice that in hole HB-6. All other experiments were run in hole HB-6.

A solution 0.17 *m* in UO_2SO_4 (93% U^{235}), 0.02 *m* in $CuSO_4$, and 0.04 *m* in H_2SO_4 gave a rate of 1.7 mpy for titanium at 250°C and 5 w/ml. This compares with a rate of 6.4 mpy for Zircaloy-2 under similar conditions.

4.3 MTR Bomb Tests. – Fabrication of equipment for the first MTR bomb test was expected to have been completed in April. The conditions for the first test will be as follows: Zircaloy-2 bomb, 0.043 *m* UO_2SO_4 (10% U^{235}), 0.05 *m* $CuSO_4$, 0.02 *m* H_2SO_4, 280°C, and a power density of 5 w/ml.

5. Laboratory Corrosion Studies

No cracking, pitting, or rapid corrosion was observed as a result of exposure of partially hardened, highly stressed, type 17-4 PH stainless steel for 1000 hr to uranyl sulfate solutions under simulated reactor conditions; fully hardened material, however, appeared to be unsatisfactory.

Inhibitor levels of 300 ppm sodium chromate in the HRT maintenance pool appear to be optimal for sustained corrosion protection combined with satisfactory visibility.

Corrosion data for type 347 stainless steel, titanium 75A, and Zircaloy-2, exposed to circulating thorium oxide slurries in stainless steel toroids, were obtained at 26-fps relative slurry velocity and 250°C, with slurry concentrations of 500 and 1000 g of thorium per kilogram of water and with 90-psi oxygen pressure. Thoria from 11 sources has been used. A maximum corrosion rate of 9 mpy was observed.

The presence of carbon dioxide resulted in a slurry which was pourable (1000 g of thorium per kilogram of water) after running for 215 hr at 26 fps and 250°C and with 90-psi oxygen. The corrosion behavior did not differ from that of a similar slurry prepared so as to be carbon-free.

PART IV. ENGINEERING DEVELOPMENT

6. Development of Fuel-System Components

Several types of heterogeneous catalysts for hydrogen-oxygen recombination were evaluated in the high-pressure recombiner loop. The electrolytic cells were modified to dilute the H_2 and O_2 with steam to prevent explosions.

Construction of the dump-valve test loop is essentially complete; it was tested hydrostatically at 3000 psi. The first tests will be made with a prototype of the HRT dump valve.

A 14-in. gas separator, with singly curved vanes, was tested. These vanes are easier to fabricate and operate better than doubly curved vanes.

A 20-cfm gas circulator was ordered from Allis-Chalmers Mfg. Co. and will be delivered in about seven months.

A 5-gpm ORNL pump, converted for gas circulation, was returned to service after an electrical failure. A 2000-psi, 5-gpm, canned-rotor pump operated for 780 hr at 300°C with water. A 1000-psi design, 5-gpm, ORNL canned-rotor pump operated for 5300 hr.

The high-frequency-induced eddy current inspection method employed on the finished ⅜-in.-OD × 0.065-in.-minimum-wall HRT heat exchanger tubing is being fully explored.

The 4000-gpm loop accumulated 700 hr of operating time. To increase ease and reliability of operation, a sample bypass was added to the high-pressure loop, and a CO_2 absorber and an O_2 flowmeter were installed in the off-gas line.

The slurry feed pump was operated as a high-pressure source of slurry for valve tests. Efforts are being made to improve the suction characteristics of the pump.

A program was initiated for the development of fabrication methods applied to titanium components of homogeneous reactor systems. Twenty-four industrial concerns were invited to bid on the submission of three items demonstrating the use of titanium: short lengths of titanium-lined 3½- and 20-in. pipe and a small titanium-clad heat exchanger. Several of these concerns indicated interest in the program. This approach, through established industrial concerns, is being supplemented at ORNL by design and fabrication studies and by metallurgical research on the fundamentals of titanium technology. The information to be supplied by this development program should ultimately permit satisfactory design of large

[redacted]

aqueous homogeneous power reactor systems utilizing titanium as the containing material in contact with the primary fuel and/or blanket solutions.

7. Development of Blanket-System Components

Operation of a 100-gpm loop with ThO_2 slurry at 290°C indicated no greater over-all attack rate on stainless steel than in a comparable test at 250°C. The optimum sulfate concentration appeared to be between 1000 and 1500 ppm at 290°C as opposed to about 3000 ppm at 250°C.

In small 5-gpm loops at 250°C the pH of the slurry was reduced with CO_2 instead of with sulfate; in tests with and without oxygen at approximately the same pH, oxygen reduced the short-term attack rate and produced a hard adherent film on stainless steel, but in the absence of oxygen no visible film formed and the short-term attack rate was roughly twice as high.

Sections of 100-gpm loops which were removed after thousands of hours of slurry service showed essentially complete freedom from general attack, although a few areas showed some localized attack.

In 5-gpm loop tests, the presence of $Na(SiO_2)_{3.25}$ caused plugging of the loop after shutdown.

In a 5-gpm loop test the rate of attack on stainless steel by ThO_2 calcined at 800°C was no greater than that by ThO_2 calcined at 650°C; in addition, ThO_2 calcined at 800°C appeared to be easier to handle at low temperatures after high-temperature circulation.

Beaten ThO_2 slurries at concentrations between 500 and 1500 g of thorium per kilogram of H_2O behave as Bingham plastics at 25°C.

The construction of the 200A slurry pump loop is 98% complete.

Five letdown valves have been tested at room temperature, and a sixth is now being tested. Difficulties encountered include abrasion, galling of close-fitting parts, and deformation of valve stems. The development of a satisfactory letdown valve appears to be possible by combining the best features of the several valves which have been tested.

A proposed inlet and outlet arrangement for slurry passing through the HRT blanket vessel appears to resuspend solids after a prolonged shutdown in tests with an 18-in.-dia model of the pressure vessel at blanket temperatures up to 175°C.

The HRT dump tanks as presently designed have been found to require modification if they are to be used with slurry.

Quantitative measurements of the height of solids in a vertical pressurizer have been made as a function of steam withdrawal rate. Rates up to 6 lb/hr did not cause excessive accumulation of solids in the pressurizer.

Construction of the HRT blanket mockup has started. The design now includes a full-size blanket vessel for tests up to 200°C, as well as provision for tests at full HRT temperature and pressure without the full-sized blanket vessel.

A method for correlating both volume-boiling and surface-boiling vapor slip velocities which was developed checked with experimental data at pressures up to 600 psi and also indicated no slip at the critical temperature and pressure.

A contract with Babcock & Wilcox Co. has been made for obtaining slip data at pressures up to 2400 psi.

8. Metallurgy

The equipment for evaluation of stress-corrosion cracking susceptibility of austenitic stainless steels was tested and modified. Tests on various materials were run in order to check the equipment. The results supported the general relation between the martensite-forming susceptibility and the stress-corrosion tendencies of stainless steels.

Specially prepared alloys of Fe-Cr and Fe-Cr-Ni were prepared and heat-treated to obtain a substantially complete sigma structure. These will be subjected to corrosion tests in HRP environments.

Work on determining the effect of oxide films on the rate of hydrogen absorption by zirconium and its alloys was confined largely to establishment of reliable experimental techniques for the use of the equipment.

Investigation of the service failure of a titanium corrosion-specimen holder continued. Metallographic and x-ray diffraction studies indicated the presence of an unidentified phase in the exposed specimens. Vacuum-fusion analysis, x-ray diffraction analysis, and metallographic examinations indicated that the phase in question is not titanium hydride, as was first suspected.

Impact tests on Zircaloy-2 specimens from the second in-pile loop run were completed, and the results were compared with those obtained with

[redacted]

[redacted]

specimens exposed to similar conditions in another test and in an out-of-pile run, as well as with unexposed control specimens. No significant change in transition temperature (judged by the energy that was required in order to break the specimens) resulted from the in-pile exposure. The values recorded in the high-temperature or ductile region of the curve, for specimens from loop run FF, are generally lower than those obtained on previous samples, but the data do not represent true impact breaks and are consequently not true measures of relative impact behavior. The apparent transition temperature (brittle to ductile fracture) did not seem to be affected by the in-pile conditions to which the specimens were exposed.

A considerable number of irradiations of materials of interest to the Project have been completed; the irradiated specimens are being tested to determine whether changes in mechanical properties have occurred. Tensile tests on irradiated austenitic stainless steels confirmed the presence of a yield point in some of these metals and revealed a strain-rate dependence of the yield stress.

PART V. CHEMICAL ENGINEERING DEVELOPMENT

9. Thermal Breeder Fuel Reprocessing

Results of further experiments with neodymium sulfate indicated that the deposition of this salt on hot metal surfaces is influenced by the metals in the system. In systems containing stainless steel, deposition from saturated solution on hot stainless steel and Zircaloy-2 surfaces was pronounced. However, in systems containing no stainless steel there was no significant deposition of neodymium sulfate on hot Zircaloy-2 surfaces. This indicates that the deposition on hot Zircaloy-2 surfaces is enhanced by a film of stainless steel corrosion products on the surface. Since Zircaloy-2 remains free of such a film under reactor conditions, deposition of rare-earth sulfates on the core tank of a TBR may not be significant.

It was found that connecting the underflow pot of a hydroclone directly to the hydroclone underflow port eliminated the necessity for recycling the hydroclone underflow. A hydroclone system of this type gave solids concentration factors of the order of 100 for 1-μ and 1000 for 4-μ ThO_2 particles suspended in water. A solids concentration factor of 100 would be adequate for TBR fuel processing. Corrosion studies indicated that a material more resistant than stainless steel may be required for the hydroclone.

A 1-in.-dia hydroclone installed on test loop B removed precipitated neodymium sulfate from simulated fuel solution; this was indicated by an increase in the neodymium concentration in the underflow. Iron oxide precipitated in this loop at 300°C and was separated with an efficiency approaching 100% by the hydroclone.

The HRT chemical processing facility will treat the reactor fuel continuously by centrifuging out, in a hydroclone system, the fission and corrosion products that are insoluble at the reactor temperature and by purging a small stream to remove those that are soluble. The purge stream and the centrifuged solids will be dried to recover the heavy water and then transported in a shielded carrier to a solvent extraction facility for recovery and decontamination of the uranium.

The preliminary designs of the principal equipment pieces are completed; valves, piping, and pumps are on order. Completion of construction is scheduled for January 1956.

10. Plutonium-Producer Blanket Processing

An autoradiograph of a zirconium tube containing adsorbed plutonium, 0.05 mg per square centimeter, indicated that PuO_2 crystallized out preferentially on surface imperfections in the metal.

Plutonium oxide that was precipitated under simulated reactor conditions and reslurried in water was concentrated in a hydroclone, with efficiencies of 15 to 70%. There was no apparent classification of the PuO_2 particles, since the same separation efficiencies were obtained upon recycling the hydroclone overflow.

The precipitation rate of PuO_2 under simulated reactor conditions was unaffected by the presence of 100 mg of iron, nickel, or copper per kilogram of H_2O. The presence of hexavalent chromium reduced the rate of precipitation and increased plutonium solubility by 50 and 150% for 20 and 100 mg of chromium per kilogram of H_2O, respectively.

11. Thermal-Breeder Blanket Processing

When irradiated ThO_2 was refluxed with 12 *N* H_2SO_4 for 4 hr, 70% of the protactinium was leached and 70% of the ThO_2 was converted to insoluble $Th(SO_4)_2$. This indicates that protactinium was bound within the ThO_2 particle and that

[redacted]

complete dissolution or metathesis of ThO_2 was necessary for removal of the protactinium to be achieved.

Slurries of ThF_4 and ThF_4-ThO_2 at 250°C under 200 psi of O_2 are too corrosive for use with Zircaloy-2. Corrosion rates were 200 to 400 mpy in static autoclave tests. The precipitation rate of PuO_2 in stainless steel equipment was approximately the same as that in a titanium vessel with 20 mg of chromium per kilogram of H_2O. In these experiments at 250°C under an atmosphere of H_2 and O_2, the chromium was present as chromate. In a reactor the chromium will be reduced, and hence the effect of chromium on plutonium behavior may be eliminated.

Temperature had a considerable effect both on the precipitation rate of PuO_2 and on plutonium solubility. As the temperature was reduced from 250 to 125°C, the precipitation rate was reduced and the plutonium solubility was increased from 15 to about 20 mg per kilogram of H_2O.

12. Summary of Work of Vitro Laboratory

The reduction of various oxidation states of iodine to the elemental form has been shown to be very rapid at 250°C in oxygenated uranyl sulfate solutions. The reduction of heptavalent iodine to the pentavalent form was too rapid to measure by present techniques. A half-period of about 2 min was measured for the reduction of pentavalent iodine to the elemental state when only a small amount of the elemental form was present. When no removal of iodine was made, equilibrium between the elemental and pentavalent states was soon attained. This indicates that the rate of diffusion of elemental iodine into the gas phase and its subsequent movement to the hot silver surface control the rate of iodine removal from the liquid and suggest the use of sweep gas to speed up this process.

PART VI. SUPPORTING CHEMICAL RESEARCH

13. Aqueous Systems at Elevated Temperatures

Studies of the pressure-volume-temperature-composition relationships in the two-liquid-phase region of the uranyl sulfate system have continued with additional measurements of volumes as functions of temperature, composition, and fractional filling. The pressure-measuring apparatus is in the final stage of construction and should be tested, calibrated, and in operation in the near future.

Phase studies of aqueous systems involving uranium trioxide, carbon dioxide, and an alkali or alkaline earth oxide have been initiated, and some data for the system UO_3-Na_2O-CO_2-H_2O at 250°C have been obtained.

Additional data on the quaternary systems, NiO-UO_3-SO_3-H_2O and CuO-UO_3-SO_3-H_2O, serve to illustrate the complexity of these systems. In the nickel system several complex basic salts have been tentatively identified. In the copper system the basic salts $4CuO{\cdot}SO_3{\cdot}3H_2O$ (brochantite) and $3CuO{\cdot}SO_3{\cdot}2H_2O$ (antlerite) dominate a large portion of the system at 25 and 100°C. Even solutions comparatively rich in uranium exist in equilibrium with these compounds. Solutions very rich in uranium yield uranium-containing complexes, none of which has been identified.

Apparatus for measuring water adsorption by ThO_2 powders has been completed, and initial testing is in progress. Experiments will be started when testing and calibration have been completed.

14. Adsorption on Inorganic Materials

Exploratory work on the adsorptive properties of various inorganic materials for ions in aqueous solutions was continued. Principal emphasis centered on the properties of zirconium hydroxide, zirconium phosphate, zirconium tungstate, and thorium hydroxide. None of these materials can be considered stoichiometric compounds; the names are used for identification only and should not be interpreted to imply any analytical data. A large fraction of the work involved determination of distribution coefficients of various tracers.

Opalescent "solutions" of thorium hydroxide in water were prepared which contained up to 2.8 g of dried hydroxide dispersed in 1 g of water. Heating these "solutions" at elevated temperatures resulted in the formation of precipitates which, under some conditions, redispersed upon cooling the system. The factors which affect the solubilization of thorium and the reversibility of the precipitation are being studied intensively because of possible application to homogeneous reactor systems.

15. Analytical Chemistry

A major concern of the analytical research directed toward support of the HRP is the determination of trace elements which are present as products

of corrosion or as additives in solutions of uranyl sulfate and slurries of thorium oxide. Procedures were developed and evaluated for the following: determination of barium in the presence of thorium, dissolution of refractory pellets of aluminum oxide and of mixtures of thorium and titanium oxide, determination of silver by flame photometry, electrodeposition of nickel and copper from uranyl sulfate solutions, photometric titration of sulfate, polarographic determination of chromium, and the use of conductivity and pH measurements for the characterization of slurries.

[redacted]

CONTENTS

SUMMARY vii

PART I. EXPERIMENTAL REACTORS

1. HOMOGENEOUS REACTOR TEST 3
   - 1.1 Project Status 3
     - 1.1.1 Procurement 3
     - 1.1.2 Construction 3
     - 1.1.3 Status of components 3
   - 1.2 Design 3
     - 1.2.1 Flowsheets 3
     - 1.2.2 Reactor cells 15
     - 1.2.3 Core vessel 15
     - 1.2.4 Reactor blast shield and cooling coils 15
     - 1.2.5 Fuel low-pressure assembly 20
     - 1.2.6 Fuel and blanket feed-pump installations 22
     - 1.2.7 Pressurizer pressure-balancing system 22
   - 1.3 Reactor Analysis 22
     - 1.3.1 HRT safety calculations 22
     - 1.3.2 Allowable rate of decrease in HRT steam pressure 25
     - 1.3.3 HRT "walk-away" and overpressure 27
   - 1.4 Component Development 28
     - 1.4.1 Pump development 28
     - 1.4.2 Fuel and blanket pumps 29
     - 1.4.3 HRT heat exchangers 29
     - 1.4.4 HRT dump test 31
     - 1.4.5 HRT mockup loop 33
     - 1.4.6 Feed pump mockup 37
   - 1.5 Controls and Instruments 37
     - 1.5.1 General design status 37
     - 1.5.2 Pneumatic weigh cell 38
     - 1.5.3 Valves and operators 39
     - 1.5.4 Liquid-level transmitter 39

PART II. THORIUM BREEDER REACTOR

2. CONCEPTUAL DESIGN 45
   - 2.1 Reactor Analysis 45
     - 2.1.1 One-region thorium breeder reactors 45
     - 2.1.2 Ratio of U^{232} to U^{233} produced in thorium breeder reactors 48
   - 2.2 Engineering Studies 48
     - 2.2.1 The reactor process flow diagram 48
     - 2.2.2 Reactor and power-plant layout 48
     - 2.2.3 Turbogenerator plant 57
     - 2.2.4 Reactor component design 57

PART III. CORROSION

3. PUMP-LOOP CORROSION TESTS 69

[redacted]

[redacted]

3.1 Pump-Loop Operation and Maintenance 69
3.1.1 Loop status 69
3.2 Results of Loop Tests 69
3.2.1 Introduction 69
3.2.2 Results 69
3.2.3 Miscellaneous 92
3.3 Sedimentation Rates of Thorium Oxide Slurries at Elevated Temperatures 92

4. RADIATION CORROSION 94
4.1 In-Pile Loop 94
4.1.1 Development and construction 94
4.1.2 LITR operations – in-pile loop corrosion test FF 99
4.1.3 In-pile loop experiment GG 109
4.1.4 Remote dismantling and inspection 109
4.2 LITR Bomb Tests 119
4.2.1 Introduction 119
4.2.2 In-pile tests 119
4.2.3 Out-of-pile tests 121
4.3 MTR Bomb Tests 123

5. LABORATORY CORROSION STUDIES 124
5.1 Corrosion of Precipitation-Hardening Stainless Steels by Simulated Reactor Environments 124
5.2 Inhibition of HRT Maintenance Pool Water 125
5.3 Boiling Nitric Acid Specification Tests 126
5.4 HRP Thorium Oxide Slurry Blanket Corrosion Studies 126
5.4.1 General 126
5.4.2 Effect of carbon dioxide in thoria slurries 127

PART IV. ENGINEERING DEVELOPMENT

6. DEVELOPMENT OF FUEL-SYSTEM COMPONENTS 133
6.1 Recombiner Development 133
6.2 Dump Valve Test Loop 133
6.3 5000-gpm Gas Separator 133
6.4 Small Reactor Components 134
6.4.1 20-cfm canned-rotor gas circulator 134
6.4.2 ORNL gas circulator 134
6.4.3 Small pumps 134
6.5 Development of Large Heat Exchangers 134
6.6 4000-gpm Loop 134
6.7 Slurry Feed Pump 135
6.8 Titanium Program 135

7. DEVELOPMENT OF BLANKET-SYSTEM COMPONENTS 137
7.1 Slurry Circulation Studies 137
7.1.1 Comparison of slurry corrosion at 290 and 250°C in 100-gpm loops 137
7.1.2 Effect of oxygen at 250°C 137
7.1.3 Long-term attack on stainless steel piping 138
7.1.4 Thickening of thorium oxide slurries 141
7.2 Pressure Drop in Slurry Systems 146

[redacted]

[redacted]

7.3 Slurry Component Development 147
7.3.1 Westinghouse 200A slurry pump 147
7.3.2 Valves 147
7.3.3 Pressure-vessel studies 148
7.3.4 Dump tank–evaporator test 150
7.3.5 Pressurizer studies 150
7.4 Slurry Blanket Mockup 156
7.5 Boiling Studies 156
7.5.1 Vapor transport 156
7.5.2 Vapor separation 160

8. METALLURGY 161
8.1 Metallurgy of Corrosion 161
8.1.1 Stress-corrosion cracking of austenitic stainless steels 161
8.1.2 Dynamic-corrosion study factors associated with grain size and sigma phase in wrought austenitic stainless steels 162
8.1.3 Effect of hydrogen on properties of zirconium and its alloys 163
8.1.4 Role of oxide films on rate of hydrogen absorption by zirconium and its alloys 163
8.2 Physical Metallurgy of Titanium and Zirconium Alloys 166
8.2.1 Commercial titanium 166
8.2.2 Zirconium alloys (Zircaloy-2) 167
8.3 Effects of Radiation on Structural Metals and Alloys 168

PART V. CHEMICAL ENGINEERING DEVELOPMENT

9. THERMAL BREEDER FUEL REPROCESSING 173
9.1 Fission-Product Chemistry 173
9.1.1 Neodymium precipitation 173
9.1.2 Neodymium solubility 174
9.1.3 Purification of neodymium tracer 175
9.1.4 Iodine removal 175
9.2 Hydroclone Development 176
9.2.1 Hydroclone underflow ratio 176
9.2.2 Hydroclone performance in an induced-underflow pot system 177
9.2.3 Hydroclone corrosion 180
9.2.4 Hydroclone test on loop B 182
9.3 HRT Chemical Processing Plant 182
9.3.1 Status of plant 182
9.3.2 Instrumentation 183
9.4 Equipment Development 184

10. PLUTONIUM-PRODUCER BLANKET REPROCESSING 185
10.1 Adsorption of Plutonium on Stainless Steel, Titanium, and Zirconium 185
10.2 Separation of PuO_2 by a Hydroclone 185
10.3 Precipitation Rate of Plutonium Dioxide 186

11. THERMAL-BREEDER BLANKET REPROCESSING 188
11.1 Leaching of Thorium Dioxide 188
11.2 Corrosion of Zircaloy-2 in ThO_2-ThF_4 Slurries 188

12. SUMMARY OF WORK OF VITRO LABORATORY 189

[redacted]

[redacted]

PART VI. SUPPORTING CHEMICAL RESEARCH

13. AQUEOUS SYSTEMS AT ELEVATED TEMPERATURES 193

13.1 Direct Sampling as a Method for Investigating the System UO_3-SO_3-H_2O Above 300°C 193
13.2 The System UO_3-SO_3-H_2O Above 300°C 193
13.3 Aqueous Systems Involving Uranium Trioxide, Carbon Dioxide, and Alkali or Alkaline Earth Oxides 194
13.4 The Quaternary Systems NiO-UO_3-SO_3-H_2O and CuO-UO_3-SO_3-H_2O 195
13.5 Adsorption of Water by ThO_2 195

14. ADSORPTION ON INORGANIC MATERIALS 197

14.1 Zirconium Phosphate 197
14.2 Zirconium Hydroxide 197
14.3 Thorium Hydroxide 199
14.4 Other Hydroxides 199
14.5 Zirconium Tungstate Precipitates 199

15. ANALYTICAL CHEMISTRY 201

15.1 Electrodeposition of Copper from Solutions of Uranyl Sulfate at a Controlled Cathode Potential 201
15.2 Electrodeposition of Nickel from Solutions of Uranyl Sulfate at a Controlled Cathode Potential 201
15.3 Conductivity and pH Measurements of Aqueous Slurries of Thorium Compounds 201
15.4 Polarographic Determination of Barium 201
15.5 Dissolution of Refractory Mixtures of Thorium and Titanium Oxides 201
15.6 Dissolution of Aluminum Oxide and Determination of Platinum 202
15.7 Flame Photometry of Silver 202
15.8 Spectrophotometric Determination of Ethylenediaminetetraacetic Acid as the Copper Complex 202
15.9 Polarographic Determination of Chromium(VI) and Total Chromium in Homogeneous Reactor Fuels 202
15.10 Photometric Titration of Sulfate in Homogeneous Reactor Fuels 202

[redacted]

Part I

EXPERIMENTAL REACTORS

S. E. Beall

1. HOMOGENEOUS REACTOR TEST

1.1 PROJECT STATUS

S. E. Beall

J. J. Hairston, Jr. J. W. Hill, Jr.
S. I. Kaplan

1.1.1 Procurement

Ninety-nine purchase orders, totaling $312,000, and two development contracts ($160,000) have been issued for HRT components and materials. Seventy purchase orders ($47,000) have been completed, leaving 29 orders ($265,256) to be procured; $141,700 of this amount is expected to be completed by July 1.

For instrumentation, 70 orders, totaling $131,000, have been issued; 42 orders ($17,000) have been received, and an additional $61,000 worth of material is expected before July 1.

1.1.2 Construction

(a) Work by Contractor. – Construction of the steel cell was completed in February. Several leaks, which were found when the cell was filled with H_2O, were subsequently repaired. Dye-penetrant inspection of the welded joints in the stainless-steel-clad portion of the tank revealed numerous (several hundred, total) cracks in the weld deposit and in the cladding adjacent to the welds, where the surface had been ground. Investigation showed that the cracks were caused by grinding the apparently highly stressed clad layer; it was possible to produce cracks by grinding alone. The cracks were repaired by rewelding without grinding.

During the final weeks of completion of the steel cell, it was decided to increase the design strength of the cell to withstand a 30-psig internal pressure (instead of the original 15 psig) and to make possible a future revision which would allow a 50-psig internal pressure. To accomplish these requirements, it was necessary to strengthen the bases of the cell columns by installing large anchor bolts at each column. The contractor was instructed to drill four 6-in.-dia holes at the base of each column and to install 2-in.-dia steel anchor bolts, fastened to the columns. Drilling of the holes has been completed, and the anchor bolts are being installed.

At the conclusion of this work, the contractor will install all process lines which pierce the shell of the steel cell and which must be welded in place. Following the installation of the penetrating lines, Amercoat 74 will be applied to all internal surfaces before the tank is released to ORNL. The contractor is also responsible for the entire steam system and the completion of the remaining concrete work (valve pit, shield walls, and floors) within the main bay of the building.

Acceptance of the steel tank by ORNL forces is expected in July, at which time the tank will be tested hydrostatically. The installation of reactor equipment will follow this test.

(b) Work by ORNL. – The preparation of the four floor levels of the control area and the installation of instrument and electrical accessories are ahead of schedule. Racks, switchgear, and conduits are in place. The entire area has been tiled and painted.

1.1.3 Status of Components

Table 1.1 summarizes the status of individual components which are being procured elsewhere or constructed in ORNL shops.

1.2 DESIGN

R. B. Briggs

R. E. Aven	J. N. Robinson
R. H. Chapman	W. Robinson
H. N. Culver[1]	W. Terry
W. R. Gall	T. H. Thomas
J. E. Kuster[2]	R. VanWinkle
R. G. Pitkin[3]	F. C. Zapp

1.2.1 Flowsheets

Final flow diagrams for the HRT system have been approved and are presented here as Figs. 1.1 through 1.5. Keys to flowsheet symbols and equipment numbers are given by Fig. 1.6 and Table 1.2.

The fuel and blanket high-pressure and low-pressure systems are shown in Fig. 1.1. The basic design data are the same as reported previously.[4] The high-pressure system is essentially the same as that reported in July 1954.[5] The pump and

[1] On loan from TVA.

[2] On loan from Maxon Construction Co.

[3] On loan from Vitro Corp.

[4] R. B. Briggs *et al.*, *HRP Quar. Prog. Rep. July 31, 1954*, ORNL-1772, Table 4, p 16.

[5] *Ibid.*, Fig. 2, p 17.

TABLE 1.1. STATUS OF HRT COMPONENTS

Component	Fabricator	Delivery Status
High-pressure equipment		
Core–pressure vessel assembly	Newport News Shipbuilding & Dry Dock Co.	August
Valves	Fulton Sylphon Division	August
Circulating pumps	Westinghouse Electric Corp.	June
Heat exchangers	Foster Wheeler Corp.	June
Feed pumps	Oak Ridge National Laboratory	May
Low-pressure equipment		
Cold traps	Oak Ridge National Laboratory	Completed
Condensate tanks	Oak Ridge National Laboratory	Completed
Recombiners	Oak Ridge National Laboratory	May
Dump tanks	Oak Ridge National Laboratory	May
Storage tanks	Oak Ridge National Laboratory	May
Valves	Fulton Sylphon Division	June

pressurizer vent lines now discharge to the low-pressure system separately, and a rupture-disc assembly has been added in parallel with the pressurizer relief valves for additional protection against pressure imbalance between the core and pressure vessel. The low-pressure system is similar to that reported in October 1954.[6] Symbols showing all instrumentation have been added.

The service systems are shown on four separate flowsheets. The cooling-water system as shown in Fig. 1.2 is designed to provide continuous cooling for all condensers and coolers in the reactor systems during operation, as well as to provide emergency cooling after shutdown in the event of complete failure of all utilities serving the building.

Water is circulated normally through the equipment and a cooling tower, with provision for make-up from the process water-supply system. A storage capacity of 15,000 gal is provided by the cooling-tower basin. In the event of failure of the circulating pump, a valve will open, allowing convection circulation through the basin. In the event of leakage of process fluids, causing contamination of cooling water in some of the equipment, a signal from a radiation monitor on the return line will cause a valve to open, dumping all return water into the reactor cell. The 15,000-gal reservoir will provide sufficient cooling for 3 to 6 hr, in which time provision can be made for pumping water into the basin from other sources.

Individual control valves and flow indicators are provided in the control area for each item of equipment being cooled.

The steam system, Fig. 1.3, is designed to remove steam from the main reactor steam generators at a controlled rate, condense it, and return feedwater to the steam generators. Some of the steam can be used to generate power, but approximately 80% at 5 Mw will be removed in an air-cooled condenser. Provision is made for preheating the reactor with 1500-psig steam from an oil-fired package boiler unit or with 240-psig steam from the ORNL steam plant.

As protection against effects of a tube rupture in the steam generators, steam drums and quick-closing valves are provided in a shielded pit adjacent to the reactor cell. The drums allow sufficient delay to permit the valves to close before any contaminated steam can reach the external piping.

The waste and vent system, Fig. 1.4, is designed to dispose of all radioactive wastes produced in

[6] R. B. Briggs *et al.*, *HRP Quar. Prog. Rep. Oct. 31, 1954*, ORNL-1813, p 7.

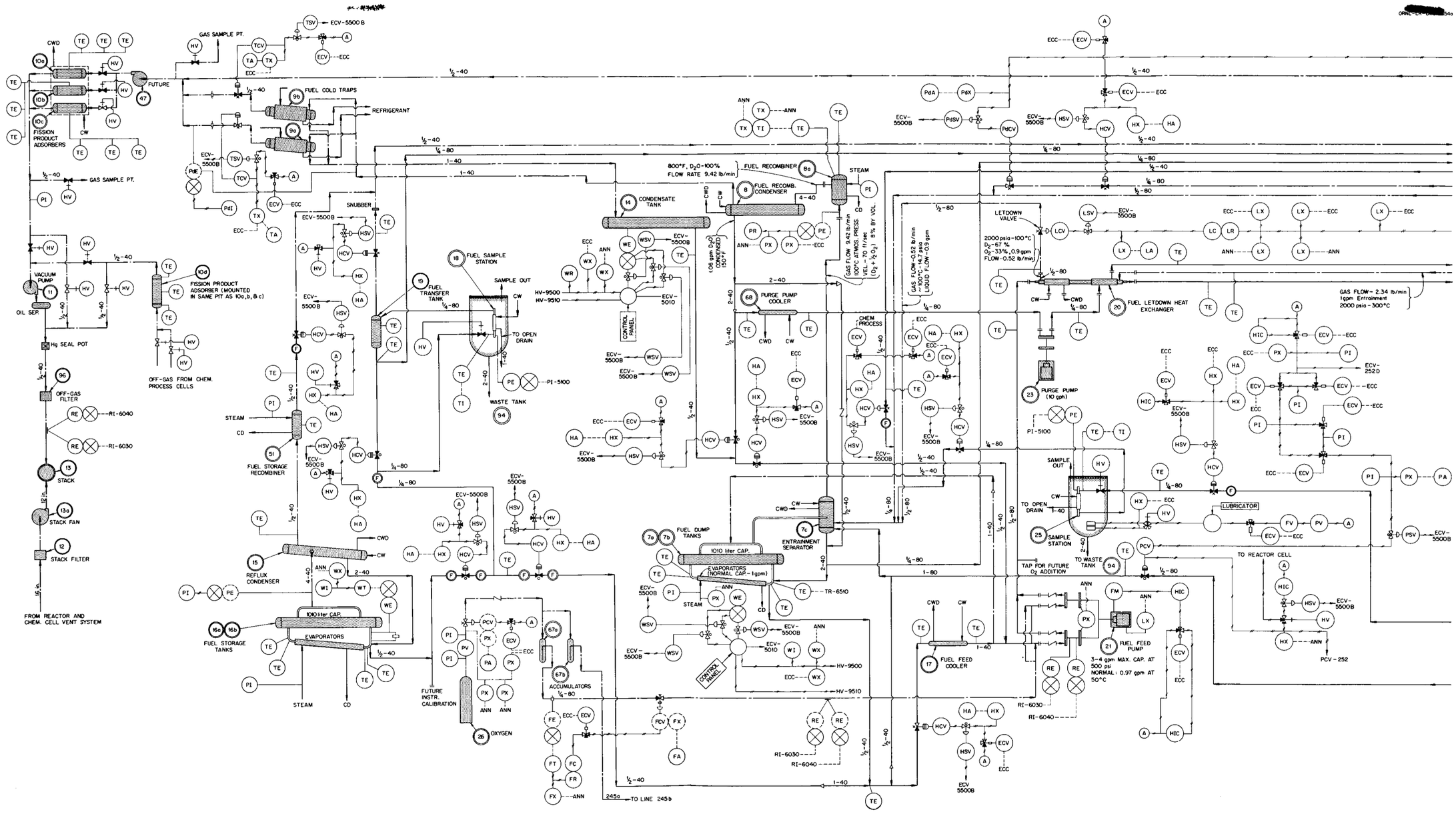

Fig. 1.1. Fuel and Blanket Systems Flowsheet.

[redacted]

ORNL-LR-DWG 6854b

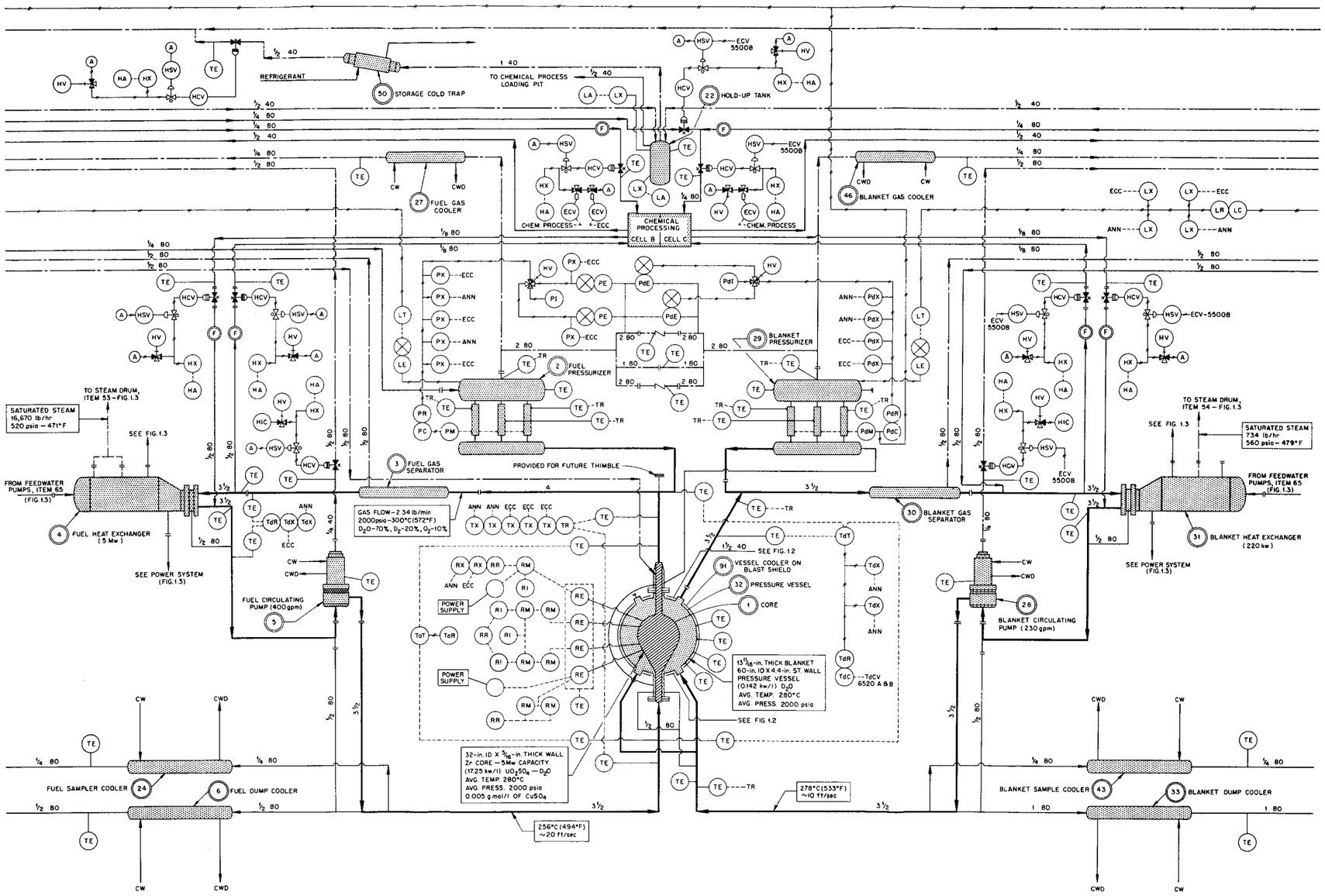

Fig. 1.1 (continued)

[redacted]
ORNL-LR-DWG 8854c

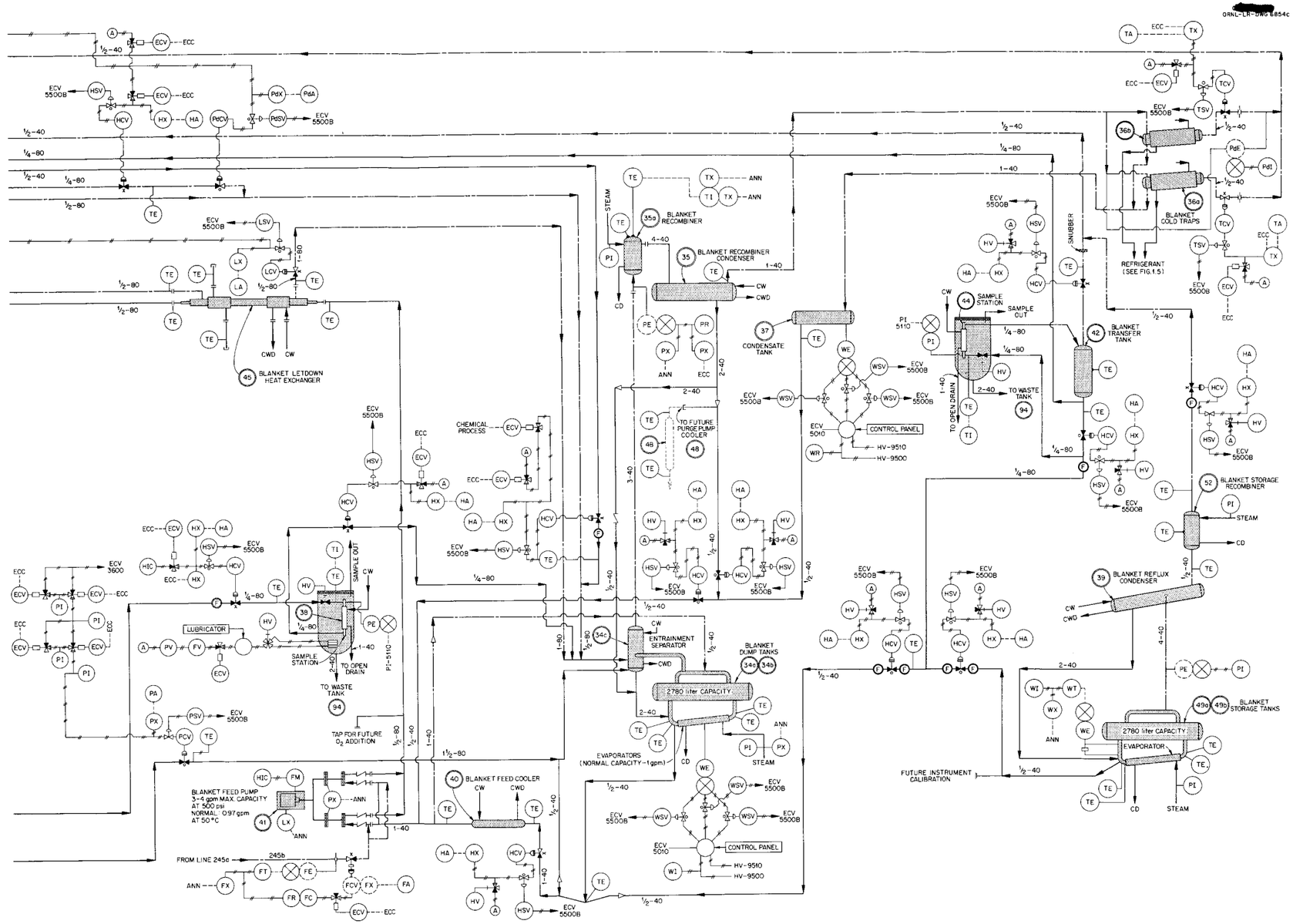

Fig. 1.1 (continued)

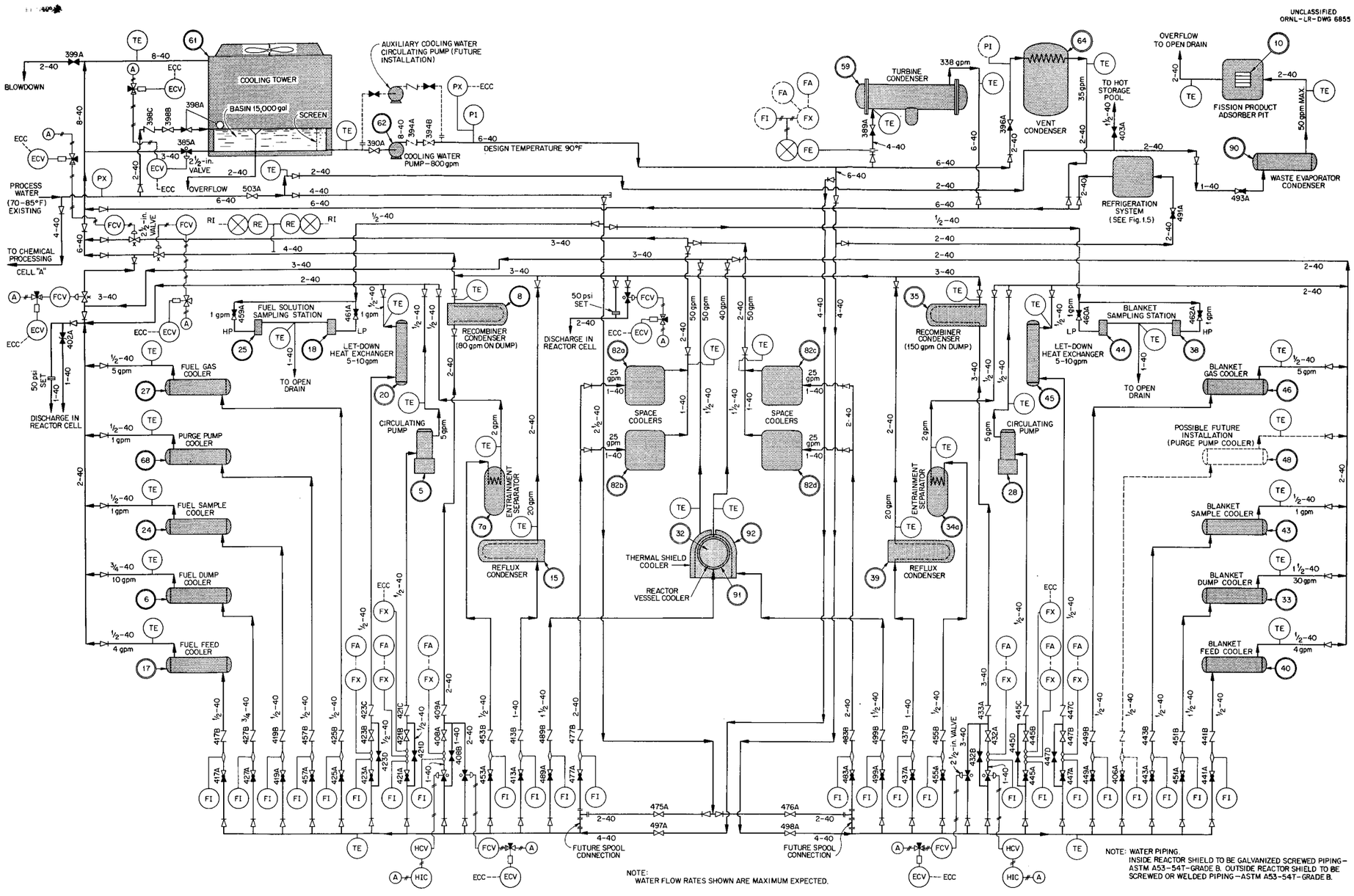

Fig. 1.2. Cooling-Water System Flowsheet.

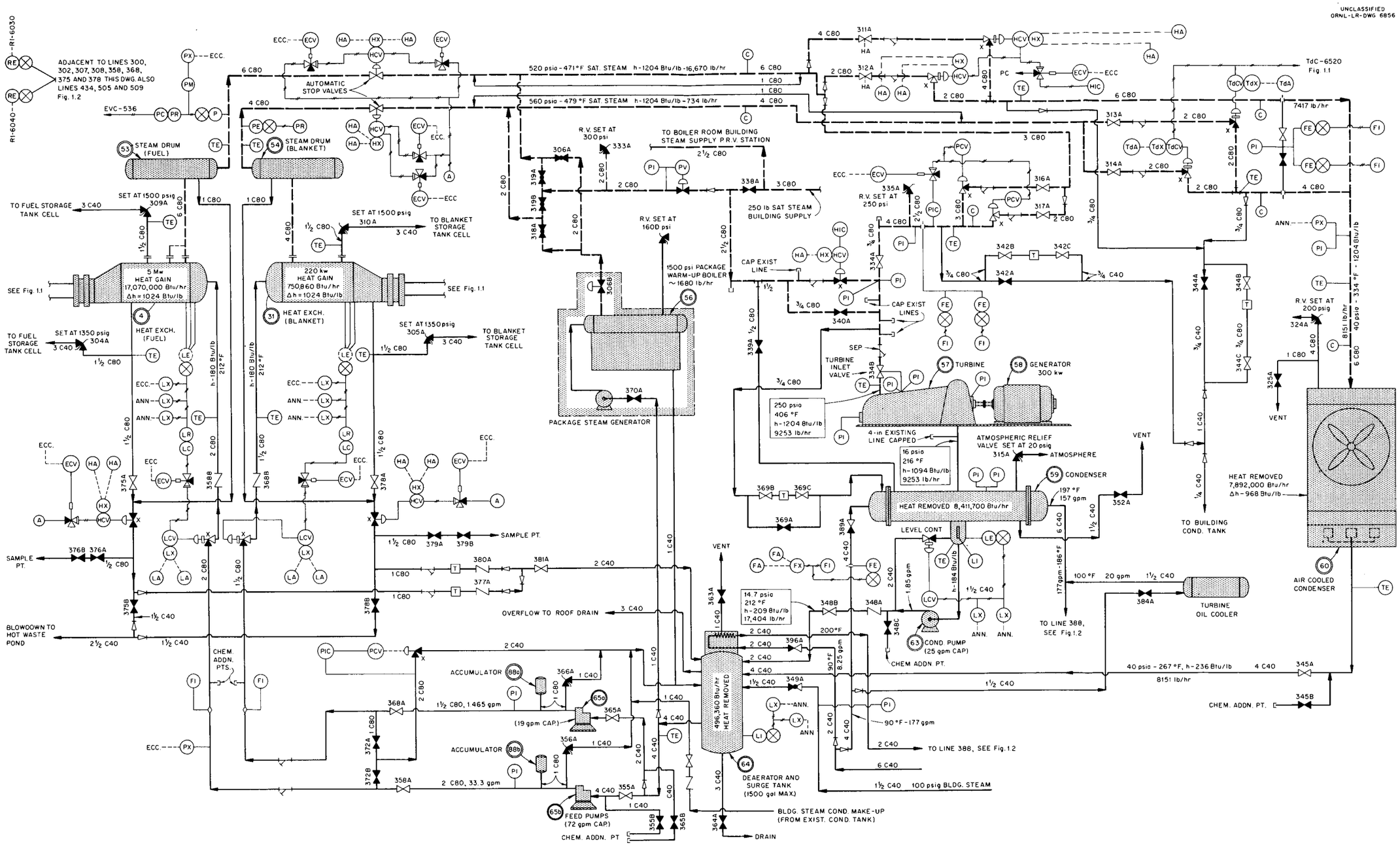

Fig. 1.3. Steam System Flowsheet.

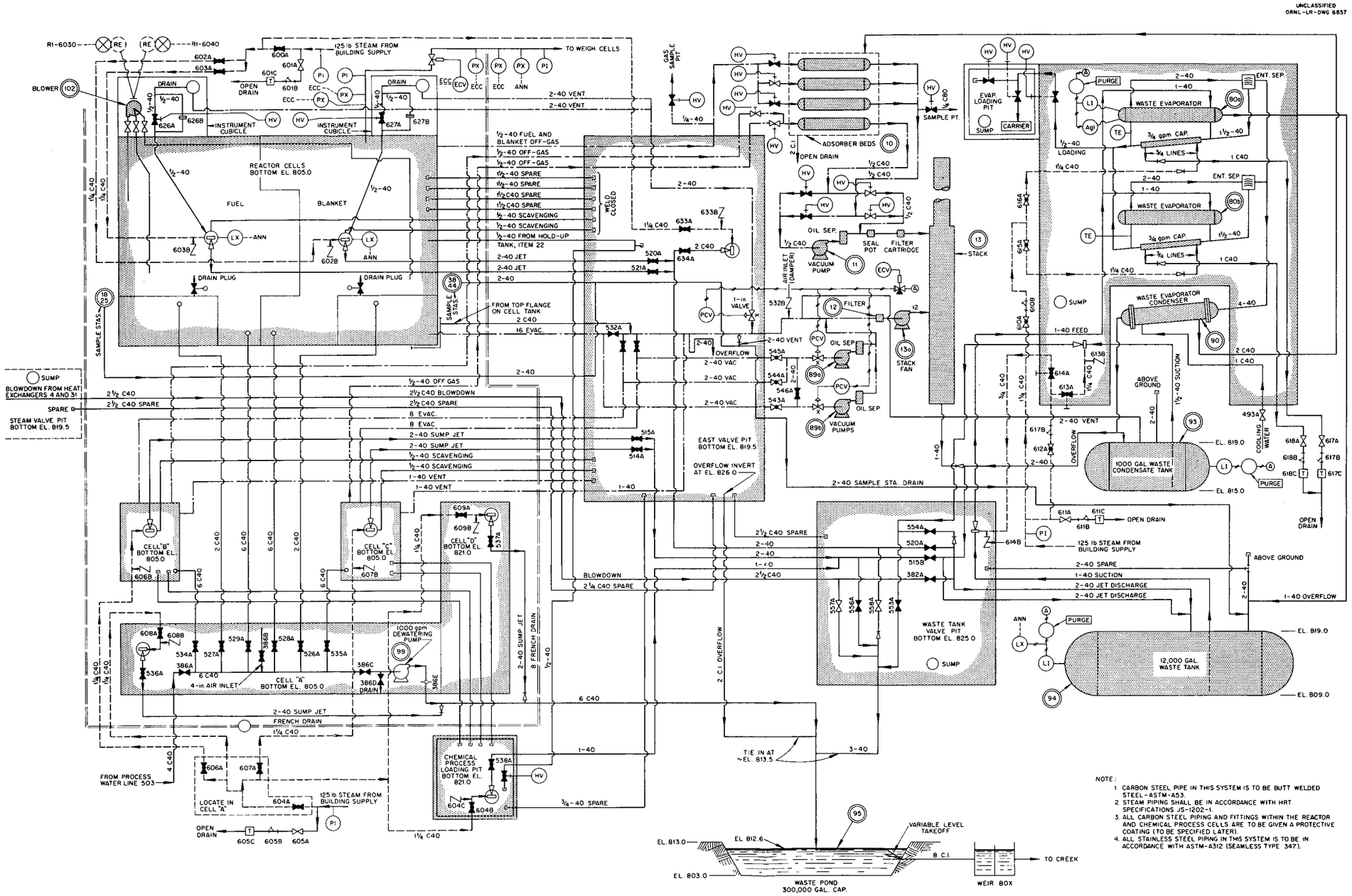

Fig. 1.4. Waste and Vent System Flowsheet.

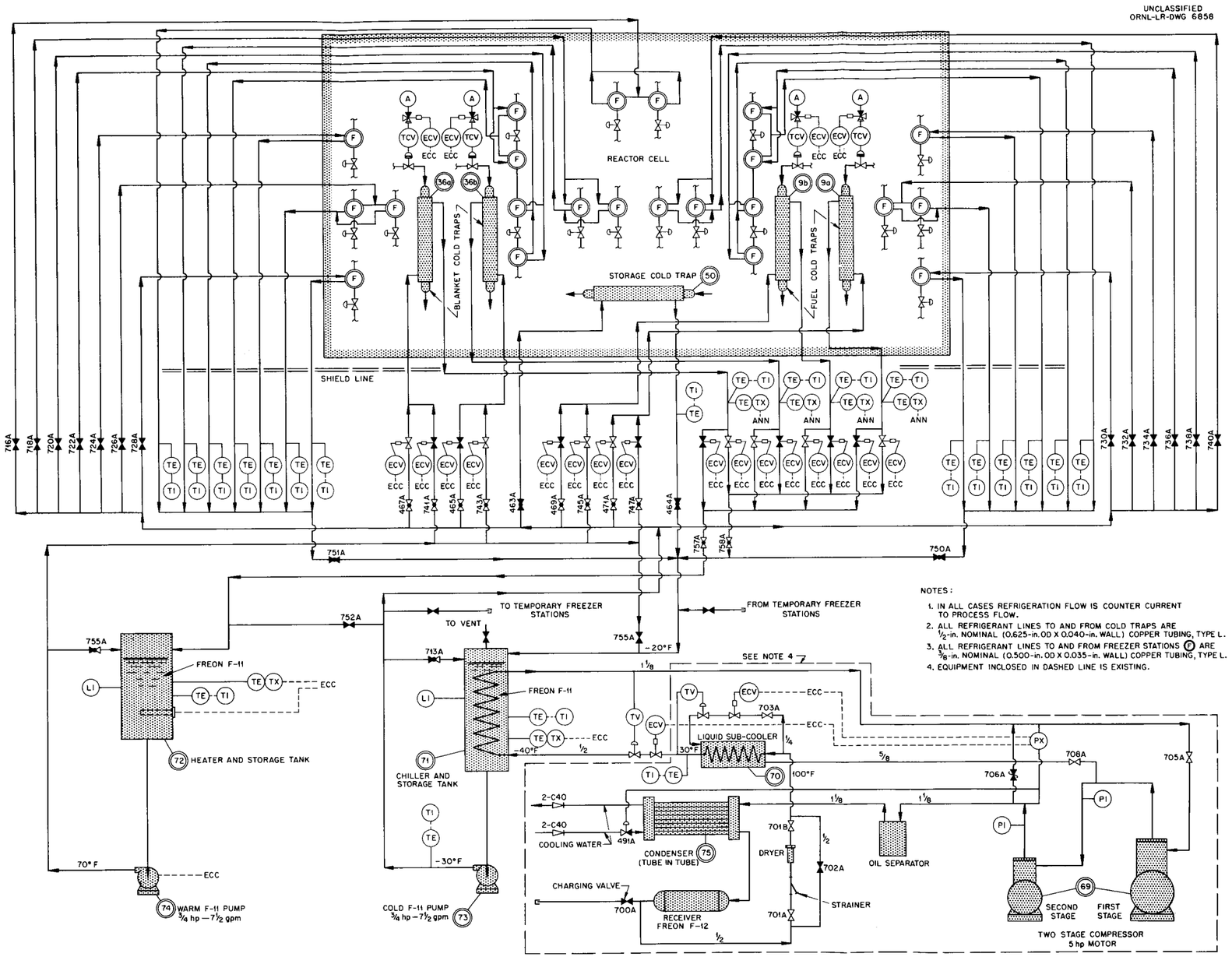

Fig. 1.5. Refrigeration and Cold-Trap System Flowsheet.

[redacted]

DWG. NO. D-18330a

NOTE: ALL PROCESS LINE INFORMATION IS FOR OPERATION AT AN OVERALL GROSS POWER OF 5220 KW.

I. LINE NUMBER NOMENCLATURE

THE LINE SCHEDULE IS DIVIDED INTO FIVE SECTIONS AS FOLLOWS·

1. PROCESS PIPING

   A) FUEL SYSTEM - LINES 100-199 INCLUSIVE

   INCLUDES ALL LINES NORMALLY CARRYING FUEL SOLUTIONS; OVERFLOW, VAPOR AND CONDENSATE, TRANSFER AND SAMPLE LINES.

   B) BLANKET SYSTEM - LINES 200-299 INCLUSIVE

   INCLUDES ALL LINES NORMALLY CARRYING BLANKET SOLUTION; OVERFLOW, VAPOR AND CONDENSATE, TRANSFER, AND SAMPLE LINES.

2. STEAM PIPING

   LINES 300-399 INCLUSIVE.

   INCLUDES ALL LINES CARRYING STEAM OR CONDENSATE, AND FEEDWATER SYSTEM.

3. SERVICE PIPING

   LINES 400-574; 601-674; 701-949; INCLUSIVE.

   INCLUDES ALL STEAM, WATER, VENT, COOLING WATER, AND REFRIGERANT LINES.

4. PROCESS INSTRUMENT PIPING

   LINES 575-600 INCLUSIVE.
   675-700 INCLUSIVE. } SHOWN IN BOX 575

5. LEAK DETECTION SYSTEM

   LINES 950-

IA. INSTRUMENT NUMBERING CODE

1. INSTRUMENT PROCESS DIVISIONS

100-199	FUEL HIGH PRESSURE
200-299	BLANKET HIGH PRESSURE
300-399	FUEL LOW PRESSURE
400-499	BLANKET LOW PRESSURE
500-699	STEAM POWER
700-799	OFF GAS
800-899	UTILITIES
900-999	MISCELLANEOUS

2.

2nd AND 3rd DIGITS	FUNDAMENTAL VARIABLE	MULTIPURPOSE NUMBERS
00-04	ANALYSIS	0000-0400
05-14	ELECTRIC	0500-1400
15-34	FLOW	1500-3400
35-44	HAND	3500-4400
45-49	LEVEL	4500-4900
50-59	PRESSURE	5000-5900
60-64	RADIATION	6000-6400
65-94	TEMPERATURE	6500-9400
95-99	WEIGHT	9500-9900

II. LINE IDENTIFICATION

LINE NUMBERS 183

SHIELD LINE . . . . . .

PRIMARY PROCESS LIQUID LINE . . . . . .

SECONDARY PROCESS LIQUID LINE . . . . . .

PRIMARY PROCESS GAS OR VAPOR LINE . . . . . .

SECONDARY PROCESS GAS OR VAPOR LINE . . . . . .

STEAM LINE . . . . . .

AIR LINE . . . . . .

ELECTRICAL LINE. . . . . .

OXYGEN . . . . . .

NITROGEN . . . . . .

III. PIPE LINE CODE

TYPICAL CODE ON LINE

1-1/2'' SCH. 80 CARBON STEEL PIPE. 1-1/2 C80

1'' SCH. 40 STAINLESS STEEL PIPE . . . . . 1 S40 OR 1-40

1/2'' SCH. 40 WROUGHT IRON PIPE 1/2 W40

1'' SCH. 80 GALVANIZED PIPE. 1 G80

IV. GENERAL LEGEND

CONDENSATE DRAIN . . . . . CD

COOLING WATER . . . . . CW

COOLING WATER DRAIN . . . . . CWD

(X - BELOW AIR OPERATED VALVE) - FAILS CLOSED - . .

(O - BELOW AIR OPERATED VALVE) - FAILS OPEN - . .

EXAMPLE:

PC-452

P C - 4 5 2

- FUNDAMENTAL VARIABLE ALLOCATION NUMBERS
- PROCESS DIVISION NUMBER
- INSTRUMENT CLASSIFICATION LETTER(S)
- FUNDAMENTAL VARIABLE CLASSIFICATION LETTER

V. VALVE AND FITTING SYMBOLS

SAFETY OR RELIEF VALVE, ... OR

MANUALLY OPERATED VALVE. . . . . .

CHECK VALVE . . . . . .

AIR OPERATED VALVE (COMMERCIAL DIAPHRAGM) . . . .

AIR OPERATED VALVE (REMOTELY OPERATED IN RADIATION FIELD) . . . . . .

AIR OPERATED VALVE WITH POSITIONER . . . . . .

MANUALLY OPERATED EXTENSION HANDLE VALVE. . . .

GATE VALVE . . . . . .

GLOBE VALVE . . . . . .

VALVE NORMALLY CLOSED. . . . . .

VALVE NORMALLY OPEN . . . . . .

VALVE THROTTLING . . . . . .

SOLENOID VALVE. . . . . .

MECH. COUPLING . . . . . .

REDUCING COUPLING (SCREWED) . . . . . .

REDUCING COUPLING (WELDED) . . . . . .

FLOW RESTRICTOR . . . . . .

FLANGED JOINT . . . . . .

UNION (THREADED). . . . . .

LOAD CELL . . . . . .

STRAINER. . . . . OR S

TRAP . . . . . T OR T

FREEZER STATION POSITION . . . . . F

PERMANENT FREEZER STATION . . . . . F

RUPTURE DISC . . . . . .

CALORIMETER CONNECTION C

VALVE (3-WAY) WITH NORMALLY BLOCKED PORT . . . . . .

VALVE (3-WAY) WITH COMMON PORT . . . . . .

VI. INSTRUMENTATION AND MISC. SYMBOLS

EQUIPMENT NO. 6

(WHEN SHOWN ON AIR OPERATED VALVES) 3 15

FIGURE TO LEFT INDICATES LOWER AIR OPER. PRESSURE

FIGURE TO RIGHT INDICATES UPPER AIR OPER. PRESSURE

INSTRUMENTS WITH SINGLE FUNCTION:

LOCALLY MOUNTED. . . . . .

TURBINE PANEL MOUNTED. . . . . .

INTERMEDIATE MOUNTED . . . . . .

CONTROL PANEL MOUNTED. . . . . .

AUXILIARY MOUNTED . . . . . .

TRANSMITTER . . . . . .

INSTRUMENTS WITH DUAL FUNCTIONS OR INSTRUMENTS WITH CLOSE MECH. COUPLING . . . . .

INSTRUMENT NOT COVERED IN CODE . . . . . .

LEADS TO ELECTRICAL CONTROL CIRCUIT . . . . . ECC

LEADS TO ANNUNCIATOR . . . . . ANN

INLINE INSTRUMENT . . . . . .

VII. INSTRUMENT CLASSIFICATION CODE

(MEANING OF LETTERS APPEARING IN INST. BALLOONS)

	FIRST LETTER	ANNUNCIATOR	PRIMARY ELEMENT	CONTROLLER	INDICATOR	AMPLIFIER, BOOSTER, RELAY - MODIFIER	RECORDER	TRANSMITTER - TRANSDUCER	SWITCH	RECORDER - CONTROLLER	INDICATOR - CONTROLLER	REMOTE OPERATED VALVE	SELF OR MANUAL OPERATED VALVE	SAFETY VALVE
2ND-3RD LETTER		A	E	C	I	M	R	T	X	RC	IC	CV	V	SV
ANALYSIS	A	AA	AE	AC	AI	AM	AR	AT	AX	ARC	AIC	ACV		ASV
ELECTRIC	E	EA	EE	EC	EI	EM	ER	ET	EX	ERC	EIC	ECV	EV	ESV
FLOW	F	FA	FE	FC	FI	FM	FR	FT	FX	FRC	FIC	FCV	FV	FSV
HAND	H	HA		HC		HM			HX		HIC	HCV	HV	
LEVEL	L	LA	LE	LC	LI	LM	LR	LT	LX	LRC	LIC	LCV	LV	LSV
PRESSURE	P	PA	PE	PC	PI	PM	PR	PT	PX	PRC	PIC	PCV	PV	PSV
RADIATION	R	RA	RE	RC	RI	RM	RR	RT	RX	RRC	RIC	RCV		
SPEED	S	SA	SE	SC	SI	SM	SR	ST	SX	SRC	SIC	SCV		
TEMPERATURE	T	TA	TE	TC	TI	TM	TR	TT	TX	TRC	TIC	TCV	TV	TSV
WEIGHT	W	WA	WE	WC	WI	WM	WR	WT	WX	WRC	WIC	WCV		
SPECIAL	X	XA	XE	XC	XI	XM	XR	XT	XX	XRC	XIC	XCV	XV	XSV

THE FOLLOWING SUBSCRIPTS MAY BE APPLIED TO THE FIRST LETTER.

a - AVERAGE
c - CONDUCTIVITY
d - DIFFERENTIAL
f - FREQUENCY
g - SPECIFIC GRAVITY
i - CURRENT
m - MOISTURE
pf - POWER FACTOR
pH - CONCENTRATION
t - TIME
v - VOLTS
w - WATTS

Fig. 1.6. Flowsheet Identification Code.

TABLE 1.2. HRT EQUIPMENT SCHEDULE

Item No.	Name	Item No.	Name
1	Core	28	Blanket circulating pump
2	Fuel pressurizer	29	Blanket pressurizer
3	Fuel gas separator	30	Blanket gas separator
4	Fuel heat exchanger	31	Blanket heat exchanger
5	Fuel circulating pump	32	Pressure vessel
6	Fuel dump cooler	33	Blanket dump cooler
7a	Fuel dump tank and evaporator	34a	Blanket dump tank and evaporator
7b	Fuel dump tank and evaporator	34b	Blanket dump tank and evaporator
7c	Entrainment separator	34c	Entrainment separator
8	Fuel recombiner-condenser	35	Blanket recombiner-condenser
8a	Fuel recombiner	35a	Blanket recombiner
9a	Fuel cold trap	36a	Blanket cold trap
9b	Fuel cold trap	36b	Blanket cold trap
10a	Fission-product adsorber	37	Blanket condensate tank
10b	Fission-product adsorber	38	High-pressure blanket sample station
10c	Fission-product adsorber	39	Blanket reflux condenser
11	Off-gas vacuum pump	40	Blanket feed cooler
12	Stack filter	41	Blanket feed pump
13	Stack	42	Blanket transfer tank
13a	Stack fan	43	Blanket-sample cooler
14	Fuel condensate tank	44	Blanket-sample station
15	Reflux condenser	45	Blanket letdown heat exchanger
16a	Fuel storage tank and evaporator	46	Blanket gas cooler
16b	Fuel storage tank and evaporator	47	Future compressor
17	Fuel feed cooler	48	Future blanket purge pump cooler
18	Fuel sample station	49a	Blanket storage tank and evaporator
19	Fuel transfer tank	49b	Blanket storage tank and evaporator
20	Fuel letdown heat exchanger	50	Storage cold trap
21	Fuel feed pump	51	Fuel storage recombiner
22	Holdup tank	52	Blanket storage recombiner
23	Purge pump	53	Fuel steam drum
24	Fuel-sample cooler	54	Blanket steam drum
25	High-pressure fuel-sample station	55	Steam calorimeter
26	Fuel oxygen supply	56	Steam separator
27	Fuel gas cooler	57	Steam turbine

TABLE 1.2 (continued)

Item No.	Name	Item No.	Name
58	Generator	80b	Waste evaporator
59	Steam condenser	81	Decontamination system
60	Auxiliary steam condenser	82a	Space cooler
61	Cooling tower	82b	Space cooler
62	Cooling-tower pump	82c	Space cooler
63	Hotwell pump	82d	Space cooler
64	Deaerator and feedwater storage tank	83	Freezers
65a	Feedwater pump	84	Corrosion-sample retainers and corrosion-study facilities
65b	Feedwater pump	85	Saurce tube and thimble
66	Packaged boiler system	86	Handling tools
67a	Oxygen accumulator	87	Leak-detector system
67b	Oxygen accumulator	88a	Feedwater accumulator
68	Purge pump cooler	88b	Feedwater accumulator
69	Refrigerant compressor	89a	Chemical vent vacuum pump
70	Refrigerant subcooler	89b	Reactor vent vacuum pump
71	Chiller and storage tank	90	Waste evaporator-condenser
72	Heater and storage tank	91	Reactor-vessel cooler
73	Cold F-11 pump	92	Thermal-shield cooler
74	Warm F-11 pump	93	1000-gal waste condensate tank
75	Refrigerant condenser	94	12,000-gal waste tank
76	High-pressure fuel loop piping	95	Waste pond
77	High-pressure blanket loop piping	96	Off-gas filter
78	High-pressure valves and fittings	97	Thermal insulation (in cell)
79	Low-pressure piping, valves, and fittings	98	Reactor blast shield
80a	Waste evaporator	99	Dewatering pump

the reactor and chemical processing systems, including water used for shielding purposes. This system includes pumps for removing high-level-activity fluids from the cells to a waste storage tank, evaporators and condensers for concentrating wastes, and a means of discharging decontaminated wastes to the creek. Gases vented from cell equipment are pumped into charcoal beds before being discharged through the stack.

The refrigeration and cold-trap system, Fig. 1.5, provides cooling for the cold traps, which freeze moisture out of all effluent gas from the reactor, and for freeze plugs, which are used to close off lines in case of valve failures or during disconnection of equipment at flanged joints. The system consists of a two-stage compressor system cooling a circulating stream of liquid Freon F-11. The liquid F-11 is pumped into a manifold which is connected to the cold traps and freeze plugs. A similar but separate circulating stream of F-11 is

pumped through a heater and serves to thaw cold traps and freezers whenever necessary. All valves in the refrigeration system are located outside the shield.

1.2.2 Reactor Cells

The HRT cell originally was designed[7] to resist a sudden pressure rise from −7.5 to +15 psig. This design was adequate to contain a constant-internal-energy expansion of the reactor liquids into the cell, for it was believed, at that time, that this was as extreme a contingency as could be reasonably considered a design criterion.

Subsequent calculations[8] by P. M. Wood of more extreme conditions (assuming simultaneous rupture of the fuel and blanket steam systems) indicated that pressures as high as 30 psig might result from such an accident in the HRT. An investigation of the design of the cell indicated that it could not reasonably be expected to remain intact at pressures in excess of 30 psig and might possibly experience damaging deformations at pressures of about 25 psig.

It was decided to modify the design of the cell in such a manner that it would contain a pressure of 30 psig. The modifications are to be such that, at a later date, further modification can make the cell capable of containing a pressure of 50 psig and thus make it adequate for a larger reactor.

Revisions required are being made in a sequence that will minimize delay in the construction of the cell components and effect a maximum economy. These revisions can be summarized:

1. Roof plugs. – The design of the upper layer of concrete roof plugs, which must resist internal pressure, was revised by the addition of more reinforcing steel before bids were requested. Because no later modification would be possible, the plugs were redesigned to resist a pressure of 50 psig. These plugs are now being fabricated.

2. Column bases. – The column bases are being anchored to the concrete base slab by a series of toggle bolts inserted through holes core-drilled in the slab. These anchorages are now being installed.

3. Roof girders. – The design of the roof girders is now being reworked to withstand a pressure of 50 psig. This revision is 90% completed.

4. North wall. – Five methods of reinforcing the wall between the cell and the control area to resist higher pressures have been investigated. It is presently proposed to test the cell to elevated pressures before deciding what, if any, revision is to be made in this area. These tests would be made after the roof structure is in place and the cell is sealed.

A general study of the remainder of the cell, with attention to specific points of local weakness, is being continued.

1.2.3 Core Vessel

A photograph of the completed core vessel is shown in Fig. 1.7. The core tank is ready for installation in the pressure vessel. After the fabrication was completed, the vessel was tested hydrostatically at an internal pressure of 775 psi to produce a stress of 20,000 psi in the wall. The hydrostatic test consisted in subjecting the vessel to the 775-psi internal pressure three times. The last time, the pressure was held for 1 hr. During the test a stethoscope and a contact microphone were used on the outside of the vessel to listen for possible failures of perforated-plate attachment welds. No failures were detected.

In an experiment prior to the hydrostatic test, it was found that the stress in the ligaments of the perforated diffuser plates was related to the test pressure by $\sigma_r = 10P$ and that the tangential stresses in the vessel wall were related to the pressure by $\sigma_t = 11P$. Since the ligament stresses in the perforated plates were somewhat less than the membrane stresses in the vessel wall, no failures were expected during the hydrostatic tests.

Following the hydrostatic tests the vessel was tested for leaks; Freon at 25 psi was used inside, and the outside surface was probed with the G-E type H halide leak detector. No leaks were found.

1.2.4 Reactor Blast Shield and Cooling Coils

Radiation effects increase the notch-brittle susceptibility transition temperature of carbon steel,[9] so there is a remote possibility that the HRT reactor vessel will fail by brittle fracture. Estimates of the probable effects of brittle fracture of the HRT pressure vessel[10] indicate that a fragment

[7] R. B. Briggs *et al.*, *HRP Quar. Prog. Rep. July 31, 1954*, ORNL-1772, p 15.

[8] P. M. Wood, *A Further Study of Pressure Rise in HRT Shield*, ORNL CF-55-1-3 (Jan. 3, 1955).

[9] E. C. Miller, *Possibility of Brittle Pressure Vessel Failure*, ORNL CF-54-4-112 (April 16, 1954).

[10] P. M. Wood, *A Study of Possible Blast Effects from HRT Pressure Vessel Rupture*, ORNL CF-54-12-100 (Dec. 14, 1954).

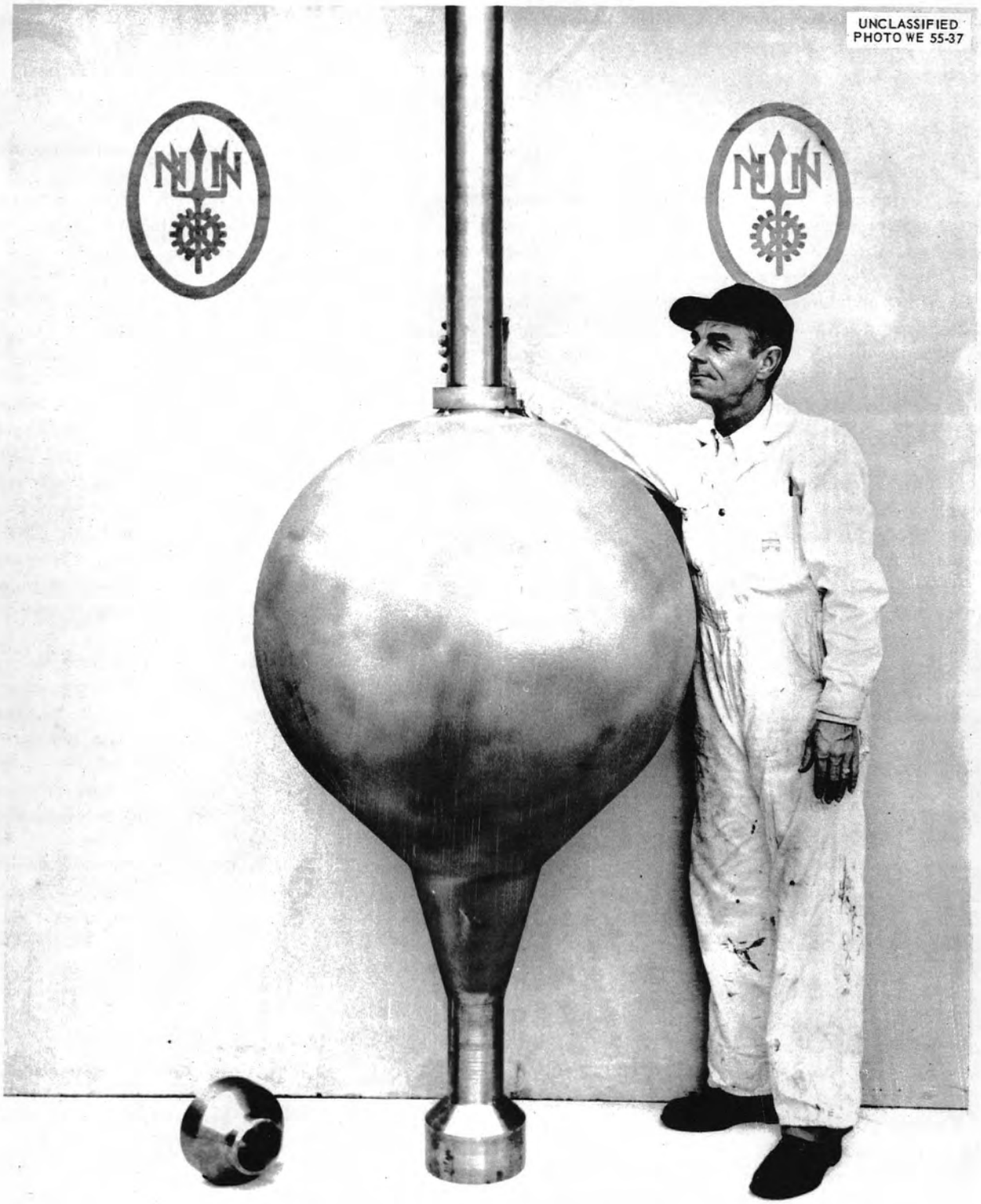

Fig. 1.7. Completed HRT Core Vessel.

of the vessel weighing as much as 1400 lb could break the restraints on the top shield plugs and thus cause leakage of radioactive materials. As protection against this hazard, a blast shield of austenitic stainless steel (type 304) is to be placed around the outside of the pressure vessel as shown in Fig. 1.8. Austenitic steels are believed to retain a substantial portion of their ductility during irradiation, although their strength and hardness are increased.[11] The shield will be 1½ in. thick and will be separated from the pressure vessel by an annulus of air 1 to 2 in. thick.

Attached to the top of the blast shield is a restraining ring to prevent the top flange assembly from being projected against the cell cover plugs if the pressure vessel ruptures. The other nozzle assemblies are not restrained, since their mass is too small to cause serious damage to the cell structure if a failure occurs.

Provisions have been made for eight thermocouples to be attached to the pressure vessel through openings in the blast shield. Also, several openings are available through which wet steam may be admitted between the blast shield and pressure vessel in case more rapid cooling is desired after reactor shutdown (see below).

Results of thermal-stress analysis of the HRT pressure vessel were reported previously.[12] It was shown that minimum total stress occurs when the outer surface of the vessel is cooled to the same temperature as the inner surface of the carbon steel. Heat-removal rates required to produce this condition at reactor power levels of 5 and 10 Mw are as follows: At 5 Mw,

$$\frac{q}{A} \cong 1000 \text{ Btu/hr}\cdot\text{ft}^2 , \qquad \sigma_t = 13{,}700 \text{ psi};$$

at 10 Mw,

$$\frac{q}{A} \cong 2000 \text{ Btu/hr}\cdot\text{ft}^2 , \qquad \sigma_t = 14{,}700 \text{ psi},$$

where q/A is the rate of heat removal from the outside surface and σ_t is the total tangential stress in the pressure-vessel wall.

These stresses increase to 15,900 and 19,200 psi for 5- and 10-Mw operation, respectively, with no exterior cooling of the pressure vessel. Results of calculations relating the maximum tangential stresses to the rate of heat removal from the outside surface of the pressure vessel are shown in Fig. 1.9.

The pressure vessel is to be cooled by radiating heat to the blast shield. The blast shield is cooled by water (at approximately 100°F) passing through ½-in. schedule-80 coils welded on its outside surface. There are 18 coils, each about 14 ft long and 6 in. apart, and they form a spiral around the spherical blast shield.

During operation the heat removal from the outside surface of the pressure vessel is about 1700 Btu/hr·ft^2. Figure 1.9 shows that the total stress in the pressure vessel is about 15,000 psi at both the 5- and 10-Mw power levels.

Figure 1.10 presents an estimate of the temperature distribution for the blast shield when it is cooled by coils on the outside surface. Since the heat is transferred from the pressure vessel to the blast shield by radiation, rather than by conduction, the temperature variation of the blast shield causes only small fluctuations (approximately 100 psi in 15,000 psi) in the total stress of the pressure-vessel wall.

When the reactor contents are dumped, the solutions are released to atmospheric pressure and consequently cooled to below 212°F. Before this solution can be pumped back into the system, the pressure vessel should be cooled to within 100°F of the temperature of the returning liquid. If cooling of the vessel is accomplished by means of the blast-shield cooling coils alone, then the cooling times given[13] in Table 1.3 will apply.

[11] J. C. Wilson, *Radiation Effects in Pressure Vessel Materials and Welds*, ORNL CF-54-10-102 (Nov. 15, 1954).

[12] R. B. Briggs *et al.*, *HRP Quar. Prog. Rep. Jan. 31, 1955*, ORNL-1853, Fig. 1.3, p 10.

[13] R. E. Aven, *Heat Removal Systems for the HRT Pressure Vessel*, ORNL CF-55-3-119 (March 14, 1955).

TABLE 1.3. COOLING TIMES AFTER A DUMPING OPERATION

T_θ (°F)	Times Required to Cool Pressure Vessel from 600°F to T_θ (hr)
600	0
500	1.87
400	4.83
300	9.84
260	13.00
240	15.00
200	20.4

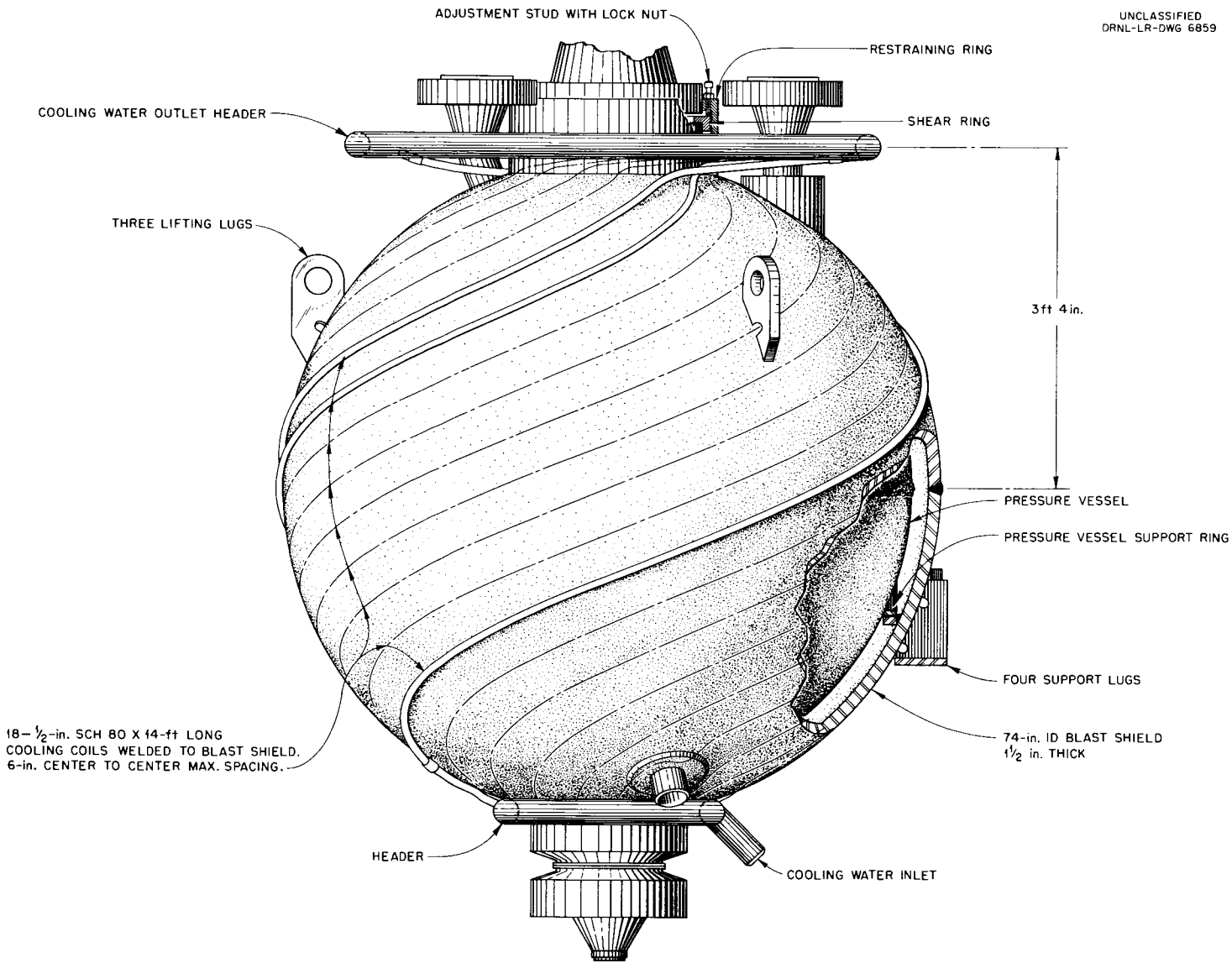

Fig. 1.8. Blast Shield and Cooling Coils.

The cooling times indicated in Table 1.3 are long and the thermal stress is small because of the slow rate of cooling. However, additional cooling may be provided after a dump, in order to get the reactor started again in as short a time as possible. This additional cooling could be accomplished by fitting steam jets at various points around the pressure vessel, so that a stream of wet steam could be sprayed directly on the vessel. The fittings could be placed in the blast shield in such a manner that the spray covers the greatest possible pressure-vessel surface. Approximately ten nozzles with a flow rate of 10 lb/min per nozzle of 95% quality steam would give cooling sufficient to reduce the cooling time to 2 to 4 hr.

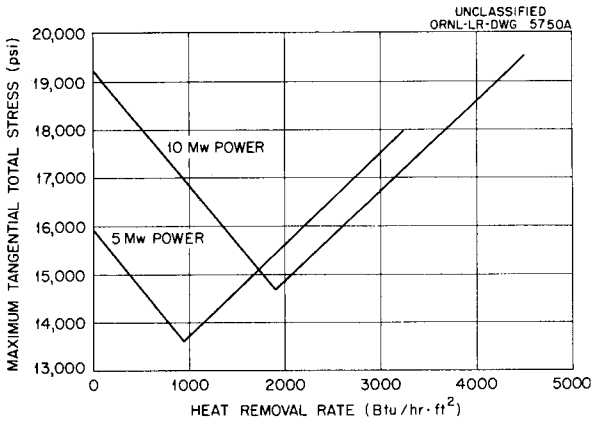

Fig. 1.9. Maximum Tangential Stress in Pressure-Vessel Wall vs Heat Removal Rate from Outside Surface.

Thermal-stress and temperature-distribution calculations have been made in order to aid in specifying reasonable rates of heating and cooling of the pressure vessel.[14] Figure 1.11 has been prepared to show the relation between the maximum thermal stress, the rate of change of surfoce temperature, and the difference in temperature between the inner

[14] R. E. Aven, *Thermal Stress in the HRT Pressure Vessel*, ORNL CF-55-2-128 (Feb. 21, 1955).

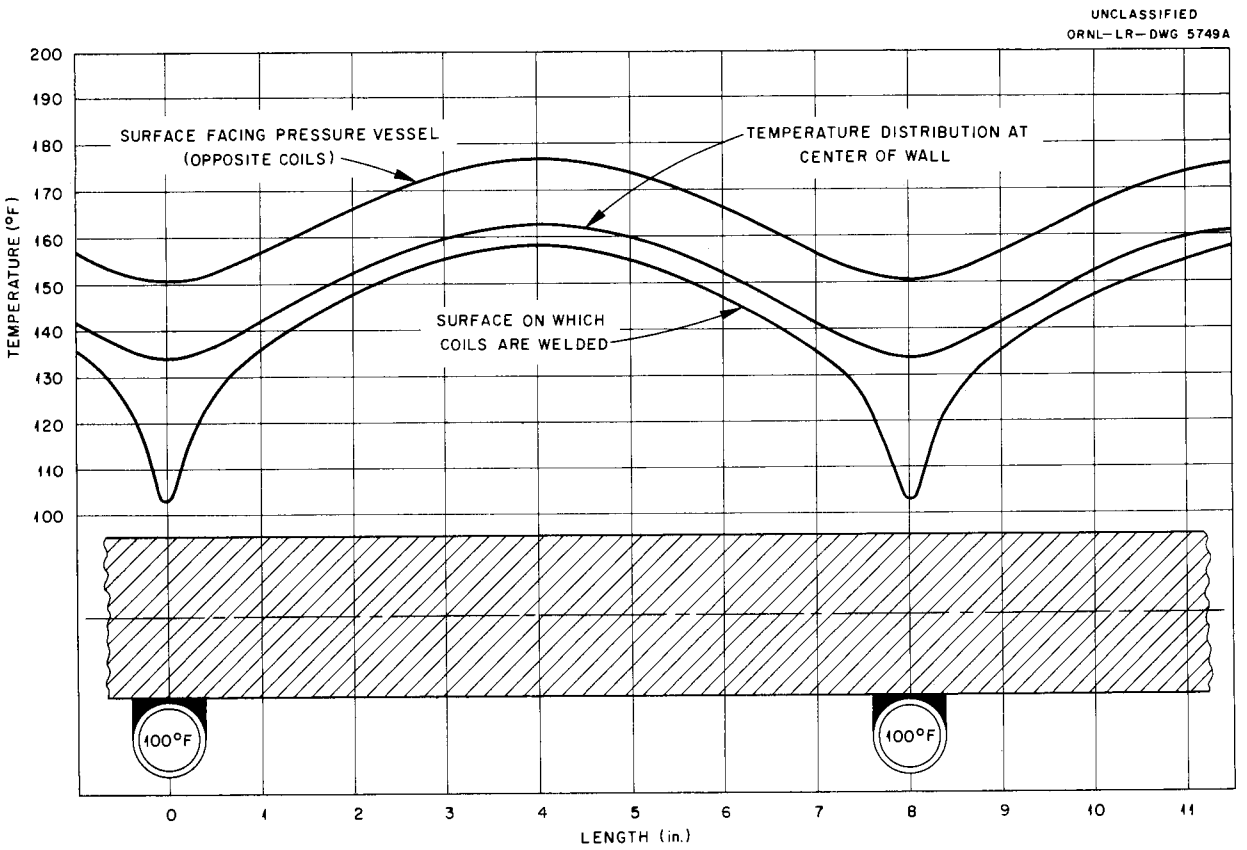

Fig. 1.10. Temperature Distribution in Blast Shield for Heat Removal Rate of 2000 Btu/hr·ft².

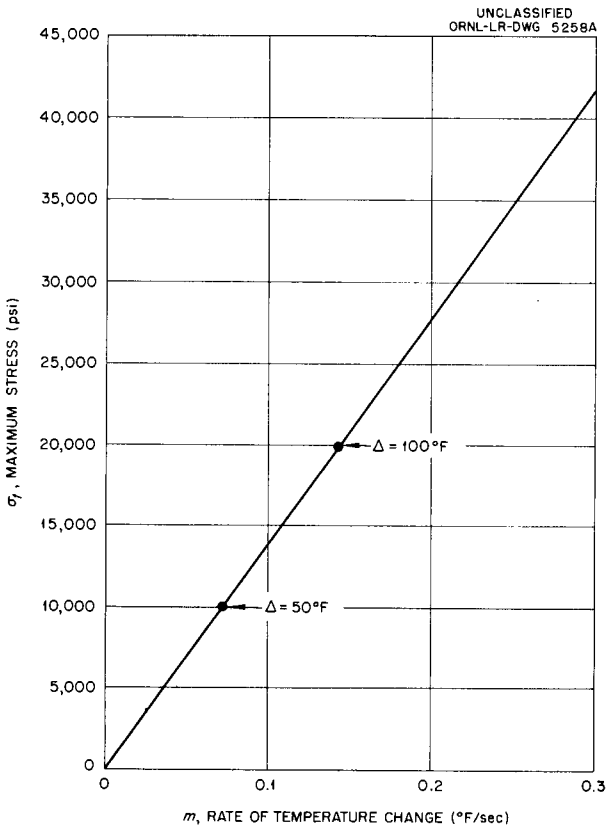

Fig. 1.11. Maximum Thermal Stress in Pressure-Vessel Wall vs Surface Heating or Cooling.

and outer surfaces of the vessel. Safe heating and cooling times have been estimated to be the following:

1. For cooling after shutdown (with no internal pressure), a cooling time of approximately 1.6 hr will keep σ_t (thermal) $\leqq$ 10,000 psi.
2. For heating during startup (with maximum internal system pressure of 2000 psi), a heating time of about 3.2 hr will keep σ_t (thermal) $\leqq$ 5000 psi.

To include a safety factor, the following times have been specified: cooling time after a dump, $\geqq$2 hr; heating time during startup, $\geqq 3\frac{1}{2}$ hr.

1.2.5 Fuel Low-Pressure Assembly

Drawings of the fuel low-pressure assembly have been approved, and it is under construction. This assembly, shown in Fig. 1.12, consists of the following (the item numbers refer to the flowsheet, Fig. 1.1):

1. inner dump tanks with their attached evaporator legs,
2. entrainment separator, item 7c,
3. recombiner and condenser, items 8a and 8,
4. cold traps, items 9a and 9b,
5. condensate tank, item 14,
6. two weigh-beam assemblies, one for the dump tanks and one for the condensate tank,
7. necessary piping for interconnecting these units and for connection to external points of attachment,
8. valves for the dump line and the feed-pump suction line,
9. framework, pipe anchors, and hangers for supporting this equipment.

A unique feature of the assembly is the provision for taking inventory by weighing the contents of the condensate and dump tanks. These tanks are supported on hangers suspended from the ends of weigh beams. There is one weigh-beam assembly for the dump tanks and one for the condensate tank. Two beams in each assembly are pivoted near their centers and are connected through a link near the center of the weigh-beam assembly to transmit the resulting force upward against a pneumatic load cell. The load cell is connected through air piping to instrumentation outside the reactor cell, where actual load measurements are taken.

The geometry of the weighing system was dictated by the need to mount the weigh cells on top, where they could be removed for maintenance. It was decided to use weigh beams operating against a single pneumatic weigh cell, rather than a cell at each end of the tanks to carry the load directly. This eliminates one cell per weigh system and its necessary instrumentation. A dual-cell system would also have required extra instrumentation to sum the signals from the two cells and would have introduced additional errors. The weigh-beam system promises to be less expensive and more accurate than the dual-cell system.

In order to obtain a reasonably accurate inventory of the contents of the condensate and dump tanks, the piping connections to these tanks must be flexible to compensate for the varying loads which result from thermal expansions and shifting of the structure.[15,16] The entire weighing system is built into a rigid framework within which the tanks are suspended on long rods. The piping associated with the components is kept flexible by confining

[15] R. G. Pitkin, *Inner Dump Tanks, Their Piping and Supports*, ORNL CF-54-8-167 (Aug. 17, 1954).

[16] R. G. Pitkin, *Inner Dump Tank Piping and Weighing System*, ORNL CF-54-10-63 (Oct. 13, 1954).

UNCLASSIFIED
ORNL-LR-DWG 6860

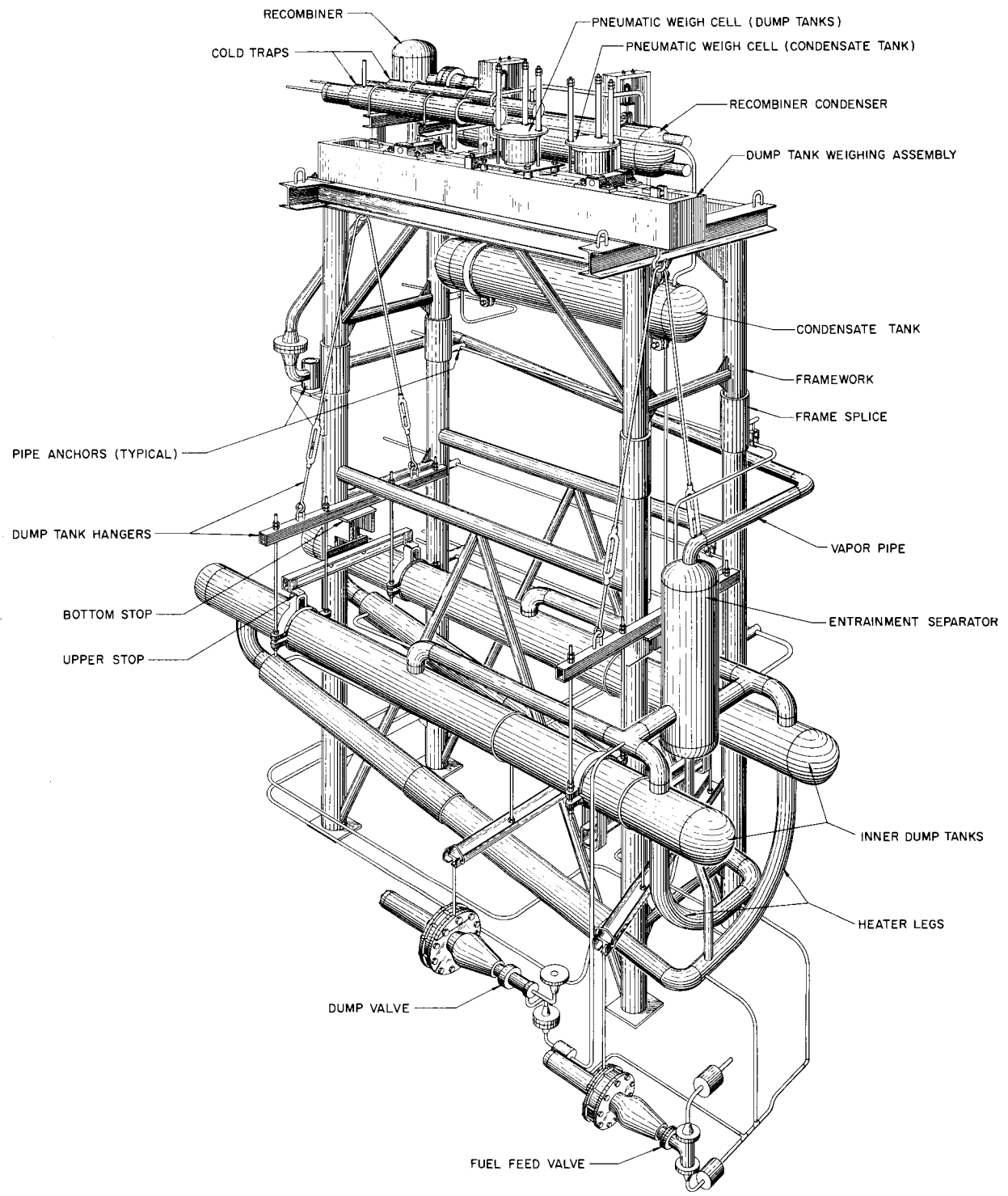

Fig. 1.12. Fuel Low-Pressure Assembly.

the piping runs to horizontal planes with anchor points on the rigid frame. This confines the pipe expansions within these planes, thus minimizing vertical thrusts which would enter into the weight measurement. The 3-in. vapor line connecting the entrainment separator to the recombiner is the least flexible pipe in the system and will act to establish the position of the dump tanks in the horizontal plane.

The total effect of thermal expansions has been calculated to be 1.0 lb, which is very small compared with the inventory of approximately 2000 lb of solution.

The weigh-beam assemblies each consist of a box frame within which a pair of beams are pivoted on Stellite knife edges. Stellite was chosen because of its hardness and resistance to corrosion. Knife-edge loading is limited to 4000 lb/in., whereas commercial practice allows up to 6000 lb/in. The mechanical accuracy of the weigh-beam system should compare with that of commercial platform scales. A total error, based on live load, of ±3.1 lb is expected.

1.2.6 Fuel and Blanket Feed-Pump Installations

A feed-pump installation design is shown in Fig. 1.13. There are two units for the core system and two for the blanket. Each pumping head has three pipe connections with flanged joints arranged for remote dismantling. Flange bolting is accomplished by means of long rods which pass through the shield. After the flanges are unbolted, the supporting carriage may be rolled back to disengage the flanges and then lifted from the cell with the crane hook. When the unit is being replaced, guides on the fixed platform serve to position the carriage on the tracks and thus align the flanges.

The process-solution inlet and outlet pipes are completely inside the cell. The only lines which pass through the shielding are the hydraulic-actuator lines connected to the pulsator unit outside.

1.2.7 Pressurizer Pressure-Balancing System

The pressurizer pressure-balancing system will prevent, by mechanical means, excessive pressure differences between the core and pressure vessels. This system is to be used in addition to the instrument control of differential pressure. Study drawings of various piping arrangements for the pressure-balancing and venting systems have been made, but a final design will await the completion of more urgent work. This system will incorporate two relief valves and two rupture discs into a single removable piping assembly, which will cost about $3000.

The pressure-balancing valves will be set to open when the differential pressure between pressurizers exceeds 75 psi. They are nominal 1½-in. valves of all-welded construction with type 347 stainless steel bodies, type 446 stainless steel plugs, and springs made of type 304 stainless steel.

An order for three pressure-balancing valves, one of which will be a prototype for testing, has been placed with the Associated Valve & Engineering Co. Delivery of the prototype valve is expected during May.

One rupture disc is designed to rupture in case the blanket pressure exceeds the core pressure by more than 200 ± 40 psi. It has a back-pressure support rated at 400 psi. Its diameter is 1½ in. The assembly will be mounted between the flat faces of two specially machined flanges which can be bolted into standard 2500-psi ring-joint flanges.

The other rupture disc is designed to rupture if the core pressure exceeds the blanket pressure by more than 400 ± 50 psi. It has a back-pressure support rated at 200 psi, and its diameter is 1 in.

The rupture-disc assemblies have been ordered from the Fike Metal Products Company, and delivery is expected by June 1.

1.3 REACTOR ANALYSIS

P. R. Kasten

H. C. Claiborne
L. Dresner
T. B. Fowler
M. K. Hullings
L. C. Noderer
M. Tobias

1.3.1 HRT Safety Calculations

An extensive survey has been performed with regard to the safety of the HRT with various blanket materials. Inasmuch as the essential effect of various blanket materials is to change the average lifetime of prompt neutrons, Oracle calculations were preformed in which the lifetime was varied from 5.7×10^{-4} to 1.1×10^{-4} sec. The Oracle results are given in graphical form in Fig. 1.14 as maximum pressure rise, p_{max}, vs m_e for different values of τ, the prompt-neutron lifetime. Since $m_e \equiv \Delta k_{eqp}/\tau$, where Δk_{eqp} is the equivalent prompt reactivity addition, Fig. 1.14 shows, in effect, the relations between p_{max} and Δk_{eqp} for the

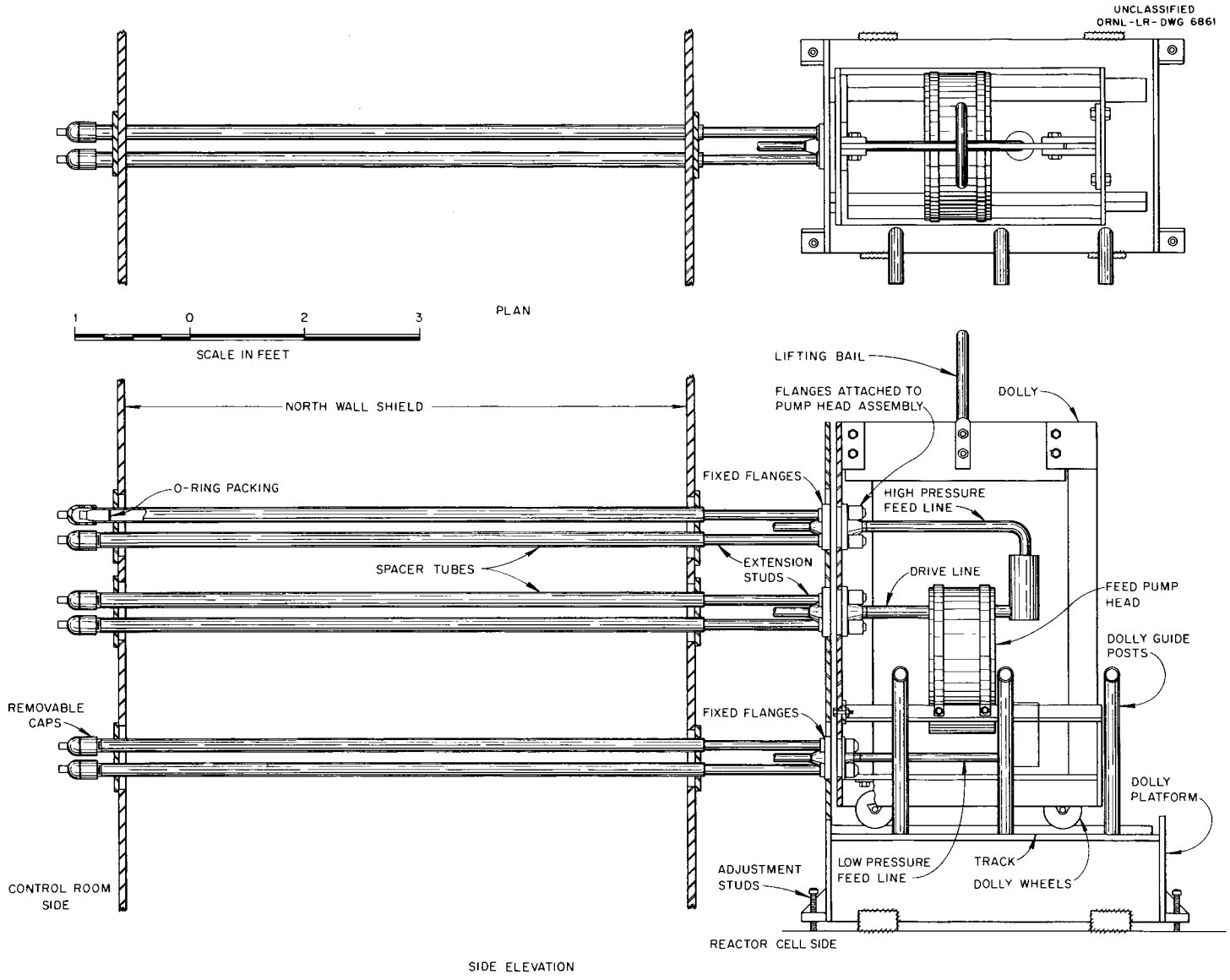

Fig. 1.13. Feed Pump Installation.

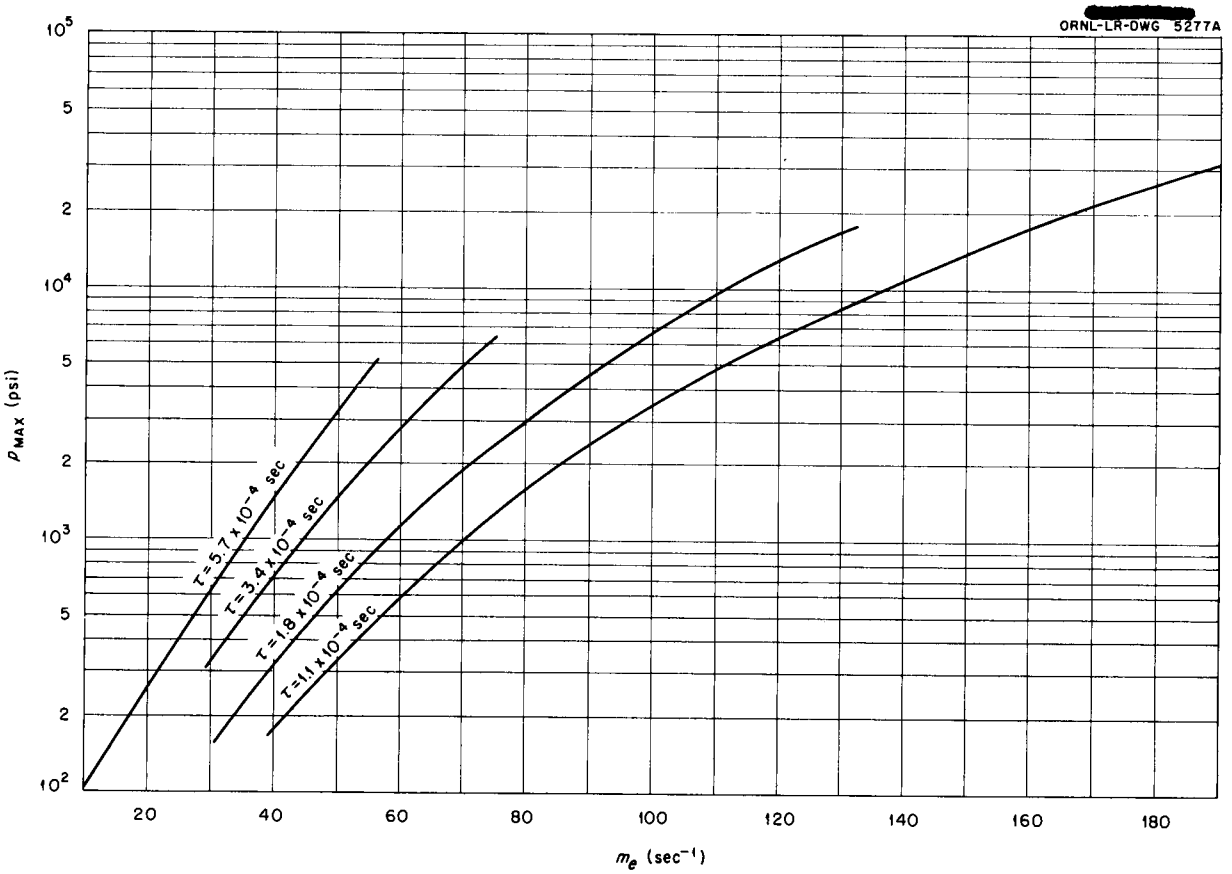

Fig. 1.14. HRT Core Pressure Rise vs Reactivity Addition for Various Prompt-Neutron Lifetimes.

different values of τ. The associated parameter values are those of the HRT and are given elsewhere.[17] The value of τ varies with the blanket material as follows:

τ (sec $\times 10^4$)	Blanket
5.7	D_2O
3.4	UO_2SO_4-D_2O solution (355 g of U per kg of D_2O)
1.8	ThO_2-D_2O (633 g of Th per kg of D_2O)
1.1	ThO_2-D_2O (1349 g of Th per kg of D_2O)

The above values pertain to operation at 280°C and 2000 psi.

The value of m_e is dependent, in a known manner, upon the initial reactor conditions and the rate of reactivity addition, as illustrated previously.[18] It is thus possible with the results of Fig. 1.14 to relate a specified pressure rise to the associated rate of reactivity as a function of τ. Figure 1.15 summarizes the relations obtained between the rate of reactivity addition, b, and τ for a specified core-pressure rise. In Fig. 1.15, $k_e(0)$ is the initial value for the effective multiplication constant, and P_0 is the initial neutron power level. As shown, the allowable rate of reactivity addition for a given p_{max} and initial conditions is relatively independent of τ, although the corresponding Δk_{eqp} is very dependent. The results state that reactors with shorter lifetime come up to power faster and do not

[17] P. R. Kasten, *HRT Safety Calculations*, ORNL CF-55-2-75 (Feb. 14, 1955).

[18] M. C. Edlund *et al.*, *HRP Quar. Prog. Rep. Jan. 31, 1955*, ORNL-1853, Figs. 1.8 and 1.9, p 22–23; P. R. Kasten, *HRP Quar. Prog. Rep. Oct. 31, 1954*, ORNL-1813, p 18–23.

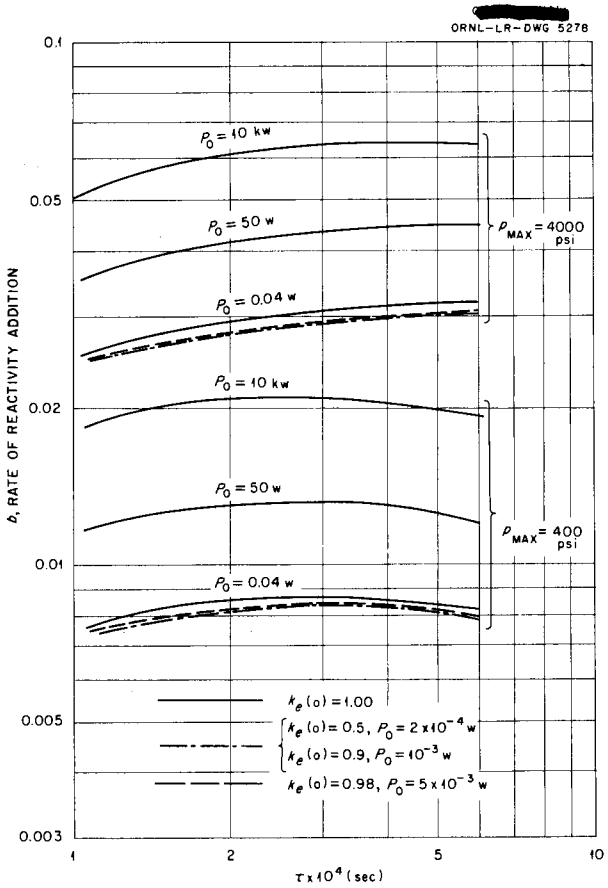

Fig. 1.15. Rate of Reactivity Addition as o Function of Lifetime of Prompt Neutrons and Initial Reactor Conditions.

allow so much reactivity to be added for a given rate of reactivity addition. For a given instantaneous reactivity addition, Fig. 1.14 indirectly shows that reactors with shorter lifetime will have the higher p_{max}, other conditions being the same. Since homogeneous reactors are to be designed on the basis of controlling the allowable rate of reactivity addition, it appears that reactors with large values of τ have only a small safety advantage over those with smaller values of τ, if rates of reactivity addition are comparable for the same operational procedure. For the lower pressure rises, it appears that there is an optimum value of τ with respect to allowable reactivity rate additions.

Figure 1.15 illustrates the increase in the allowable value of b as the initial reactor fission power increases, and shows that the fission power and not the initial value of k_e is the important parameter.

1.3.2 Allowable Rate of Decrease in HRT Steam Pressure

With the reactor initially subcritical and the 400A pump running at full speed, venting the steam side of the core heat exchanger could add reactivity to the reactor at an undesirable rate. An analysis pertaining to allowable rates of steam-temperature decrease was therefore performed to aid in the design of a proper control system. The rate of reactivity addition is related to the average rate of change of reactor core temperature; so the problem is to determine the rate of core temperature change for the conditions of interest.

The core temperature, T_c, is the average fluid temperature within the core, and, so long as no heat generation exists, dT_c/dt will be given approximately by

$$(1) \quad \frac{dT_c}{dt} = C_p w S_c [T(L,t - a_1) - T(L,t - a_2)] \ ,$$

where

T_c = average temperature of fluid within core region, °C,

a_1 = time required for fluid to travel from heat-exchanger outlet to core inlet, sec,

a_2 = time required for fluid to travel from heat-exchanger outlet to core outlet, sec,

S_c = reciprocal heat capacity of core fluid, °C/Btu,

$C_p w$ = mass flow rate times heat capacity of fluid, Btu/°C·sec,

$T(L,t)$ = temperature of fluid leaving heat-exchanger outlet at time t, °C,

t = time, sec,

L = length of heat-exchanger tubes, ft.

The problem is therefore to find $T(L,t)$.

The temperature of the fuel fluid leaving the heat exchanger is a function of the average heat-transfer coefficient and flow rate of the fluid and is determined from the differential equation

$$(2) \quad -wC_p \frac{\partial T}{\partial X} - hn\pi D(T - T_s) = C_p \rho A \frac{\partial T}{\partial t}$$

where

$n\pi D$ = total perimeter of all heat-exchanger tubes, ft,

n = number of heat-exchanger tubes,
A = cross-sectional area of all heat-exchanger tubes carrying fuel fluid, ft^2,
T_s = temperatures on shell side of heat exchanger, °C,
wC_p = mass flow rate times heat capacity of fluid, Btu/°C·sec,
T = $T(X,t)$ = temperature of fuel fluid at position X and time t, °C,
X = distance from heat-exchanger inlet along a tube, ft,
h = average heat-transfer coefficient, Btu/°C·ft^2·sec,
$C_p\rho$ = heat capacity times density of fuel fluid, Btu/°C·ft^3,
t = time, sec.

If the fuel fluid and shell-side fluid are initially at the same temperature $T(0)$, and $T_s = T(0) + f(t)$,[19] where $f(t)$ is an arbitrary function of time, $T(X,t)$ is given by

$$(3)\quad T(X,t) - T(0) = \frac{a}{b}\int_0^t f(t-\omega)e^{-(a/b)\omega}\,d\omega + \sum_{n=0}^{\infty} e^{-(X+Ln)a}\int_0^t f(t-\omega)[F_d(\omega) - F_l(\omega)]\,d\omega\ ,$$

where

$$F_d(\omega) = 0 \text{ for } \omega < d,$$
$$= e^{-(a/b)(\omega-d)} \text{ for } \omega > d,$$
$$F_l(\omega) = 0 \text{ for } \omega < l,$$
$$= e^{-(a/b)(\omega-l)} \text{ for } \omega > l,$$
$$d = b(X + nL) + \tau(n+1),$$
$$l = b(X + nL) + n\tau,$$
$$a = hnDn/wC_p,\ ft^{-1},$$
$$b = C_p\rho A/wC_p = \text{reciprocal of velocity of fluid in tubes, } fps^{-1}.$$

On the assumption that $f(t) = -rt$, where r is a positive constant, it was found by means of the ORNL analogue computer that the maximum value for $|dT_c/dt|$ occurred during the second transit time. For times during the second transit time, Eq. 3 simplifies to

$$(4)\quad T(L,t) - T(0) = \frac{a}{b}\int_0^t f(t-\omega)e^{-(a/b)\omega}[1 - S_{bL}(\omega) - e^{(a/b)\tau}S_{2bL+\tau}(\omega)]\,d\omega$$

where

$$S_x(\omega) = 0 \text{ for } \omega < x,$$
$$= 1 \text{ for } \omega > x.$$

From Eqs. 1 and 4 it can be shown that if $f(t) = -rt$, any increase in $|dT_c/dt|$ is due to the step-type behavior of $T(L,t)$. Thus only the step-type behavior of $T(L,t)$ need be considered in the evaluation of $|dT_c/dt|_{max}$, leading to

$$(5)\quad \left|\frac{dT_c}{dt}\right|_{max} \leq C_p wrS_c[(a_2 - a_1) + e^{-aL}(bL - a_2 + a_1)] < r\ ,\ °C/sec\ .$$

Since the allowable rate of reactivity addition is approximately 0.005/sec at source power and the temperature coefficient of reactivity is about −0.002/°C, the allowable rate of temperature drop in the heat-exchanger fluid is approximately 2.5°C per second at 280°C. At 280°C, a drop of 1°C in saturated-water temperature corresponds to a 14-psi drop in steam pressure, so an allowable rate of core-temperature drop of 2.5°C per second would correspond to a 35-psi/sec decrease in shell-side steam pressure. In the foregoing, it is assumed, of course, that the shell side of the heat exchanger is operating under saturation conditions.

At lower initial temperatures the temperature coefficient is lower, but a given rate of pressure drop will result in a higher rate of temperature decrease. To obtain a better over-all picture of the situation, the information given in Table 1.4 was compiled.

In deriving the values shown in Table 1.4, it was assumed that the temperature coefficient of reactivity consists essentially of the density coefficient. This assumption is valid at high temperatures; however, at temperatures near 100°C, the nuclear temperature coefficient is about the same magnitude as the density coefficient. If this correction were applied, the allowable rate of pressure drop at atmospheric pressure would be roughly 24 psi/sec. Obviously, such a rate could not exist for any appreciable period of time, since the starting pressure is 15 psi. At 160°C, this correction would raise the allowable rate of pressure drop to above 20 psi/sec.

[19] P. R. Kasten and R. S. Stone, *Cooling of HRT Fuel Solution as a Result of Changing Heat Exchanger Operating Conditions*, ORNL CF-55-4-19 (April 1, 1955).

TABLE 1.4. ALLOWABLE RATES* OF STEAM-PRESSURE DECREASE IN SHELL SIDE OF HEAT EXCHANGER**

$T(0)$ °C	$T(0)$ °F	$p(T_0)$ Saturated (psi)	dp/dT (psi/°F)	dT/dp (°F/lb/ft^3)	$dp/d\rho$ (psi/lb/ft^3)	Allowable dp/dt (psi/sec)
280	536	940	7.7	15.4	118	35
260	500	680	7.6	18.9	144	42
240	464	490	6.5	20.9	135	40
220	428	340	5.3	22.2	117	35
200	392	225	4.0	23.8	95	28
160	320	90	2.2	28.6	63	18
100	212	15	0.9	28	41	12

*To keep rate of reactivity increases below 0.005/sec.

**Saturation conditions for water obtained from J. H. Keenan and F. G. Keyes, *Thermodynamic Properties of Steam*, Wiley, New York, 1936.

It requires about 2.7 sec for fluid to travel from the heat-exchanger outlet to the core inlet. Once the pump is stopped, the fluid flow rate drops rapidly[20] (from 400 gpm to 270 gpm in 0.5 sec, to 150 gpm in 1 sec, to 80 gpm in 1.5 sec, to 50 gpm in 2 sec, and to 40 gpm in 3 sec); so a time delay in stopping the pump of about 1 sec appears to be reasonable. It would be desirable to have the faster pressure-decrease rates trip the actuating device in proportionately shorter periods of time.

1.3.3 HRT "Walk-Away" and Overpressure

"Walk-away" stability calculations were performed for the HRT operating at 5 and 10 Mw, under the assumption that sufficient copper was used to recombine all decomposed heavy water except that amount corresponding to 1-Mw operation. The results given here concern the effect of overpressure on walk-away for the HRT and supplemental studies previously reported.[21] In the present calculations the effect of varying overpressure over a range of 0 to 1350 psi was examined. As in the previous report, the stability criterion was the maximum permissible value of the heat-removal temperature coefficient, a, for which the HRT could operate without walk-away.

The numerical results are displayed in Figs. 1.16 and 1.17 and show how a varies with overpressure at temperatures between 235 and 300°C. It is apparent that the limiting value of a is only mildly temperature dependent for a given overpressure.

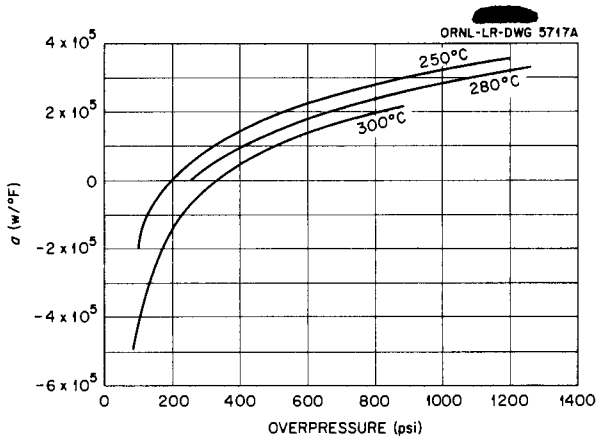

Fig. 1.16. Variation of Limiting Value of Power Removal Temperature Coefficient a vs Overpressure for the HRT Operated at 5 Mw at Various Temperatures. Enough copper was used to recombine all decomposed heavy water except that corresponding to 1 Mw operation.

While it is difficult to create instability by reducing the fuel feed rate or increasing the amount of fuel held in the low-pressure system, a walk-away condition can easily be created by reducing overpressure. An eightfold reduction in injection rate at 10 Mw and 250°C would reduce a by a factor

[20] J. L. Redford, *Slow Startup of the 400A Westinghouse Pump*, intercompany correspondence (Nov. 18, 1954).

[21] M. C. Edlund *et al.*, *HRP Quar. Prog. Rep. Jan. 31, 1955*, ORNL-1853, p 23 ff.

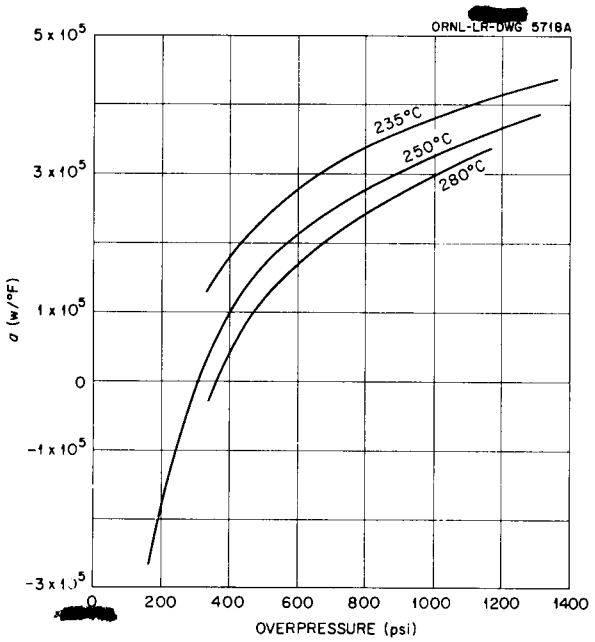

Fig. 1.17. Variation of Limiting Value of Power Removal Temperature Coefficient *a* vs Overpressure for the HRT Operated at 10 Mw at Various Temperatures. Enough copper was used to recombine all decomposed heavy water except that corresponding to 1 Mw operation.

of 2, while halving the overpressure from 800 to 400 psi would reduce *a* by a factor of 3.

1.4 COMPONENT DEVELOPMENT

C. B. Graham

L. J. Bell
J. S. Culver
K. E. Estes
C. H. Gabbard
L. F. Goode
J. A. Hafford
P. F. Pasqua[22]
W. L. Ross
J. W. Skillern
I. Spiewak
D. S. Toomb
R. VanWinkle

E. L. Youngblood

1.4.1 Pump Development

L. J. Bell K. E. Estes
W. L. Ross

All HRT-size development pumps have been received. The pump casing for the second 400A pump, which was shipped to the manufacturer for repair in November 1954, has not been returned.

[22]Consultant.

The 300A pump was assembled with the 230-gpm impeller and installed in a loop with a vertical pressurizer. The pump has been run a few hours on water at low temperatures and appears to be operating satisfactorily. Figure 1.18 shows the pump characteristics for the 230-gpm pump.

The first 400A pump has been run since January 19, 1955, on a UO_2SO_4 solution containing approximately 30 g of uranium per kilogram of solution, 0.005 *m* $CuSO_4$, and 10 mole % excess H_2SO_4. After approximately 46 hr at 300°C, the unit became noisy and was shut down. Examination revealed that the greater part of several locking cups had been dissolved. Spectrographic analysis revealed that the locking cups were Inconel X instead of type 304 stainless steel. The lower Graphitar radial bearing was soft and swollen and appeared to have burned or lost some material. The tip end of the Stellite journal which operates adjacent to the burned area had suffered some corrosion.

The design of the thermal barrier was checked closely after this near failure. It was discovered that the design and fabrication of the thermal barrier allowed it to seat on two faces rather than one. The result was that it seated only partially and allowed hot 300°C liquid to leak into the space around the lower radial bearing. The thermal barrier was then machined so that only one surface would make the seal, in order to prevent excess leakage of hot fluid around the barrier. Four bolts were added to bring the thermal barrier down snugly. A sleeve was installed between the base of the Kingsbury thrust bearing and the thermal barrier to keep hot liquid away from a new lower Graphitar bearing. A thermocouple was installed at the outer periphery of the thermal barrier to check the actual temperature of the stagnant liquid between the thermal barrier and the Kingsbury thrust bearing.

New locking cups were made from stainless steel.

Several pump shutdowns due to high current occurred after these modifications were made. The failures were caused by seizing of the lower radial bearing on the shaft as a result of inadequate flow of cool fluid through the bearing. The bearing was then altered so that it has three grooves which run the length of the bearing and permit it to operate at a lower temperature. Since this modification a run of 1000 hr has been made with the 30-g/kg uranyl sulfate solution at 300°C. Figure 1.19 shows the variation in uranium, copper, oxygen,

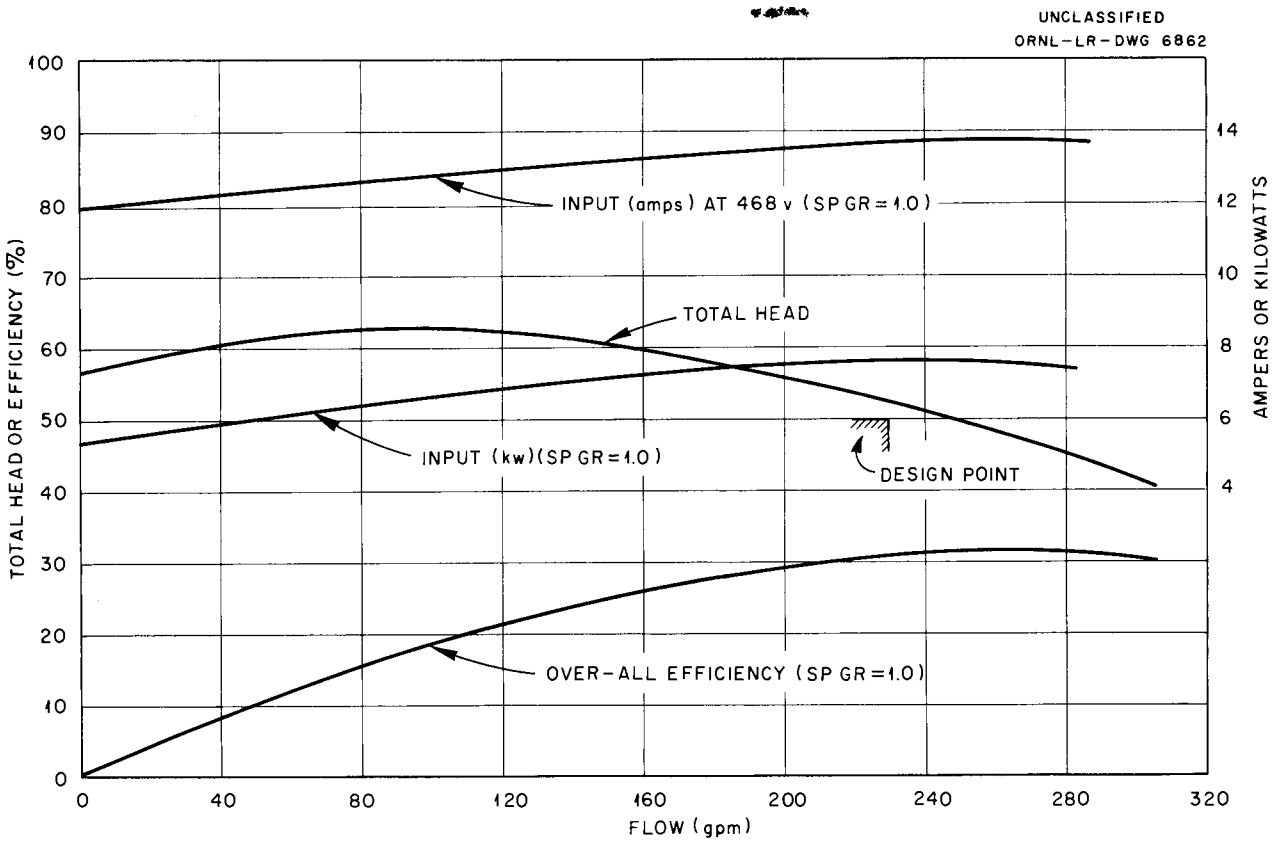

Fig. 1.18. Characteristics of Type W150 Pump (230 gpm; 50-ft Total Design Head).

nickel, and cobalt concentrations for the first 25 days of operation.

The temperature in the stagnant region above the thermal barrier has run between 170 and 190°C. This temperature range compares with 300°C in the hot region and about 55°C in the motor. A new thermal-barrier design has been tested satisfactorily by the manufacturer and is being proposed for all pumps at ORNL.

The HRT fuel mockup pump was assembled with the 300-gpm impeller. Figure 1.20 shows the pump characteristics for the 300-gpm pump. The pump first operated in the mockup on February 22, 1955, and its performance was satisfactory. After 51 hr of operation the pump was disassembled and inspected. Measurements of pump parts indicated normal wear. The thrust-bearing shoes had a few light polish marks. No other damage or wear was observed. The pump has returned to mockup operations and has accumulated a total of about 75 hr on water and cleaning solutions.

1.4.2 Fuel and Blanket Pumps

L. J. Bell W. L. Ross

Final fabrication, inspection, and testing of the first 230- and 400-gpm HRT pumps have been delayed by a change in the thermal barrier. This change will cause a postponement in delivery of the first two HRT pumps to June 1955.

Fabrication is approximately 20% complete on the second pair of HRT pumps. Titanium for these pumps was purchased, and its certified chemical analysis and physical properties comply with HRT titanium specifications. These two alternate pumps will be built according to the ORNL specifications HRT-1028 and HRT-1005.

1.4.3 HRT Heat Exchangers

L. F. Goode W. L. Ross

Fabrication of the HRT fuel and blanket heat exchangers at the Foster Wheeler Corp., Carteret, New Jersey, is nearing completion. Both units

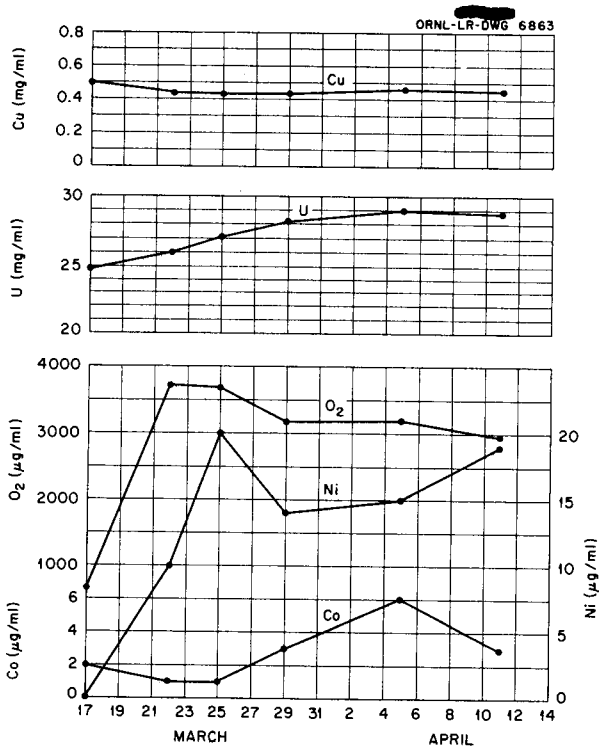

Fig. 1.19. Concentration Changes of UO_2SO_4 Solution.

have been tubed, and the primary nozzle welds have been completed satisfactorily.

All the exchanger tubing passed dye-penetrant inspection on the outside diameter of the bent portion of the tubes. Inspection was made with Spotcheck, and any indication of a flaw was cause for rejection. The rejection rate was very low; no questionable tubes are to be used in the exchangers. After the tube sheets were tubed and the tubes were rolled to 0.001 to 0.002 in. beyond contact, the units were subjected to a leakage demonstration to prove that a final helium leak test would be a test of the weld integrity, and not of the tightness of the rolled joint. Attempts to show leakage through the joints with nitrogen gas being used to bubble through acetone placed in the weld-joint preparation groove were not successful for most of the joints. Each joint was shown to leak, however, when Freon gas pressure was applied on the shell side of the exchanger and a G-E type H halogen leak detector was used on the channel side of the tube sheet.

Several difficulties arose in the tube-joint welding of the first unit, and similar welding of the second exchanger is being deferred until these difficulties have been resolved. Figure 1.21 shows the details

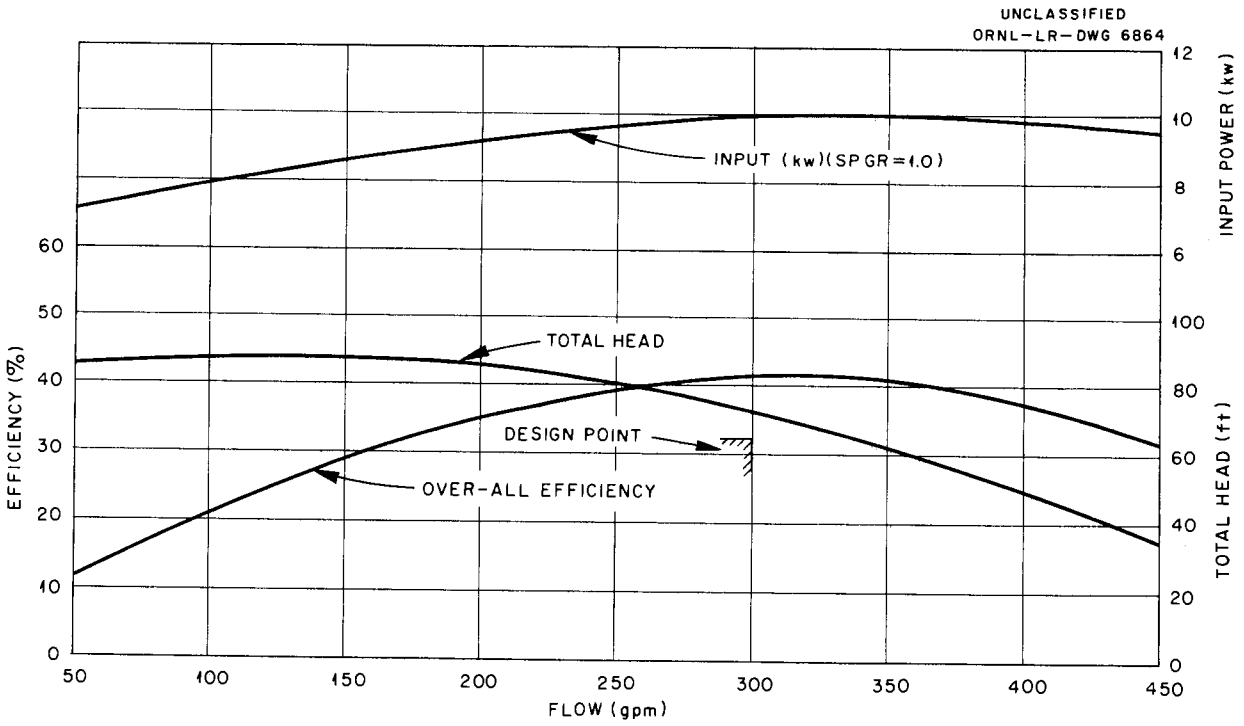

Fig. 1.20. Characteristics of Type 150-Al Pump (300 gpm; 65-ft Total Design Head).

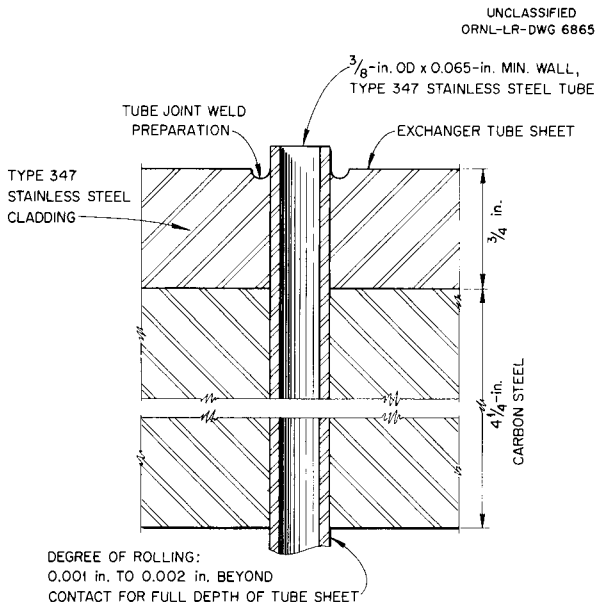

Fig. 1.21. HRT Heat-Exchanger Tube-Joint Weld Details.

of the heat-exchanger tube joint. Of major concern is the presence of crater cracks in a high percentage of the first-pass welds. Most of the cracks were not visible until the deposition of adjacent second pass welds, and it is not known whether any of the cracks were inadvertently welded over with second passes before the trouble was discovered by ORNL inspectors. All detectable cracks were ground out and repaired.

Foster Wheeler is currently preparing a series of test welds in a piece of the actual tube-sheet material in order to investigate the nature and extent of the cracks and to determine the extent of removal of first-pass crater cracks by second-pass welding. This information will be used to establish a revised procedure for the second heat-exchanger unit. The most plausible explanation of the cracking is that the tube-sheet material has a high carbon and sulfur content, although within the limits of applicable HRP and ASTM specifications. The foregoing trouble was not encountered in any of the tube-joint welds made during development and qualification.

Quality-control welds are made periodically during the tube-joint welding of an exchanger and are subsequently examined by radiographic and metallographic methods. An apparent lack of fusion or the presence of inclusion has been noted on several of these test welds and is being investigated.

Owing to the unforseen difficulties encountered in tube welding, the delivery date now appears to be June 1, 1955.

1.4.4 HRT Dump Test

C. H. Gabbard P. F. Pasqua
R. VanWinkle

The HRT dump test is being conducted to develop a control system which will maintain a pressure balance between the core and blanket during a dump of the reactor. It is hoped that the pressure differential can be maintained at 50 psi or less.

The object of the first phase of the dump test was to obtain fundamental information on the pressure-time curves of the pressure vessel, pressure drops through the discharge line and dump valve, and mass flow rates. The test apparatus, shown in Fig. 1.22, consists of a pressure vessel and a dump tank connected by a dump line, which is a mockup of the reactor-core dump line as it existed in an early piping layout. In the present HRT flowsheet the line between the dump valve and the dump tank has been shortened. A comparison of the test apparatus with the reactor is shown in Table 1.5. The volume ratio between the components of the test apparatus and the reactor core system is 1:3.63.

After a total of 30 runs the first phase of the test is nearing completion. Pressure-time curves were taken by Brush recorders at the pressurizer, dump-line entrance, valve entrance, valve discharge, and dump-line discharge. A curve of mass discharge vs time was obtained by recording the rate of liquid-level rise in the dump tank. Runs were made with saturated liquid at the following temperatures: 182, 240, 270, and 300°C. Pressurized runs were made under the following conditions: 240°C, 1250 psi; 240°C, 2000 psi; 270°C, 2000 psi; and 300°C, 2000 psi. In addition, tests were made to determine the effect of throttling the valve and of cooling the dump line. A typical set of curves for a pressurized run is shown in Fig. 1.23. The curves indicate that the pressure drops in ½-in. line, valve, and 1-in. line are essentially equal when the valve is wide open. Figure 1.24 shows a comparison of two runs at 300°C, one saturated and the other pressurized to 2000 psi. With the exception of the initial drop to the saturation pressure, the curves are essentially the same. The effect of throttling the dump valve is shown in

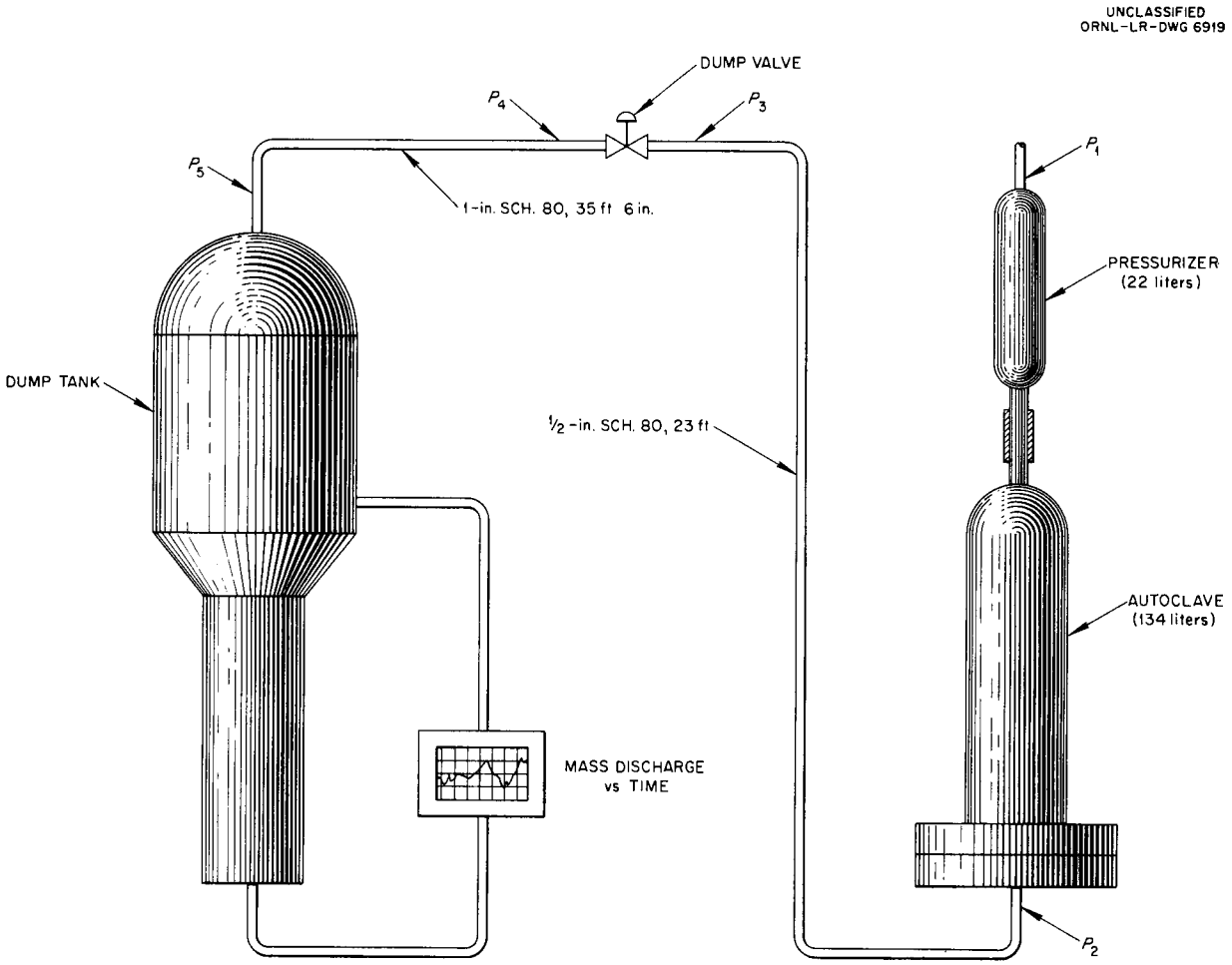

Fig. 1.22. Mockup of Reactor-Core Dump Line.

Fig. 1.25 – a comparison of a run in which the valve was wide open with one in which the valve was opened only 10%. The curves show the relative ineffectiveness of throttling the valve to control the rapid initial drop in pressure to saturation. This fact was verified further by using smaller valve trim. Throttling the valve also has relatively little effect on the mass discharge rate, since the large pressure drop across the valve is counteracted by a smaller drop in the entrance line. The following two equations, relating the mass flow rate in the existing dump line to the total system pressure, have been derived by P. N. Haubenreich:

$$\text{Saturated-steam flow (lb/sec)} = 0.0009P ,$$

$$\text{Flashing liquid flow (lb/sec)} = 0.047P^{0.6} ,$$

where P = total pressure (psia).

If the core and blanket of the reactor are operated at different temperatures, it may be necessary to close off completely one of the dump valves in order to maintain the pressure balances. A test was conducted in which the dump valve was completely closed in 1 sec. It was found that the valve could be closed without causing a pressure surge in the line as long as flashing occurred in the upstream line.

At the present time, the test apparatus is being modified to simulate bleeding-off of the superpressure through the pressurizer vent valve. This should allow the time for the initial drop (approximately 5 sec) to be extended easily past 60 sec, and should also give better control, since the vent valve will be operating in essentially pure vapor. At the conclusion of these tests, the apparatus

TABLE 1.5. COMPARISON OF SYSTEMS

	Dump Test Phase No. 1	HRT Core System	HRT Blanket System
Compressed liquid volume, liters	134	482	1740
Pressurizer liquid volume, liters	22	11	11
Pressurizer vapor volume, liters		73	73
Total system volume, liters	156	566	1824
Dump line upstream of valve	½-in. sched. 80	½-in. sched. 80	1-in. sched. 80
Inside diameter, in.	0.546	0.546	0.957
Flow area, in.^{2}	0.234	0.234	0.719
Length, ft	23	28.5	31
Valve size, in.	½	½	1
Dump line downstream of valve	1-in. sched. 80	1-in. sched. 80	1½-in. sched. 80
Inside diameter, in.	0.957	0.957	1.50
Flow area, in.^{2}	0.719	0.719	1.767
Length, ft	35	11	11

will be modified into a two-region system for additional tests.

1.4.5 HRT Mockup Loop

J. A. Hafford I. Spiewak
J. W. Skillern D. S. Toomb

The HRT mockup loop completed the water phase of its operation. The performance of the system and of the HRT-type components was excellent.[23]

The basic flowsheet of the mockup loop in water operation is presented in Fig. 1.26. The high-pressure system contains a 300A Westinghouse pump similar to the HRT blanket pump, a titanium flow-metering orifice installed in a ring joint flange, a shell-and-tube heat exchanger, an air supply, an HRT-type pressurizer, an HRT gas separator, and a lens ring flange. The gas takeoff from the separator goes through an HRT letdown heat exchanger, through a letdown valve, and into a low-pressure dump tank. Liquid is returned to the high-pressure system with HRT injection heads. The high-pressure air simulating reactor off-gas is supplied by a 20-scfm air compressor. Heat losses are balanced with an 80-kw electric boiler.

The mockup letdown system has been operated at temperatures from 30 to 300°C, pressures from 1500 to 2100 psi, liquid flows from about 0.1 to 1.6 gpm, and gas flows from about 10 to 45 scfm. During these tests there was no sign of oscillations such as were observed on the HRE mockup and, to a lesser degree, on the HRE itself. The letdown valve pressure was steady at all times when gas was present. There was no detectable gas by-passing the gas separator even during periods when gas surges were introduced or the level set point changed gradually. The superior performance of the letdown system is believed to be due to the following:

1. The letdown heat exchanger and the lines connecting it to the gas separator and letdown valve are constructed to give turbulent mixing of gas and liquid at all points. This is accomplished by including flow "spoilers" in the connecting lines which give them the same type of annular flow geometry with spacers as is present in the letdown exchanger.

2. The gas separator is capable of removing

[23] J. A. Hafford, I. Spiewak, and D. S. Toomb, *HRT Mockup Loop Water Operation*, ORNL CF-55-4-92 (April 15, 1955).

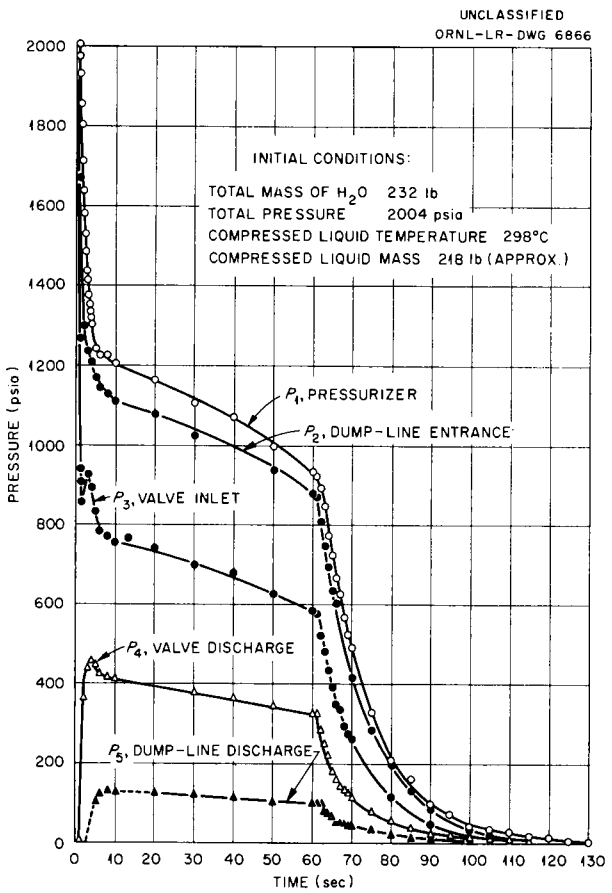

Fig. 1.23. Pressure vs Time (Pressurized Run).

large amounts of gas, with liquid entrainment rates dictated by the pressurizer level controller.

3. The letdown valve was sized properly. The HRE letdown valve was three times as large as necessary.

The control of liquid level in the mockup pressurizer is accomplished by means of a D/P cell which regulates the letdown-valve setting. This instrument maintained the level to within 1 in. of the set point at steady state and was able to adjust to transients rapidly and smoothly. An HRT-type float level controller will be tested in the near future.

The pressurizer maintained a very steady superpressure on the high-pressure loop. Its response to changes in pressure demand was quite slow because of its high heat capacity. There was no observable gas collection in the pressurizer and only a trivial amount of liquid mixing with the main stream.

The performance of the circulating and injection pumps was good. The circulating pump did not collect gas and was able to circulate liquid containing up to 7% gas by volume. There was considerable vibration in some of the small injection-pump lines; these will have to be supported securely to prevent fatigue. The total operating time on the circulating pump is now 76 hr; that on the injection pump is 430 hr.

The shell-and-tube heat exchanger, which contains tube joints similar to those of the main HRT exchangers, showed no leaks when tested with a helium leak detector after seven thermal cycles between room temperature and 300°C. The flanges, also, developed no leaks during this period.

After the completion of water operation, the loop was modified to include water injection to the circulating pump and the pressurizer and oxygen addition at the suction line of the injection pump. A uranyl sulfate run of four to six weeks duration is next on the agenda.

During the period of modification, some additional experience was obtained which is of interest in the HRT. Welding scale and stainless steel filings from weld preparation had accumulated in the high-pressure system. To remove this trash, trisodium phosphate solution was circulated with the Westinghouse pump and the dump valve was partially opened to transfer the trash to the low-pressure system. The trash was collected in a sedimentation tank in the injection suction line.

Following this, the loop was treated with 5% HNO_3 for 12 hr. The purpose of this operation was to dissolve any remaining scale and to reveal the presence of foreign construction materials by chemical analysis of the solution in the loop. The results of these analyses are shown in Fig. 1.27. They are similar to results that would be expected from the HRT. The fact that none of the elements continued to build up after about 4 hr indicates that the loop is clean and free of foreign materials.

Another test run on the mockup involved venting the pressurizer steam to a low-pressure receiver, simulating transfer of steam from the core pressurizer of the HRT to the blanket pressurizer. Phosphate was used as a tracer ion to determine liquid entrainment rates. The phosphate concentration in the vent stream was below 1 ppm as compared with 5000 ppm in the pressurizer liquid, at a vent rate of 7 lb/min. For a 35-lb/min vent, phosphate concentration increased to 15 ppm. The

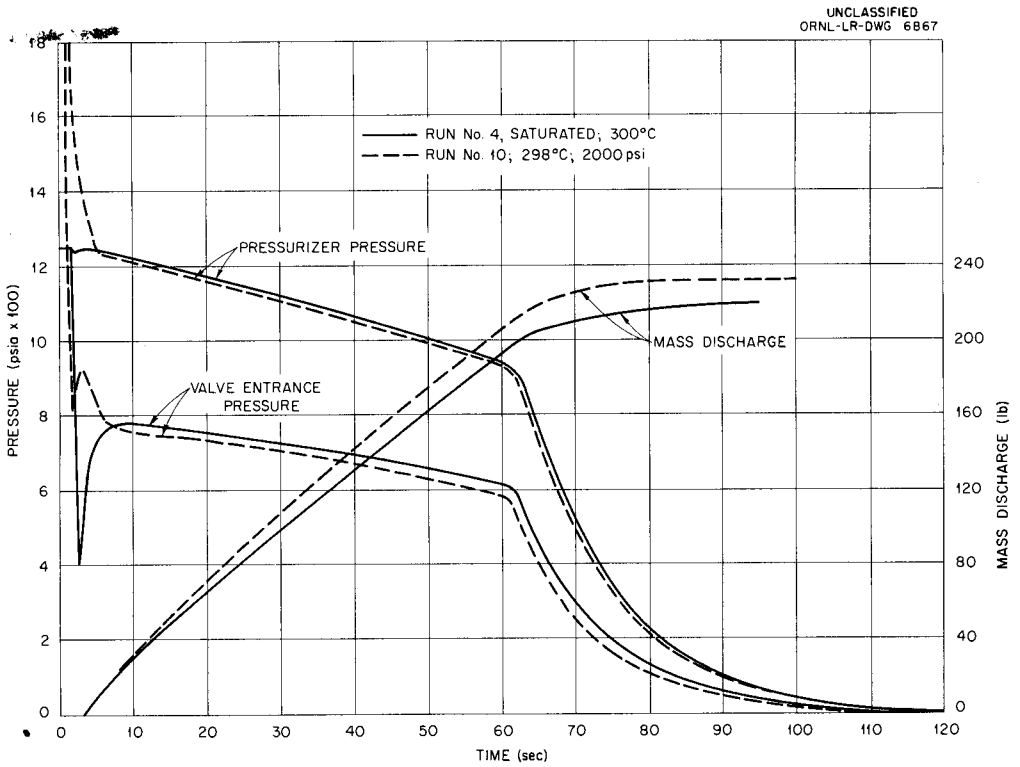

Fig. 1.24. Dump Test (Comparison of Runs 4 and 10).

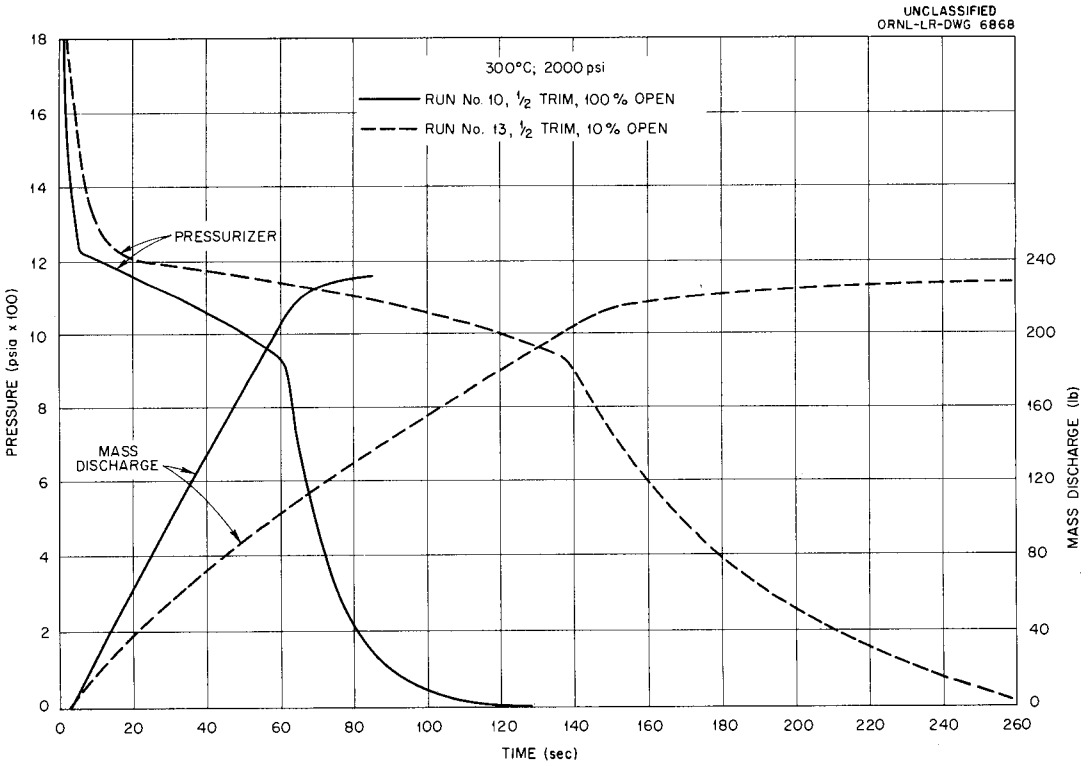

Fig. 1.25. Dump Test (Effect of Throttling).

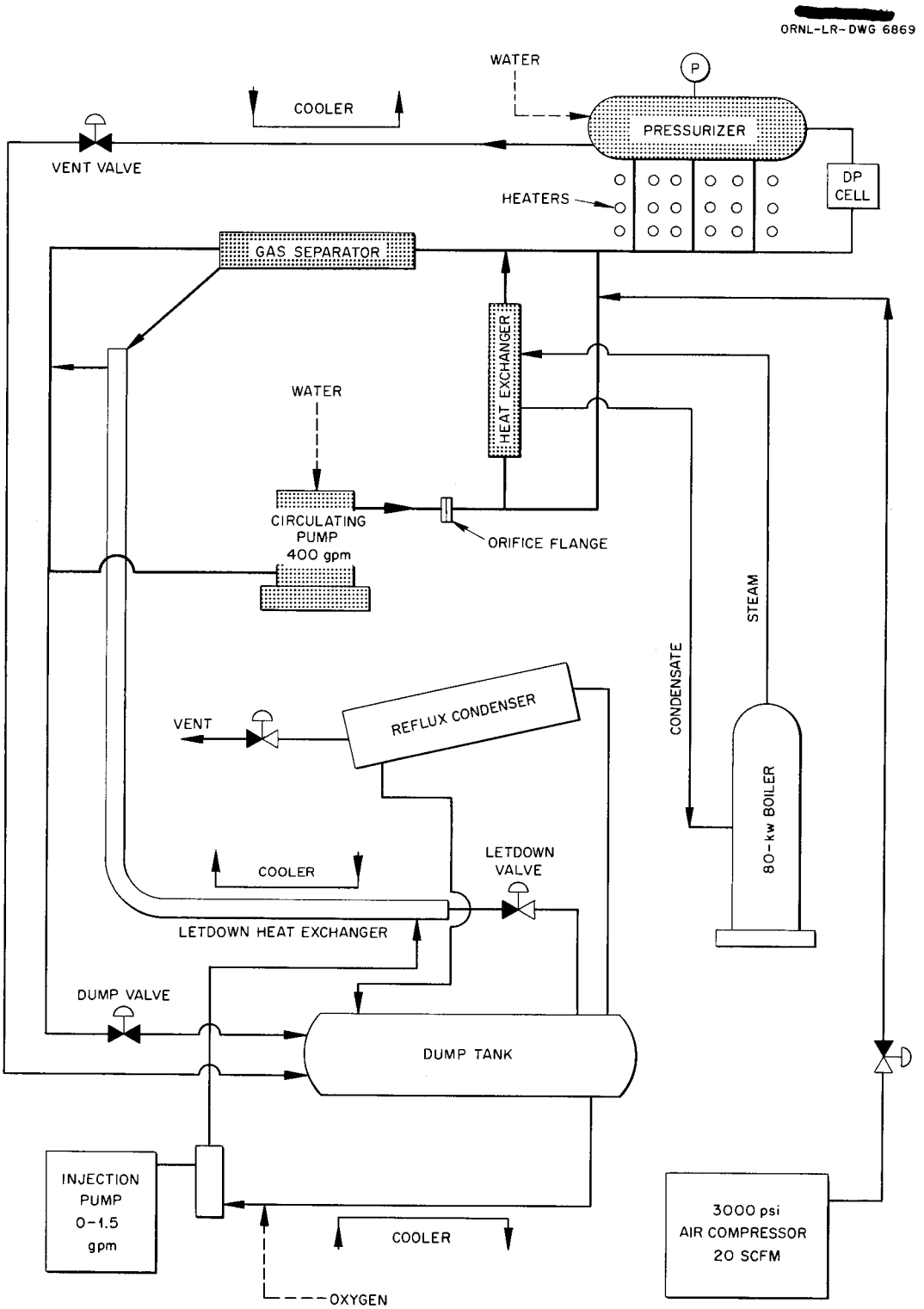

Fig. 1.26. Elevation Flowsheet of HRT Mockup Loop.

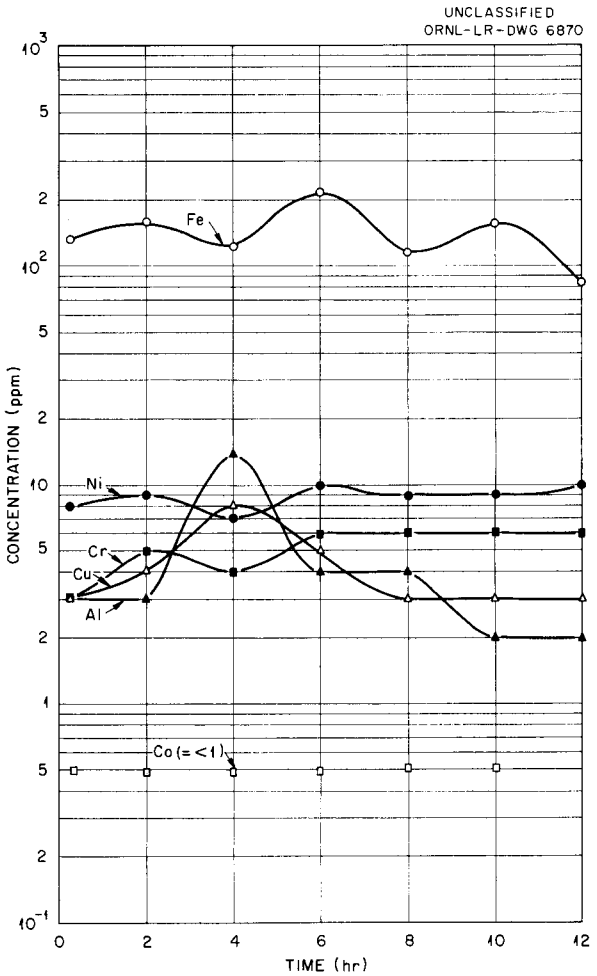

Fig. 1.27. Results of Nitric Acid Wash of HRT Mockup Loop.

conclusions drawn from this test are that no uranium transfer will occur between pressurizers in normal operation and that only a trivial amount (below ¼ g) will occur during a wide-open dump. Water injection to the pressurizer should eliminate even this small amount.

1.4.6 Feed Pump Mockup

E. L. Youngblood J. S. Culver

The HRT feed pump system has been studied on a mockup which utilized a Scott & Williams P-14 drive unit and HRE-type diaphragm heads.[24] The purpose of the study was to determine the capabilities and limitations of this feed pump under HRT operating conditions.

The HRT fuel pump is required to pump 1.5 gpm at 2000 psi, and the reflector pump must have a maximum output of 3.5 gpm. The Scott & Williams type of feed pump appears to be fully capable of meeting these requirements. The over-all operation of the unit was considered to be good, and the arrangement of the suction line and standpipe as designed for the HRT was satisfactory.

The power requirement of the pump at various pumping rates is given in Fig. 1.28 for 500- and 2000-psi discharge pressures. The 500-psi test was intended to simulate conditions during the filling operation. Figure 1.29 shows the effect of discharge pressure on the output of the pump. The effect of low-pressure gas addition to the feed-pump suction is also shown in Fig. 1.29. Satisfactory operation was obtained at gas rates up to 500 cc/min and at temperatures up to 70°C.

The system operated satisfactorily for over 1200 hr; only minor difficulties, such as leaks, occurred, and they are expected to be entirely eliminated by slight modifications in the design.

1.5 CONTROLS AND INSTRUMENTS

W. P. Walker

M. C. Becker	R. L. Moore
A. M. Billings	L. R. Quarles[25]
J. R. Brown	R. E. Toucey
J. S. Culver	E. Vincens
C. H. Gabbard	K. W. West

1.5.1 General Design Status

All drawings have been completed for the electrical work that is to be performed by the HRT subcontractor. This includes the mounting of equipment and conduit and the interconnection wiring of all electrical equipment and power distribution outside the control-room area. Interconnection conduit for personnel monitors and the intercommunication system for the building are also to be installed.

Detailed layouts of instruments on the main and auxiliary control panels have been completed. Approval for construction is being deferred in order to include anticipated flowsheet changes.

Preliminary designs for the pressure cells and differential-pressure cells have received approval. Corrosion tests are being performed on submitted

[24] E. L. Youngblood, *Feed Pump Mockup*, ORNL CF-55-2-52 (Feb. 9, 1955).

[25] Consultant.

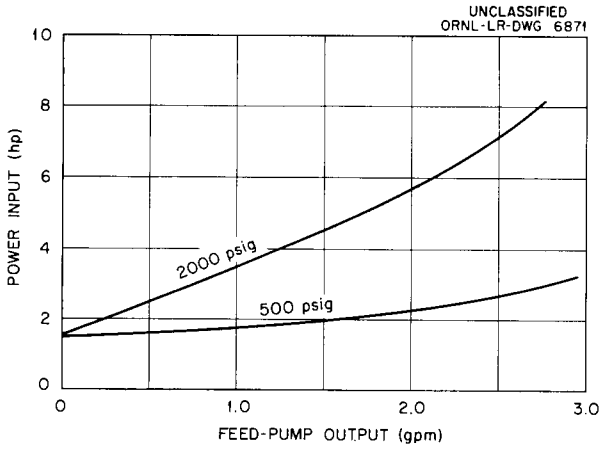

Fig. 1.28. Power Requirement of Scott and Williams Type Feed Pump.

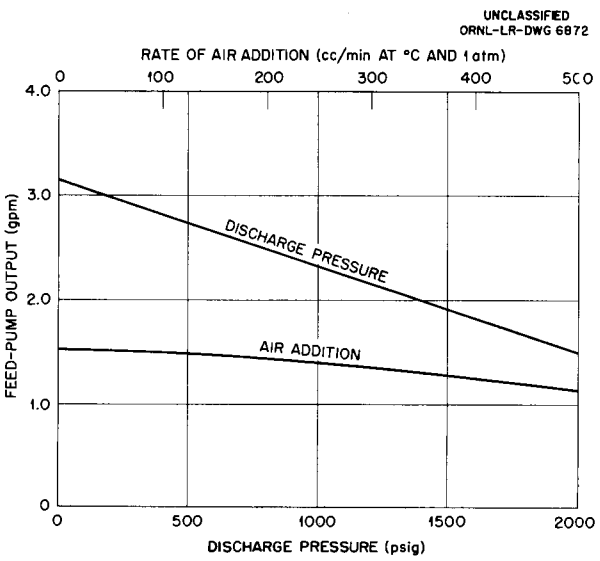

Fig. 1.29. Effect of Discharge Pressure and Gas Addition on the Feed-Pump Output.

material samples; more than 50% of the samples have failed to pass the tests, but approved material for approximately 75% of the items is now on hand.

1.5.2 Pneumatic Weigh Cell

R. L. Moore

A pneumatic weighing system,[26] utilizing a force developed with compressed air to oppose the load applied to the weigh cell (see Fig. 1.30), was chosen to measure the dump- and condensate-tank inventories. It is capable of high accuracy under conditions of high radiation and varying ambient pressure, and it is unaffected by submersion in water. A baffle-nozzle within the cell, in combination with a pilot relay (located in the auxiliary control area), regulates the pressure in the weighing section of the cell so that the product of this pressure and the effective weighing area is equal to the load applied to the cell. This pressure, proportional to the load, is measured by a pressure gage which is calibrated in terms of weight. For precise weighing, the pressure will be measured by means of a mercury manometer.

The tare loading, developed by the dead weight of the tanks and any pipe stresses present,[27] is counterbalanced by a force, developed by an externally regulated pressure, which is applied to unbalanced areas in the lower "tare" section of the weigh cell. This pressure is regulated differentially with respect to the ambient "shield" pressure surrounding the cell, and this differential regulation, together with special connection of ambient and atmospheric pressures to various portions of the cell, provides automatic compensation for variations in shield pressure. Greater accuracy is realized from the use of tare compensation, since the weighing section is required to measure only over the range of the live load. Factory calibrations of these cells show a maximum deviation of ¼% in linearity. If the expected precision is realized, a calibration curve could be used to obtain higher accuracies. The deflection of the cell is less than 0.001 in. for full load; therefore the cell, together with the beam system,[27] forms a rigid assembly; no appreciable pipe loads will be introduced as a result of movement of the tanks.

All materials used in the weigh cells are metallic (see Fig. 1.31), and no problem of radiation damage exists. The main body of the cell is aluminum, and the flexible diaphragms are stainless steel. With the exception of the nozzle, which can be cleaned by back-pressuring, all components that might give trouble are located in the auxiliary control area, where they are easily accessible for maintenance.

[26] The A. H. Emery Co., Pine & Grove Sts., New Canaan, Connecticut.

[27] R. B. Briggs *et al.*, Chap. 1.2, this report.

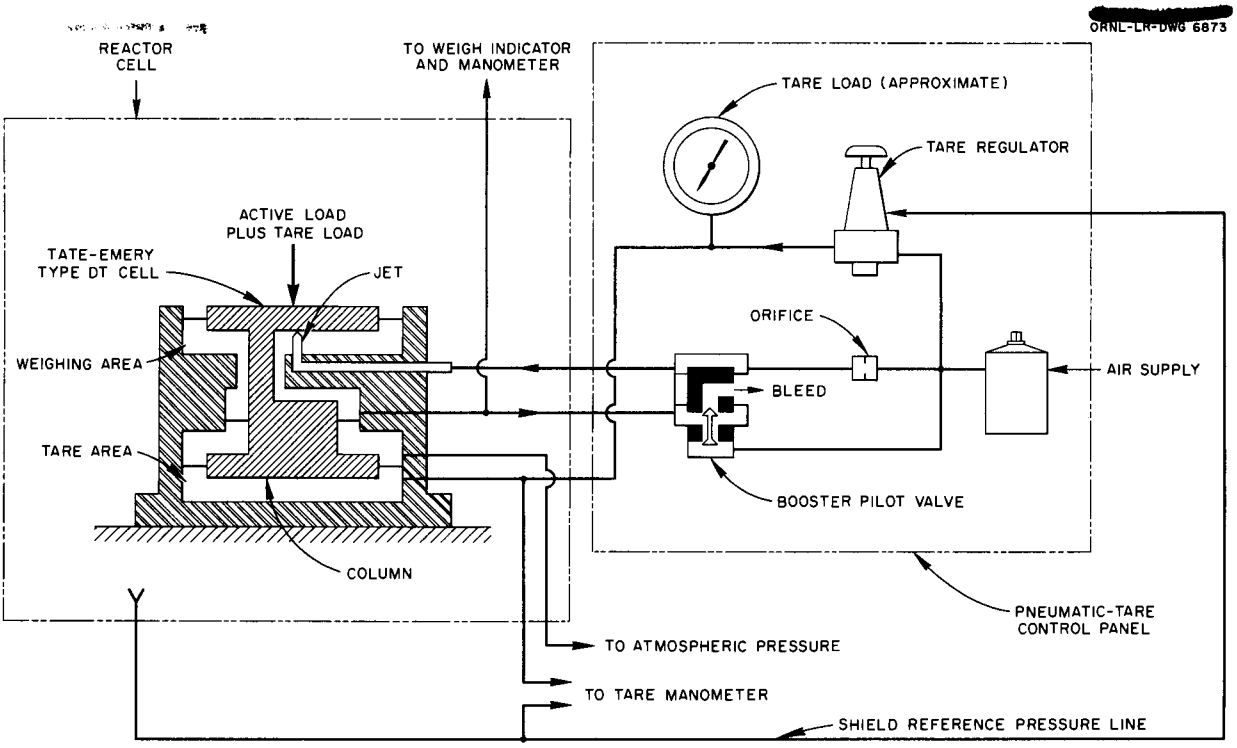

Fig. 1.30. Pneumatic Weigh System.

1.5.3 Valves and Operators

A. M. Billings

The vendor's design for the low-pressure valve[28] (½-in., 500 psi, 250°C) has been approved for construction. Delivery is scheduled in May. This design features integral ring-joint flange grooves for through-bolting installation. A unit has been received, and a thermal-cycle test for flange leaks has been made. After being heated to an equilibrium temperature of 150°C with steam, the valve was cooled with water to 30°C in 6 min. No leakage was detected during this test nor in 500-psi gas tests after the thermal cycling. The bolting materials were ASTM A-193 grade B7 and A-194 grade 2H for the bolts and nuts, respectively.

The requirements for the HRT valve actuators specified a sealed unit capable of operating while being exposed to a radiation dosage of 5×10^9 r. The cylinder-type actuator, shown in Fig. 1.32, was selected. The actuator piston has an area of 50 in.^{2} and uses nylon O-rings for the seal. Positive steam sealing is assured by the use of a small metallic bellows. The pressure rating of the unit is 100 psi, and external materials have been selected or plated to withstand corrosion under water. The design includes a spring loading mechanism which may be adjusted or even reversed in the field without the loss of actuation during adjustment.

1.5.4 Liquid-Level Transmitter

Operation of the HRE and subsequent experimental loops indicated that a major design improvement was desirable for the displacement-type liquid level transmitter.[29] The method of float suspension and the method of pickup and electronic circuitry of the receiving instrument were studied.

A compact suspension system with dual spiral springs milled from a flat sheet 0.030 in. thick was tested at 200°C. The first test was performed with cold-rolled type 347 stainless steel springs. Lateral stability was good, but the change in the

[28] J. N. Baird *et al.*, *HRP Quar. Prog. Rep. Oct. 31, 1954*, ORNL-1813, p 37.

[29] L. R. Quarles and W. P. Walker, *A Manual of HRE Control and Instrumentation*, ORNL-1094, p 24 (Jan. 23, 1952).

[redacted]

ORNL-LR-DWG 6874

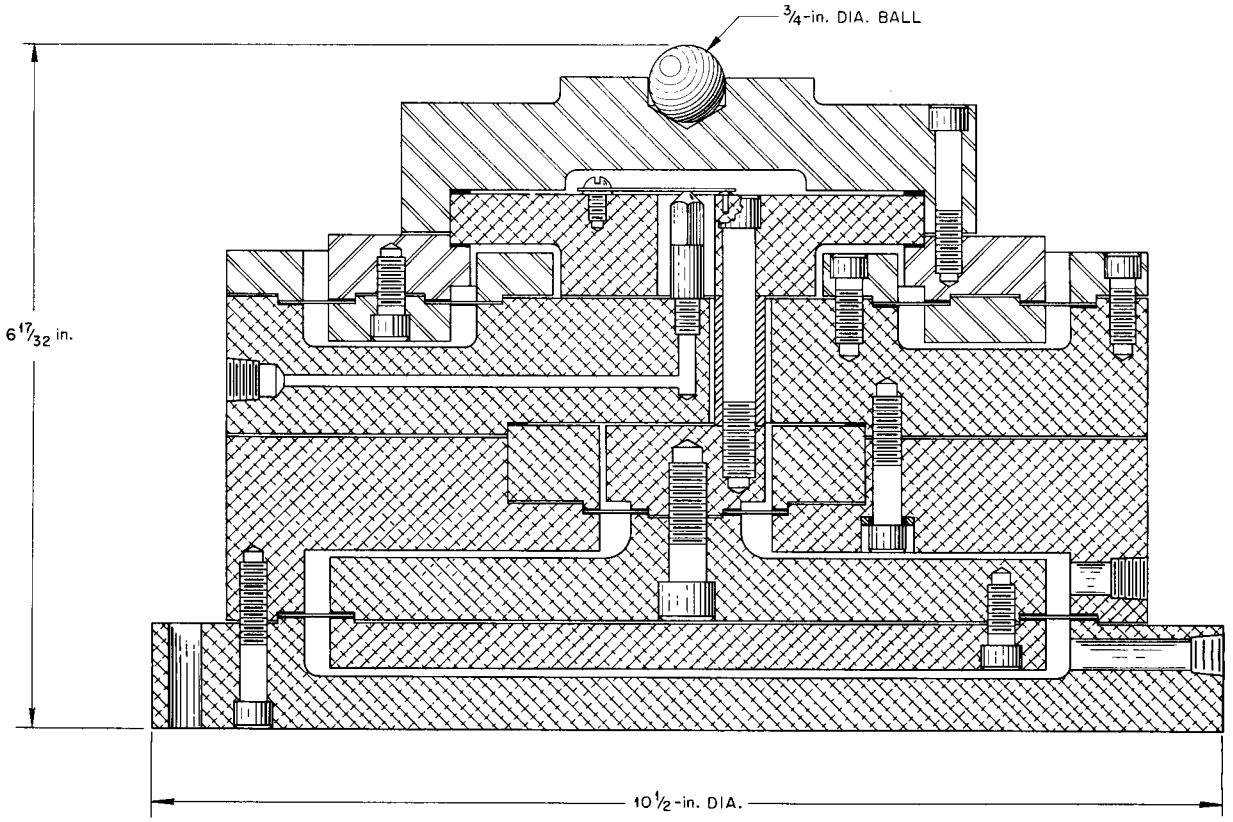

Fig. 1.31. Pneumatic Weigh Cell.

[redacted]

ORNL-LR-DWG 6875

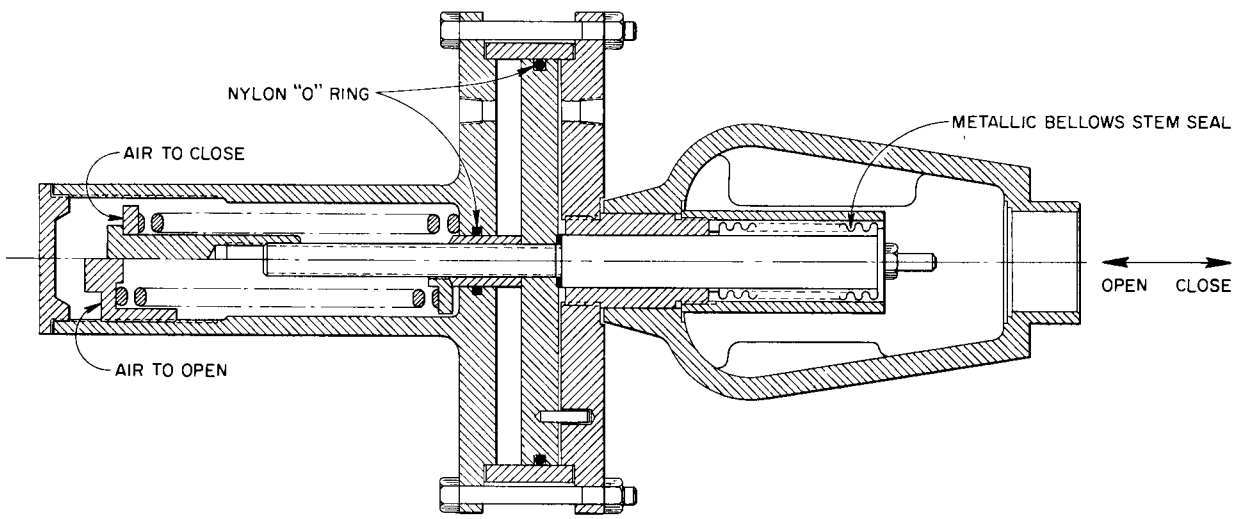

Fig. 1.32. Cylinder-Valve Actuator.

modulus of elasticity resulted in a 0.007-in. or 35% contraction at the elevated temperatures. Some difficulty with creep and permanent deformation was also experienced. An expansion of only 0.001 in. or 5% was measured after the first thermal cycle of a set of springs made from Iso-Elastic spring alloy.[30] Corrosion tests will be initiated on this material.

Observations of the operation of the HRE pressurizer-level instrument indicated that changes in temperature affected the sensitivity and electronic zero of the instrument. Other factors, such as pressure, changing modulus of elasticity, and fuel-solution density, made it impossible to determine, under operating conditions, the extent to which the electronic portion of the instrument was affected. In order to isolate the electronic effect, a jig was constructed which simulated the upper portion of the HRE pressurizer-level sensing element. The jig was provided with a micrometer adjustment for positioning the core and with thermocouples for determining temperatures at various points along the stainless steel tube and on the core. Provisions were made to heat the coil evenly or to produce temperature gradients along the coil.

Investigations showed that the HRE-type coil and circuit was very temperature sensitive and that the instrument could be rendered insensitive under certain conditions. Isolation of various effects present showed that the temperature effects were due mainly to variation in the impedance reflected into the coil. (A previous theory that the temperature effect was due to changes in primary resistance was found to be invalid. It was also determined that, owing to reflected impedance effects, the Q of the coil could not be materially increased by raising the frequency.)

The addition of an output phasing network greatly improved operation, but zero shifts and some loss of sensitivity (sluggishness) were still present. Further investigation and analysis showed that an improvement in the temperature effect could be obtained by reducing the number of turns of the coil in a manner that would reduce the percentage of total impedance that was reflected. The microformer-type circuitry has demonstrated a lower temperature effect, with the ability to function under differential temperature.

A circuit with a microformer and an output phasing network was installed in a Foxboro Dynalog instrument. Tests showed a zero drift of less than 2% and very little quadrature voltage development when the coil-assembly temperature was increased to 150°C. Further tests will be conducted at higher temperature after coils with high-temperature insulation are wound.

A complete level-indicator unit featuring the microformer-type coil and the spiral-spring suspension is now being fabricated for test under operating conditions on the HRT mockup.

[30] John Chatillon & Sons, 90 Cliff Street, New York 38, N. Y. Composition: 36% nickel, 8% chromium, 0.5% molybdenum, balance iron.

Part II

THORIUM BREEDER REACTOR

J. A. Lane R. B. Briggs

2. CONCEPTUAL DESIGN

2.1 REACTOR ANALYSIS

M. C. Edlund P. R. Kasten
H. C. Claiborne L. Dresner

2.1.1 One-Region Thorium Breeder Reactors

The study of one-region thorium-uranium reactors was made for the purpose of direct comparison with the two-region reactors previously reported.[1,2] Process characteristics and cost factors were similar to those used in the two-region study, with two exceptions:

1. No attempt was made to estimate the fixed costs for the one-region reactors. For initial comparison purposes, it was assumed that these costs are approximately equal for the two reactor types.

2. The nature of the fuel (UO_3 and ThO_2 suspended in D_2O) assumed for the one-region reactor appears to preclude the use of a precipitation process with removal of poisons by hydraulic separators. In one-region reactors, all chemical processing must be done by use of the more expensive Thorex process.

All results are for 125 Mw of electrical power delivered to a power grid for a one-region reactor operating at an average temperature of 280°C (equivalent to 480.8 Mw of heat, with a net station efficiency of 26%). An external power density of 20 kw/liter was used in all cases.

The unit cost of power is shown as a net partial cost in Table 2.1 and in Figs. 2.1 through 2.3. This cost is the sum of the inventory charges,

[1] M. C. Edlund *et al.*, *HRP Quar. Prog. Rep. Oct. 31, 1954*, ORNL-1813, p 44–47.

[2] M. C. Edlund *et al.*, *HRP Quar. Prog. Rep. Jan. 31, 1955*, ORNL-1853, p 41–43.

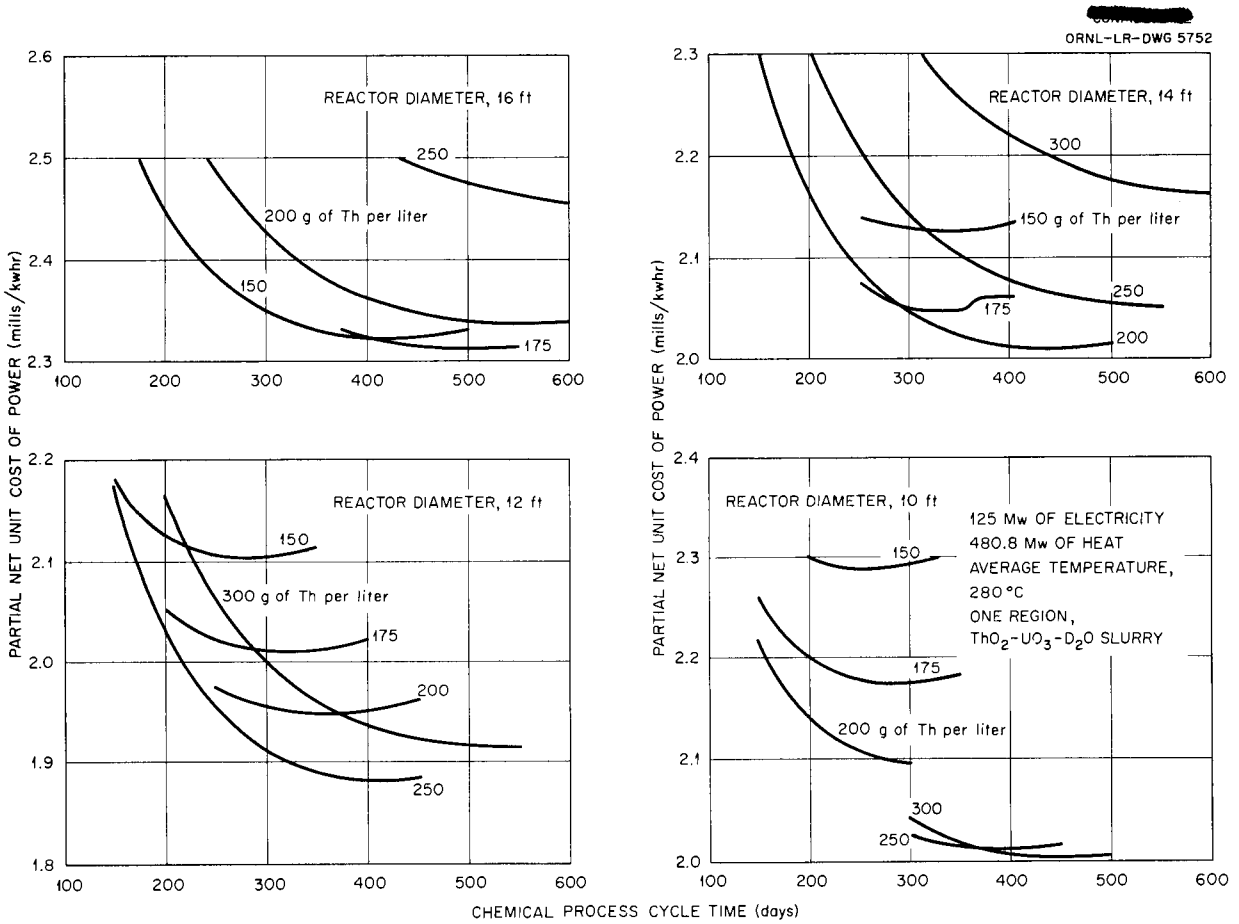

Fig. 2.1. Effect of Process Cycle Time on Unit Cost.

TABLE 2.1. COST BREAKDOWNS AND NEUTRON BALANCES FOR SEVERAL REACTORS* NEAR OPTIMUM CONDITIONS

Process Characteristics and Costs					
Reactor diameter, ft	10	11	12	13	14
Thorium concentration, g/liter	300	300	250	250	200
Process cycle time, days	450	400	400	500	450
Net partial cost of power, mills/kwhr	2.00	1.92	1.88	1.93	2.01
Uranium (U^{233} and U^{235}) credit, mills/kwhr	0	0.04	0.05	0.15	0.11
Chemical processing (less fixed costs), mills/kwhr	0.17	0.20	0.18	0.16	0.16
Feed costs (Th, D_2O, U), mills/kwhr	0.40	0.22	0.25	0.28	0.32
D_2O inventory, mills/kwhr	0.52	0.58	0.66	0.75	0.86
Uranium inventory, mills/kwhr	0.92	0.96	0.84	0.89	0.77
Reactor volume, liters	14,800	20,000	25,600	32,600	40,700
Total system volume, liters	38,900	43,800	49,700	56,600	64,700
Power density in reactor, kw/liter	32.4	24.1	18.8	14.8	11.8
Gross breeding ratio	0.957	1.011	1.012	1.035	1.025
Net breeding ratio	0.956	1.009	1.010	1.034	1.024
Net breeding gain (U^{233} and U^{235}), g/day	0	5.79	6.3	20.4	14.3
Critical concentration, g of U^{233} per kg of D_2O	7.99	7.62	5.82	5.60	4.15
Critical concentration, g of U^{235} per kg of D_2O	1.18	0.71	0.56	0.46	0.37
Uranium concentration, g of U per kg of D_2O	26.08	17.60	13.42	10.68	8.50
U^{233} in product, wt fraction	0.306	0.433	0.434	0.524	0.487
U^{235} in product, wt fraction	0.042	0.038	0.038	0.040	0.040
Thorium feed, g/day	528	560	561	580	572
U^{235} feed, g/day	26.7	0	0	0	0
Reactor poisons, %	5.49	4.93	5.46	6.10	6.34
Neutron Balances					
Absorptions and losses					
Pa^{233}	0.0191	0.0186	0.0214	0.0206	0.0235
U^{233}	1.0000	1.0000	1.0000	1.0000	1.0000
U^{234}	0.1090	0.1019	0.1040	0.0910	0.0986
U^{235}	0.1599	0.1009	0.1029	0.0883	0.0966
U^{236}	0.0235	0.0095	0.0095	0.0044	0.0061
D_2O	0.0070	0.0073	0.0095	0.0099	0.0133
Poisons	0.0573	0.0491	0.0545	0.0601	0.0629
Th^{232} (thermal)	0.5516	0.5775	0.6269	0.6516	0.6998
Th^{232} (resonance)	0.4687	0.4520	0.4063	0.4043	0.3488
Fast leakage	0.1873	0.1518	0.1309	0.1123	0.0993
Slow leakage	0.07081	0.0623	0.0694	0.0622	0.0730
Total neutrons absorbed and lost	2.6541	2.5309	2.5351	2.5046	2.5218
Production					
Neutrons from U^{233}	2.3200	2.3200	2.3200	2.3200	2.3200
Neutrons from U^{235}	0.3341	0.2109	0.2151	0.1846	0.2018
Total neutrons produced	2.6541	2.5309	2.5351	2.5046	2.5218

*125 Mw of electricity, 480.8 Mw of heat; average temperature 280°C, external power density, 20 kw/liter.

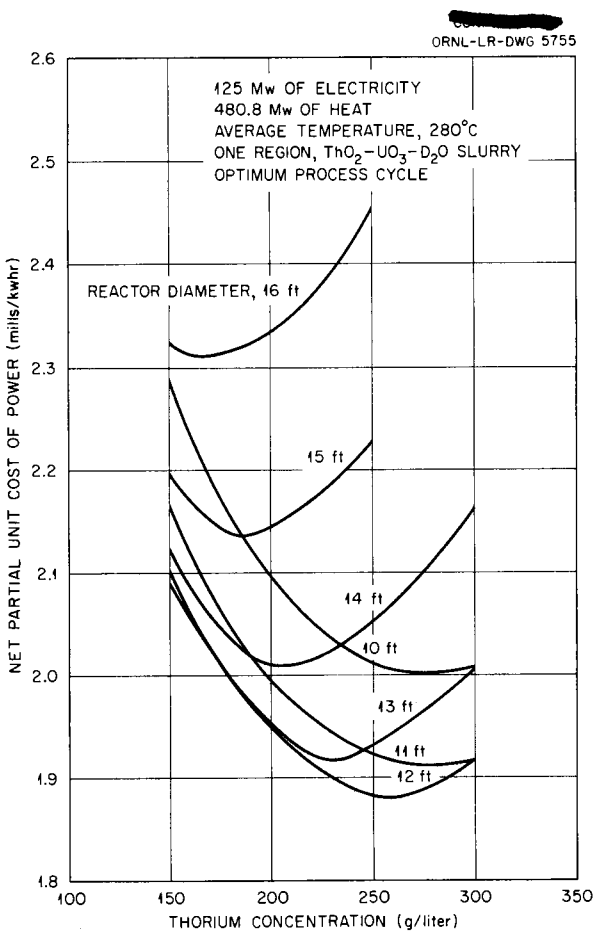

Fig. 2.2. Effect of Thorium Concentration on Unit Cost.

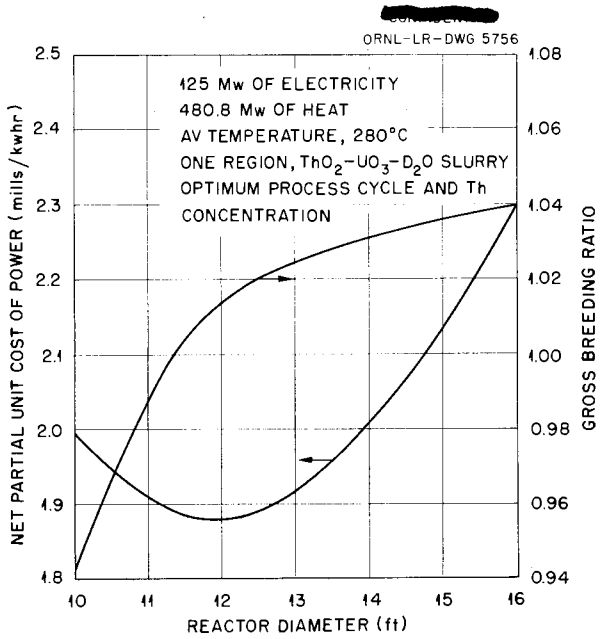

Fig. 2.3. Effect of Reactor Size on Unit Cost and Breeding Ratio.

feed (thorium, and for nonbreeders, U^{235}), D_2O makeup, and chemical processing charges that are a function of throughput, minus the credit for breeding gain, if any. Costs not included are the fixed charges on the plant investment (reactor, turbogenerator, and chemical processing), fixed operating costs for the chemical processing plant, and operating and maintenance cost, which is usually taken as a percentage of the plant investment (3% in the two-region study). The comparable fixed cost for the two-region reactors is 5.25 mills/kwhr. Consequently, for initial comparison, the total unit cost can be obtained by adding the fixed cost of 5.25 mills/kwhr to the net partial unit cost shown.

The results for five reactor sizes near optimum conditions are presented in Table 2.1. It is apparent that, for one-region reactors near optimum cost conditions, large breeding gains cannot be obtained and high isotopic purity (approximately 95%) U^{233} cannot be produced without a protactinium recovery process. This would involve separation of protactinium from the uranium isotope mixture as soon as it is practical after discharge from the reactor. Such a procedure ordinarily would not be required for the two-region reactor, since a product of about 95% purity is expected.

The effect of the chemical processing cycle (which determines the fission poison level) is shown in Fig. 2.1 for reactor diameters from 10 to 16 ft. In general, the optimum cycle time increases with increase in thorium concentration and reactor diameter; the optimum cycle times for the reactors near optimum cost appear to be about twice as large as for a two-region machine. For nonbreeders it was assumed that a 30-day supply of U^{235} feed was on hand, but no reserve supply of fissionable material was assumed for breeders. Thus the loss in credit from the breeding gain and the additional inventory charge cause the abrupt change in slope of the curve in Fig. 2.1 at the point of change from breeder to nonbreeder.

The net partial cost as a function of diameter and thorium concentration at optimum cycle time is

shown in Fig. 2.2. For the reactor sizes of interest, the optimum thorium concentrations are between 200 and 300 g/liter.

The effect of reactor diameter on the partial unit cost of power for optimum process cycle times and thorium concentrations is shown in Fig. 2.3. The minimum partial unit cost of 1.88 mills/kwhr occurs for a reactor size of 12 ft, with a thorium concentration of 260 g/liter. From a cost viewpoint there is little variation in the range of reactor sizes from 10 to 14 ft, the maximum difference being only 0.12 mill/kwhr.

The comparable minimum partial cost for the two-region reactor is 0.97 mill/kwhr. Therefore, a cost differential of 0.9 mill/kwhr seems to exist in favor of the two-region reactor, provided the fixed costs for the two types of reactors are equal. It is believed that the fixed charges will be somewhat smaller for the one-region reactor because of simpler construction and operation. Also, the relative power costs of one-region and two-region reactors may be dependent on the size of the plant, which has not been varied in this study. A more complete discussion of one- and two-region thorium breeder reactors will be presented in a forthcoming report.[3]

2.1.2 Ratio of U^{232} to U^{233} Produced in Thorium Breeder Reactors

An expression for the $(n,2n)$ cross section of fissionable nuclei has been applied to the production of U^{232} in thorium breeder reactors. Preliminary results for the optimum-cost one-region breeder give the U^{232}/U^{233} ratio as approximately 2×10^{-4}, while for the optimum-cost two-region system the U^{232}/U^{233} ratio is 4×10^{-5}. The ratio is roughly proportional to the thermal-neutron flux and to the chemical processing cycle time.

2.2 ENGINEERING STUDIES (TBR DESIGN – CASE A)

R. B. Korsmeyer

A. L. Gaines
P. N. Haubenreich
M. C. Lawrence[4]
M. I. Lundin
R. G. McGrath[5]
C. L. Segaser

W. F. Taylor[6]

With the use of the results of the optimization studies as a basis,[7,8] the major plant components have been under preliminary design during the last quarter, and a plant layout has been considered. The process flow diagram of the reactor plant has been completed.

2.2.1 Reactor Process Flow Diagram

The diagram shown in Figs. 2.4 through 2.7 is the first of four flowsheets to be studied.[9] It follows closely the flowsheet for the HRT, differing mainly in the consolidation of the outer dump tanks of the three reactors into two common storage systems supplying the cores and blankets, respectively, of the reactors. The common storage is not shown.

2.2.2 Reactor and Power-Plant Layout

If underwater maintenance in the operating areas can be shown to be feasible, the station layout shown in Figs. 2.8 and 2.9 can be used. The arrangement of the turbogenerator plant was patterned after the TVA Kingston Steam Plant, which utilizes turbogenerator units of a physical size not greatly differing from those chosen for the TBR.

Three turbogenerator sets, each of 100,000 kw capacity, are required. They are approximately 90 ft long by 32 ft wide and are arranged laterally on 96-ft centers in a room 360 ft long by 114 ft wide. The center line of each set is midway between building columns in order to facilitate maintenance of the generator rotor. Auxiliary power-plant items, such as feed pumps, feed-water heaters, condenser hot-well pumps, etc., are located in the basement.

An area 26 ft wide by 300 ft long located between the turbogenerator plant and reactor plant is designated as the control area. Each reactor and its turbogenerator unit are individually controlled. The main control rooms are at ground level on the operating floor and are 26 ft wide, 48 ft long, and of sufficient height to accommodate the main instrument panel. Directly below the main control room is shown an auxiliary control room. This room houses the various valves and

[3] H. C. Claiborne and M. Tobias, *Thorium Breeder Reactor Studies*, ORNL-1810 (to be published).

[4] On loan from General Dynamics Corp.

[5] On loan from Westinghouse Electric Corporation.

[6] On loan from Pioneer Service & Engineering Co.

[7] W. C. Moore *et al.*, *HRP Quar. Prog. Rep. Oct. 31, 1954*, ORNL-1813, p 43–59.

[8] J. A. Lane, R. B. Briggs, *et al.*, *HRP Quar. Prog. Rep. Jan. 31, 1955*, ORNL-1853, p 41–52.

[9] R. B. Korsmeyer *et al.*, *HRP Quar. Prog. Rep. Jan. 31, 1955*, ORNL-1853, p 44.

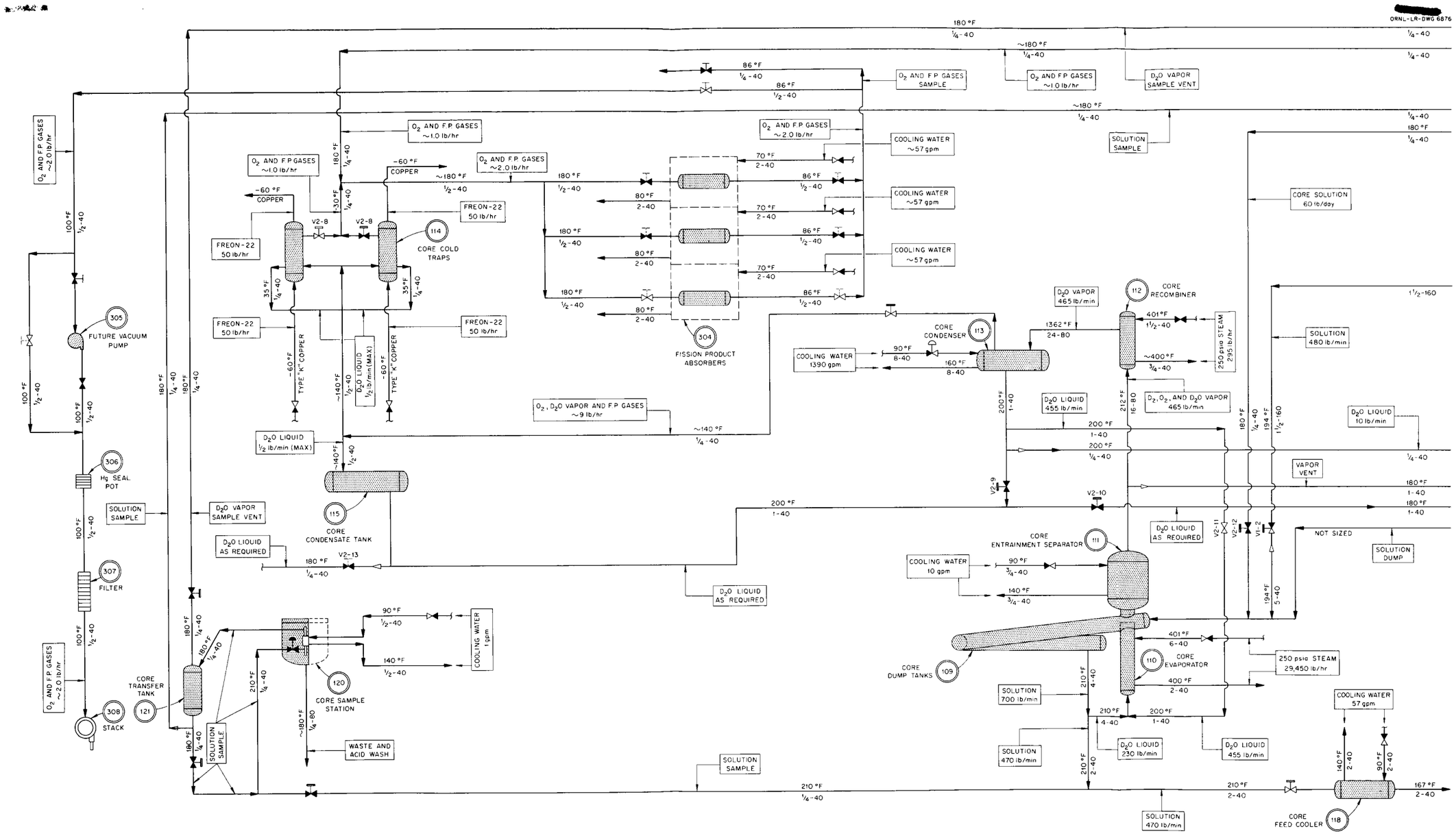

Fig. 2.4. Reactor Process Flow Diagram, Part I.

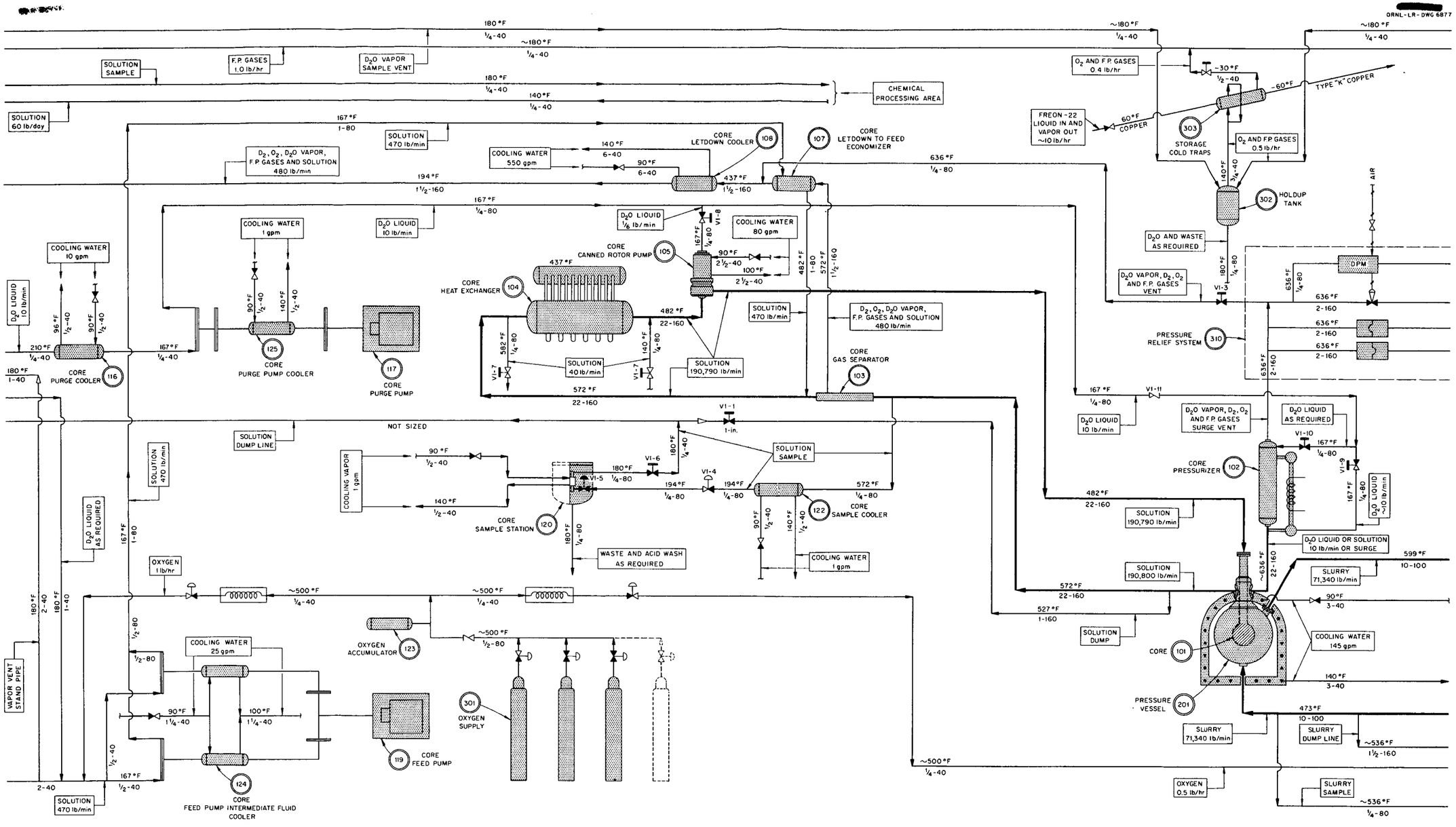

Fig. 2.5. Reactor Process Flow Diagram, Part II.

[redacted]
ORNL-LR-DWG 6878

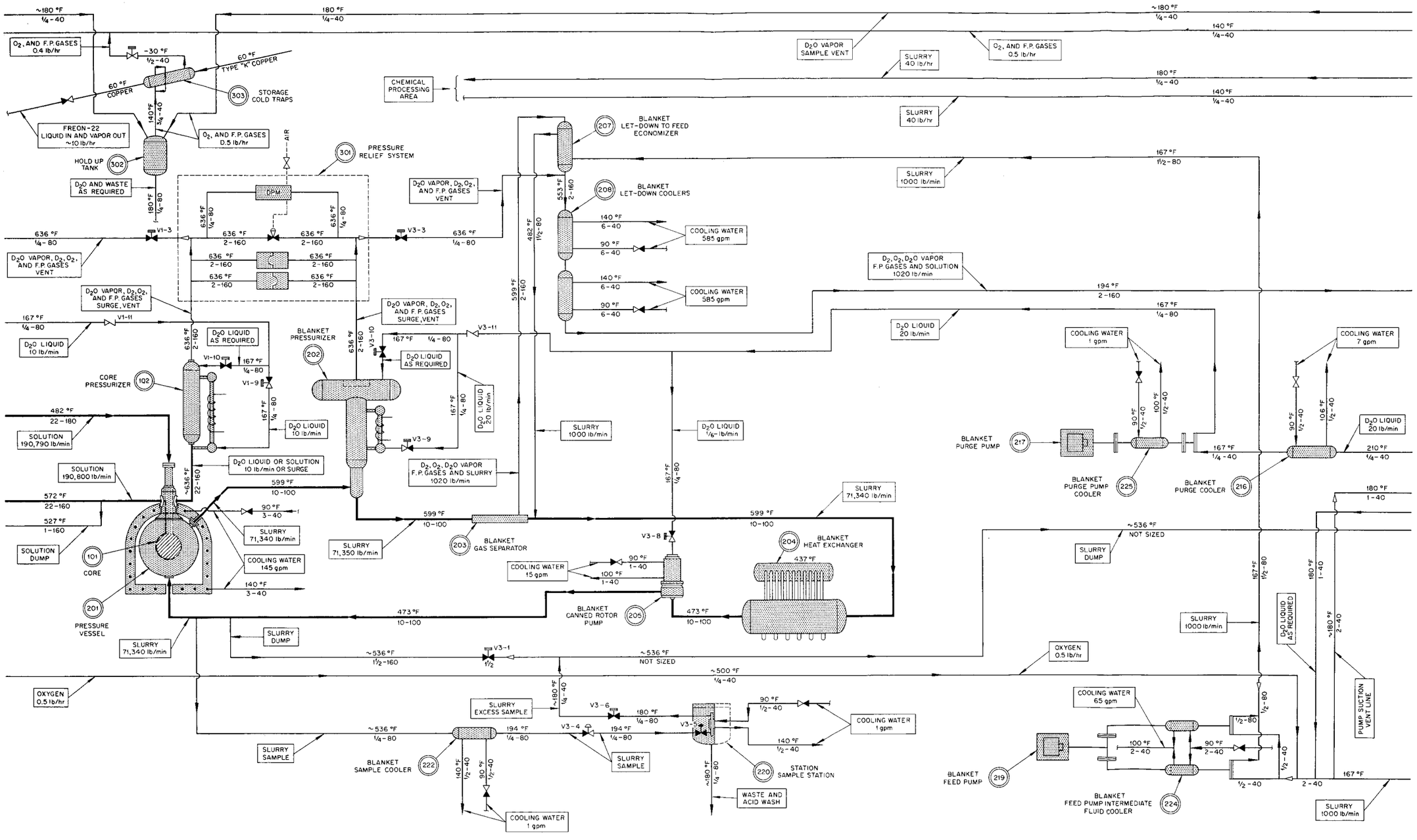

Fig. 2.6. Reactor Process Flow Diagram, Part III.

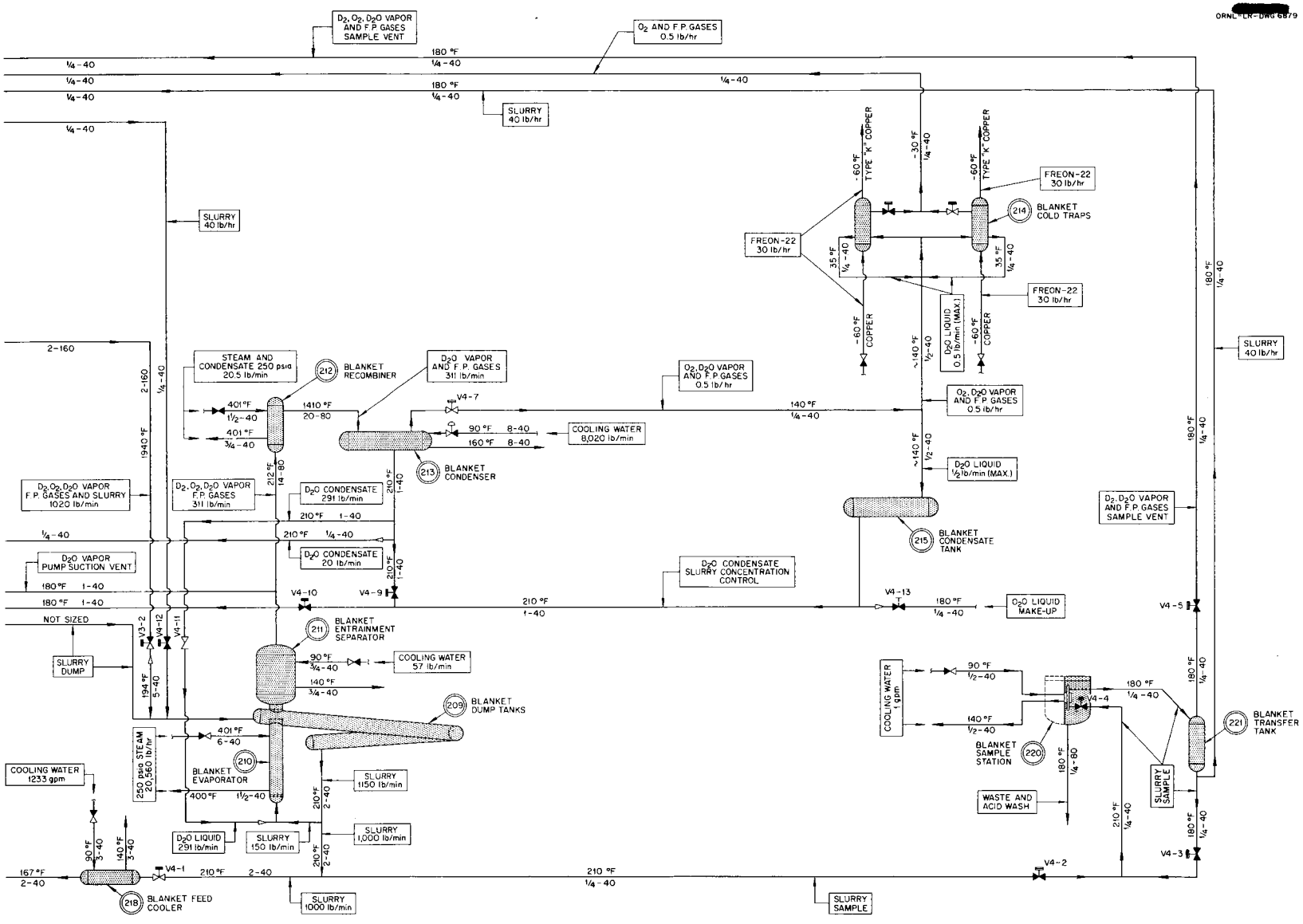

Fig. 2.7. Reactor Process Flow Diagram, Part IV.

[redacted]
ORNL-LR-DWG 6880

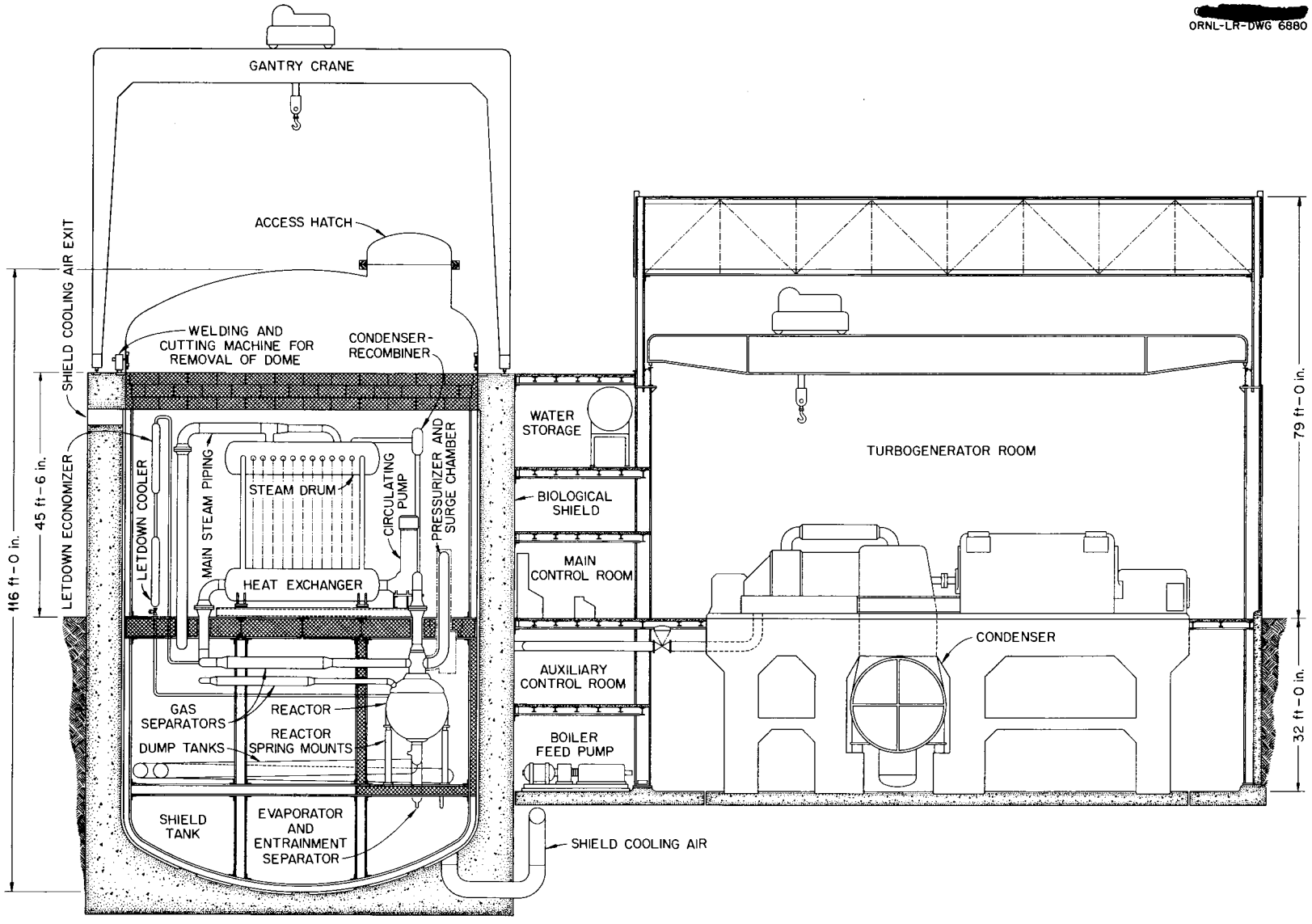

Fig. 2.8. TBR Power Plant (Elevation).

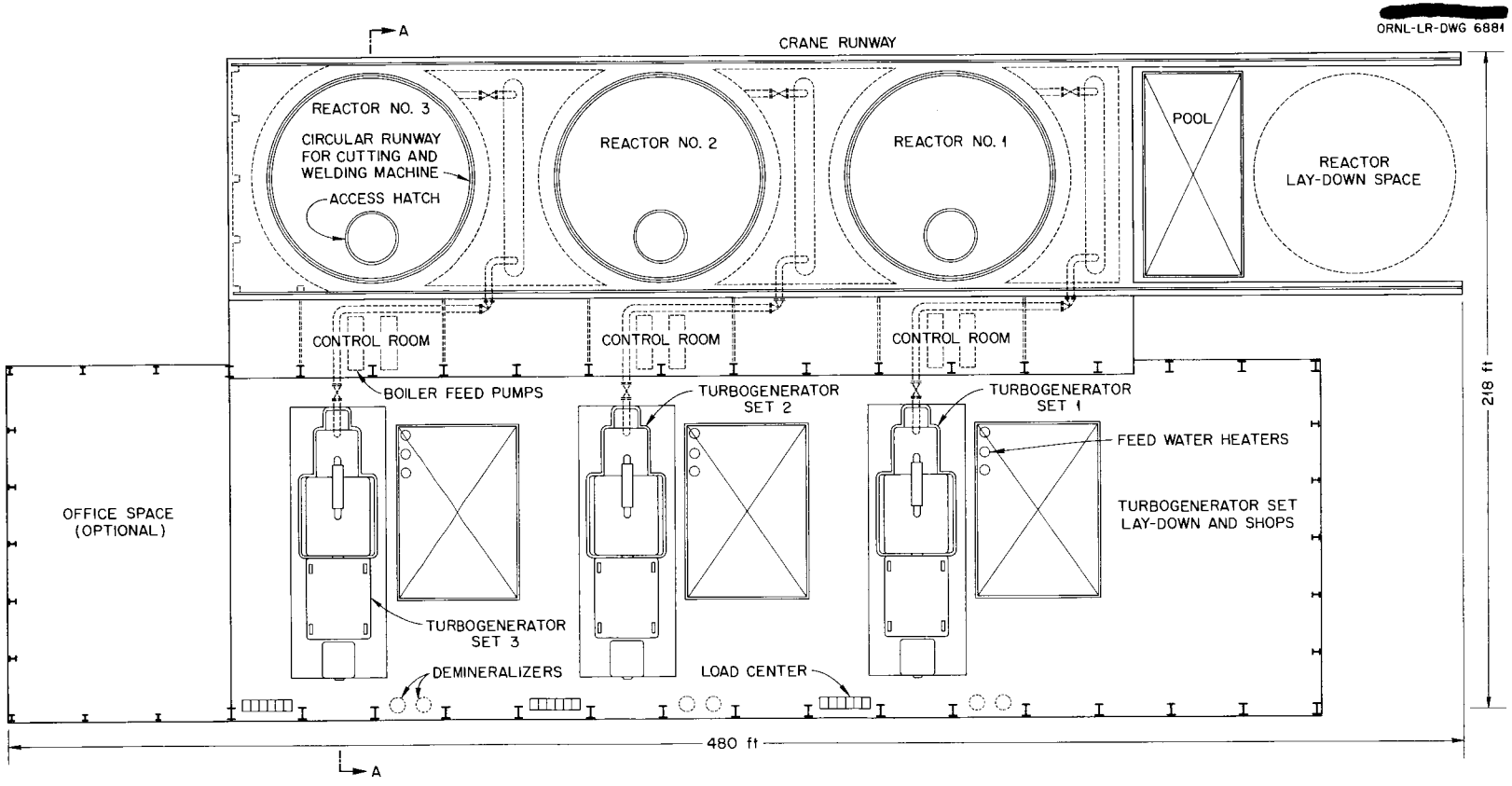

Fig. 2.9. TBR Power Plant (Plan View).

control equipment for cooling water, steam, etc. not otherwise necessary in the main control room. Undesignated areas over the main control room are also shown. It is anticipated that equipment requiring elevation, such as water storage tanks, deaerating feed-water heaters, and power-plant evaporators, normally found in a power plant may be located here. Also, part of the control area can be utilized for office space, wash rooms, etc. and will provide space for elevator hatches and stairways.

The reactor plant occupies a space 80 ft wide and 300 ft long that is 45 ft 6 in. above ground level. A storage pool is located at one end of the structure for items freshly removed from the shield tank. A gantry crane services the reactors, and the runway extends a distance beyond the shield in order to provide access to the pool and to provide lay-down space for a reactor shield tank dome. Three cylindrical shield tanks are provided to contain the reactors, the steam generators, and most of the radioactive components. The problems considered in laying out the systems for each tank are discussed below.

(a) Equipment Rupture. – In the event of a line rupture or equipment failure resulting in gross leakage of reactor fluids, the resultant leakage products must be contained. This is accomplished in the proposed layouts by placing the reactor and components in a cyclindrical tank 66 ft in diameter by 116 ft in height. Seven to eight feet of concrete is poured around this tank to a height of 45 ft 6 in. above ground level for biological shielding. Calculations indicate that the pressure in the tank may rise to 50 psig in the event of a catastrophic rupture of the reactor. Normally, the tank will operate at a pressure of 7.5 psia.

(b) Equipment Maintenance. – All maintenance in the tank must be accomplished remotely behind shielding. It will be observed that items such as circulating pumps, pressurizer heater elements, and evaporators, for which the probability of maintenance is high, are grouped on one side of the tank and are more or less under an access hatch in the tank dome. This hatch may be removed without removing the dome, and enough of the top shielding blocks may be displaced for access to these items from above. For servicing the reactors, the following procedure might be used:

1. The lower half of the tank may be flooded with water for partial shielding from the reactor and dump tanks.

2. A lead coffin equipped with remote manipulators and large enough to contain a man can be constructed. This coffin may be lowered from the gantry crane through the access hatch to a position adjacent to the equipment to be serviced. If the radiation is too intense, a team may work until each man has received his maximum radiation dosage.

The circulating pumps are shown welded to the steam generator and cannot be removed without removing the steam generators too. However, the pumps are constructed in such a way that the electrical components and impeller shaft and bearings can be removed without removing the pump; hence, it may be practicable to service the pumps in place.

If one of the steam generators should fail, it would have to be removed from the shield. To do this the circulating pump would also have to be removed, since it has a welded tie to the generator. To facilitate this procedure, only two flanged connections in the high-pressure system are provided, and both flanges face upward for access to the bolting from above. To gain access to the steam generators, the top dome of the shield tank must be removed. With such a large tank designed for 50 psig internal pressure, bolting of the tank in place is not considered feasible. Hence the dome is welded to the tank and may be removed with a specially designed cutting and welding machine guided by circular tracks. After the dome is removed, the top shield plugs may be removed. As before, the bottom half of the flanged pipe connections is above the top level of flooding; hence, when the system is opened, light water cannot get into the reactor and contaminate the heavy water. The coffin can now be lowered to the system piping, the flanged connections can be disconnected (also the steam piping, etc.), and the entire unit can be removed and transported to the storage pool. A new standby unit can then be lowered and connected. The old unit may be allowed to remain in the pool until the radioactivity has decayed sufficiently to permit maintenance. At all times, air must be exhausted from the tank when it is open, in order to maintain a draft into the opening to prevent spread of activity to adjoining operating areas. When the entire dome is removed, the opening is too large for general

exhaust and ducts must be temporarily installed to the locations where the process system is to be opened.

If maintenance is required on the equipment below the level of the steam generator, the entire process system must be not only drained but also washed with nitric acid to reduce the residual activity enough to permit either essentially complete disassembly of the reactor or exposure of personnel at below-tolerance levels for fairly long periods of time.

(c) Pipe Stresses and Minimum Inventory. – In the high-pressure fuel and blanket systems particular consideration must be paid to pipe stresses arising from thermal expansion and to nonproductive external holdup of fluids. Obviously, these are conflicting desiderata. If the reactor, the circulating pump, and the steam generator are all at anchor points, the piping must be sufficiently flexible to absorb expansion. This implies a number of loops and bends in the pipe, since bellows-type expansion joints probably do not have the reliability required. Excessive loops and bends will greatly increase the holdup. However, if only the circulating pump is fixed and the reactor and steam generator are allowed to move with the piping, both low holdup and reasonably low pipe stresses may be obtained. It will be noted in the layouts that this scheme has been followed. The circulating pump is bolted to the framework supporting the steam generator, and the latter is supported on rollers similar to the mounting of high-pressure boiler drums. The reactor is mounted on spring supports similar to the mounting of the turbine condensers.

(d) Tank and Shield Cooling. – Considerable amounts of heat will be generated within the tank and in the concrete shielding from thermal and radioactive sources. To remove this heat a shield cooling-air supply duct is indicated. Calculations have not been made to prove the effectiveness of such a system, but, in theory, air is introduced through an annulus between the cylindrical steel tank and the concrete shield. Space coolers will also be used to cool the contents of the shield as required, and cooling coils may need to be placed in the concrete near the reactor.

2.2.3 Turbogenerator Plant

(a) Turbine Cycle Heat Balance. – The heat balance for the TBR turbine cycle has been completed. Three stages of feed-water heating and one stage of moisture separation are employed, as shown in Fig. 2.10. The choice of the turbine will depend on the exhaust end required to handle the steam flow at $1\frac{1}{2}$ in. Hg absolute pressure when 106 Mw of power is developed, which figure includes the auxiliary power requirements of the reactor and turbine plant.

(b) Quick-Closure Valves. – If a leak develops in the main heat exchanger of either the core or blanket system, the steam flow to the turbine must be shut off immediately to prevent the spread of contamination beyond the biological shield. According to information received from turbine manufacturers, the throttle valves furnished as a part of the turbine can be closed in half a second or less, the speed of operation being independent of size or steam pressure. In the TBR design, the turbine throttle valve is used in combination with a holdup drum for immediate action, and additional motor-operated, isolation valves are provided in the steam exits from the reactor tank, thus allowing a reduction in the design pressure requirements of the subsequent steam piping and holdup drum. All the valves will be energized simultaneously on indication of radioactive release.

2.2.4 Reactor Component Design

Preliminary conceptual design of nearly all the reactor components has been completed. Designs of some of the major items of equipment which have been evolved are presented below.

(a) Reactor Vessel and Pressurizer. – A possible design of a reactor vessel and core-system pressurizer is shown in Fig. 2.11. The basic dimensions of the reactor vessel are the same as those reported heretofore.[10] From a consideration of the power-density distribution in the reactor[11] it is apparent that considerable boiling would take place in the blanket next to the core vessel wall unless means are provided for high circulation in this area. One possible method is to divide the blanket inlet flow into three streams: the first passes between the thermal shield and the pressure-vessel wall as a coolant, the second stream passes into the main body of the blanket at comparatively low velocity, and the third stream is

[10] R. B. Korsmeyer *et al.*, *HRP Quar. Prog. Rep. Oct. 31, 1954*, ORNL-1813, Fig. 2.11, p 55.

[11] R. B. Korsmeyer *et al.*, *HRP Quar. Prog. Rep. Jan. 31, 1955*, ORNL-1853, Fig. 2.13, p 52.

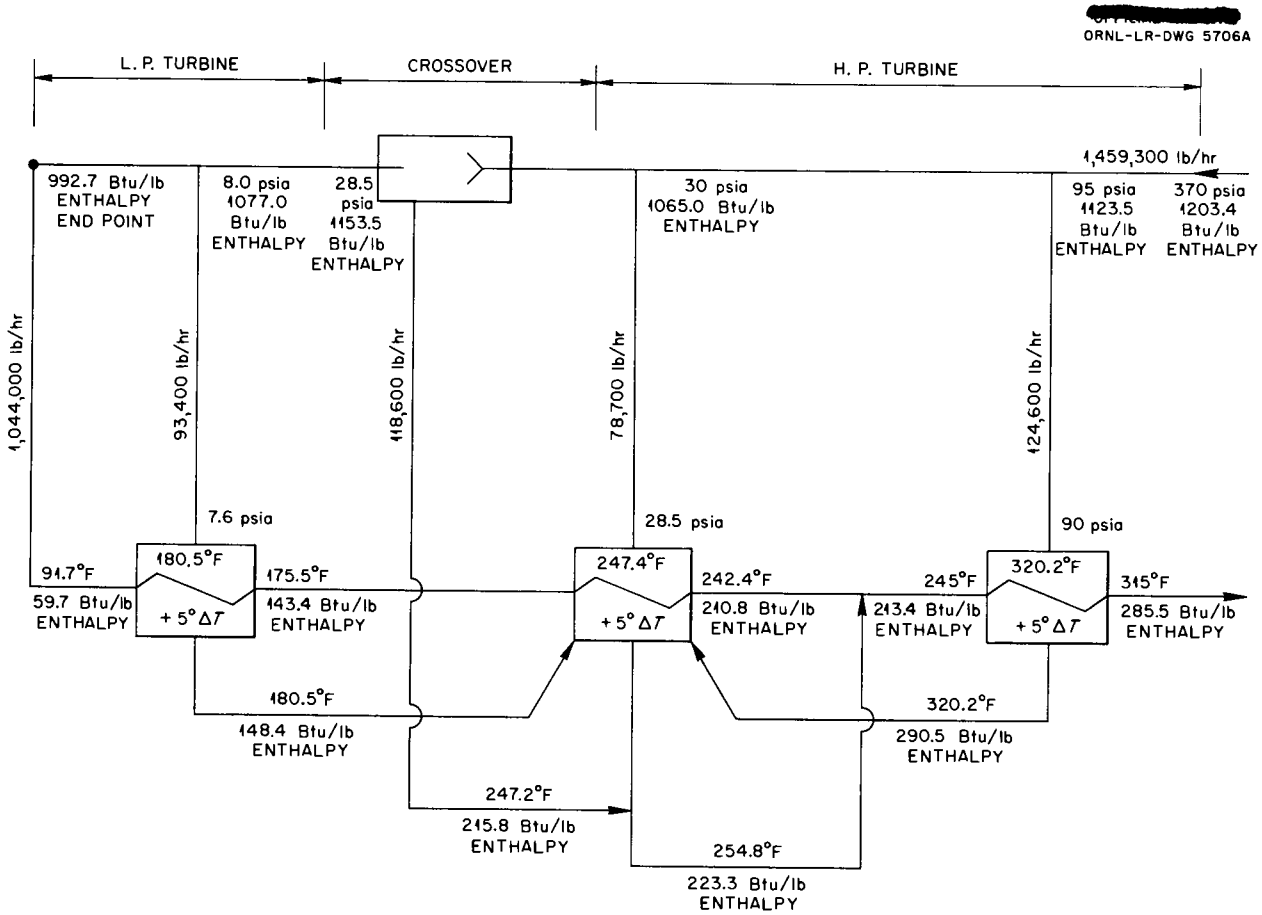

Fig. 2.10. Turbine Cycle Heat Balance.

directed with much greater velocity around the core vessel by means of a spherical baffle set at an appropriate distance from the core wall.

For safety considerations in the event of a rapid increase in reactivity, a surge volume, which can accommodate liquid expelled from the core on rapid temperature rise, is closely connected to the reactor core. In order to limit the pressure surge within the core vessel to about 400 psi, a surge volume of at least 1000 liters above the liquid surface is required, and it must be located not more than 10 ft from the core, with the cross section of the connecting pipe not less than 2 ft^2. As shown in Fig. 2.11, a surge volume of adequate capacity is connected to the core outlet on the opposite side from the main circulation piping to minimize the size of pipe connections required. The surge volume also serves as the pressurizer which maintains the total pressure of the core fluid at 2000 psi. The overpressure is developed by heating the fluid in parallel legs in the base of the surge volume.

The blanket pressurizer (not shown but of similar design) is connected to a separate opening in the pressure vessel. Provision is made to introduce a small stream of D_2O to keep the ThO_2 slurry at a low concentration in the heated region. In both pressurizers a small bleed-off of steam is provided to prevent accumulation of noncondensable gases. Tentative specifications for core and blanket pressurizers are shown in Table 2.2.

(b) **Core and Blanket Circulating Pumps.** – A single canned-rotor centrifugal pump is specified for each of the two main circulating loops. The pumps are sized for operating in the cold legs of each circuit at full reactor power, with an internal pressure of about 2000 psi. The system parameters used in sizing the pumps are shown in Table 2.3.

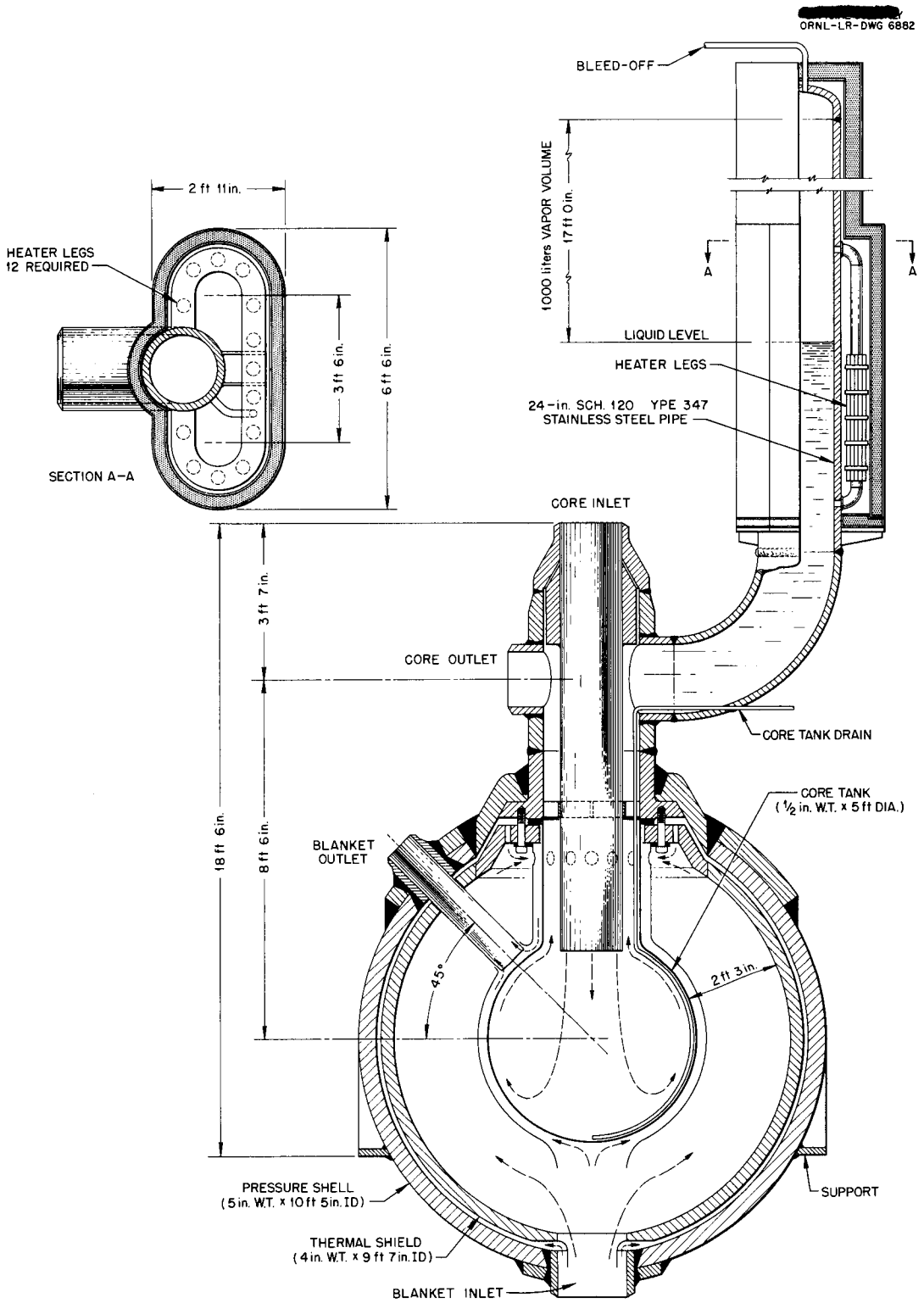

Fig. 2.11. Reactor Vessel and Pressurizer.

[redacted]

TABLE 2.2. PRESSURIZER SPECIFICATIONS

Operating temperature, °F	635 (335°C)
Operating pressure, psia	2000
Material	Type 347 stainless steel
Nominal heating capacity, kw	100
Steady-state heat losses, kw	11
Approximate time to pressurize	1 hr 45 min
Approximate fuel holdup, lb	570
Vapor volume, liters	1000
Maximum allowable heater wall stress, psi	12,000
Maximum strip-heater sheath temperature, °F	1200
Allowable heater power density, w/in.^{2}	12
Allowable heater rating, w	1390
Initial heat requirements, kwhr	175
Maximum purge rate, gph	20
Maximum operating heat flux, kw/ft^2	2.25
Operating temperature of heaters, °F	930
Maximum operating power, kw	64
Heat flux into fluid, Btu/hr·ft^2	7700

TABLE 2.3. CIRCULATING-PUMP SPECIFICATIONS

System Parameters	Core Pump	Blanket Pump
System pressure, psi	2000	2000
Temperature (cold leg), °F	482	473
Density, lb/ft^3	56.8	125
Flow rate, lb/min	190,300	70,300
Pump head, psi	68 (173 ft)	75 (86 ft)
Pumping load, hp	996	184
Efficiency (E), %	70 to 75	70 to 75
Power to pump, shaft hp	1422 ($E = 70$)	263 ($E = 70$)
Impeller diameter, in.	15	11
Synchronous pump speed, rpm	1800	1800

The pump heads are based upon calculated pressure drops across the heat exchangers, gas separators, reactor, and piping; they are summarized in Table 2.4. The expected efficiencies are based upon operating experience with smaller pumps of this type.

Degassed D_2O, at a pressure of 2000 psi, is introduced into the pump can above the motor section. This flow (10 lb/min to the core pump and 20 lb/min to the blanket pump) is effective in removing gases which may accumulate in the motor section. In flowing down over the shaft and

TABLE 2.4. SYSTEM PRESSURE DROPS

	Core Loop		Blanket Loop	
	psi	ft	psi	ft
Gas separator	8.0	20.3	16.0	18.4
Heat exchanger	43.9	111.0	43.6	50.2
Reactor	14.4	36.5	12.2	14.1
Lines	1.8	4.6	3.2	3.7
Total	68.1	172.6	75.0	86.4

upper section of the impeller, the D_2O limits entry of radioactive loop fluids into these parts. The D_2O passes into the high-pressure circulating loops at the impellers.

Light water flowing through heat exchangers built into each pump removes excess heat. This water, circulating at low pressure, is completely separate from the high-pressure system.

(c) Core and Blanket Steam Generators. – The main heat exchangers in the reactor station are the core and blanket steam generators. The designs of these items have been optimized for the number of tubes which will give the lowest annual charges when inventory, pumping, and capital costs are considered. The core unit is designed to transfer 1,219,000,000 Btu/hr (357 Mw) and the blanket unit is designed to transfer 293,000,000 Btu/hr (83 Mw) from the core fluid and blanket slurry, respectively, to generate steam at 437°F (370 psia). The tubes are stainless steel welded into stainless-clad tube sheets. The channels and nozzles can be designed for minimum holdup volume without causing channeling of flow through the tube bundle by providing filler pieces for a standard dished head or by designing a special transition nozzle.

The specifications for both core and blanket generators complete with risers and steam drums are shown in Table 2.5, and side and end elevations of the design are shown in Fig. 2.12.

(d) Recombiners. – The recombiners for the core and blanket systems are of the low-pressure, catalytic type, containing $^1/_8 \times {}^1/_8$ in. cylindrical pellets of 0.3% platinized alumina in a cylindrical annulus. Sufficient catalyst is provided to assure complete recombination of the deuterium and oxygen at maximum power, resulting in bed volumes of 3 and 2 ft^3 for the core and blanket recombiners, respectively.

Due to the extremely exothermic reaction, the water vapor leaves the recombiners superheated several hundred degrees. Consequently, the exit pipe is several sizes larger than the inlet pipe. A typical cross section for the core recombiner is shown in Fig. 2.13.

To assure dryness of the bed, the inlet pipe is jacketed (not shown) so that plant steam can be used to heat the gases from the dump-tank evaporators during startup periods.

(e) Core and Blanket System Dump Tanks. – Dump tanks are required for the core and blanket systems of the TBR in order to provide ever-safe storage capacity for the contents of the systems in the event of a complete dump for maintenance purposes and to provide surplus fuel and moderator for operation of the reactor. For storage of a solution containing fissile material, the design is limited to tanks of comparatively small diameter (or large pipes) arranged horizontally.[12] A further requirement of the dump-tank system is that the solution or slurry must be maintained in circulation in order to keep the contents well mixed. A proposed dump-tank system for the TBR core and blanket is shown in Figs. 2.14 and 2.15. As can be seen, the dump tanks are located concentrically inside the reactor tank, with an evaporator on one end of each. A circulating loop is provided by means of a pipe from the opposite end of the tank to the bottom of the evaporator. The evaporator has an entrainment separator at the top, since the steam used to dilute the radiolytic gas is generated at this point. Tentative specifications for the core and blanket tanks are given in Table 2.6.

(f) Fission-Gas Disposal System. – The method proposed for disposal of fission gases from the TBR is the same as that employed in the HRT; the fission gases and excess oxygen are taken from the cold traps to beds of activated charcoal. The beds provide sufficient holdup time to reduce the activity so that the gases may be discharged through a stack to the atmosphere.

The design of the system is strongly influenced by the 10-year half-life Kr^{85} activity, which cannot be reduced significantly by reasonable holdup times. If the reactor station is located in a populated area (i.e., no large exclusion area) a stack about 250 ft tall will permit discharge of all the

[12] R. B. Korsmeyer *et al.*, *HRP Quar. Prog. Rep. Jan. 31, 1955*, ORNL-1853, Fig. 2.12, p 52.

TABLE 2.5. STEAM GENERATOR SPECIFICATIONS

	Core	Blanket
Reactor fluids, forced circulation		
Inlet temperature, °F	572	599
Outlet temperature, °F	482	473
Flow rate, lb/hr	11,448,000	4,280,000
Pressure, psia	2000	2000
Velocity through tubing, fps	17.8	11.8
Steam, natural recirculation		
Feedwater temperature, °F	315	315
Generation temperature, °F	437	437
Pressure, psia	370	370
Generation rate, lb/hr	1,326,000	319,000
Heat load		
Btu/hr	1,219,000,000	293,000,000
Mw	357	83
Steam generator		
Number of $\frac{3}{8}$-in. 18 BWG tubes	7800	1950
Number of tube passes	1	1
Effective length of tubing, ft	24.1	23.1
Heat transfer surface, ft^2	18,450	4420
Shell internal diameter, in.	61	30
Shell thickness, in.	5	$2\frac{1}{2}$
Tube sheet thickness, in.	$8\frac{1}{4}$	$4\frac{3}{8}$
Reactor fluid connections, in. NPS	22	10
Feedwater connection, in. NPS	10	6
Number of risers	12	12
Number of downcomers	6	6
Size of risers ond downcomers, in. NPS	10	5
Steam drum		
Internal diameter, in.	60	36
Length, ft	18	18
Wall thickness, in.	$1\frac{7}{8}$	$1\frac{7}{8}$
Height above generator, ft	20	15
Steam nozzle, in. NPS	20	10

[redacted]

[redacted]

[redacted]
ORNL-LR-DWG 6884

	A	B	C	D	E	F	G
CORE	20 ft	65 in.	20 in.	22 in.	66 in.	18 ft	28 ft
BLANKET	15 ft	38 1/2 in.	10 3/4 in.	10 3/4 in.	32 1/2 in.	15 ft.	25 ft

[redacted]

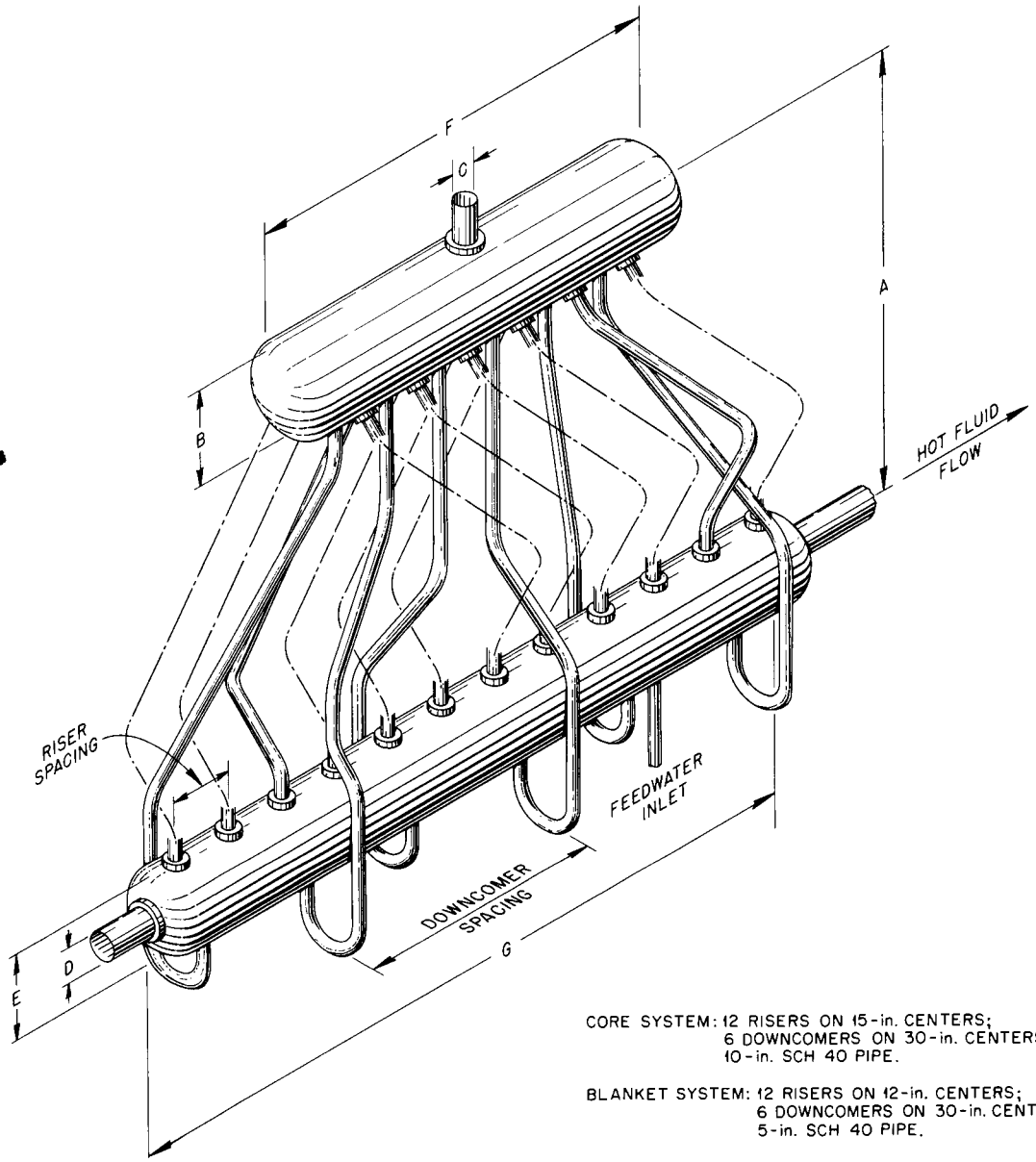

CORE SYSTEM: 12 RISERS ON 15-in. CENTERS;
6 DOWNCOMERS ON 30-in. CENTERS.
10-in. SCH 40 PIPE.

BLANKET SYSTEM: 12 RISERS ON 12-in. CENTERS;
6 DOWNCOMERS ON 30-in. CENTERS.
5-in. SCH 40 PIPE.

Fig. 2.12. Steam Generator.

[redacted]
ORNL-LR-DWG 6885

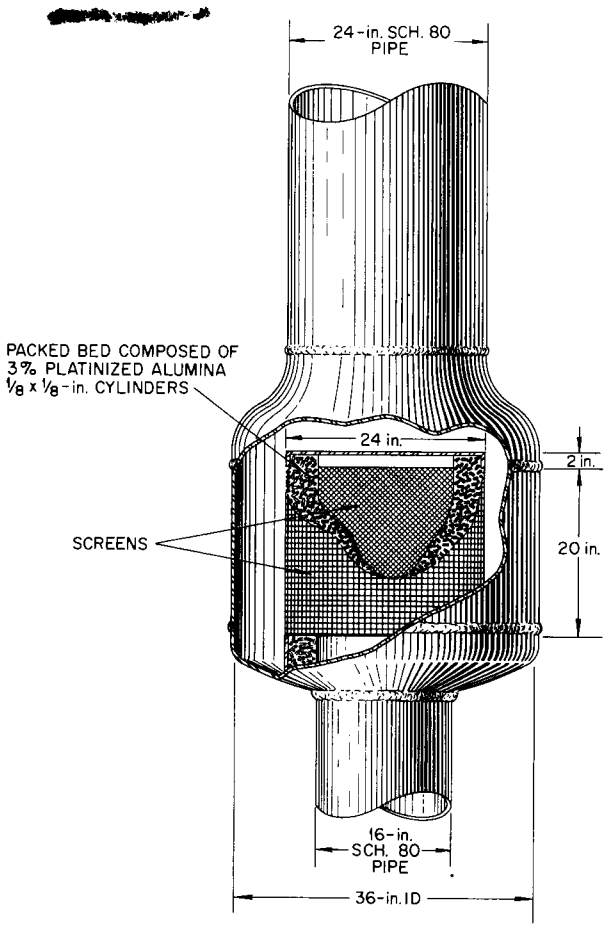

Fig. 2.13. Core Recombiner.

Kr^{85} produced by three reactors under nearly all meteorological conditions. The charcoal beds are designed to remove essentially all other activities and to provide storage for periods of adverse weather when the stack discharge rate must be reduced.

The conditions for which the beds are designed are as follows: pressure, 14.7 psia; average temperature, 30°C; xenon holdup time, 200 days; oxygen flow rate, 0.25 scfm. The size of the beds is quite sensitive to the amount of oxygen dilution. The stated oxygen flow is equivalent to a concentration of 50 and 25 ppm above the stoichiometric quantities of radiolytic gas in the letdown streams from the core and blanket, respectively. For the above conditions, 6900 lb of charcoal per reactor

[redacted]
ORNL-LR-DWG 6886

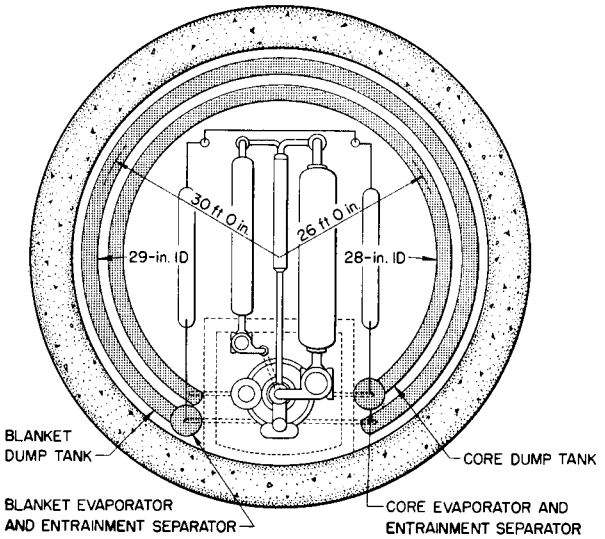

Fig. 2.14. TBR Dump Tanks (Plan View).

[redacted]
ORNL-LR-DWG 6887

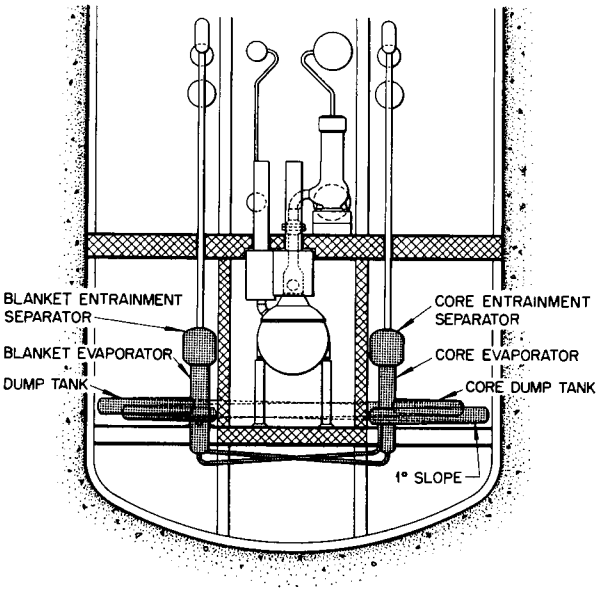

Fig. 2.15. TBR Dump Tanks (Elevation).

is required. This is divided among three beds, each having the dimensions shown in Fig. 2.16. In operation, 85 kw of heat is generated in each bed by radioactive decay. Therefore, the beds are kept cool by immersion in a pool of water.

TABLE 2.6 DUMP-TANK SPECIFICATIONS

	Core	Blanket
Volume – high-pressure system, ft^3	344	487
Volume – condensate tanks, ft^3	60	25
Volume – high-pressure system and condensate tanks, ft^3	404	512
Required volume of dump tank, ft^3	517	730
Radius of dump tank, ft	26	30
Minimum length of dump tank, ft	122	159
Inside diameter of dump tank, in.	28	29
Fuel inventory, kg of $U^{235} + U^{233}$	27.1	45.1
Linear concentration of fuel, kg/ft	0.22	0.28
Design pressure, psig	600	600
Design temperature, °F	500	500
Material	Type 347 stainless steel, HRP specifications	
Wall thickness, in.	3/4	3/4
Corrosion allowance, in.	0.12	0.09

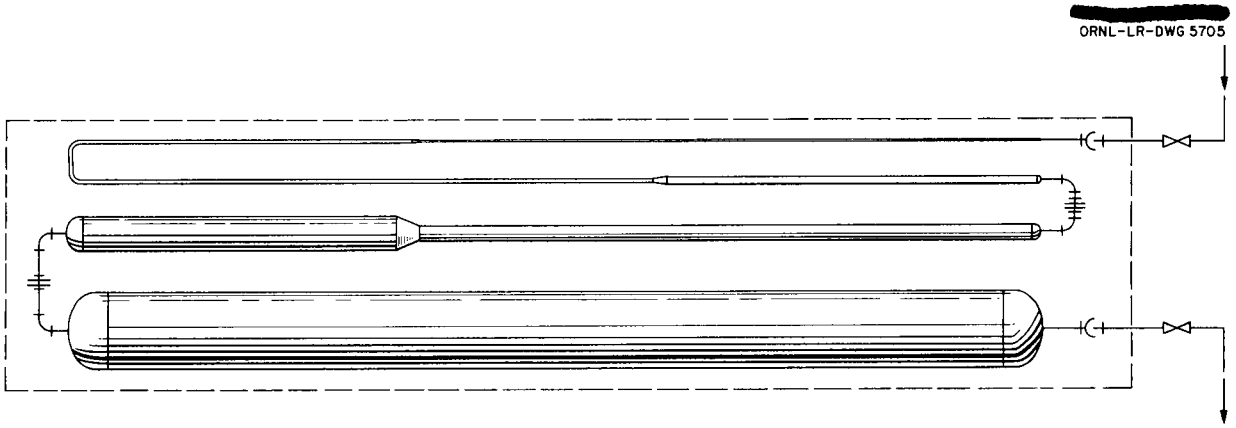

SECTIONS CONTAINING CHARCOAL:

PIPE SIZE	LENGTH	PIPE SIZE	LENGTH
1/2 in.	15 ft	4 in.	15 ft
1 in.	25 ft	10 in.	10 ft
2 in.	10 ft	24 in.	25 ft

TOTAL CHARCOAL: 77 ft^3 (2300 lb)

Fig. 2.16. Typical Charcoal Adsorber.

Part III

CORROSION

E. G. Bohlmann

3. PUMP-LOOP CORROSION TESTS

J. C. Griess H. C. Savage
R. S. Greeley
S. A. Reed
F. J. Walter

3.1 PUMP-LOOP OPERATION AND MAINTENANCE

H. C. Savage F. J. Walter

3.1.1 Loop Status

(a) Solution. – Operation of 13 dynamic-corrosion test loops is proceeding in a routine manner, with no significant changes or difficulties. Test loops K, L, and M are being used to make long-term measurements of the corrosion of stainless steels by the uranyl sulfate solution composition presently planned for the HRT. Table 3.1 shows the operating conditions and total accumulated operating time to date for these long-term experiments.

(b) Slurry. – The 100A loop Cs,[1] which was designed to measure the corrosion of various materials by thorium oxide slurries, began operation during this quarter. Loop operation and control have been checked by isothermal operation with water at 250 and 300°C. The system is now operating with 280 g of thorium (as ThO_2) per kilogram of H_2O containing approximately 1000 ppm dissolved oxygen at 250°C and approximately 900 psig. In the test now in progress, the five sample barrels contain different types of standard pin and coupon corrosion specimens exposed to bulk flow velocities ranging from 9 to 78 fps.

[1]H. C. Savage, F. J. Walter, and R. M. Warner, *HRP Quar. Prog. Rep. Oct. 31, 1954*, ORNL-1813, p 63 and Fig. 3.2, p 66.

3.2 RESULTS OF LOOP TESTS

J. C. Griess R. S. Greeley

3.2.1 Introduction

The Dynamic Corrosion Group has continued to test the corrosion resistance of several different alloys to uranyl sulfate solutions. In addition, the corrosion resistance of several stainless steels to nitric, chromic, sulfuric, and phosphoric acids has been studied, with the expectation that the results may be helpful in the interpretation of the data obtained with uranyl sulfate solutions. Preliminary runs in which a salt of sulfuric acid was incorporated in the uranyl sulfate solution have shown a substantial decrease in the extent of corrosion, both at high and low flow rates. The results of all experiments completed during the past quarter are reported in the following sections.

3.2.2 Results

(a) General Corrosion Rates. – It has been the custom in past quarterly reports to present all of the pin data obtained during the quarter in tabular form. In the present report the pin data are presented in Table 3.2. The form of the table is the same as that used in previous reports,[2] and the

[2]J. C. Griess, J. M. Ruth, and R. E. Wacker, *HRP Quar. Prog. Rep. Jan. 1, 1953*, ORNL-1478, Table 8, p 65; also, ORNL-1554, p 51; ORNL-1605, p 76; ORNL-1658, p 46; ORNL-1678, p 51; ORNL-1753, p 64; ORNL-1772, p 62; ORNL-1813, p 68; ORNL-1853, p 57.

TABLE 3.1. LONG-TERM LOOP TESTS WITH HRT SOLUTION

Composition of solution: 0.04 *m* UO_2SO_4 + 0.006 *m* H_2SO_4 + 0.005 *m* $CuSO_4$ + 1000 ppm O_2

Loop	Temperature (°C)	Pressure (psi)	Over-all Generalized Corrosion Rate Based on Nickel Analysis (mpy)	Total Accumulated Time* (hr)
K	300	1500	0.06	5350
L	200	500	0.07	2500
M	250	900	0.05	4678

*Through April 11, 1955.

TABLE 3.2. CORROSION RATES OF PIN-TYPE CORROSION SPECIMENS IN URANYL SULFATE SOLUTIONS

Run No.	Test Conditions: UO_2SO_4 Concentration (m)	Temperature (°C)	Time (hr)	Additions	Flow Rate (fps ± 10%)	Pin Material	Number of Pins	Corrosion Rate (mpy): Minimum	Average	Maximum
A-73	0.17	250	15	1000–2000 ppm O_2	18	Type 302B SS (stainless steel)	2	250	270	280
						304L SS	7	95	100	110
						309 SCb SS	4	66	75	84
						322W SS	1		120	
						322W SS[a]	1		140	
						347 SS	8	86	100	150
						347 SS[b]	1		120	
						17-4 PH SS	1		180	
						17-4 PH SS[a]	1		140	
						17-7 PH SS	1		110	
						17-7 PH SS[a]	1		140	
					61	304L SS	6	100	120	130
						304 SS[b]	1		120	
						309 SCb SS	4	72	81	96
						321 SS	4	77	96	110
						347 SS	12	87	110	120
						347 SS[b]	1		130	
A-74	0.17	250	1000	1000–2000 ppm O_2	19	302B SS	2	13	15	16
						304L SS	3	12	47	49
						309 SCb SS	3	6.2	6.6	7.4
						316 SS	2	14	18	21
						316L SS	2	26	34	41
						321 SS	3	9.5	18	25
						322W SS	1		5.8	
						322W SS[a]	1		1.9	
						347 SS	6	5.8	6.9	8.4
						347 SS[b]	1		130	
						17-4 PH SS	1		3.5	
						17-4 PH[a] SS	1		3.6	
						17-7 PH SS	1		3.5	
						17-7 PH SS[a]	1		2.7	

TABLE 3.2 (continued)

Run No.	Test Conditions: UO_2SO_4 Concentration (m)	Temperature (°C)	Time (hr)	Additions	Flow Rate (fps ± 10%)	Pin Material	Number of Pins	Corrosion Rate (mpy): Minimum	Average	Maximum
A-75	0.17	250	400	1000–2000 ppm O_2	19	347 SS	12	16	22	32
						430 SS	2	3.8	9.0	14
						443 SS	2	25	44	62
						446 SS	2	7.5	59	110
						Titanium alloy[c]	2	0.77	0.81	0.84
A-76	0.17	250	201	1000–2000 ppm O_2 0.1 m Na_2SO_4	16	302B SS	2	2.0	23	25
						304L SS	3	8.1	8.9	9.4
						309 SCb SS	3	3.0	6.4	8.7
						347 SS	3	2.4	9.1	14
						Titanium 75A	1		1.4	
						Titanium, Electromet	1		0.60	
						Zircaloy-2	1		0	
					18	304L SS	5	15	51	71
						309 SCb SS	4	9.9	15	25
						316L SS	3	67	69	71
						321 SS	3	3.3	3.6	4.2
						347 SS	8	22	27	35
						347 SS[b]	1		2.4	
						430 SS	2	1.2	4.7	8.2
						Platinum	1		0.03	
						Titanium RC-55	1		0.76	
A-77	0.17	250	200	1000–2000 ppm O_2 0.075 m Na_2SO_4 0.025 m H_2SO_4	16	304L SS	4	22	27	32
						309 SCb SS	3	18	19	19
						347 SS	4	5.2	20	26
						Titanium 75A	1		0.46	
						Titanium, Electromet	1		0	
						Zircaloy-2	1		0	
					18	304L SS	5	110	110	120
						309 SCb SS	4	98	100	110

TABLE 3.2 (continued)

Run No.	Test Conditions: UO_2SO_4 Concentration (m)	Temperature (°C)	Time (hr)	Additions	Flow Rate (fps ± 10%)	Pin Material	Number of Pins	Corrosion Rate (mpy): Minimum	Average	Maximum
A-77	0.17	250	200	1000–2000 ppm O_2	18	316L SS	3	91	100	110
				0.075 m Na_2SO_4		321 SS	3	110	120	120
				0.025 m H_2SO_4		347 SS	8	37	50	64
						347 SS[b]	1		120	
						430 SS	2	29	30	30
						Platinum	1		0.48	
						Titanium RC-55	1		0.31	
A-78	0.17	250	200	1000–2000 ppm O_2	16	304L SS	4	2.1	2.2	2.3
				0.17 m $MgSO_4$		309 SCb SS	3	2.1	2.2	2.3
						347 SS	4	1.4	1.7	2.0
						Titanium 75A	2	0.15	0.30	0.45
						Zircaloy-2	1		0	
					18	304L SS	5	6.5	7.4	8.2
						309 SCb SS	4	6.2	6.9	8.1
						316L SS	3	5.7	7.0	8.5
						321 SS	3	2.0	5.2	8.7
						347 SS	8	1.6	4.0	6.6
						347 SS[b]	1		5.5	
						430 SS	2	1.2	1.4	1.6
						Platinum	1		0.06	
						Titanium RC-55	1		0.30	
E-34	0.04	175	700	1000–2000 ppm O_2	16	302B SS	1		14	
				0.006 m H_2SO_4		304L SS	4	3.3	4.7	5.7
						309 SCb SS	2	2.4	2.6	2.7
						321 SS	2	4.5	4.6	4.7
						347 SS	5	3.4	5.6	7.2
					31	302B SS	1		34	
						304L SS	8	4.0	4.5	5.1
						309 SCb SS	4	2.6	2.7	2.9

TABLE 3.2 (continued)

Run No.	Test Conditions: UO_2SO_4 Concentration (m)	Temperature (°C)	Time (hr)	Additions	Flow Rate (fps ± 10%)	Pin Material	Number of Pins	Corrosion Rate (mpy): Minimum	Average	Maximum
E-34	0.04	175	700	1000–2000 ppm O_2 0.006 m H_2SO_4	31	316L SS	4	4.9	5.3	5.6
						318 SS	1		4.3	
						321 SS	2	4.4	4.6	4.8
						347 SS	7	4.0	5.5	6.2
						347 SS[b]	1		4.1	
					73	304L SS	4	4.6	5.1	5.7
						309 SCb SS	2	3.2	3.5	3.8
						318 SS	1		8.4	
						321 SS	2	5.2	6.2	7.1
						347 SS	4	5.8	10	23
						347 SS[b]	1		4.8	
E-35	0.04	175	300	1000–2000 ppm O_2 0.006 m H_2SO_4	16	302B SS	1		18	
						304L SS	4	5.4	6.9	8.8
						309 SCb SS	2	2.6	2.8	2.9
						321 SS	2	4.2	4.9	5.5
						347 SS	5	5.5	6.1	6.9
					32	302B SS	1		16	
						304L SS	8	4.8	5.9	6.5
						309 SCb SS	4	2.7	3.0	3.4
						310 SS	1		4.8	
						316L SS	4	5.6	6.3	6.7
						321 SS	2	5.2	5.5	5.7
						322W SS[a]	1		11	
						347 SS	6	5.1	6.0	6.9
						430 SS	1		26	
					71	304L SS	4	6.0	6.8	7.7
						309 SCb SS	2	3.2	3.5	3.8
						318 SS	1		5.7	
						321 SS	2	8.2	8.9	9.5

TABLE 3.2 (continued)

Run No.	Test Conditions: UO_2SO_4 Concentration (m)	Temperature (°C)	Time (hr)	Additions	Flow Rate (fps ± 10%)	Pin Material	Number of Pins	Corrosion Rate (mpy): Minimum	Average	Maximum
E-35	0.04	175	300	1000–2000 ppm O_2 0.006 m H_2SO_4	71	322W SS[a]	1		24	
						347 SS	4	6.2	8.0	8.9
E-36	0.17	250	6	600–800 ppm O_2 120 ppm Mo added as H_2MoO_4	15	316 SS	3	71	73	74
						347 SS	8	62	73	91
						Titanium, Electromet	2		b	
						Zircaloy-2	1		7.2	
					70	316 SS	3	77	86	96
						347 SS	8	65	82	91
						Titanium, Electromet	2	5.1	7.6	10
						Zircaloy-2	1		11	
E-37	0.17	250	200	600–800 ppm O_2 120 ppm Mo added as H_2MoO_4	16	316 SS	3	23	23	23
						347 SS	8	22	23	24
						Titanium, Electromet	2		d	
						Zircaloy-2	1		d	
					70	316 SS	2	210	270	320
						347 SS	8	190	270	340
						Titanium, Electromet	2		d	
						Zircaloy-2	1		d	
E-38	0.17	250	202	200–500 ppm O_2 400 ppm Mo added as H_2MoO_4	16	316 SS	3	81	82	84
						347 SS	8	53	68	82
						Titanium, Electromet	2		d	
						Zircaloy-2	1		d	
					70	316 SS	3	120	130	140
						347 SS	8	140	17	210
						Titanium, Electromet	2	6.2	6.6	7.0
						Zircaloy-2	1		3.5	

TABLE 3.2 (continued)

Run No.	Test Conditions: UO_2SO_4 Concentration (m)	Temperature (°C)	Time (hr)	Additions	Flow Rate (fps ± 10%)	Pin Material	Number of Pins	Corrosion Rate (mpy): Minimum	Average	Maximum
F-51	0.17	250	200	1000–2000 ppm O_2	13	302B SS	1		0.17	
				0.034 m H_2SO_4		304L SS	3	0.17	1.2	2.3
				0.01 m $K_2Cr_2O_7$		309 SCb SS	1		0.68	
				0.03 m $CuSO_4$		347 SS	3	1.1	1.5	2.0
						Platinum	1		0.06	
						Titanium, Electromet	1		0	
						Zircaloy-2	1		*d*	
					74	302B SS	2	510	580	650
						304L SS	3	310	350	370
						309 SCb SS	3	310	340	360
						347 SS	3	320	350	370
						Platinum	1		0.35	
						Titanium, Electromet	1		*d*	
						Zircaloy-2	1		*d*	
F-52	0.17	250	200	1000–2000 ppm O_2	13	304L SS	4	1.7	1.9	2.0
				0.02 m H_2SO_4		309 SCb SS	3	1.5	1.6	1.6
				0.01 m $K_2Cr_2O_7$		347 SS	4	1.5	1.8	1.9
				0.03 m $CuSO_4$		Platinum	1		0	
						Titanium, Electromet	1		*d*	
						Zircaloy-2	1		*d*	
					74	304L SS	4	530	570	620
						309 SCb SS	3	420	500	540
						347 SS	4	640	670	700
						Platinum	1		*d*	
						Titanium, Electromet	1		*d*	
						Zircaloy-2	1		4.0	

TABLE 3.2 (continued)

Run No.	Test Conditions: UO_2SO_4 Concentration (m)	Temperature (°C)	Time (hr)	Additions	Flow Rate (fps ± 10%)	Pin Material	Number of Pins	Corrosion Rate (mpy): Minimum	Average	Maximum
H-55	0.17	250	200	1000–2000 ppm O_2 0.034 m H_2SO_4 0.01 m $K_2Cr_2O_7$	17	302B SS	2	5.8	6.0	6.2
						304L SS	3	4.2	4.3	4.5
						309 SCb SS	3	4.6	4.6	4.7
						347 SS	3	5.2	5.3	5.5
						Platinum	1		*d*	
						Titanium, Electromet	1		0	
						Zircaloy-2	1		0	
					64	302B SS	2	92	130	160
						304L SS	3	250	260	280
						309 SCb SS	3	280	320	360
						347 SS	3	230	250	270
						Platinum	1		0.81	
						Titanium, Electromet	1		0.90	
						Zircaloy-2	1		2.6	
I-23	0.11	200	200	1000–2000 ppm O_2 0.016 m H_2SO_4	12	302B SS	2	19	22	25
						304 SS	1		29	
						304 SS[b]	2	19	20	21
						304L SS	2	19	20	20
						309 SCb SS	2	13	14	14
						310S SS	2	12	12	12
						316 SS[b]	2	25	26	26
						316L SS	1		21	
						318 SS	2	16	17	18
						321 SS	2	17	18	18
						322W SS	2	25	27	28
						322W SS[a]	2	23	24	24
						347 SS	4	23	25	28
						347 SS[b]	2	20	26	31
						410 SS	2	28	40	51
						410 SS[a]	2	52	55	57

TABLE 3.2 (continued)

Run No.	Test Conditions: UO_2SO_4 Concentration (m)	Temperature (°C)	Time (hr)	Additions	Flow Rate (fps ± 10%)	Pin Material	Number of Pins	Corrosion Rate (mpy): Minimum	Average	Maximum
I-23	0.11	200	200	1000–2000 ppm O_2 0.016 m H_2SO_4	12	416 SS	2	52	55	57
						416 SS[a]	2	60	69	77
						420 SS	2	140	150	160
						420 SS[a]	2	98	110	130
						430 SS	2	63	100	140
						440C SS	2	290	410	530
						440C SS[a]	2	72	82	91
						443 SS	2	15	16	16
						446 SS	2	11	12	13
						17-4 PH SS	2	25	26	26
						17-4 PH SS[a]	2	32	36	40
						17-7 PH SS	2	25	26	27
						17-7 PH SS[a]	2	72	81	90
						Carpenter 20 SS	2	12	14	16
						Durimet 20	2	13	24	34
						Misco B	1		19	
						Miscro 4	2	140	160	170
						Stellite 1	2	84	92	100
						Stellite 3	2	440	480	520
						Stellite 6	2	78	85	91
						Stellite 25	2	21	24	26
						Stellite 98M2	2	290	310	320
						Worthite SS	2	13	14	15
						Worthite SS[b]	2	34	120	210
						Incoloy	1		21	
						Inconel	1		190	
						Inconel X	1		54	
						Inconel (low carbon)	1		340	

TABLE 3.2 (continued)

Run No.	Test Conditions					Pin Material	Number of Pins	Corrosion Rate (mpy)		
	UO_2SO_4 Concentration (m)	Temperature (°C)	Time (hr)	Additions	Flow Rate (fps ± 10%)			Minimum	Average	Maximum
I-24	0.02	100	200	1000–2000 ppm O_2 0.005 m H_2SO_4	12	302B SS	2	0.17	0.17	0.17
						304 SS	1		0.42	
						304 SS[b]	2	0.34	0.34	0.34
						304L SS	2	0.25	0.34	0.42
						309 SCb SS	2	0.34	0.34	0.34
						310S SS	2	0.34	0.28	0.42
						316L SS	1		0.25	
						316 SS[b]	2	0.51	0.60	0.68
						318 SS	2	0.17	0.34	0.51
						321 SS	2	0.34	0.34	0.34
						322W SS	2	0.25	0.30	0.34
						322W SS[a]	2	0.17	0.26	0.34
						347 SS	4	0.25	0.27	0.34
						347 SS[b]	2	0.17	0.21	0.25
						410 SS	2	0.17	0.21	0.25
						410 SS[a]	2	20	75	130
						416 SS	2	0.76	4.2	7.7
						416 SS[a]	2	0.76	3.3	5.8
						420 SS	2	360	370	370
						420 SS[a]	2	130	140	150
						430 SS	2	0.17	0.26	0.34
						440C SS	2	840	850	850
						440C SS[a]	2	230	270	310
						443 SS	2	0.17	0.17	0.17
						446 SS	2	0.08	0.13	0.17
						17-4 PH SS	2	0.25	0.38	0.51
						17-4 PH SS[a]	2	0.25	0.25	0.25

TABLE 3.2 (continued)

Run No.	Test Conditions: UO_2SO_4 Concentration (m)	Temperature (°C)	Time (hr)	Additions	Flow Rate (fps ± 10%)	Pin Material	Number of Pins	Corrosion Rate (mpy): Minimum	Average	Maximum
I-24	0.02	100	200	1000–2000 ppm O_2 0.005 m H_2SO_4	12	17-7 PH SS	2	0.34	0.38	0.42
						17-7 PH SS[a]	2	0.17	0.30	0.42
						Carpenter 20 SS	2	0.34	0.34	0.34
						Durimet 20	2	0.42	0.51	0.60
						Misco B	1		0.17	
						Miscro 4	2	1.8	1.8	1.8
						Stellite 1	2	0.68	0.94	1.2
						Stellite 3	2	1.2	1.5	1.8
						Stellite 6	2	0.51	0.68	0.85
						Stellite 25	2	0.25	0.34	0.42
						Stellite 98M2	2	1.3	1.4	1.4
						Worthite SS	2	0.17	0.26	0.34
						Worthite SS[b]	2	0.68	0.72	0.76
						Incoloy	1		0.42	
						Inconel	1		0.42	
						Inconel X	1		0.25	
						Inconel (low carbon)	1		0.51	
I-25	0.02	150	200	1000–2000 ppm O_2 0.005 m H_2SO_4	12	302B SS	2	1.9	2.1	2.3
						304 SS	1		1.1	
						304 SS[b]	2	1.0	1.2	1.4
						304L SS	2	0.87	0.87	0.87
						309 SCb SS	2	0.35	0.44	0.52
						310S SS	2	0.61	0.66	0.70
						316L SS	1		0.61	
						316 SS[b]	2	1.4	1.5	1.5
						318 SS	2	0.52	0.74	0.96
						321 SS	2	0.52	0.65	0.78
						322W SS	2	1.0	1.2	1.3
						322W SS[a]	2	4.1	4.1	4.1
						347 SS	4	0.78	0.87	0.96
						347 SS[b]	2	0.61	0.74	0.87

TABLE 3.2 (continued)

Run No.	Test Conditions: UO_2SO_4 Concentration (m)	Temperature (°C)	Time (hr)	Additions	Flow Rate (fps ± 10%)	Pin Material	Number of Pins	Corrosion Rate (mpy): Minimum	Average	Maximum
I-25	0.02	150	200	1000–2000 ppm O_2 0.005 m H_2SO_4	12	410 SS	2	3.3	24	44
						410 SS[a]	2	37	59	80
						416 SS	2	45	46	47
						416 SS[a]	2	41	52	62
						420 SS	2	65	74	82
						420 SS[a]	2	69	75	80
						430 SS	2	1.5	1.6	1.6
						440C SS	2	270	360	440
						440C SS[a]	2	72	83	94
						443 SS	2	0.52	1.3	2.0
						446 SS	2	0.44	0.57	0.70
						17-4 PH SS	2	1.8	2.0	2.1
						17-4 PH SS[a]	2	1.3	1.6	1.9
						17-7 PH SS	2	0.44	0.77	1.1
						17-7 PH SS[a]	2	90	130	160
						Carpenter 20 SS	2	0.52	0.61	0.70
						Durimet 20	2	0.61	0.91	1.2
						Misco B	1		1.8	
						Miscro 4	2	170	180	190
						Stellite 1	2	2.4	3.3	4.1
						Stellite 3	2	12	19	25
						Stellite 6	2	2.1	2.2	2.2
						Stellite 25	2	1.4	1.5	1.6
						Stellite 98M2	2	12	13	13
						Worthite SS	2	0.61	0.66	0.70
						Worthite SS[b]	2	3.1	3.8	4.5
						Incoloy	1		0.61	
						Inconel	1		0.78	
						Inconel X	1		0.96	
						Inconel (low carbon)	1		32	

TABLE 3.2 (continued)

Run No.	Test Conditions: UO_2SO_4 Concentration (m)	Temperature (°C)	Time (hr)	Additions	Flow Rate (fps ± 10%)	Pin Material	Number of Pins	Corrosion Rate (mpy): Minimum	Average	Maximum
I-26	0.17	200	200	1000–2000 ppm O_2	12	302B SS	2	16	19	22
						304 SS	1		27	
						304 SS[b]	2	27	31	35
						304L SS	2	18	21	24
						309 SCb SS	2	14	15	16
						310S SS	2	15	20	25
						316L SS	1		18	
						316 SS[b]	2	25	27	29
						318 SS	2	20	20	20
						321 SS	2	20	20	20
						322W SS	2	24	26	28
						322W SS[a]	2	18	20	22
						347 SS	4	23	27	29
						347 SS[b]	2	22	23	24
						410 SS	2	56	57	58
						410 SS[a]	2	45	51	57
						416 SS	2	57	62	66
						416 SS[a]	2	56	58	60
						420 SS	2	59	76	92
						420 SS[a]	2	92	96	100
						430 SS	2	22	23	23
						440C SS	2	300	400	500
						440C SS[a]	2	53	56	59
						443 SS	2	17	19	21
						446 SS	2	13	15	16
						17-4 PH SS	2	21	22	23
						17-4 PH SS[a]	2	29	33	35
						17-7 PH SS	2	24	25	25
						17-7 PH SS[a]	2	21	28	35
						Carpenter 20 SS	2	14	15	15
						Durimet 20	2	15	18	20

TABLE 3.2 (continued)

Run No.	Test Conditions: UO_2SO_4 Concentration (*m*)	Temperature (°C)	Time (hr)	Additions	Flow Rate (fps ± 10%)	Pin Material	Number of Pins	Corrosion Rate (mpy): Minimum	Average	Maximum
I-26	0.17	200	200	1000–2000 ppm O_2	12	Misco B	1		19	
						Miscro 4	2	51	64	77
						Stellite 1	2	72	81	90
						Stellite 3	2	240	260	270
						Stellite 6	2	86	110	130
						Stellite 25	2	17	19	20
						Stellite 98M2	2	210	240	260
						Worthite SS	2	15	16	17
						Worthite SS[b]	2	27	49	70
						Incoloy	1		21	
						Inconel	1		160	
						Inconel X	1		72	
						Inconel (low carbon)	1		260	
N-1	1.34	275	1512	500–2000 ppm O_2	4	304L SS	5	2.8	3.0	3.3
						309 SCb SS	2	2.6	2.6	2.6
						347 SS	5	2.8	3.8	4.6
N-2	1.34	275	200	1000–2000 ppm O_2	4	304L SS	5	100	130	190
						309 SCb SS	2	86	180	270
						347 SS	5	85	97	110

[a]Hardened by suitable heat treatment.

[b]Pin machined from cast bar.

[c]A titanium alloy containing 6% aluminum and 4% vanadium.

[d]Surface oxide of iron and chromium not removed; hence, specimens showed weight gain.

same precautions for interpretation that were given then still apply.

The pin data obtained during runs in which the mineral acids were used are not given in the table but are discussed in the appropriate section. Also, a number of pins and coupons containing welds have been exposed to uranyl sulfate solutions, and the results of these tests are discussed in Sec. 8 of this report.

(b) Corrosion of Stainless Steel by 0.04 *m* Uranyl Sulfate at 175°C. – Three runs in which 0.04 *m* uranyl sulfate containing 0.006 *m* sulfuric acid was circulated at 175°C have been made. Table 3.1, run E-33, in the last quarterly report[3] showed the corrosion rates of pin-type specimens after a 1111-hr exposure, and runs E-34 and E-35 in Table 3.2 of this report show the corrosion rates after 700 and 300 hr, respectively.

In general, all the stainless steels, with two exceptions, showed similar corrosion rates. The two exceptions were type 302B, which had a considerably higher corrosion rate than any of the other steels, and type 309 SCb, which had a lower corrosion rate than did the other stainless steels.

The corrosion rate of stainless steel was nearly independent of flow rate. All specimens developed films which were composed of a hydrated iron oxide. That the oxide was not protective was shown by the fact that all specimens corroded at a constant rate regardless of velocity. The corrosion rates were: type 347, 6 mpy; type 304L, 5 mpy; type 309 SCb, 3 mpy; type 302B, 15 mpy.

(c) Corrosion by 1.34 *m* Uranyl Sulfate at 275°C. – Two runs with 1.34 *m* uranyl sulfate at 275°C have been made in loop N, which was especially designed for operation with high-concentration uranyl sulfate solutions. The loop was constructed with type 347 stainless steel, except for some special test sections and the pump, which were made of titanium. Areas of high turbulence were eliminated as far as possible in design and construction of the loop, except for one special test section. In addition, the bulk velocity of the circulating solution in the 1½-in. pipe was reduced to about 5.5 fps by reducing the pump speed.

The first run, N-1, lasted for more than 1500 hr, after which the corrosion specimens and the loop were examined. The pin specimens were exposed to a bulk flow rate of only 3.9 fps, and the coupons were exposed over the range of 2.3 to 21.5 fps. At the end of the run all specimens had a smooth black film on their surfaces and all showed average corrosion rates of less than 5 mpy, with most rates between 2 and 3 mpy. The coupons showed no critical velocity effect. The interior surface of the loop had a complete coating similar to the specimens, except in one small area of a stainless steel test section on the downstream side of a tee. At this point corrosion had been so severe that the pipe wall was nearly penetrated.

The nickel and chromium concentrations increased rapidly during the early stages of the run and then leveled off after a few days. The average corrosion rate of the system as a whole was about 2 mpy based on the nickel found in solution. The agreement between this figure and the 2 to 5 mpy observed on the specimens is considered fair.

A second run, identical with the first in all respects, was made for 200 hr. At the end of this run, examination of the specimens revealed heavy corrosion even at flow rates as low as 4 fps. The 347 stainless steel coupons were partially free of film at rates of 6 fps and above, and a corrosion rate of more than 1-in. penetration per year was observed at 17 to 22 fps. The loop itself did not change in appearance during the second run. That the loop did not corrode to any measurable extent during the second run was shown by the fact that the presence of all the nickel in solution at the end of the run could be accounted for by the dissolving of the steel from the corrosion specimens.

The phenomenon observed with regard to the corrosion in runs N-1 and N-2 is not new and has been reported previously.[4] Usually, when a new loop is used for the first time, the loop corrodes heavily and the specimens show less corrosion than in subsequent runs. In later runs the loop corrodes only slightly, but the specimens show a greater attack than in the first run. It seems that the corrosion products originating from the large surface area of a new loop help protect the specimens during the first run.

(d) Corrosion of Selected Alloys. – In the last quarterly report[3] a discussion of the corrosion behavior of a number of alloys was given, and the results of four runs (I-19 through I-22) were pre-

[3] J. C. Griess and R. S. Greeley, *HRP Quar. Prog. Rep. Jan. 31, 1955*, ORNL-1853, p 56.

[4] J. C. Griess and R. E. Wacker, *HRP Quar. Prog. Rep. July 31, 1953*, ORNL-1605, p 74.

sented in Table 3.1. During this report period four additional runs with the same types of specimens as those used in the previous runs have been completed. Corrosion in the temperature range of 100 to 300°C has been examined at 50°C intervals with the use of a 0.02 *m* uranyl sulfate solution containing 0.005 *m* sulfuric acid, and the effect of uranium concentration has been investigated from 0.02 to 0.17 *m* at 200°C. The results of the measurements of individual pins, as well as the conditions of each run, can be seen in Table 3.2, runs I-23 through I-26, and in the previous quarterly report,[3] Table 3.1, runs I-19 through I-22. In each run, only pin-type corrosion specimens were exposed at 12 fps for 200 hr. Figure 3.1 shows the effect of temperature on the corrosion of most of the alloys tested in 0.02 *m* uranyl sulfate containing 0.005 *m* sulfuric acid. The data are presented on a semilog scale so that alloys showing both high and low weight losses can be shown on the same coordinates. The weight loss of type 347 stainless steel is shown for comparison.

From Fig. 3.1 it is obvious that most alloys showed a maximum corrosion rate at 200°C. For most austenitic stainless steels the maximum is actually at 225°C, and it is possible that the same maximum would have been observed here had specimens been exposed at 225°C.

Since all runs were of 200 hr duration, true corrosion rates were not obtained. However, previous experience has shown that at temperatures up to 200°C the corrosion rates of most alloys are constant with time; hence the rates reported at temperatures up to 200°C probably represent fairly reliable corrosion rates. At temperatures above 200°C the austenitic stainless steels corrode at a very low rate, probably less than 1 mpy, after a film has formed. Thus the average corrosion rate of the austenitic stainless steels would decrease as the exposure time increased. In other cases, particularly the ferritic stainless steels (except 430, 443, and 446), the extent of corrosion was so great that from a practical point of view the corrosion rates were not worth determining. In all tests, types 443 and 446 stainless steel showed corrosion rates similar to, but slightly less than, the rate for type 347 stainless. Type 430 stainless steel corroded at a faster rate than did type 347 stainless steel in solutions which contained added acid, but in solutions which contained only uranyl sulfate, type 430 stainless steel had a corrosion resistance equal to that of type 347.

On the other hand, the nickel- and cobalt-base alloys do not form protective surface films at any temperature and, as a result, show a rather constant corrosion rate at all temperatures. Thus, in the case of the Stellites and Inconels, the reported corrosion rates should be reasonably accurate for the particular conditions used in the test. Descriptions of the appearance of the corroded specimens and the chemical compositions of the alloys were reported previously.[3]

Table 3.3 shows how the extent of corrosion varied with changes in the uranium and sulfuric acid concentrations at 200°C. The acid concentrations were those deemed necessary to give a stable solution at 300°C. From the data it is apparent that the acid concentration was quite important in determining the extent of corrosion. For example, in most cases the weight losses were as high, or higher, at the 0.11 *m* level with 0.016 *m* sulfuric acid as at the 0.17 *m* level with no added acid.

(e) Additions of Magnesium and Sodium Sulfates.— It has been known for some time that the uranyl ion forms a rather stable complex with sulfate ions, at least at room temperature. Furthermore, there is evidence to indicate that under a given set of conditions the extent and/or rate of corrosion are proportional to the uranyl ion concentration. Therefore, it was believed that the addition of a salt of sulfuric acid might be beneficial in that it might reduce the uranyl ion concentration at high temperature and thereby reduce the rate of corrosion.

A first run, A-76, was made in which 0.17 *m* uranyl sulfate containing 0.1 *m* sodium sulfate was circulated at 250°C for 200 hr. The results of this run indicated a substantial decrease in the corrosion of stainless steel, both at high and low flow rates, although the solution was not completely stable. The concentration of uranium decreased slowly during the run, and the pH also decreased. The sulfate ion concentration, however, remained constant throughout the run.

A second run, A-77, was made in which the conditions were the same as in run A-76, except in this case the concentration of sodium sulfate was 0.075 *m* and the concentration of sulfuric acid was 0.025 *m*. During this run the uranium concentration increased slightly, apparently as a result of resolution of some of the precipitated uranium from

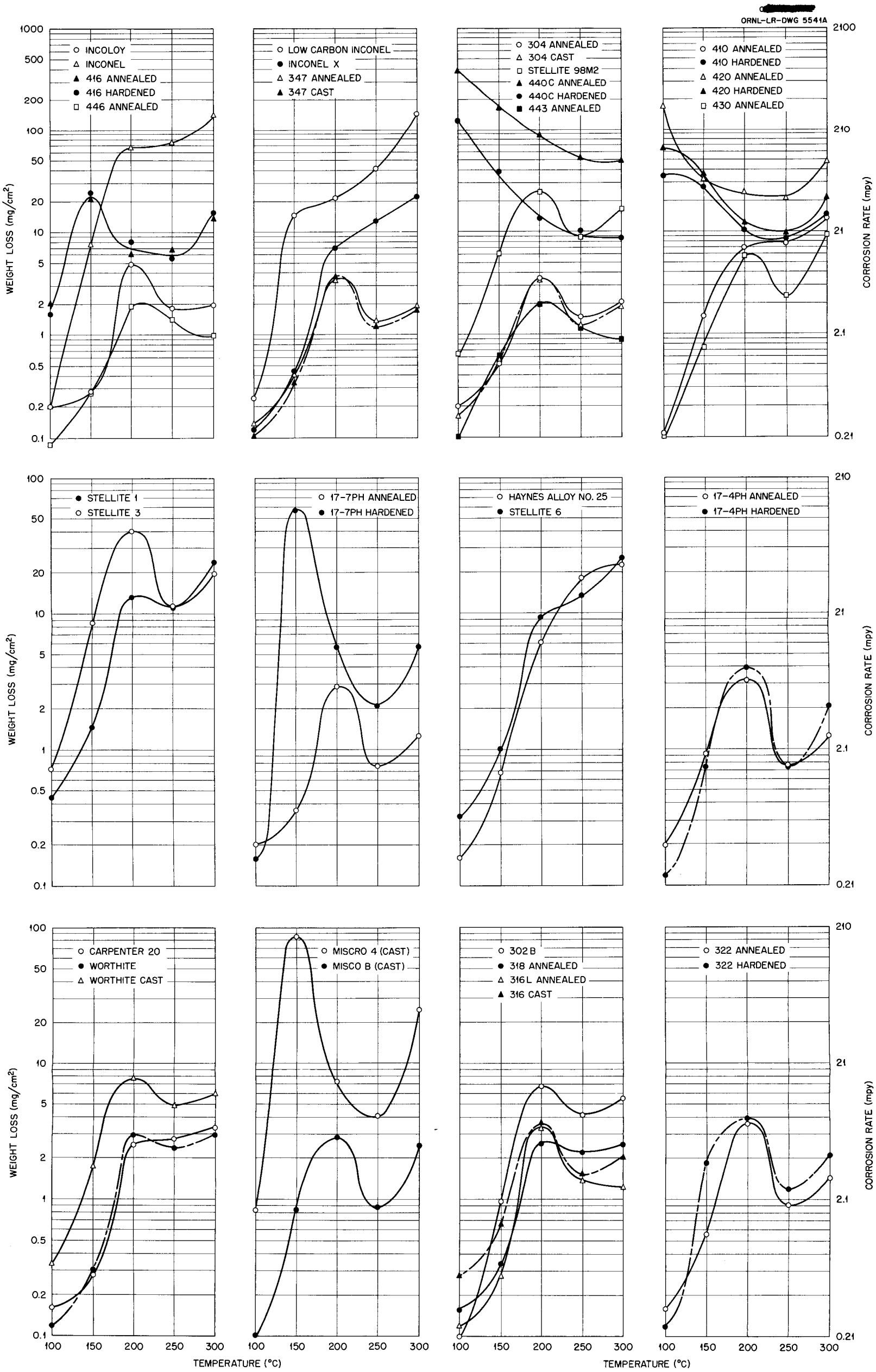

Fig. 3.1. Corrosion of Various Alloys in 0.02 *m* UO_2SO_4 Containing 0.005 *m* H_2SO_4 at Different Temperatures. Time of each run, 200 hr; flow rate, 12 fps.

TABLE 3.3. AVERAGE WEIGHT LOSSES OF DIFFERENT ALLOYS IN URANYL SULFATE SOLUTIONS AT 200°C AFTER AN EXPOSURE OF 200 hr

Alloy	Average Weight Loss* (mg/cm^2)			
	0.02 *m* UO_2SO_4 + 0.005 *m* H_2SO_4	0.06 *m* UO_2SO_4 + 0.006 *m* H_2SO_4	0.11 *m* UO_2SO_4 + 0.016 *m* H_2SO_4	0.17 *m* UO_2SO_4
Stellite 1	13.2	30.1	42.8	38.0
Stellite 3	39.5	91.8	224	119
Stellite 6	9.4	21.5	39.6	51.2
Stellite 98M2	24.2	79.6	145	112
Haynes alloy 25	6.0	8.5	11.1	8.9
Type 410 SS (stainless steel)	7.2	13.1	18.7	26.9
410 SS**	9.7	16.4	25.7	25.8
416 SS	6.0	15.5	25.5	29.1
416 SS**	8.3	18.2	32.2	27.3
420 SS	24.0	36.6	50.0	34.8
420 SS**	12.2	22.2	52.4	45.2
440C SS	88.9	115	194	187
440C SS**	13.6	28.7	38.5	26.4
430 SS	5.6	32.6	47.6	10.4
443 SS	2.0	2.9	7.2	9.2
446 SS	2.0	2.6	5.7	6.6
17-4 PH SS	3.4	7.8	11.8	10.2
17-4 PH SS**	3.9	8.6	16.8	15.0
17-7 PH SS	2.9	[illegible]	12.3	11.7
17-7 PH SS**	5.6	8.9	38.2	10.1
322W SS	3.6	6.9	12.7	12.2
322W SS**	3.9	6.2	11.2	9.5
302B SS	6.6	9.7	10.3	8.9
304 SS	3.4	6.7	13.8	13.2
304 SS (cast)	3.5	9.9	9.4	14.7
304L SS	3.5	4.9	9.3	9.9
309SCb SS	2.0	3.2	6.4	7.3
310S SS	1.8	2.4	5.6	9.4
316L SS	3.4	4.9	10.0	8.7
316 SS (cast)	3.6	5.5	12.0	12.7
318 SS	2.6	3.8	8.0	9.4
321 SS	3.0	4.3	8.1	9.6
347 SS	3.4	5.2	11.8	12.6
347 SS (cast)	3.6	6.7	11.9	10.8
Carpenter-20 SS	2.5	3.4	6.6	6.9
Durimet 20 (cast)	2.8	3.4	11.1	8.1
Worthite SS	3.0	4.0	6.8	7.6
Worthite SS (cast)	7.7	13.7	56.3	22.9
Misco B (cast)	2.8	4.3	8.8	8.8
Miscro 4 (cast)	7.4	25.6	73.0	30.2
Incoloy	4.8	5.8	9.8	10.0
Inconel	67.0	50.6	88.0	75.0
Inconel (low carbon)	21.5	109	160	120
Inconel X	7.0	13.6	25.6	33.7

*A weight loss of 10 mg/cm^2 in 200 hr corresponds to an approximate corrosion rate of 20 mpy.

** Hardened.

the previous run. The extent of corrosion was greater than in A-76 but less than is usually observed in 0.17 *m* uranyl sulfate under the same conditions.

On the basis of a few quartz-tube experiments it appeared that magnesium sulfate would be more soluble than sodium sulfate in high-temperature uranyl sulfate solutions; as a result, run A-78 was made at 250°C for 200 hr with 0.17 *m* uranyl sulfate containing 0.17 *m* magnesium sulfate. As in run A-76, the pH of the system decreased slightly. However, the extent of corrosion as observed on the corrosion specimens was very low, about an order of magnitude lower than is normally observed with 0.17 *m* uranyl sulfate.

The results obtained with coupon-type specimens in runs A-76 through A-78 can be seen in Fig. 3.2. A typical curve, obtained by using 0.17 *m* uranyl sulfate at 250°C for 200 hr, is shown for comparison. From the graph the beneficial effect of added sulfate is apparent. It should be noted that the addition of the salt had little, if any, effect on the critical velocity but lowered the corrosion at all velocities. The results from the pin-type specimens can be seen in Table 3.2.

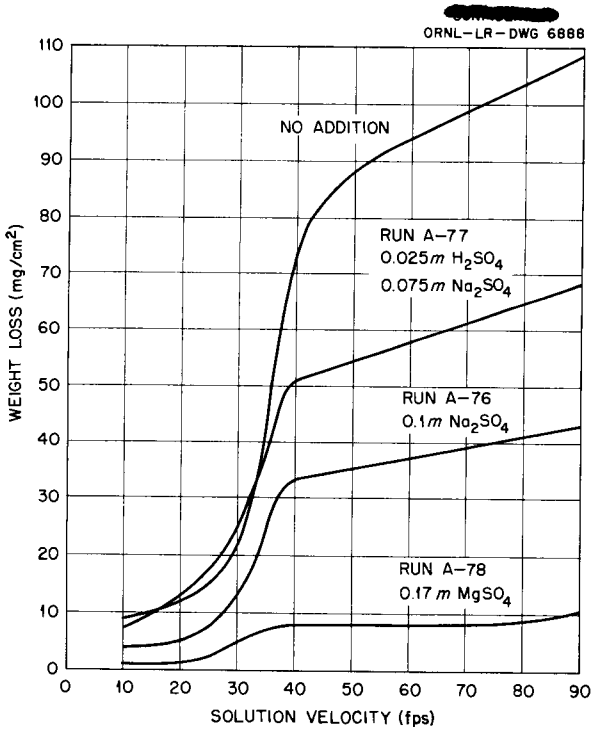

Fig. 3.2. Effect of Inorganic Sulfate Additions on the Corrosion of Type 347 Stainless Steel Coupons in 0.17 *m* UO_2SO_4 at 250°C.

In view of the encouraging results obtained to date, other studies in which a salt of sulfuric acid is added to uranyl sulfate solutions are in progress.

(f) Corrosion in Acid Media at 200 to 300°C. – Corrosion of several stainless steels, four titanium alloys, two zirconium alloys, and platinum has been explored in nitric, sulfuric, chromic, and phosphoric acids in the temperature range 200 to 300°C. Approximate corrosion rates for type 347 stainless steel are given in Table 3.4; those for titanium, zirconium, platinum, and stainless steels other than 347 are given in Table 3.5. The rates listed are of value only for comparative purposes, since the data were obtained in 100- to 200-hr runs, which are insufficient to establish true corrosion rates encountered once a film has formed.

With some significant exceptions, all stainless steels tested behaved similarly to type 347. Types tested were 302B, 304L, 309 SCb, 310, 316, 316L, 321, and 347. (Not all steels were tested in all solutions.) In 0.16 *m* nitric acid at 200°C, type 304L was superior to 347 in corrosion resistance. In all sulfuric and chromic acid solutions tested, type 309 SCb was four to ten times more resistant than 347. In 0.25 *m* phosphoric acid at 300°C, type 309 SCb was far superior to 347 and almost as resistant as platinum.

The titanium alloys tested were Ti-75A, Ti-100A, RC-55, and Electromet titanium. The zirconium alloys were crystal-bar zirconium and Zircaloy-2. In general, the titanium, zirconium, and platinum corroded only in the more concentrated acids at high velocity, although Table 3.5 lists a few exceptions.

(1) Nitric Acid. – In nitric acid solutions at 250°C with 1000 ppm oxygen in solution, corrosion of austenitic stainless steels was very similar to that observed in uranyl sulfate solution. Stainless steel coupons showed a critical velocity effect, and nickelous and chromium(VI) ion concentrations increased in solution with time. Corrosion was initially rapid, but in 0.16 *m* solution the chromium(VI) concentration increased rapidly and served as an efficient corrosion inhibitor. In 0.16 *m* nitric acid the chromium(VI) concentration increased to 400 to 500 ppm within 100 to 150 hr. The addition of 300 ppm chromium(VI) initially caused a marked decrease in corrosion and increased the critical velocity, as shown in Fig. 3.3.

TABLE 3.4. APPROXIMATE CORROSION RATES FOR TYPE 347 STAINLESS STEEL IN ACID SOLUTIONS

Conditions[a]		Corrosion Rates[b] (mpy)						
Temperature (°C)	Velocity (fps)	HNO_3 0.04 *m*	HNO_3 0.16 *m*	H_2SO_4 0.015 *m*	H_2SO_4 0.05 *m*	H_2CrO_4 0.20 *m*	H_3PO_4 0.05 *m*	H_3PO_4 0.25 *m*
200	20	*c*	100	30	*c*	25	*c*	*c*
	60	*c*	200	30	*c*	750	*c*	*c*
250	20	6	25	100	550	10	4	270
	60	20	150	100	550	10	7	400
300	20	*d*	*d*	*c*	150	*c*	*c*	1500
	60	*d*	*d*	*c*	150	*c*	*c*	2000

[a] 1000 ppm oxygen in solution.
[b] 100- to 200-hr runs.
[c] Not tested.
[d] NO_3^- begins to decompose at 280°C.

TABLE 3.5. APPROXIMATE CORROSION RATES FOR TITANIUM, ZIRCONIUM, PLATINUM, AND SEVERAL STAINLESS STEELS

Acid	Concentration (*m*)	Gas	Temperature (°C)	Velocity (fps)	Corrosion Rate* (mpy) Ti	Zr	Pt	304L	309 SCb	302B	316L	321
HNO_3	0.16	O_2	250	20	0	0	0	35	32			
				60	1.2	0	2.2	200	170			
		He	250	20	0	0	0	55	78			
				60	0	0	25	330	560			
H_2SO_4	0.10	O_2	250	20				1700	120			1100
				60				1000	100		850	440
	0.05	O_2	250	20				750	60		860	540
				60				180	9		380	260
			300	20				180	160		220	120
				60				>8700	45		3100	380
**				60	20–30	40	0	160	300			210
H_2CrO_4	0.20	O_2	200	20	20	0.2	0	30	40			
				60	30	5	0	800	670			
			250	20	0	0	0	8.0	13			7.2
				60	0	0	0	75	37			51
H_3PO_4	0.05	O_2	250	20	0	0	0	3.3	2.5	8.0	6.9	
				60	1	1	0	7.9	5.4	15	8.0	
		He	250	20	0	0	0	6.0	6.1	11	5.1	
				60	0	0	0	22	18	35	21	
	0.25	O_2	250	20	15	0	0	350	180	710		
				60	50	0	0	300	260			
			300	20	15	2	0	690	1000		1400	
				60	100	30	30	2400	100		2000	

*100- to 200-hr runs.
**Plus 300 ppm Cr(VI).

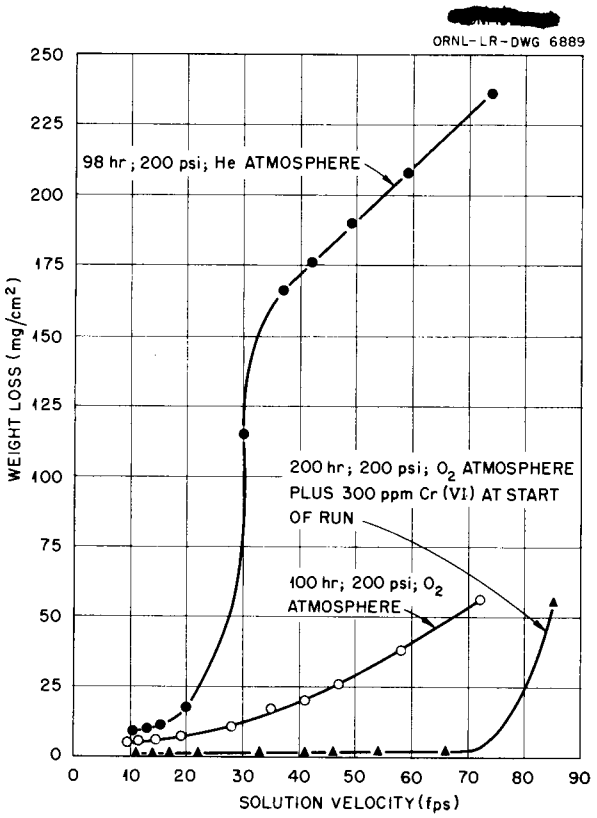

Fig. 3.3. Corrosion of Type 347 Stainless Steel Coupons in 0.16 *m* HNO_3 at 250°C.

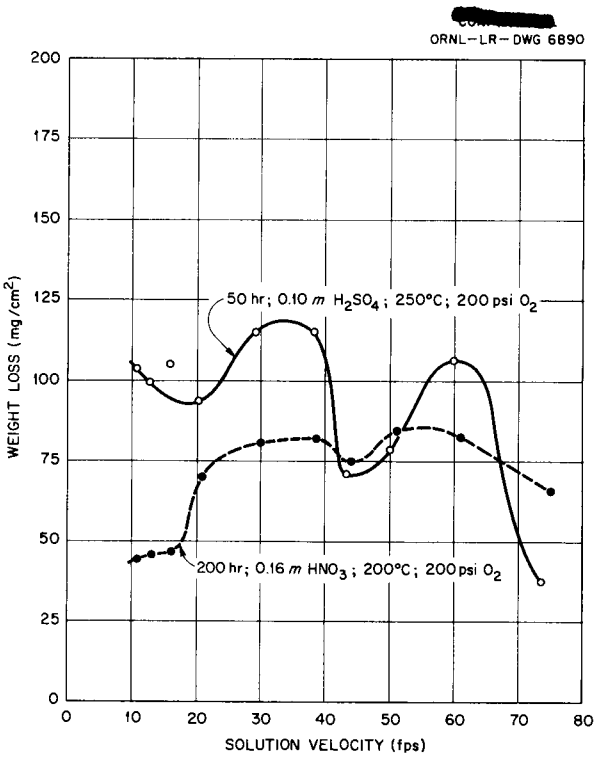

Fig. 3.4. Corrosion of Type 347 Stainless Steel Coupons in Nitric and Sulfuric Acids.

In the absence of oxygen, with helium used as the pressurizing gas, nitrate ion acted as the oxidant for the steel, and the chromium(VI) concentration did not build up in solution. As a result, corrosion continued for a somewhat longer time at the high initial rate, but, since nickelous ions going into solution replace hydrogen ions, the acidity ultimately decreased enough to reduce corrosion considerably.

Corrosion of stainless steel in the gas space over dilute nitric acid at 250°C was severe. Type 321 stainless steel rupture disks failed, in two successive 50-hr runs over 0.04 *m* HNO_3, as a result of corrosion.

At 200°C, corrosion of stainless steel is more severe than at 250°C. Curiously, at 200°C, stainless steel shows no simple dependence of corrosion on velocity, and in this respect the nitric acid acted more like sulfuric acid than like uranyl sulfate (see Fig. 3.4).

(2) Sulfuric Acid. – In sulfuric acid solutions oxygen must be present to prevent very rapid attack of stainless steel. Therefore, no runs have been made with other than oxygen pressurization. Oxygen must be present at the steel surface to oxidize ferrous to ferric iron in order to form a protective film of ferric oxide on the surface. This produces an inverse velocity effect: generally, the higher the solution velocity over the steel surface, the lower the rate of corrosion. Actually, the corrosion vs velocity curve is camel-shaped, as shown in Fig. 3.4; this may be due to an uneven flow along the coupons caused by the geometry of the coupon holder. This same velocity dependence has been noted in 0.015, 0.05, and 0.1 *m* sulfuric acid at 250 and 300°C and in 0.17 *m* nitric acid at 200°C.

The nickelous ion concentration increased in dilute sulfuric acid solutions at 250 to 300°C and indicated the extent of corrosion, but chromium(VI) did not form. When 300 ppm chromium(VI) was added initially to 0.05 *m* sulfuric acid at 300°C, corrosion decreased markedly, but, at the end of 50 hr, only 35 ppm chromium was left in solution. The effects of velocity, temperature, time, and

chromium(VI) concentration on corrosion of type 347 stainless steel are shown in Fig. 3.5.

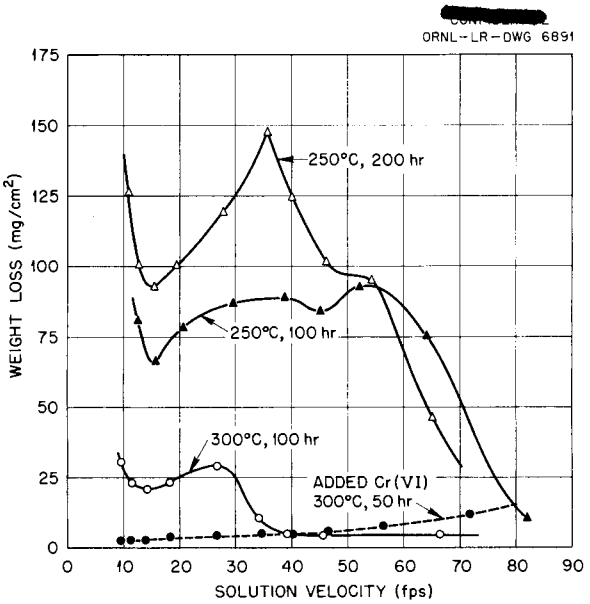

Fig. 3.5. Corrosion of Type 347 Stainless Steel Coupons in 0.05 *m* H_2SO_4 at 200 psi O_2 and at 250 and 300°C.

(3) Chromic Acid. – Corrosion in chromic acid was much less than in nitric or sulfuric acids, but at high solution velocity severe pitting occurred. As can be seen in Fig. 3.6, at 250°C in 0.2 *m* chromic acid no sharp critical velocity was observed, but at 200°C a sharp increase in corrosion rate occurred at about 35 fps. Weight losses at 60 fps were ten times greater at 200 than at 250°C. The explanation for this large increase in high-velocity corrosion and the appearance of a sharp critical velocity at the lower temperature may be associated with a change in the oxidizing power of oxygen. If uniform oxidation of the steel is assumed, it can be inferred from the decrease in chromium(VI) concentration and the increase in nickelous ion concentration during the runs that at 250°C oxygen oxidized about 25% of the total steel corroded and that chromium(VI) oxidized 75%, whereas at 200°C oxygen oxidized none of the steel and chromium(VI) oxidized all the steel.

(4) Phosphoric Acid. – In runs with 0.05 and 0.25 *m* phosphoric acid at 250 and 300°C, phosphate and hydrogen ions uniformly disappeared from solution simultaneously. With the use of

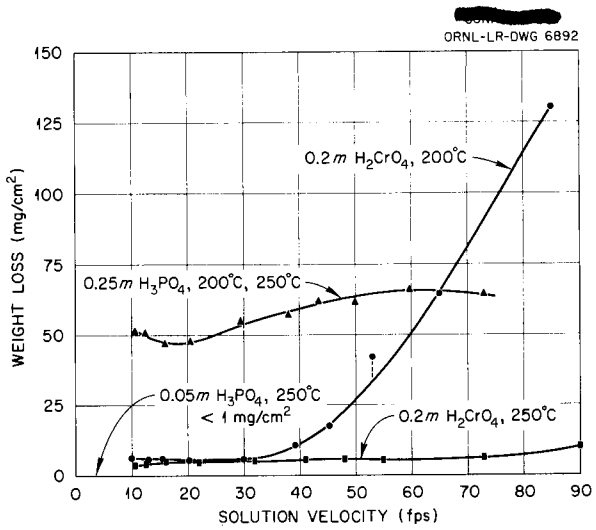

Fig. 3.6. Corrosion of Type 347 Stainless Steel Coupons in 0.2 *m* H_2CrO_4 and 0.25 *m* H_3PO_4 Containing About 1000 ppm Oxygen.

x-ray and electron diffraction studies, it has not been possible to identify either the pinkish-gray film formed on the specimens at 250°C or the greenish film formed at 300°C; evidently the films are mixed iron, chromium, and nickel phosphates and oxides. No accumulation of nickel, chromium, or iron concentrations in solution occurred during the runs. In a run in which helium pressurization was used instead of oxygen, the extent of corrosion was about twice that when oxygen was used. Figure 3.6 shows the appearance of the velocity curve for stainless steel in 0.25 *m* phosphoric acid at 250°C.

In the helium run, one solution sample was analyzed for dissolved hydrogen gas to determine whether hydrogen ion or phosphate ion was the stronger oxidant at 250°C. No hydrogen was found, but, since the amount involved was near the limit of analysis, no definite conclusion can be drawn. Since the normality of the acid and the molarity of phosphate ion decreased in the ratio 1:1 during the runs, it may be that, as the hydrogen ions oxidized the steel, precipitation of insoluble iron, chromium, and nickel phosphates occurred.

(5) General Conclusions. – The type of attack by acids on metals at 200 to 300°C depends greatly on the relative oxidizing power of the ions and gases present in solution. This relative oxidizing power varies with temperature and also from one

acid to another. For instance, oxygen will readily oxidize chromium to the hexavalent state at 250°C in nitric acid but not in sulfuric acid solution. The degree of attack usually depends on the ability of the metal to form and hold on its surface a protective film of corrosion products. Titanium and zirconium quickly form tenacious oxide films when exposed to most acids (for exceptions see Table 3.5), while platinum is chemically very inert. Of the stainless steels, type 309 SCb, with its high chromium content, seems to be the most resistant, particularly in solutions which do not have sufficient oxidizing power to oxidize chromium to the hexavalent state. Thus in sulfuric and phosphoric acids, type 309 SCb is superior to either type 304L or 347, but in chromic and nitric acids, type 309 SCb is similar to the other stainless steels investigated.

3.2.3 Miscellaneous

Most of the data presented in Table 3.2 have already been discussed or are sufficiently clear to need no further discussion. However, there are several runs whose significance may not be apparent from the table alone; it is to call attention to these runs that this section is written.

Runs A-73 and E-36 were of very short duration because of mechanical difficulties. It is of interest to note that all specimens showed high corrosion rates, essentially independent of flow. Had the runs continued for longer periods, the specimens at low flow rates would have nearly stopped corroding, and those at high flow would have continued to corrode at even faster rates than those shown in the table. These data are in agreement with other short-term runs.

In runs A-76 through A-78, pins were exposed at 16 and at 18 fps. Those pins exposed at 16 fps showed average corrosion rates, as expected for flow rates less than the critical velocity, but those exposed at 18 fps were partially free of film and showed high corrosion rates. These runs serve as a good example to demonstrate how much the film stability, and consequently the corrosion, depends on the flow rate of the solution.

Previous loop results have shown that the addition of molybdate ions to uranyl sulfate solutions had no effect on the corrosiveness of the solution, although static tests have always shown a marked decrease in corrosion when the system contained molybdate ions. The only chemical difference between the two systems was that in the loop tests the system was pressurized with oxygen gas, whereas the static systems were indirectly pressurized with hydrogen peroxide. The addition of hydrogen peroxide to uranyl sulfate solutions results in a decrease in pH and a precipitation of uranium peroxide. As the system is heated, the peroxide decomposes, and the system is then pressurized with oxygen.

It seemed possible that the beneficial effect of molybdate ions noted in the static tests could have been due to the presence of a complex or a compound formed as a result of a reaction between molybdate ions and hydrogen peroxide. Therefore, in runs E-37 and E-38 the system was pressurized with helium, and hydrogen peroxide was added to supply the oxygen. The results of the runs confirmed previous loop data and showed that the presence of molybdate ions had no effect on the corrosiveness of uranyl sulfate solutions.

Runs F-51, F-52, and H-55 showed that, at flow rates less than the critical velocity, dichromate ions very greatly reduced the corrosion of stainless steel by uranyl sulfate solutions, even at high acidities. At flow rates in excess of the critical velocity the corrosion rate of stainless steel was very high, but in each case the critical velocity was about 40 fps, as compared with about 15 fps for the same system in the absence of dichromate ions. While the presence of dichromate ions decreased the corrosion at low flow rates, the corrosion rate of the film-free metal was increased by as much as a factor of 3.

3.3 SEDIMENTATION RATES OF THORIUM OXIDE SLURRIES AT ELEVATED TEMPERATURES

S. A. Reed

Additional tests were made in order to study the sedimentation characteristics of thorium dioxide slurries. Sedimentation rates of slurries made from four different thorium dioxide preparations were determined at 100, 150, 200, 250, and 300°C for concentrations of 250, 500, and 1000 g of thorium per kilogram of water. Results of completed tests are shown in Table 3.6.

It is apparent from these data that the sedimentation rates for all materials tested were severalfold greater than would be expected on the basis of particle sizes (0.02 to 0.05 μ dia) calculated from surface-area data or electron diffraction

TABLE 3.6. SEDIMENTATION RATES OF ThO_2 SLURRIES AT ELEVATED TEMPERATURES

Slurry Identification*	Approximate Concentration (g of Th per kg of H_2O)	Rate of Sedimentation (cm/sec)				
		100°C	150°C	200°C	250°C	300°C
P-1	250	**	0.05	0.17	0.23	0.29
	500	**	**	0.12	0.18	0.25
	1000	**	**	**	**	**
L-8	250	**	0.04	0.16	0.24	0.33
	500	**	**	0.10	0.16	0.24
	1000	**	**	**	**	**
D-10	250			Test incomplete		
	500	**	**	0.13	0.19	0.28
	1000	**	**	**	**	**
H-5-A	250			Test incomplete		
	500	**	**	0.05	0.06	0.08
	1000			Test incomplete		

*P-1 – prepared from thorium formate, 650°C calcination (cf. S. A. Reed, *HRP Quar. Prog. Rep. Jan. 31, 1955*, ORNL-1853, p 83).

L-8 – Lindsay Chemical Company preparation: oxalate precipitation, 900°C calcination.

D-10 – ORNL production batch, two-stage calcination.

H-5-A – ORNL experimental batch: two-stage calcination, contained 7800 ppm SO_4^{--}.

**In compaction (no hindered settling was apparent).

measurements, indicating an association of ThO_2 particles and water or of the solid particles themselves. Calculations of effective particle size, based on the assumption that association does occur, are now being made.

Tests have been initiated to study the sedimentation characteristics of other ThO_2 preparations, especially those to be used in making dynamic-corrosion studies. Slurries prepared with D_2O are also being investigated.

4. RADIATION CORROSION

G. H. Jenks H. C. Savage

A. L. Bacarella R. J. Davis R. A. Lorenz R. M. Warner
J. E. Baker H. O. Day J. R. McWherter K. S. Warren
W. N. Bley H. A. Fisch A. R. Olsen L. F. Woo
N. C. Bradley D. N. Hess M. D. Silverman W. C. Yee
W. E. Clark D. T. Jones H. H. Stone

4.1 IN-PILE LOOP

H. C. Savage G. H. Jenks

W. N. Bley J. E. Baker
N. C. Bradley R. A. Lorenz
D. T. Jones A. R. Olsen
R. M. Warner

4.1.1 Development and Construction

(a) HB-4 Mockup. – During the past quarter, in-pile loop assembly GG was completed and installed in beam hole HB-4 in the LITR. Loop GG, a duplicate of FF, is the third corrosion test loop installed in this facility; it contains Zircaloy-2 corrosion specimens in Zircaloy-2 holders in both the in-line and core positions, as well as Zircaloy-2 impact specimens in the core. The circulating pump in loop GG contains hardened 17-4 PH stainless steel journal bushings and Graphitar No. 14 bearings, as did the pump in loop FF.

The next in-pile loop to be installed in beam hole HB-4 in the LITR will be loop EE. This loop, with type 347 stainless steel corrosion coupons, was previously assembled but was set aside because of the greater urgency of obtaining radiation corrosion data on Zircaloy-2 corrosion coupons incorporated in loops GG and FF. (There was a high priority on Zircaloy-2 data because the core tank of the HRT is fabricated of this alloy.) The corrosion specimens in loop EE were removed, and new corrosion specimen assemblies, as described below, were installed in order to obtain additional radiation corrosion data:

1. The width of the coupons was decreased from $\frac{1}{2}$ in. to $\frac{1}{4}$ in. in order to increase the number of coupons from 12 to 24 in each holder.
2. Three different metals under consideration for use in homogeneous reactors, namely, type 347 stainless steel, Zircaloy-2, and titanium, were chosen for corrosion coupons. Eight coupons of each metal were arranged in each holder in an attempt to evaluate statistically the effects of radiation level, solution velocity, and any galvanic coupling between pairs of different metals. The arrangement was worked out by the ORNL Mathematics Panel.
3. Stressed specimens of type 347 stainless steel, Zircaloy-2, and titanium were installed in the core position of loop EE, replacing the impact specimens. Each stress-specimen assembly consists of two strips $\frac{3}{8}$ in. wide by $3\frac{1}{2}$ in. long by 0.060 in. thick, stressed over a center fulcrum.
4. As a further test of the possibility of a galvanic couple effect under radiation, a coupled specimen assembly was made up consisting of nine pairs of coupled specimens of type 347 stainless steel, Zircaloy-2, and titanium, assembled on a rod and separated by spacers. Two of these assemblies were installed in loop EE, surrounding the core coupon holder, along with the stressed specimens.

Figure 4.1 is a photograph of the corrosion specimen assembly installed in the core position of loop EE, showing the coupons and the stressed and coupled specimens.

(b) LITR HB-2 Mockup. – Work is under way to design and build an in-pile loop assembly for installation in beam hole HB-2 in the LITR. This will provide two facilities at the LITR for radiation corrosion data from circulating in-pile loops. With the higher neutron flux available in beam hole HB-2, radiation corrosion data can be obtained for higher power densities than can now be obtained in beam hole HB-4. In addition, the loop is being designed to operate at temperatures and pressures up to 300°C and 2000 psi.

The loop will have essentially the same design as the present in-pile loop.[1] In order that the loop package might fit beam hole HB-2, a few changes in the dimensions of the package will be required. At present, an accurate measurement of HB-2 is being made by means of a dummy wood plug.

The circulating pump for the 2000-psi loop for

[1] G. H. Jenks, H. C. Savage, *et al.*, *HRP Quar. Prog. Rep. April 30, 1954*, ORNL-1753, p 81–94.

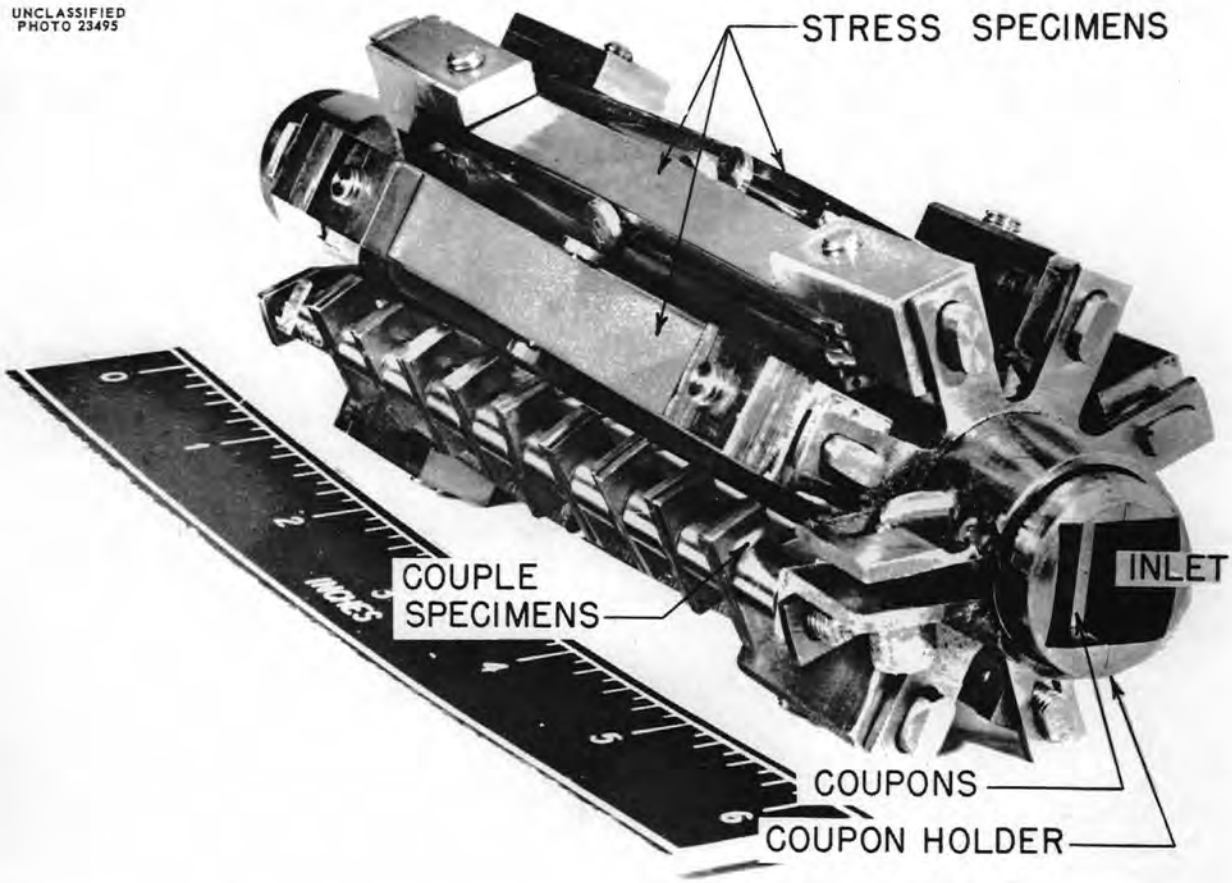

Fig. 4.1. Corrosion Specimen Assembly, In-Pile Loop Core (EE).

beam hole HB-2 will be a canned-rotor pump designed and built by the Byron Jackson Co. This pump, of smaller diameter than the present pump, is a two-stage centrifugal type developing a 40-ft head at a flow rate of 5 gpm. Bearings and journal bushings are of pure sintered aluminum oxide instead of the hardened 17-4 PH stainless steel–Graphitar No. 14 combination used in the present circulating pump. A test model of the Byron Jackson pump has been received which has a flanged head end to facilitate test operations. Pumps installed in the in-pile loop will be welded shut.

The instrumentation and panel board for the HB-2 in-pile loop will be similar to those used in the present system. Design of the panel board is essentially complete.

Engineering also has been started on the adaptation of the present flowsheet of the HB-4 loop for installation at HB-2. The physical sizes and locations of the valve boxes have been specified, and detailed changes of the HB-4 drawings are in progress. This engineering is scheduled for completion by June 1. Fabrication completion is scheduled for September 1, 1955. Procurement of material based on HB-4 requirements is almost complete.

(c) In-Pile Slurry Loop. – Work is being continued for establishing the feasibility of circulating thorium oxide slurry in an in-pile loop, with minimum modification of the present design. Following the plugging difficulties[2] which were experienced in an initial attempt to circulate thorium oxide slurry in an in-pile type of loop,[1] revisions were made to the loop design. Since the oxide had been found to accumulate and cake primarily in the ¼-in. tubing in the pressurizer and pressurizer heater

[2]H. C. Savage *et al.*, *HRP Quar. Prog. Rep. Oct. 31, 1954*, ORNL-1813, p 63–65.

portion of the loop, the principal design changes were in the pressurizer section of the loop. A diagram of the revised loop is presented in Fig. 4.2.

The horizontal pressurizer was replaced with a vertical pressurizer with side inlet and bottom outlet. A set of vertical baffles was placed around the inside wall of the straight section of the holder to prevent the flow through the pressurizer from forming a vortex near the outlet.

The pressurizer heater section of the original in-pile loop design was replaced with a $\frac{3}{8}$-in. side inlet line to the pressurizer. The pressurizer and pressurizer inlet line are heated with resistance wire wrapped around the outside of the pipe and pressurizer; the heat supplied to the pressurizer is that required to vaporize water for feed to the rear of the pump. As shown by Fig. 4.2, both the side inlet line and the main loop line contain orifice-type flow restrictors to permit the main loop and pressurizer flow rates to be varied to any desired ratio.

Following satisfactory preliminary loop runs with water at 250°C, a slurry of thorium oxide containing 200 g of thorium per kilogram of water was prepared from the D-17 oxide (ORNL production batch) by stirring in a small Waring Blendor for 2 hr; the slurry was then charged to the loop. Loop operating conditions were 250°C in the line and 255 to 265°C in the pressurizer with oxygen overpressure.

A $\frac{3}{8}$-in.-dia orifice flow restrictor installed in the side inlet line to the pressurizer resulted in a maximum calculated flow rate of 0.6 gpm through the pressurizer, compared with an estimated 5.8 gpm flow in the main loop piping.

Loop sampling was accomplished through a $\frac{1}{4}$-in. line located in the loop piping approximately 6 in. from the pump discharge. Since the total loop volume is relatively small, the volume of the sample was measured each time a sample was withdrawn, and an equal quantity of distilled water was added to the loop to maintain liquid level in the pressurizer. This practice decreased the oxide concentration in the loop but allowed the inventory volume to be held constant.

The first run was terminated, after approximately 65 hr of operation at elevated temperature, because of a slow increase of temperature in the pressurizer. During the last 16-hr period of operation the temperature gradually rose from 265 to 290°C. The reason for this was not readily apparent, since removal of the flanged cap on the pressurizer showed that both the pressurizer and side inlet line were open and free from plugging or caking. However, small quantities of sludge were found in the bottom of the side inlet line. Samples HT-11-6 and HT-11-8 taken during this run are listed in Table 4.1 under run No. HT-11-1. Both are well below the theoretical thorium concentration of the

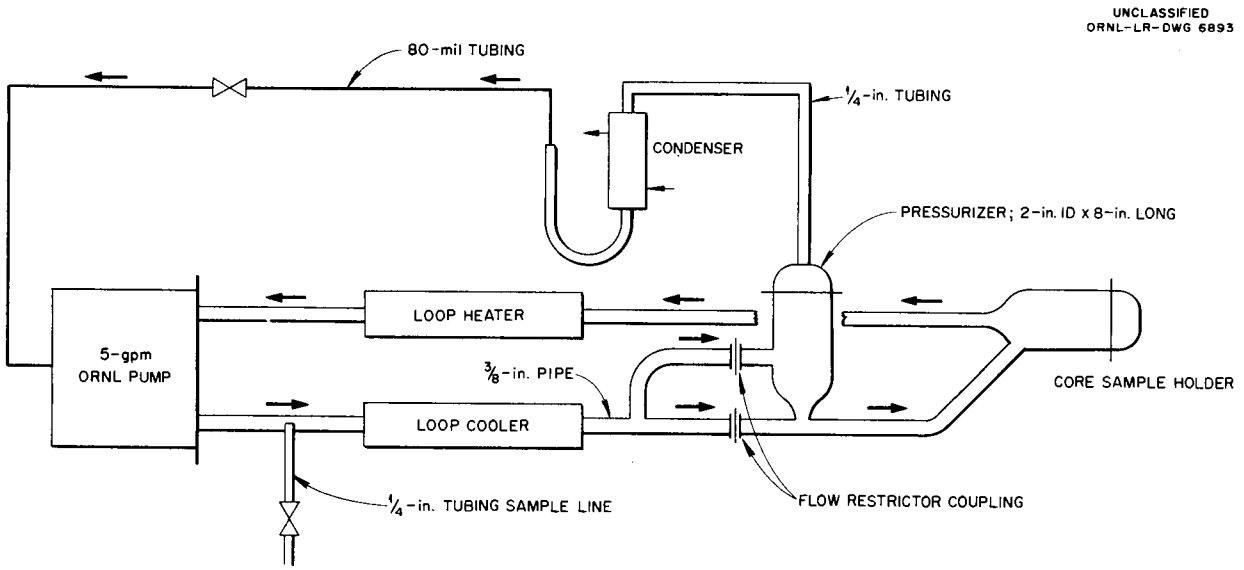

Fig. 4.2. Thorium Oxide Slurry Experimental In-Pile Loop.

TABLE 4.1. ANALYSIS OF SAMPLES WITHDRAWN FROM IN-PILE TYPE OF SLURRY LOOP

Sample No.	Time of Withdrawal (hr)	Th Concentration (g of Th per kg of H_2O)		Solids (mg per g of Th)				Liquid		Gas (ppm)		
		Theoretical Loop Concentration	Sample Analysis	Fe	Ni	Cr	SO_4^{--}	pH	SO_4^{--} (ppm)	O_2	CO_2	H_2
				Run No. HT-11-I*								
HT-11-6	0.7	200	104	0.29	0.05	0.10	1.77	8.8	<10	Not sampled		
HT-11-8	18.9	204	138	0.85	0.08	0.17	0.27	9.2	<10	Not sampled		
				Run No. HT-11-II**								
HT-11-10	0.9	251	195	0.20	0.03	0.04	0.12	9.0	Not analyzed	Not sampled		
HT-11-12	18.6	252	239	0.53	0.06	0.36	0.11	9.2	108	66	34	None
HT-11-14	114.4	241	246	1.18	0.13	0.68	0.11	8.4	56	None	None	None
HT-11-16	162.7	232	299	1.21	0.10	0.62	0.07	8.5	17	11	33	None

*Loop charge, 200 g of Th per kg of H_2O + 60 psia O_2 at room temperature; run time approximately 65 hr, loop temperature 250°C, pressurizer 255 to 265°C.

**Loop charge, 251 g of Th per kg of H_2O + 60 psia O_2 at room temperature; run time approximately 165 hr, loop temperature 250°C, pressurizer 255 to 265°C.

loop, indicating that the solids were concentrated somewhere in the loop.

For the second run the ⅜-in.-dia flow restrictor was removed from the pressurizer side inlet line to increase the flow through the pressurizer. New material was prepared as described previously, and a concentration of 250 g of thorium per kilogram of water was used. The loop was operated at 250°C and the pressurizer at 255 to 265°C with oxygen overpressure.

Following 165 hr of operation at temperature, the loop was shut down to observe the samples in the core sample holder. Analyses of slurry and gas samples withdrawn during this run are also presented in Table 4.1 under run No. HT-11-II. It should be noted that the gas analyses of samples HT-11-14 and HT-11-16 show very low oxygen concentrations in spite of the initial loop charge. This was due to a slow leak through a fitting in the back of the pump can; the leak was discovered after approximately 70 hr of operation. Although the leak was repaired, it apparently was not discovered in time to prevent the loss of practically all the oxygen from the loop. The thorium concentration values in slurry samples removed during operation were erratic; the deviations may have been due to poor sampling techniques or to thorium oxide retained in the loop. The quantities of sulfate ion which were reported in the solids of the samples withdrawn during both runs were consistently above the 100 ppm sulfate reported in the analysis of the D-17 oxide. No explanation of this is apparent at present.

The type 347 stainless steel corrosion test specimens, contained in the tapered titanium coupon holder[3] in the core sample holder section of the loop during both the previously described slurry runs, were removed and examined (see Fig. 4.3). Visual inspection of the coupons revealed that all but three in the higher-velocity sections of the holder were covered with a light-brown, smooth, extremely thin film. The three coupons in the high-velocity region of the holder had highly polished, bare metal surfaces and several sharply pitted areas. Microscopic examination showed these pits to range from 0.5 to 2.4 mils in depth. The inside surfaces of the titanium holders bore no visual evidence of attack.

[3] G. H. Jenks, H. C. Savage, *et al.*, *HRP Quar. Prog. Rep. April 30, 1954*, ORNL-1753, Figs. 63 and 64, p 84–85.

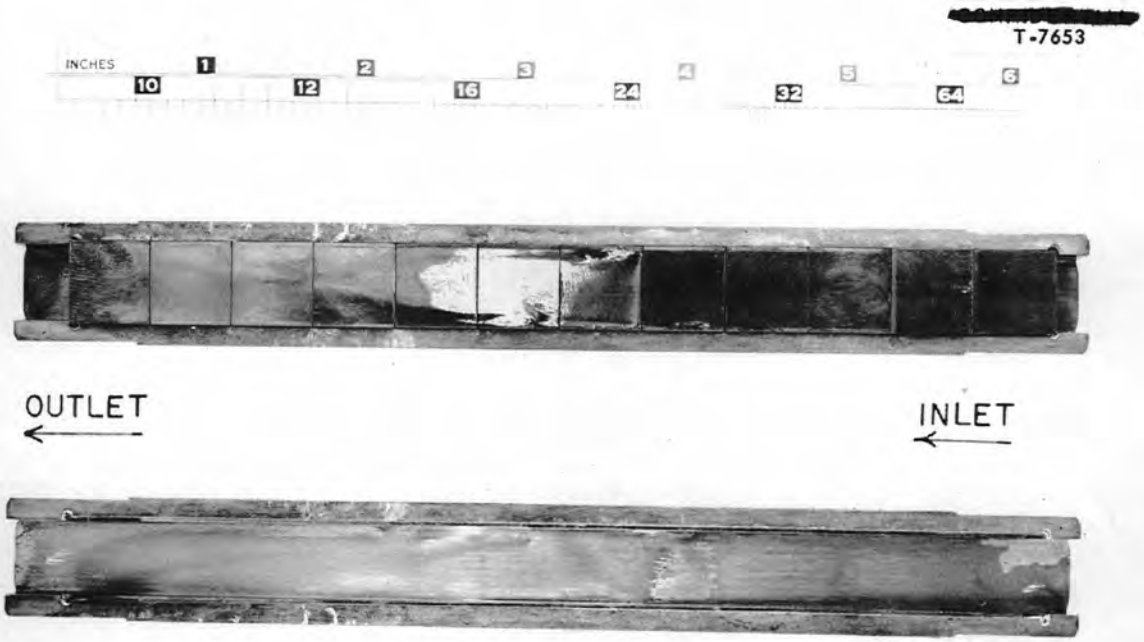

Fig. 4.3. Coupon Assembly in the Core Sample Holder of the HT In-Pile Slurry Loop.

Table 4.2 presents the corrosion rates for the coupons as a function of velocity. Unfortunately, neither the loop nor the 5-gpm pump has as yet been calibrated for slurry circulation. Thus, the velocities listed are based on the assumption that the main loop flow rate was 5.8 gpm (based on previous values obtained for water flow rates in the in-pile type of loop). A flow calibration with slurry will be made prior to another corrosion test.

Upon disassembling the ORNL 5-gpm pump at the end of the second run, dilute slurry was found in the extreme rear of the pump can. However, no evidence of an accumulation of solids in a cake or sludge form was found in the pump. Measurements preceding and following both runs showed no detectable wear of the bearings and rotor. The pump scroll, impeller, and thermal spacer were all covered with the same type of light-brown film found on the stainless steel coupons in the lower-velocity sections of the coupon holder.

Additional runs with slurries of various thorium oxide concentrations will be made to determine the feasibility of circulating these slurries in an in-pile loop and to measure corrosion and/or erosion attack on corrosion specimens.

TABLE 4.2. CORROSION OF TYPE 347 STAINLESS STEEL COUPONS IN IN-PILE TYPE OF LOOP*

Velocity Range** (fps)	Weight Loss (mg/cm^2)	Average Corrosion Rate (mpy)
9.5–11.1	0.27	0.51
11.1–13.4	0.29	0.55
13.4–16.8	0.29	0.55
16.8–21.9	0.21	0.40
21.9–32.2	0.46	0.87
32.2–37.2	1.18	2.22
37.2–44.2	4.18	7.90
44.2–27.1	3.72	7.00
27.1–19.3	1.64	3.09
19.3–14.5	1.14	2.15
14.5–11.6	0.89	1.68
11.6–10.1	0.53	1.00

*Runs HT-11-I and HT-11-II (ThO_2 slurry).

**Approximate; based on previous water data from similar loops.

4.1.2 LITR Operation – In-Pile Loop Corrosion Test FF

4.1.2.1 Introduction

A second in-pile loop experiment, designed to determine the effect of reactor radiation on the corrosion of Zircaloy-2 by uranyl sulfate solutions at 250°C, has been completed. The methods and procedures which were followed in this experiment were similar to those previously reported[4] for the first experiment DD, and reference is made to the previous report for details not included here.

4.1.2.2 Construction and Preparation of Loop

As before, constructional material for the loop was type 347 stainless steel. An ORNL 5-gpm canned-rotor pump was used to effect circulation.

Specimens of Zircaloy-2, clamped in holders of the same material, were contained in the core (in the neutron flux) and in in-line (out of the neutron flux) positions. A set of Zircaloy-2 impact specimens was also placed in the core. A summary of the loop and sample specifications is presented in Tables 4.3 and 4.4.

Details of the construction of the loop and of the preparatory operation have been described.[5] A summary of the preparatory operations is presented in Table 4.5; a tabulation of the results of solution analyses during these operations is presented in Table 4.6. The very high rate of accumulation of corrosion products during the initial 80 hr of operation is ascribed to the defective pump.[5] After the pump was replaced, the loop operation was satisfactory, and the corrosion behavior was normal. The aluminum in the sample of enriched solution was not a product of corrosion. The enriched material which is employed with these experiments contains aluminum in approximately the same proportion as that found.

4.1.2.3 In-Pile Operation

(a) General Operating Conditions and Procedures. – The solution which was charged for the in-pile operation was of the following composition:

UO_2SO_4	39.95 g of uranium per liter (U^{235}/total U = 0.888)
$CuSO_4$	0.031 *m*
H_2SO_4	0.04 *m*

A solution of the same composition was used to replace liquid withdrawn from the loop during sampling operations. Some excess sulfuric acid must be added to the loop solutions in order to prevent hydrolytic precipitation of copper and uranium, since hydrogen ions are lost from solution during the corrosion of stainless steel. A large excess of acid was added to the solution for this loop in the hope that a prolonged exposure would be feasible.

In-pile operation of the loop with enriched solution was for a period of 661.5 hr (total circulation time with this solution was 692.3 hr). The energy output of the LITR during this time was 1401 Mwhr. Essentially all this energy was liberated at full reactor power. The reactor operating schedule for the exposure is shown in Fig. 4.4.

The schedule for solution sampling is also shown in Fig. 4.4. Two successive samples of about 2 ml each were taken on the occasion of each sampling. With the exception of FF-1-52, the samples were withdrawn after the reactor had been at zero power for several hours. Sample FF-1-52 was taken while the reactor was at power. The time which elapsed between reactor shutdown and sample withdrawal is listed in Fig. 4.4 for each sample.

Temperature control for the first portion of the operation was essentially as before.[4] However, after 380 hr of circulation, the thermocouple attached to the pressurizer jacket heater failed. For the subsequent operation, the power to the jacket heater was adjusted manually to a value for which the temperature of the liquid in the pressurizer and the measured partial pressures of steam, oxygen, and radiolytic gas were the same as before the failure. Another loop thermocouple, between the pressurizer line heater and the pressurizer, failed after 529 hr of circulation. Normally, this thermocouple was used to control the pressurizer heater and, thus, the temperature of the pressurizer. After the failure, one of the two thermocouples in the pressurizer thermocouple well was employed for the temperature control. The degree of control which was achieved with this arrangement was ±0.5°C. Control with the normal system is within ±0.1°C.

(b) Results. – In-pile loop corrosion measurements and results are given in the numbered paragraphs that follow.

[4] G. H. Jenks, H. C. Savage, *et al.*, *HRP Quar. Prog. Rep. Jan. 31, 1955*, ORNL-1853, p 88.

[5] G. H. Jenks, H. C. Savage, *et al.*, *HRP Quar. Prog. Rep. Jan. 31, 1955*, ORNL-1853, p 86.

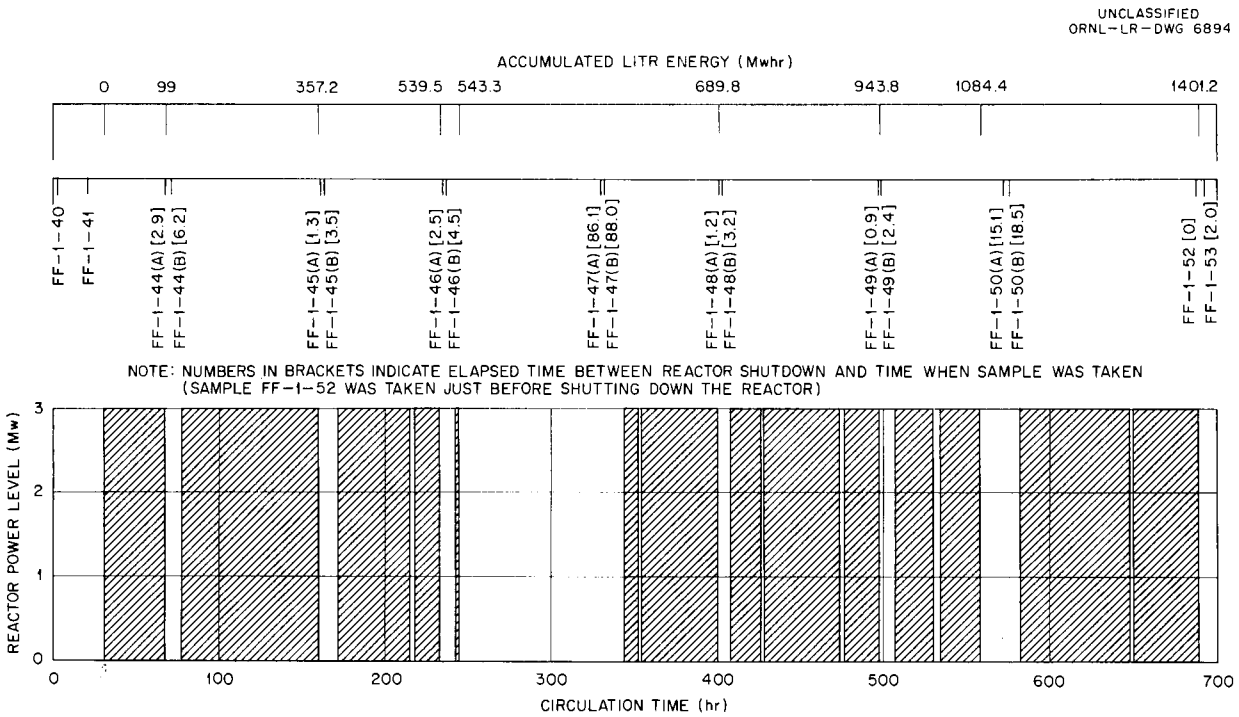

Fig. 4.4. Reactor Operating Schedule During In-Pile Operation.

1. Solution analyses. – The results of solution analyses for constituents other than products of irradiation are tabulated in Table 4.7. As shown in the column labeled "uranium," the uranium concentrations for a majority of the samples were appreciably less than those calculated for the loop solution. The same was true of the samples which were obtained in experiment DD; in that case the difference was ascribed to dilution with wash water during sampling.[4] Although the sampling procedure for this experiment was altered to minimize the possibility of dilution, it may have been encountered and may be, in part, the explanation for the low uranium concentration. The basis for this statement is primarily evidence which has been obtained with the third in-pile loop experiment GG now in progress. For the latter portion of experiment GG, sample dilution was determined quantitatively by adding a known amount of lithium sulfate to the wash water and analyzing for lithium in the samples. As with FF, low uranium concentrations were found; however, lithium was also found. When the results were corrected for dilution, as indicated by the amount of lithium, the uranium concentration in each case was in fair agreement with the calculated concentration for the loop solution.

The sample dilution factor listed in Table 4.7 is, in each case, the ratio of the calculated uranium concentration to the reported concentration in the sample. This factor was used to obtain for SO_4^{--} and Cu the "corrected concentrations" which are listed. These corrected values are plotted in Fig. 4.5. Reported values and calculated concentrations are also plotted for comparison. It is clear that the results for copper lend no support as to the accuracy of the dilution factor. The uncorrected reported values are in better agreement with the calculated values than are the corrected values. The deviation of the corrected values from the calculated ones is in the direction that would have been expected if the samples had not been diluted. The observed and corrected values for SO_4^{--} deviate in approximately equal amounts from the calculated values.

From the above results, it appears that the validity of the dilution factor is questionable. However, the calculated values for the other elements listed in Table 4.7 were obtained through use of the dilution factors. The values for cobalt,

TABLE 4.3. LOOP SPECIFICATIONS

Loop volume (including pressurizer), cc	1560
Pressurizer volume, cc	509
Flow rates	
Pressurizer, ml/sec	6
Core, gpm	5.8
Pump bearing material	Graphitar No. 14
Pump journal material	17-4 PH stainless steel
Pressure at which system was checked, psi	1200
Corrosion sample units	
Specimen materials	Zircaloy-2
In-line holder	Zircaloy-2 (No. 8)
Core holder	Zircaloy-2 (No. 9)
Minimum clearance, in.	
Core holder	0.050
In-line holder	0.046
Impact sample units	
Material	Zircaloy-2
Identification numbers	36, 38, 39, 40, 42, 44, 46, 50

TABLE 4.4. LOOP AREAS EXPOSED TO HIGH-TEMPERATURE SOLUTIONS

Component	Area Exposed (cm^2)
Stainless Steel*	
Total main circulation lines (not including pump and core)	1553
Pressurizer	
Total	(706)
Area wetted when filled with 300 ml of solution	414
Pressurizer lines	300
Core	445
Pump	
Scroll	272
Impeller	159
Total	3143
Zircaloy-2	
Core holder	162
In-line holder	162
Specimens	
12 core specimens	34
12 in-line specimens	34
8 impact specimens	152
Total	544

*Areas are nominal.

TABLE 4.5. SUMMARY OF PREPARATORY OPERATIONS

Time (hr)	Conditions
20.8	H_2O
4.0	3 wt % tribasic sodium phosphate + N_2 (partial pressure 85 psi), 100°C
18.4	5 wt % HNO_3 + N_2 (partial pressure 70 psi), 100°C
4.0	5 wt % HNO_3 + N_2 (partial pressure 70 psi), 100°C
22.0	Distilled H_2O + O_2 (partial pressure 30 psi), 250°C
12.7	37 g of U per liter of UO_2SO_4 (88% enrichment) + 0.03 *m* $CuSO_4$ + 0.03 *m* H_2SO_4 + O_2 (partial pressure 10 to 100 psi), 250°C
New pump installed	
4.3	Distilled H_2O + O_2 (partial pressure 50 psi), 250°C
4.2	37 g of U per liter of UO_2SO_4 (88.8% enrichment) + O_2 (partial pressure 80 psi), 250°C
8.0	Distilled H_2O + O_2, 250°C
123.5	27.1 g of U per liter of UO_2SO_4 (normal) + 0.031 *m* $CuSO_4$ + 0.0085 *m* H_2SO_4 + O_2, 250°C

TABLE 4.6. ANALYSES OF SAMPLES FROM LOOP INVENTORY DURING PREPARATORY OPERATIONS*

Solution	Sample No.	Total Circulation Time for Each Solution (hr)	Inventory at Time of Sampling (ml)	Uranium		Sulfate		pH	Copper		Cobalt		Nickel		Chlorine		Chromium		Iron		Aluminum	
				Conc (mg/ml)	Total (g)	Conc (mg/ml)	Total (g)		Conc (μg/ml)	Total (mg)	Conc (μg/ml)	Total (mg)	Conc (μg/ml)	Total (mg)	Conc (μg/ml)	Total (mg)	Conc (μg/ml)	Total (mg)	Conc (μg/ml)	Total (mg)	Conc (μg/ml)	Total (mg)
H_2O		20.8	1100																			
3% TSP	FF-1-1A	4.0	1320								1	1.3	1	1.3	13	17			1.2	1.6		
5% HNO_3	FF-1-4	18.4	1210						20	24.2	2.2	2.7	278	336	1	1.2	495	599	1854	2243	7.7	9.3
5% HNO_3 (2nd run)	FF-1-8	4.0	1200						1	1.2	1	1.2	5	6.0			3	3.6	28	34	24	29
H_2O	FF-1-13	22.0	1054						1	1.1	1	1.1	1	1.1	2	2.1			1	1.1	1	1.1
Enriched UO_2SO_4	FF-1-21	12.7	1092	37.0	40.4	20.8	22.7	1.53	1800	1966			212	232	2	2.2	1	1.1	42	46		
New pump installed																						
H_2O	FF-1-26	4.3	1190																			
Enriched UO_2SO_4	FF-1-28	4.2	975																			
H_2O		8.0	1130																			
Normal UO_2SO_4	FF-1-38	123.5	984	27.1	26.7			1.92	1770	1742			63	62			12	11.8	1	1.0	15	14.8

*Constituent concentrations and totals shown are not cumulative but represent the quantities present for operation with each solution.

TABLE 4.7. ANALYSES OF SAMPLES FROM LOOP INVENTORY DURING ENRICHED-SOLUTION OPERATIONS[a]

Sample	Total Circulation Time (hr)	Accumulated LITR Energy (Mwhr)	Elapsed Time from LITR Shutdown to Sample (hr)	Inventory Volume (25°C) at Time of Sample (ml)	Sample Dilution Factor	Uranium		Sulfate			Copper			Cobalt		Nickel		Chlorine		Chromium		Iron		Aluminum		Zirconium		pH	Specific Gravity
						Rep (mg/ml)	Calcd[b] (mg/ml)	Rep (mg/ml)	Cor (mg/ml)	Calcd[c] (mg/ml)	Rep (mg/ml)	Cor (mg/ml)	Calcd[c] (mg/ml)	Rep (mg/ml)	Calcd Total[d] (g)	Rep (mg/ml)	Calcd Total[d] (g)	Rep (mg/ml)	Calcd Total[e] (g)	Cor (mg/ml)	Calcd Total[e] (g)	Cor (mg/ml)	Calcd Total[e] (g)	Rep (mg/ml)	Calcd Total[d] (g)	Cor (mg/ml)	Calcd Total[e] (g)		
Original solution																													
FF-1-42, FF-1-43	0	0	0	1170	1.0	39.95 (G)	39.95	25.15 (IE)	25.15	25.15	1.785 (P)	1.785	1.785	(ND) (C)	(ND)	(ND) (C)	(ND)	<0.001 (T)	<0.0017	0.025 (C)	0.0293	(ND) (C)	(ND)	0.0021 (S)	0.0025	(ND) (C)	(ND)	1.3	1.056 (G)
Y-12 operation																													
FF-1-40	1.5	0	0	1186	0.99	39.99 (T)	39.43	25.06 (IE)	24.82	24.82	1.872 (P)	1.853	1.762	(ND) (C)	(ND)	(ND) (C)	(ND)	<0.001 (T)	<0.0017	0.004 (C)	0.0047	(ND) (C)	(ND)	0.0011 (S)	0.0013	(ND) (C)	(ND)	1.45	1.05+ (G)
FF-1-41	20.8	0	0	1151	0.99	39.94 (T)	39.43	23.44 (IE)	23.21	24.82	1.837 (P)	1.819	1.762	(ND) (C)	(ND)	0.016 (C)	0.018	0.005 (T)	0.0057	0.019 (C)	0.0219	0.011 (C)	0.0127	0.0042 (S)	0.0044	(ND) (C)	(ND)	1.3	1.05+ (G)
Pump[f] shut down	23.1	0																											
X-10 operation[g]	30.8	0																											
FF-1-44 (a)	67.8	99.0	2.9	1142	1.00	39.4 (T)	39.4	23.9 (IE)	23.9	24.8	1.75 (P)	1.75	1.76	0.016 (T)	0.019	0.178 (P)	0.204	0.005 (T)	0.007	0.030 (C)	0.034	0.092 (C)	0.105			0.072 (C)	0.082	1.55	
(b)	71.1	99.0	6.2	1121	1.03	38.3 (T)	39.4	22.6 (IE)	23.3	24.8	1.73 (P)	1.79	1.76	0.013 (T)	0.015	0.168 (P)	0.198	0.004 (T)	0.005	0.014 (C)	0.016	0.095 (C)	0.107			0.061 (C)	0.068	1.55	
FF-1-45 (a)	161.2	357.2	1.3	1054	1.11	35.6 (T)	39.4	21.7 (IE)	24.1	24.8	1.76 (P)	1.96	1.76	0.133 (T)	0.157	0.520 (P)	0.624	0.003 (T)	0.004	0.017 (C)	0.018	0.033 (C)	0.035	0.050 (C)	0.059	0.139 (C)	0.146	1.65	
(b)	163.4	357.2	3.5	1043	1.09	36.2 (T)	39.4	23.4 (IE)	25.5	24.8	1.81 (P)	1.97	1.76	0.021 (T)	0.026	0.579 (P)	0.680	0.005 (T)	0.006	0.007 (C)	0.007	0.058 (C)	0.061	0.048 (C)	0.055	0.065 (C)	0.068	1.65	
FF-1-46 (a)	234.4	536.5	2.5	1051	1.23	32.0 (T)	39.3	21.5 (IE)	26.5	24.8	1.60 (P)	1.96	1.76	0.021 (T)	0.028	0.581 (P)	0.783	0.004 (T)	0.006	0.011 (C)	0.012	0.085 (C)	0.089	0.069 (C)	0.091	0.076 (C)	0.080	1.70	
(b)	236.4	536.5	4.5	1038	1.21	32.6 (T)	39.3	24.4 (IE)	29.5	24.8	1.84 (P)	2.22	1.76	0.019 (T)	0.024	0.451 (P)	0.608	0.004 (T)	0.006	0.007 (C)	0.007	0.068 (C)	0.071	0.081 (C)	0.104	0.053 (C)	0.055	1.75	
FF-1-47 (a)	330.1	543.3	86.1	1047	1.12	35.0 (T)	39.3	21.8 (IE)	24.4	24.8	1.74 (P)	1.95	1.76	0.022 (T)	0.027	0.660 (P)	0.823	0.014 (T)	0.005	0.047 (C)	0.049	0.041 (C)	0.043	0.051 (C)	0.064	0.047 (C)	0.049	1.50	
(b)	332.0	543.3	88.0	1034	1.20	32.7 (T)	39.3	21.9 (IE)	26.3	24.8	1.64 (P)	1.97	1.76	0.020 (T)	0.029	0.648 (P)	0.863	0.004 (T)	0.006	0.070 (C)	0.072	0.050 (C)	0.052	0.045 (C)	0.061	0.058 (C)	0.056	1.75	
FF-1-48 (a)	401.6	689.8	1.2	1054	1.17	33.5 (T)	39.3	22.2 (IE)	26.0	24.8	1.71 (P)	2.00	1.76	0.025 (T)	0.035	0.855 (P)	1.124	0.006 (T)	0.008	0.025 (C)	0.026	0.034 (C)	0.036	0.032 (C)	0.045	0.036 (C)	0.038	1.70	
(b)	403.6	689.8	3.2	1041	1.23	31.9 (T)	39.3	23.5 (IE)	28.9	24.8	1.67 (P)	2.05	1.76	0.026 (T)	0.038	0.800 (P)	1.107	0.006 (T)	0.009	0.025 (C)	0.026	0.043 (C)	0.045	0.032 (C)	0.047	0.043 (C)	0.045	1.70	
FF-1-49 (a)	497.3	943.8	0.9	1053	1.23	31.9 (T)	39.3	22.0 (IE)	27.0	24.8	1.55 (P)	1.90	1.76			0.928 (P)	1.299	0.006 (T)	0.009	0.012 (C)	0.013	0.032 (C)	0.034	0.028 (C)	0.043	0.082 (C)	0.086	1.88	
(b)	498.8	943.8	2.4	1041	1.27	30.9 (T)	39.3	21.0 (IE)	26.6	24.8	1.61 (P)	2.04	1.76	0.022 (T)	0.035	0.078 (P)	1.272	0.006 (T)	0.009	0.023 (C)	0.024	0.034 (C)	0.035	0.027 (C)	0.043	0.041 (C)	0.043	1.88	
FF-1-50 (a)	572.1	1084.4	15.1	1052	1.14	34.6 (T)	39.3	20.0 (IE)	22.8	24.8	1.75 (P)	1.99	1.76	0.034 (T)	0.047	0.820 (P)	1.111	0.006 (T)	0.009	0.046 (C)	0.048	0.050 (C)	0.053	0.053 (C)	0.071	0.023 (C)	0.024	1.80	
(b)	575.5	1084.4	18.5	1039	1.16	34.0 (T)	39.3	24.0 (IE)	27.8	24.8	1.86 (P)	2.16	1.76	0.017 (T)	0.027	0.729 (P)	1.017	0.005 (T)	0.007	0.046 (C)	0.048	0.035 (C)	0.036	0.069 (C)	0.091	0.022 (C)	0.023	1.80	
FF-1-52[h]	687.9	1401.2	0	1050	1.05	37.4 (T)	39.3	24.3 (IE)	25.5	24.8	1.80 (P)	1.90	1.76			0.818 (P)	1.054	0.006 (T)	0.008	0.013 (C)	0.014	0.028 (C)	0.029	0.060 (C)	0.076	0.029 (C)	0.031	1.90	
FF-1-53	692.3	1401.2	3.5	1038	1.08	36.4 (T)	39.3	22.8 (IE)	24.7	24.8	1.72 (P)	1.85	1.76			0.802 (P)	1.061	0.005 (T)	0.007	0.025 (C)	0.026	0.029 (C)	0.030	0.060 (C)	0.078	0.041 (C)	0.043	1.90	

[a]Where no values are given, either an analysis was not requested or the analytical results were not reliable.
G Gravimetric; P Polarographic; C Colorimetric; S Spectrographic; IE Ion exchange, volumetric; ND Not detected; T Titrimetric

[b]Determined from calculated uranium and inventory balance.

[c] $\frac{\text{(Original concentration)} \times \text{(Calculated uranium concentration at time of sample)}}{\text{(Original uranium concentration)}}$

[d]Corrected for sample dilution and for amounts withdrawn in previous samples.

[e]From calculated inventory and from concentration corrected for sample dilution.

[f]Loop inoperative about 170 hr between shutdown at Y-12 and startup at X-10. (Inventory was not removed from loop during this period.)

[g]Started reactor at 3 Mw.

[h]Taken with reactor on.

[redacted]

ORNL-LR-DWG 6895

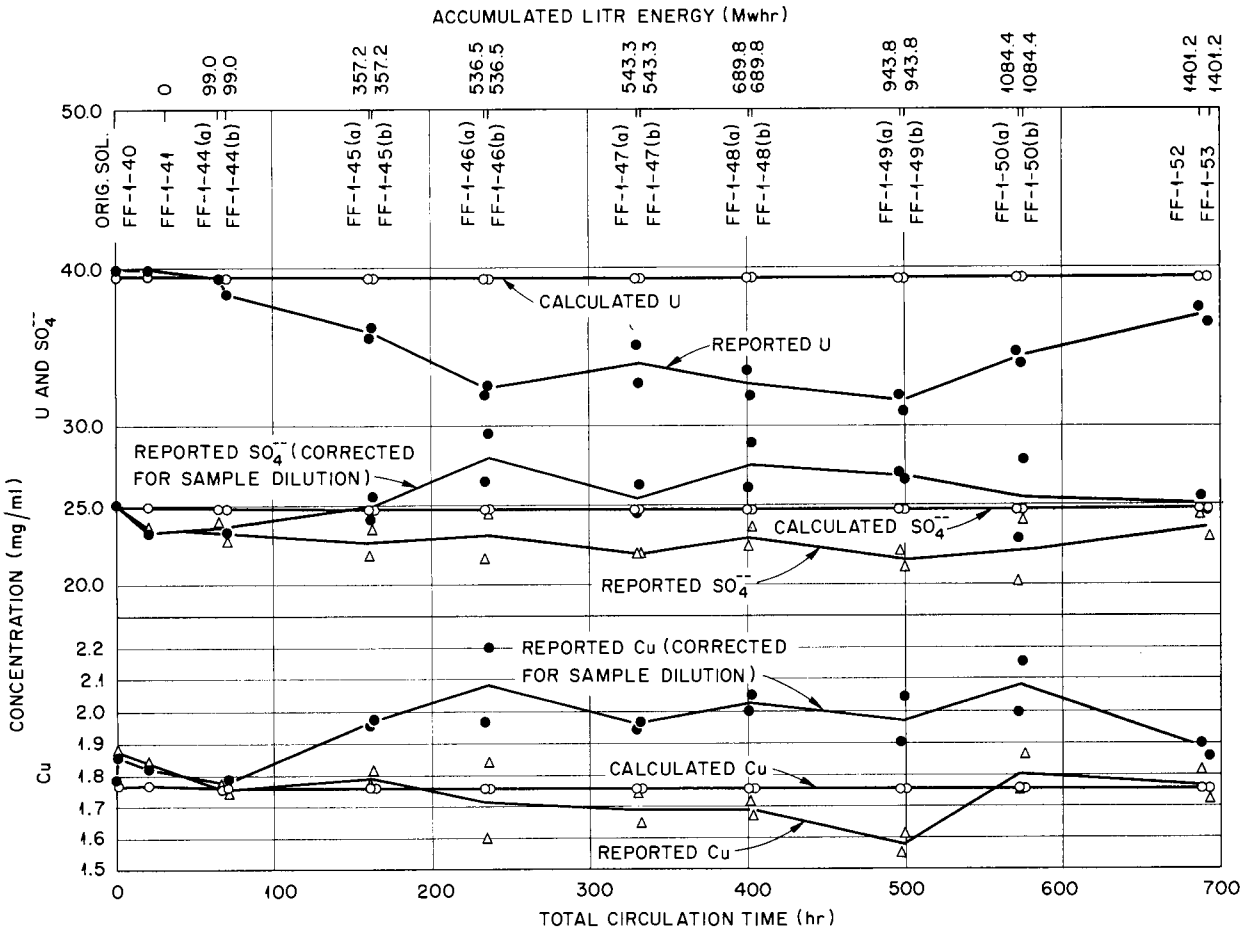

Fig. 4.5. Concentration of U, SO_4^{--}, and Cu in Solution Samples.

nickel, chlorine, and aluminum were also corrected for the amount of the material withdrawn in sampling. No correction was applied to pH measurements. The calculated values are plotted against circulation time in Fig. 4.6.

2. *Oxygen consumption.* – The results of oxygen depletion measurements are shown in Table 4.8. For conversion from gas volumes to pressures in the loop at operating temperatures, the factor, 100 psi = 1050 cc at STP, is applicable.

3. *Fission power in loop.* – The results of solution analyses for total fissions are presented in Table 4.9. A sample cooling period of three months preceded these analyses, so that interference from 13-day Cs^{136} was presumably eliminated. The reported values were corrected by the sample dilution factor described above and were also corrected for the amounts of cesium withdrawn from the loop in sampling. The values for fission power were calculated from the corrected cesium analytical results. Thus, the values represent the average power from the start of irradiation to the time of sampling.

The difference between the electrical power required to maintain loop temperature with and without the reactor at power averaged 865 w. No significant change in the power was observed throughout the operation. The maximum deviation from the average was about 3%.

The neutron flux at a given specimen position in the core was determined from comparison between the induced activity in the specimens and the induced activity in a control specimen which was irradiated for a known nvt in the ORNL Graphite

TABLE 4.8. OXYGEN CONSUMPTION IN LOOP FF

Remarks	Sample No.	LITR Energy (Mwhr)	Total Solution Circulation Time (hr)	O_2 Additions to Loop (cc at STP)	O_2 Withdrawn from Loop* (cc at STP)	Total O_2 Charged to Loop Less O_2 Withdrawn in Sampling (cc at STP)	O_2 Volume at Time of Sample (cc at STP)	O_2 Consumed Since Last Sample (cc at STP)	Cumulative Amount of O_2 Consumed (cc at STP)	Calculated Corrosion Penetration of Type 347 Stainless Steel (mils)
Mockup operation										
Original O_2 fill		0	0	1124	0	1124		0	0	
	FF-1-40	0	1.5		24	1100				
	FF-1-41	0	20.8		7	1093				0.002
Circulating pump shut down		0	23.1		0	1093	1052		41	
LITR operation										
Reactor started up		0	30.9	0	0	1093	1052		41	0.002
	FF-1-44 (a)	99.0	67.8	0	13	1093	342	713	751	0.04
	(b)	99.0	71.1	0		1093	291	51	802	0.04
O_2 addition FF-1			71.8	1361	0	2441	1641			
	FF-1-45 (a)	357.2	161.2	0	3	2441	290	1349	2151	0.12
	(b)	357.2	163.4	0		2441	252	38	2189	0.12
O_2 addition FF-2			165.0	1092	0	3530	1344			
	FF-1-46 (a)	536.5	234.4	0	10	3530	714	627	2816	0.15
	(b)	536.5	236.4	0		3530	697	17	2833	0.15
O_2 addition FF-3			238.7	610	0	4130	1324			
	FF-1-47 (a)	543.3	330.1	0	10	4130	928	369	3202	0.17
	(b)	543.3	332.0	0		4130	928	0	3202	0.17
	FF-1-48 (a)	689.8	401.6	0	7	4120	617	301	3503	0.19
	(b)	689.8	403.6	0		4120	606	11	3514	0.19
O_2 addition FF-4			473.9	799	0	4912				
	FF-1-49 (a)	943.8	497.3	0	10	4912	908	490	4004	0.21
	(b)	943.8	498.8	0		4912	902	6	4010	0.22
	FF-1-50 (a)	1084.4	572.1	0	7	4902	582	310	4320	0.23
	(b)	1084.4	575.5	0		4902	568	14	4334	0.23
O_2 addition FF-5			576.0	682	0	5577	1245			
Sample taken with reactor on	FF-1-52	1401.2	687.9	0	9	5577	697	546	4880	0.26
Reactor shut down		1401.2	687.9			5577				
	FF-1-53	1401.2	692.3	0		5577	687	10	4890	0.26
Circulating pump shut down		1401.2	693.0	0		5577	683	4	4894	0.26

*Calculated amount removed as O_2 dissolved in sample.

[redacted]

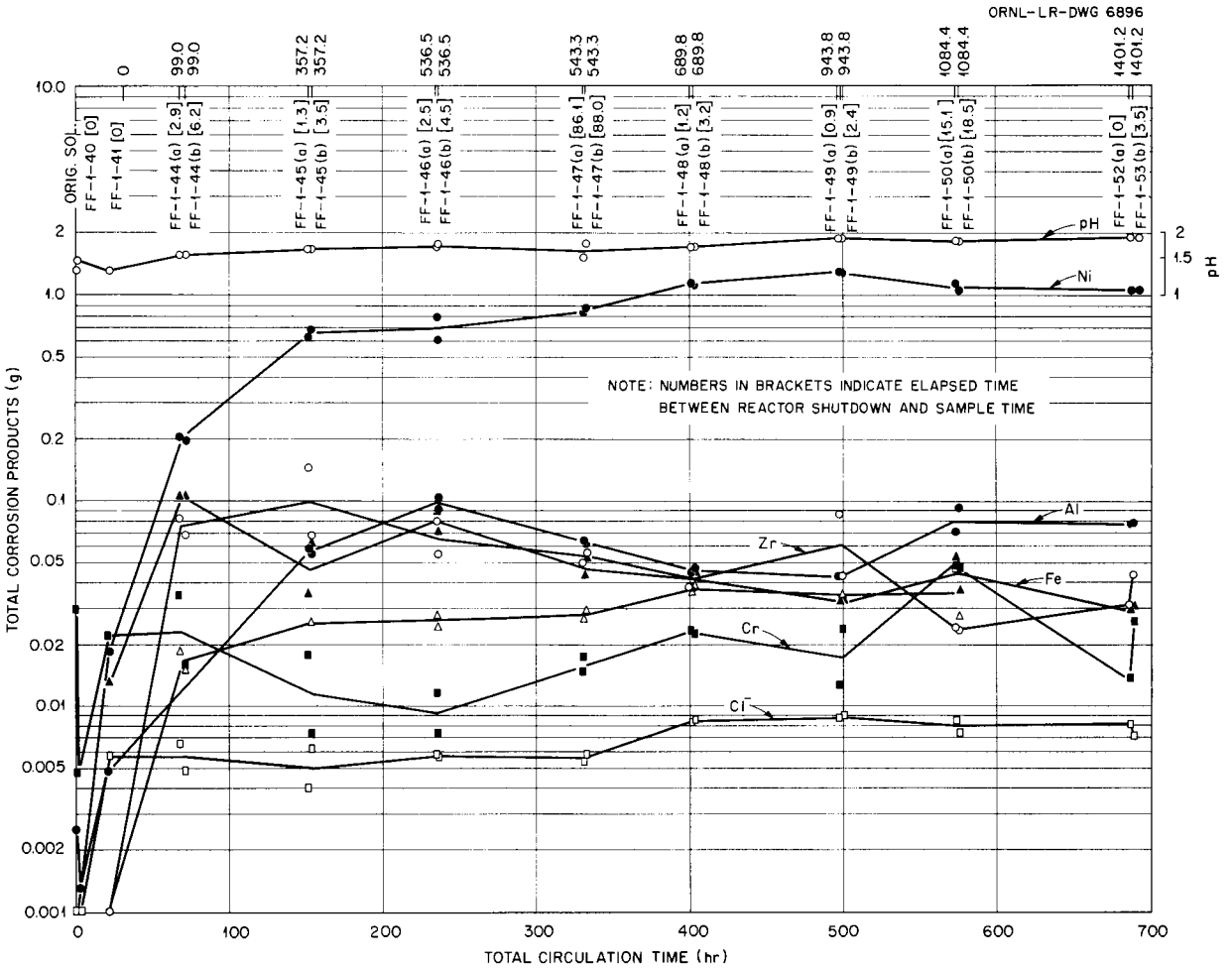

Fig. 4.6. Total Corrosion Products in Solution During Enriched-Solution Operation.

TABLE 4.9. FISSIONS IN LOOP SOLUTION

Sample No.	Accumulated LITR Energy (Mwhr)	Inventory Volume at Time of Sample (ml at 25°C)	Calculated Uranium Concentration (mg/ml)	Total Fissions per ml × 10^{-15}		Total Fission Power in Loop Solution at 3 Mw (w)
				Analysis	Corrected*	
FF-1-44 (a)	99.0	1142	39.39	2.00	2.00	614
FF-1-45 (a)	357.2	1054	39.36	7.07	8.02	629
FF-1-46 (a)	536.5	1051	39.34	9.48	11.99	625
FF-1-47 (a)	543.3	1047	39.32	10.00	11.81	606
FF-1-48 (a)	689.8	1054	39.34	11.7	14.60	595
FF-1-49 (a)	943.8	1053	39.32	16.1	21.05	625
FF-1-50 (a)	1084.4	1052	39.34	19.1	23.57	609
FF-1-52	1401.2	1050	39.33	23.9	27.44	541
FF-1-53	1401.2	1038	39.33	26.0	30.77	606

*Corrected to include amounts withdrawn in previous samples and for sample dilution.

Reactor. The activity which was employed was that of Zr^{95}-Nb^{95}. These isotopes are also produced in fission and are known to adsorb strongly on Zircaloy-2 under the conditions of the experiment. Hence, it was necessary to clean the specimens thoroughly before they were counted. Chemical cleaning was employed with a solution comprised of HF, HCl, HNO_3, and H_2O in the volume ratios 0.4:1:2:5; concentrated acids were used. Six washings were given each specimen, and fresh solution was used for each wash. After cleaning, the core specimens appeared free of oxide film.

As a check on the degree of removal of fission products in this treatment, two of the in-line specimens, which are free of induced activity, were cleaned in a similar fashion and were analyzed for Zr-Nb along with the core specimens. However, visual inspection showed that the oxide film was not completely removed from these surfaces. Hence, it was anticipated that some Zr-Nb activity would be found on the in-line specimens; the amount of activity actually found was approximately equal to that of core specimen L. However, the gross activity of the in-line specimen, as measured with a cutie pie, was three times that of core specimen L, so that if the fission-product Zr-Nb contamination is assumed to be proportional to the gross activity, the maximum contribution of fission-product Zr-Nb to the total Zr-Nb activity of core specimen L would be 30%. If this contamination is also assumed to be constant for all core specimens, the possible maximum contribution of the fission-product Zr-Nb to the total Zr-Nb activity will be inversely proportional to the total measured. For example, the maximum contribution to the activity of specimen A would be 5%.

The results of the analysis of these data are shown in Table 4.10. The control specimen was irradiated for 315 hr in an average flux of 6.15×10^{11} neutrons/cm^2/sec. The elapsed time between termination of exposure and counting was 7.5 days.

TABLE 4.10. INDUCED Zr-Nb ACTIVITY IN CORE SPECIMENS

Coupon Position	Cleaned Weight When Counted (g)	Zr-Nb Activity (0.76-Mev gamma)		Neutron Flux at 3 Mw (neutrons/cm^2/sec $\times 10^{-12}$)	Power Density at 3 Mw* (w/ml)
		Counts/min/coupon $\times 10^{-6}$	Counts/min/g $\times 10^{-6}$		
		Core Specimens			
A	1.4688	8.29	5.64	2.77	3.66
C	1.4962	6.65	4.44	2.18	2.88
D	1.4989	5.87	3.92	1.93	2.54
E	1.5147	5.13	3.39	1.66	2.20
F	1.5190	4.30	2.83	1.39	1.83
H	1.5009	3.39	2.26	1.11	1.46
I	1.5094	2.80	1.86	0.91	1.20
J	1.4962	2.52	1.68	0.83	1.09
L	1.4997	1.61	1.07	0.53	0.69
		In-Line Specimens			
E	1.5288	1.64	1.07		
F	1.5424	1.45	0.94		
		Control Specimen			
	1.6045	1.58	0.98	6.15×10^{11}	

*Uranium concentration, 39.3 mg/ml; 88.8% enrichment.

For the loop specimens, 61 days elapsed between termination of exposure and counting. Calculated values for the power density, which are proportional to the neutron flux at the surface of the specimen, are also tabulated. A uranium concentration of 39.3 mg/ml, 88.8% enriched, was the basis for the calculation.

The results of cesium analyses and electrical-power measurements and the effects of induced activities indicate that the intensities of reactor radiation for this experiment were appreciably higher[4] than those for experiment DD. This increase is ascribed to a rearrangement of the fuel elements in the LITR between experiments. In this rearrangement, three fuel elements were placed in front and to the right of the adjacent beam hole, HB-5.

4. *Uranium balance.* – The amount of uranium initially charged to the loop was 47.02 g. An additional 8.77 g was added to the loop during operation by means of fuel additions.

Data obtained in the determination of the weight of uranium removed from the loop are shown in Table 4.11, together with the amounts charged to the loop.

TABLE 4.11. ACTUAL URANIUM BALANCE

Source	Solution Weight (g)	Specific Gravity	Solution Volume (ml)	Uranium Concentration by Analysis (mg/ml)	Weight of Uranium (g)
		Charged to Loop			
Original solution charged to system	1244	1.056	1178	39.95	47.02
Solution additions during operation			220	39.95	8.77
Total					55.79
		Recovered from Loop			
From weigh tank *after* sampling of contents [sample purges and flushes through sample 50 (b)]	4470[a]	1.0[b]	4470	2.40	10.73
From weigh tank *after* sampling of contents (purges from samples 52 and 53 plus loop contents and rinses)	7530[a]	1.0[b]	7530	6.18	46.54
Loop inventory samples sent to laboratory			77.3	40.0 to 36.4	2.91
Weigh tank samples sent to laboratory[c]					
Samples 51 (a) and (b) [weigh tank contents, sample purges, and flushes through sample 50 (b)]			2.1	2.40	0.01
Samples 54 (a) and (b), 55, 57, and 58 [weigh tank contents, sample purges, and flushes for samples following 50 (b), plus inventory drained from loop and loop rinses]			6.80	6.18	0.04
Total					60.23

[a] From weigh tank reading.

[b] Assumed.

[c] Weigh tank was drained of sample purges and flushes after sample 50 (b). Therefore, final contents of tank included purges and flushes from samples 52 and 53 plus loop inventory and loop rinses.

As in the first loop, the resulting value for the total weight of uranium removed is 8% greater than the value for the charged weight. No explanation for this discrepancy is apparent other than that of experimental error.

5. *Radiolytic gas pressures.* – The steady-state pressures of radiolytic gases which were observed under irradiation were in the range 8 to 11.5 psi. These data will be correlated with those from the first loop and will be reported later.

(c) Corrosion Indicated by Nickel and Oxygen Data. – Values for corrosive penetration have been calculated which correspond to the amount of nickel found in the different samples and to the oxygen depletion data. It was assumed in these calculations that all steel surfaces in contact with high-temperature solutions corroded uniformly and that steel surfaces in the cool rotor region of the pump did not corrode. It was also assumed that oxygen was consumed only in the oxidation of steel. Calculated values are plotted against circulation time in Fig. 4.7. Other quantities of interest are shown on additional scales. The curves are of the same general type as those obtained in experiment DD, although the indicated rates of corrosion are greater than before. As calculated from the oxygen data, the corrosion rate for the first 200 hr was about 6 mpy. From the end of the 200-hr exposure to the end of the test, the rate was constant at 2.2 mpy. The nickel results were very erratic. However, if the corrosion of the Zircaloy-2 in the core is taken into account and

[redacted]

ORNL-LR-DWG 6177A

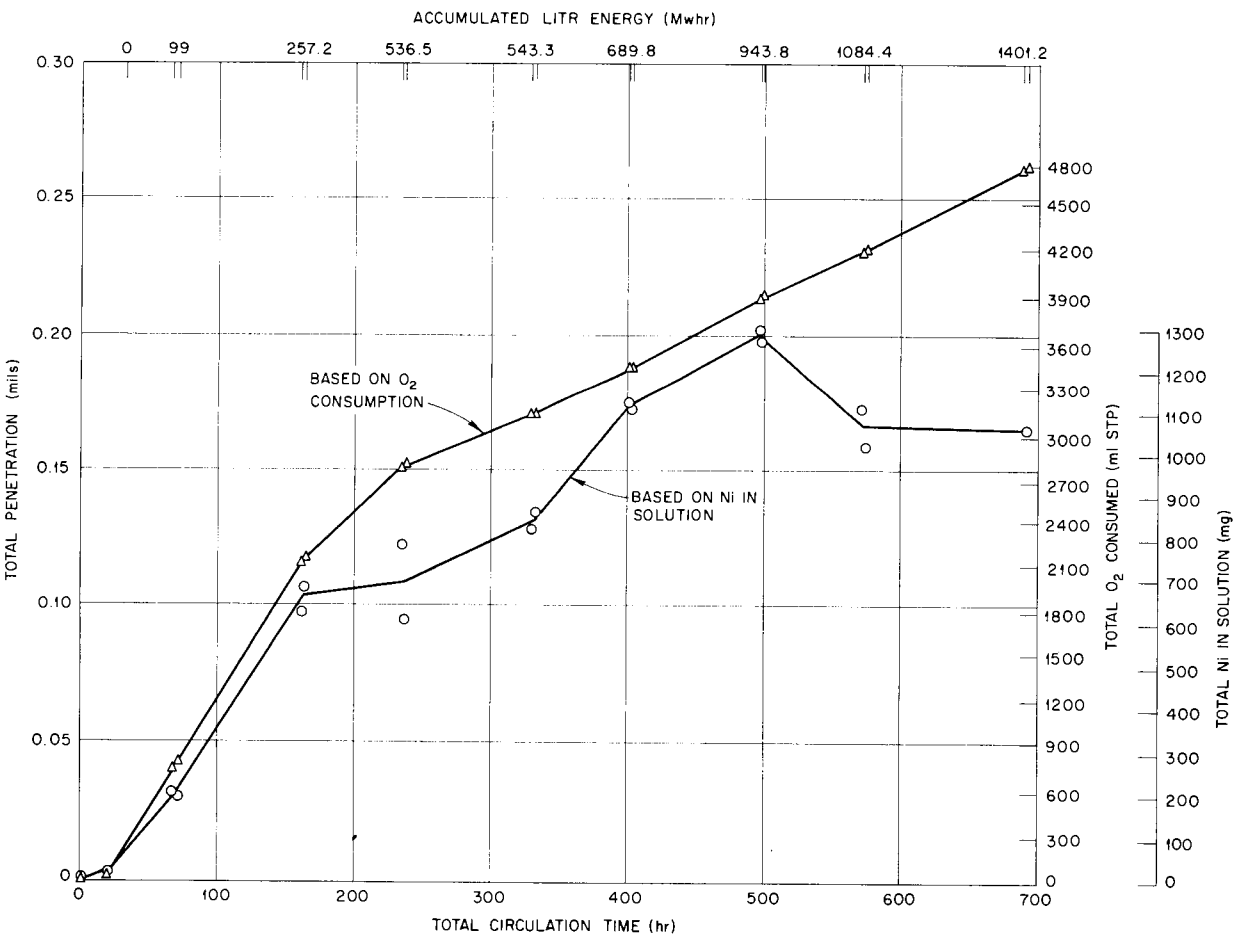

Fig. 4.7. Over-all Corrosion Penetration of Type 347 Stainless Steel (FF Loop).

a comparison made between the oxygen and nickel results at 500 hr, good agreement is obtained. As will be reported later, the estimated average corrosion rate of Zircaloy-2 in the core was 1.5 mpy. At this rate approximately 200 cc of O_2 was consumed by the Zircaloy-2 during 500 hr of exposure. If the oxygen curve in Fig. 4.7 is lowered by this amount, the point at 500 hr is in near agreement with the points from the nickel data.

(d) Performance of Equipment. – With the exception of the thermocouples noted previously, the performance of the equipment was satisfactory.

4.1.3 In-Pile Loop Experiment GG

The exposure of a third in-pile loop in the LITR has been completed. This experiment was similar to the previous experiment, FF. The circulation time for the installed loop was 1064 hr. The LITR energy during this time was 2692 Mwhr.

4.1.4 Remote Dismantling and Inspection

4.1.4.1 Dismantling, Loop FF

Operation of the dismantling cell in Building 4501 was generally satisfactory. Some difficulty was experienced because of the off-center attachment of the cable which is used for lowering the assembly into the cell. With this arrangement, the loop can does not hang vertically, and remote centering in the chuck is difficult. A new clamp has been designed and constructed which should eliminate centering difficulties.

An attempt was made to determine the cause of failure of the thermocouple between the pressurizer heater and the pressurizer before dismantling of the loop. This thermocouple appeared to be firmly attached to the loop, and the cause of failure remains unknown.

The portions of the loop which were removed and transferred to the Solid State Division hot cells were the core, the in-line sample holder, the pressurizer, a portion of the pressurizer heater, a sample of the piping which included the sample line filter, and the pump.

Two additional pieces of piping were removed from the entrance and exit of the core for decontamination studies by the Chemical Technology Division.

Removal of the remainder of the loop was normal. Arrangements have been made for the separate burial of this loop and all future loop remnants, so that a specific loop may be recovered if the need arises.

4.1.4.2 Results of Inspection and Evaluation, Loop FF

(a) Qualitative. – All surfaces outside the core area were covered with a heavy rust-like scale. Figures 4.8 and 4.9 are photographs of the pressurizer and pump, respectively. They show a uniform deposit of scale with no apparent localized attack, even in the high-velocity areas. Figure 4.10 is a photograph of the in-line coupon assembly after it was removed from the loop (as-removed condition). The clamping bands on either end are stainless steel, and the holder is Zircaloy-2; both materials were covered with the typical heavy scale. Figure 4.11 is a picture of the coupons and interior surface of the in-line assembly; it shows that there was no apparent velocity effect upon the amount of deposited scale.

Figure 4.12 is a photograph of the core coupon and impact specimen assembly in the as-removed state. All the stainless steel components in this area were covered with a rust-like scale. However, the deposit appeared to become thinner with increasing flux. The Zircaloy-2 holder and impact specimens were free from any scale deposit in the higher-flux regions. The only visible scale on the Zircaloy holder was located around the spider at the low-flux end of the assembly. Figure 4.13

PHOTO 13791

Fig. 4.8. HRP In-Pile Loop FF Pressurizer.

[redacted]

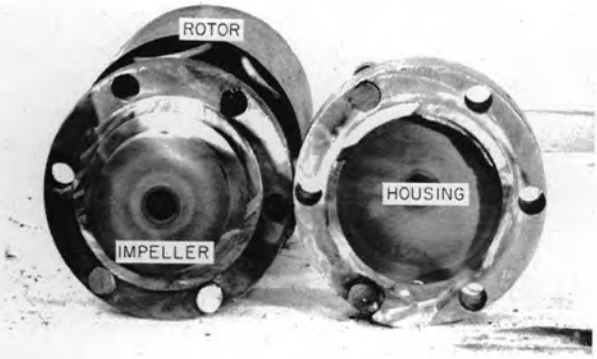

Fig. 4.9. HRP In-Pile Loop FF Pump.

is a view of the core coupons and holder after disassembly. The machining marks and stamped identifications were clearly visible on both holder and coupons.

Corrosion coupons, coupon holders, and impact specimens were all removed from the loop and weighed in the as-removed condition. An attempt was then made to defilm the coupons to determine more accurately the amount of corrosion. In out-of-pile experience no successful method has been found for removing the zirconium oxide film without subjecting the metal to attack; however, since this oxide is generally quite thin it was hoped that removal of the bulky deposited iron oxide scale would permit the determination of more accurate comparative weight data. Although microscopic examination of the heavy scale on the in-line

[redacted]

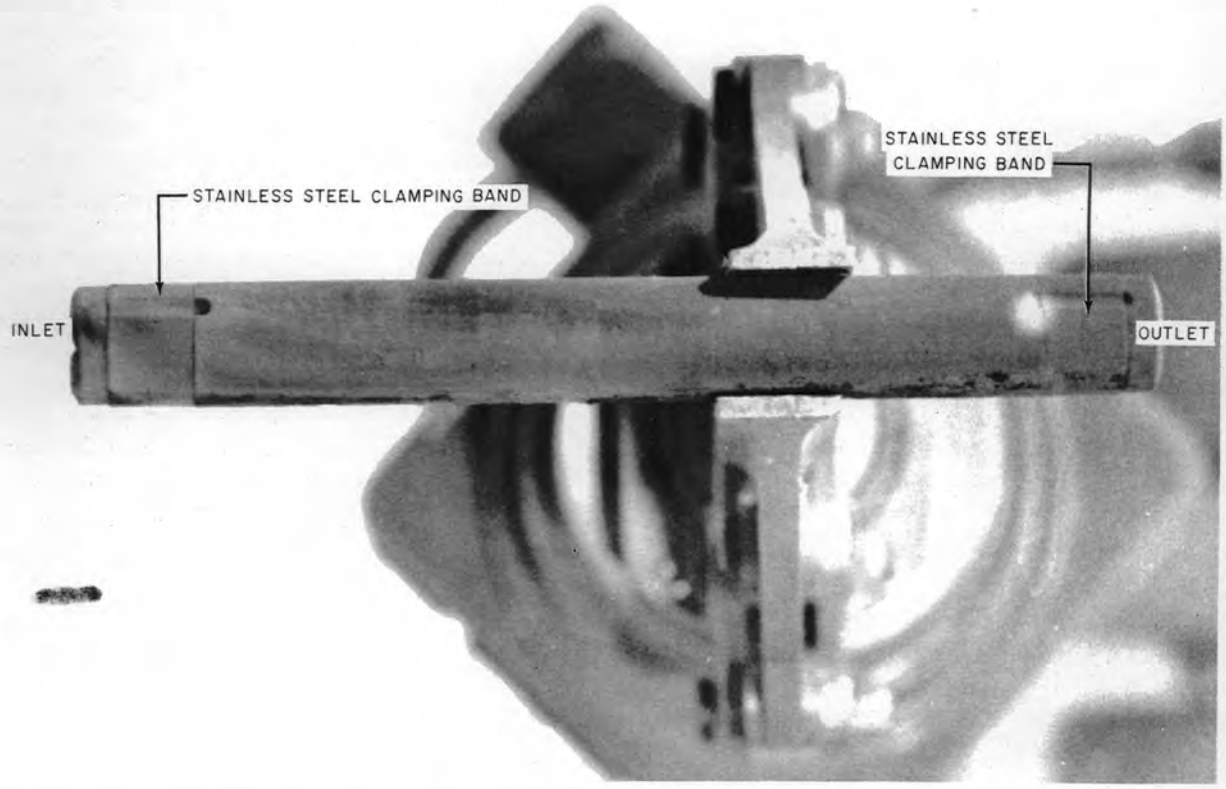

[redacted]

Fig. 4.10. HRP In-Pile Loop FF In-Line Coupon Assembly, as Removed from the Loop. Outside of Zircaloy-2 holder.

[redacted] [redacted] [redacted]

PHOTO 13789

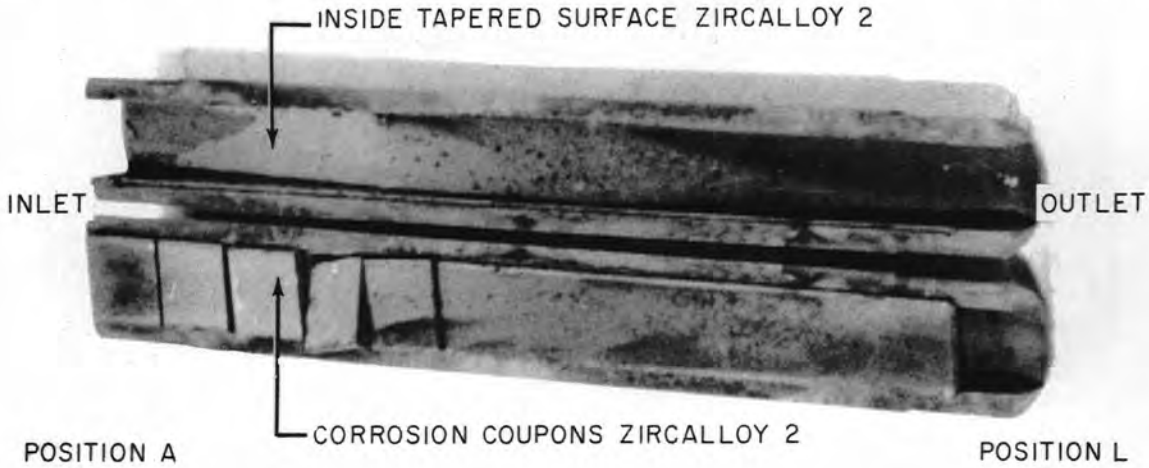

Fig. 4.11. HRP In-Pile Loop FF In-Line Coupon Assembly Before Defilming.

[redacted]

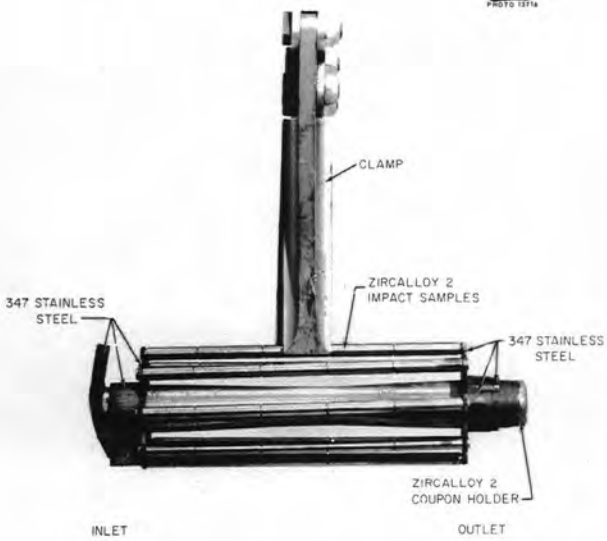

Fig. 4.12. HRP In-Pile Loop FF Core Specimen Assembly.

[redacted]

Fig. 4.13. HRP In-Pile Loop FF Core Coupon Assembly.

coupons showed that it had flaked off in some areas, prolonged cathodic treatment and mechanical brushing failed to remove this scale. Some of the scale was pulled from the metal surface by the use of Scotch tape, but this method was not completely effective either. This is evident from the "defilmed" weight of the in-line coupons shown in Table 4.12. Figures 4.14 and 4.15 are individual photographs of representative coupons, after defilming, from the core and in-line assemblies, respectively. There is no obvious indication of increased attack in the areas not protected by the holders, as was seen with the loop DD stainless steel core coupons.[4]

Examination of the stainless steel core body and cap surfaces indicated that the only change in the covering oxide scale was a reduction, with increasing flux, in the amount deposited, in contrast with the rather distinctive change in character observed[4] on the previous loop DD. Generally, there was no apparent evidence of localized attack. However, during the preirradiation testing of the loop at Y-12 a pin-hole leak was detected in the reducer at the rear, or low-flux end, of the core assembly. This leak was repaired by grinding out the metal in that area and back-filling with weld

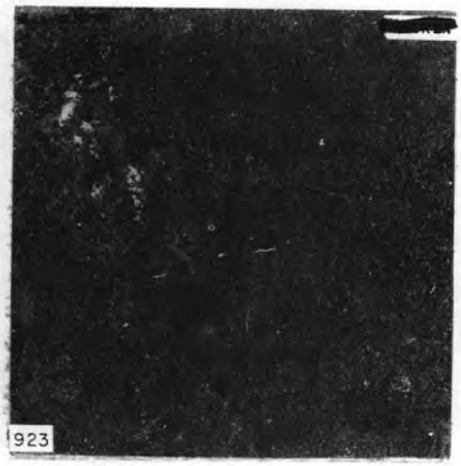

POSITION A (HIGH FLUX - LOW VELOCITY)

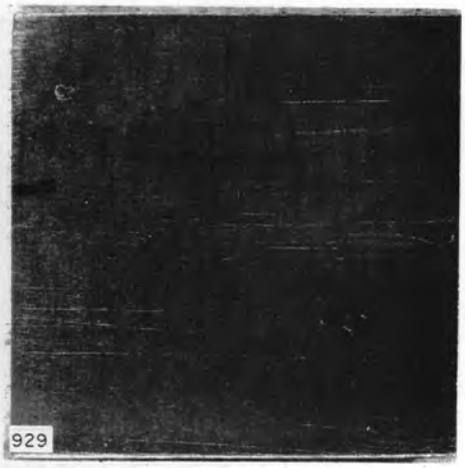

POSITION G (MEDIUM FLUX - HIGH VELOCITY)

POSITION L (LOW FLUX - LOW VELOCITY)

Fig. 4.14. Defilmed Zircaloy-2 Corrosion Coupons from the Core Array of In-Pile Loop FF. (A) High flux, low velocity; (G) medium flux, high velocity; (L) low flux, low velocity.

POSITION A (LOW VELOCITY)

POSITION G (HIGH VELOCITY)

POSITION L (LOW VELOCITY)

Fig. 4.15. Defilmed Zircaloy-2 Corrosion Coupons from the In-Line Array of In-Pile Loop FF. (A) Low velocity, (G) high velocity, (L) low velocity.

TABLE 4.12. CORROSION DATA FOR ZIRCALOY-2 CORROSION SPECIMENS

Sample No.	Position	Exposed Coupon Area (cm^2)	Flow Velocity at Leading Edge (fps)	Initial Weight (g)	As-Removed Weight (g)	Defilmed Weight (g)	Weight Change (mg)	Corrosion Penetration (mils)	Corrosion Rate* (mpy) 696 hr	Corrosion Rate* (mpy) 467 hr	Surface Appearance, As-Removed	Surface Appearance, After Defilming
								Core Coupons				
923 A	A	3.00	9.7	1.5679	1.5594	1.5590	−8.9	0.1797	2.27	3.36	All surfaces have fibrous texture	All surfaces have fibrous texture; little change
924 A	B	2.80	11.3	1.5759	1.5686	1.5678	−8.1	0.1752	2.21	3.27	All surfaces deeply etched; one corner scratched	Fine texture or deeply etched; one corner scratched
925 A	C	2.80	13.7	1.5710	1.5630	1.5628	−8.2	0.1774	2.24	3.32	All surfaces deeply etched	Fine texture or deeply etched
926 A	D	2.80	17.1	1.5731	1.5658	1.5656	−7.5	0.1622	2.05	3.04	All surfaces deeply etched	Fine texture or deeply etched
927 A	E	2.80	22.9	1.5796	1.5731	1.5729	−6.7	0.1449	1.83	2.71	All surfaces deeply etched	Fine texture or deeply etched
928 A	F	2.80	35.8	1.5822	1.5772	1.5769	−5.3	0.1146	1.45	2.15	All surfaces stained	Fine texture or deeply etched
929 A	G	2.80	41.5	1.5778	1.5730	1.5730	−4.8	0.1038	1.31	1.94	Some film	Fine texture or deeply etched; machine marks visible
930 A	H	2.80	50.5	1.5720	1.5678	1.5677	−4.3	0.0930	1.17	1.73	Some film	Fine texture or deeply etched; machine marks visible
931 A	I	2.80	28.2	1.5654	1.5619	1.5614	−4.0	0.0865	1.09	1.62	All surfaces covered with film	Fine texture or deeply etched; machine marks visible
932 A	J	2.80	19.9	1.5735	1.5722	1.5701	−3.4	0.0735	0.93	1.38	All surfaces covered with film; some scale	Fine texture or deeply etched; some scale remaining
933 A	K	2.80	15.2	1.5717	1.5686	1.5683	−3.4	0.0735	0.93	1.38	All surfaces covered with scale	Fine texture or deeply etched; some scale remaining
934 A	L	3.00	12.1	1.5657	1.5640	1.5631	−2.6	0.0525	0.66	0.98	All surfaces covered with scale	Fine texture or deeply etched
								In-Line Coupons				
911 A	A	3.00	9.7	1.5625	1.5756	1.5644	+1.9				Rusty scale covered all surfaces	Thin adherent film on all surfaces; some scale along edges; machine marks visible
912 A	B	2.80	11.3	1.5750	1.5906	1.5758	+0.8				Rusty scale covered all surfaces	Thin adherent film on all surfaces; some scale along edges; machine marks visible
913 A	C	2.80	13.7	1.5734	1.5871	1.5782	+4.8				As above but flaked	As above; flake film spots and small arc burn
914 A	D	2.80	17.1	1.5747	1.5886	1.5778	+3.1				As above but flaked	As above; flake film spots and small arc burn
915 A	E	2.80	22.9	1.5741	1.5864	1.5792	+5.1				As above but flaked	Black film covered with scale flakes
916 A	F	2.80	35.8	1.5774	1.5896	1.5780	+0.6				As above but flaked	Thin adherent film on all surfaces; some scale along edges; machine marks visible
917 A	G	2.80	41.5	1.5604	1.5722	1.5617	+1.3				As above but flaked	Thin adherent film on all surfaces; some scale along edges; machine marks visible
918 A	H	2.80	50.5	1.5730	1.5864	1.5759	+2.9				As above but flaked	Thin adherent film on all surfaces; some scale along edges; machine marks visible
919 A	I	2.80	28.2	1.5748	1.5878	1.5775	+2.7				As above but flaked	Thin adherent film on all surfaces; some scale along edges; machine marks visible
920 A	J	2.80	19.9	1.5673	1.5811	1.5696	+2.3				As above but flaked	Thin adherent film on all surfaces; some scale along edges; machine marks visible
921 A	K	2.80	15.2	1.5634	1.5767	1.5650	+1.6				As above but flaked	Thin adherent film on all surfaces; some scale along edges; machine marks visible
922 A	L	3.00	12.1	1.5857	1.6000	1.5894	+3.7				As above but flaked	Thin adherent film on all surfaces; some scale along edges; machine marks visible

*Two corrosion rates are presented: one based on the total operation time of 696 hr and the other based on the total radiation time of 467 hr (3 Mwhr of reactor time equivalent to 1 hr of total radiation time).

metal. When the core was sectioned after irradiation, a rather large pit or cavity was found in the area of this repair. Figures 4.16 and 4.17 are general views of the core sections showing the extent of this cavity. Figure 4.18 is a photograph, taken through the remote microscope, of the surface of the largest portion of the cavity. Since the other welds in the core showed no apparent concentrated attack, it is difficult to explain the cause of this cavity. It is hoped that metallographic examination of this area and the adjacent girth weld will help explain this phenomenon.

Additional metallographic sections have been taken from the core cap, the pressurizer, the pressurizer heater, and a section of the piping near the pump. These examinations, together with the metallographic examination of core coupons B, G, and K and in-line coupons B and G, will be made by the Remote Metallography Group of the Solid State Division.

Fig. 4.16. HRP In-Pile Loop FF Type 347 Stainless Steel Core Section, as Removed from Loop.

(b) Quantitative. – Sample-weight data for in-line and core specimens, with calculated values for corrosive penetration, are presented in Table 4.12. Descriptions of the surface appearance before and after defilming are included. The defilmed in-line specimens showed increases over the initial weights; hence, corrosion rates could not be calculated for these specimens. No correction has been applied for corrosion which occurred during loop operation before reactor insertion, but this corrosion was probably negligible.

Values for corrosive penetration of the core specimens are shown in Fig. 4.19 plotted vs the neutron flux to which the specimen was exposed when the reactor was operating at 3 Mw. Determination of these fluxes was described previously. The letter adjacent to each point identifies the coupon position. The number is the value for the solution velocity in fps past the leading edge of the specimen. The flux was not determined for three specimens, B, G, and K, since these were withheld for metallographic examination. The weight-loss data for these coupons are plotted separately at the left.

The data exhibit a linear relationship between neutron flux and weight loss, except for coupon A, which was in the highest flux. No effect of velocity on the corrosive attack is apparent. If the linear portion of the curve is extrapolated, the corrosion rate at 5 w/ml is 5.6 mpy. This is in near agreement with corrosion rates measured in bomb experiments at a power density of 5 w/ml and with rates for solution conditions similar to those employed in this loop.

Weight data for the in-line and core specimen holders and for the impact specimens are shown in Table 4.13. No attempt was made to defilm these pieces, and it was apparent from visual inspection that some oxide film remained on the core pieces. The in-line holder was heavily covered with oxide. Average corrosion rates estimated from the weight data for the core pieces are in approximate agreement with the average corrosion rates of the core coupon specimens.

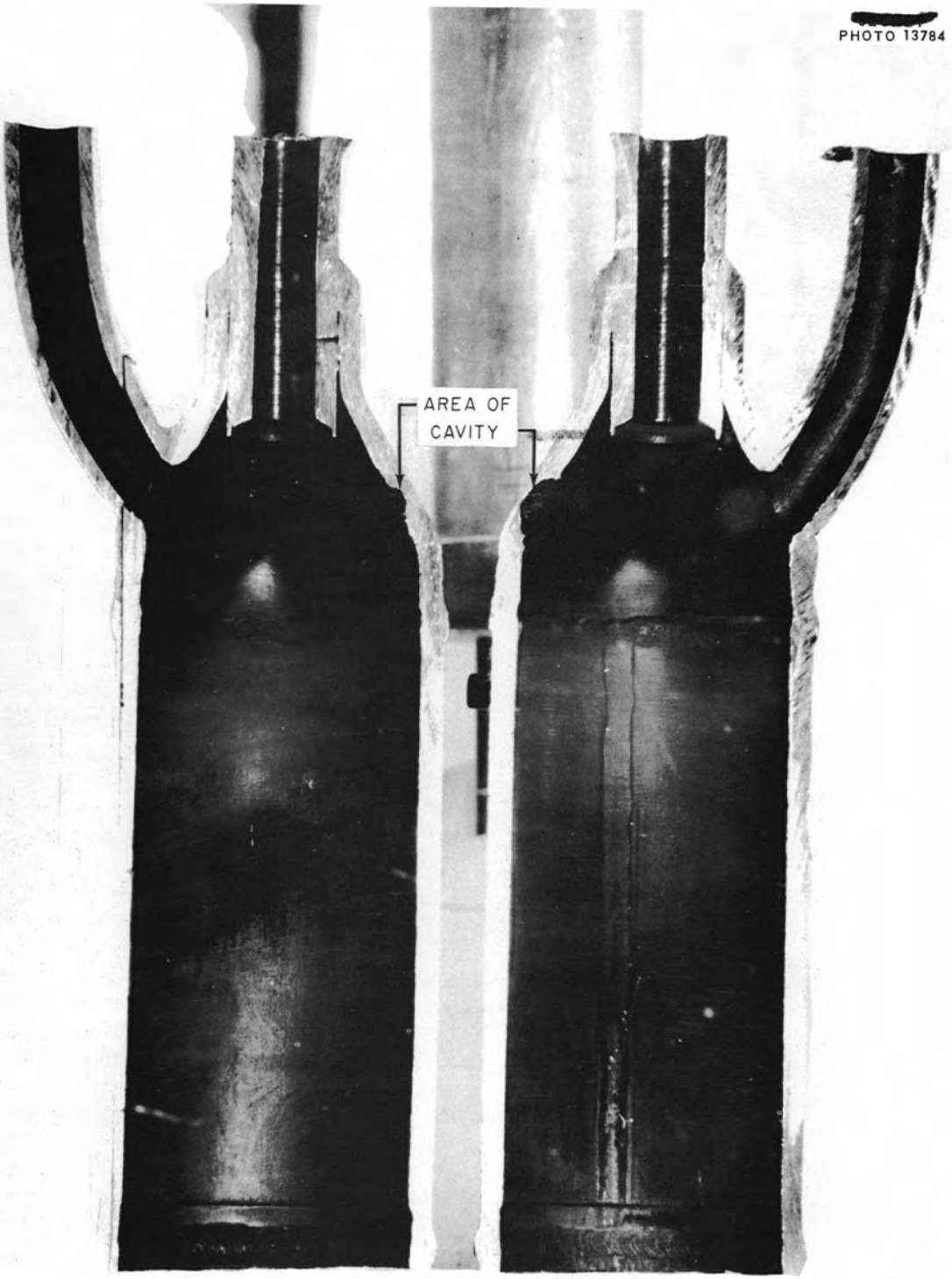

Fig. 4.17. HRP In-Pile Loop FF Type 347 Stainless Steel Core Sections, as Removed from Loop.

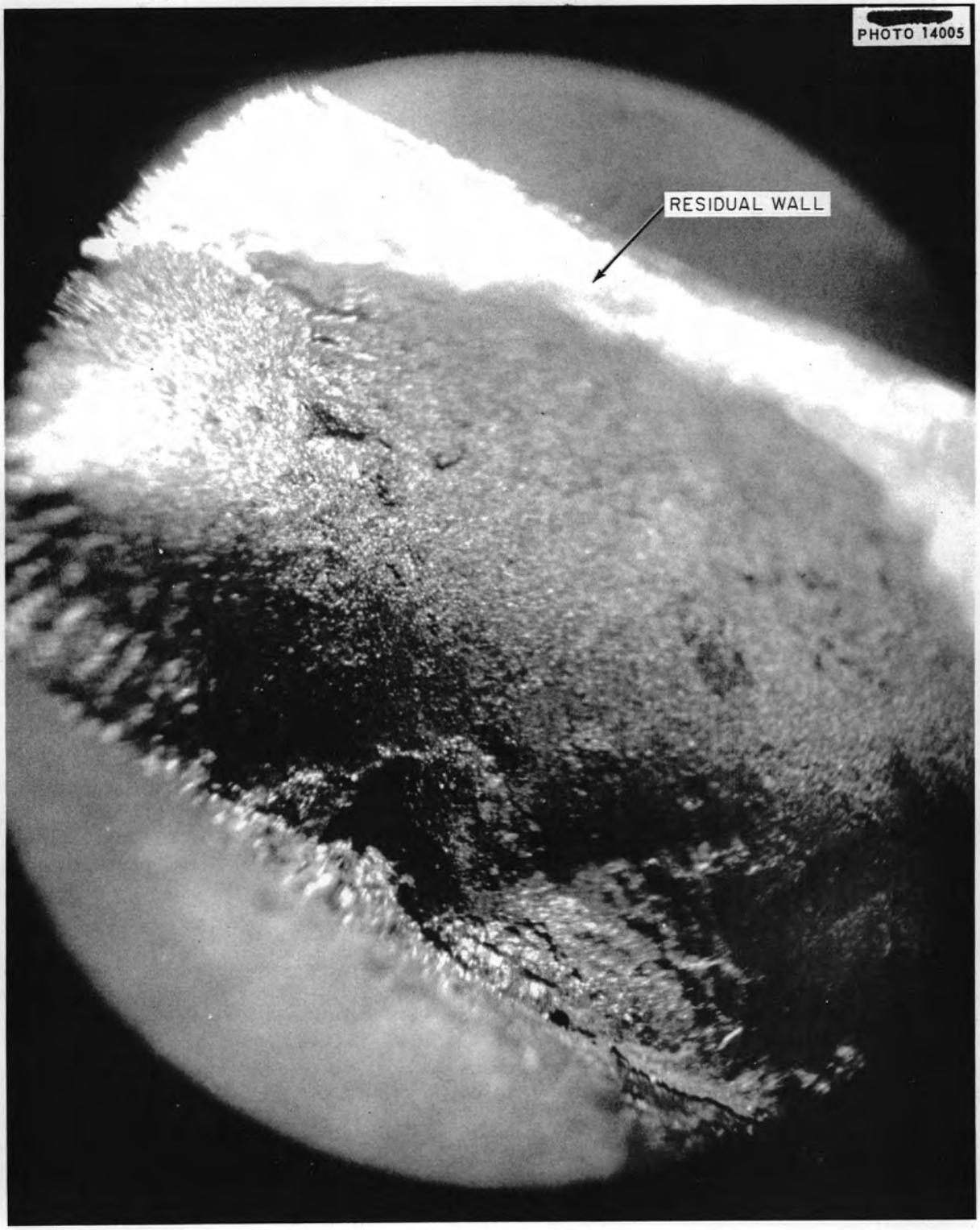

Fig. 4.18. Microscopic View of Surface of Cavity in the Stainless Steel Core Reducer Wall of In-Pile Loop FF. 10X. Reduced 17%.

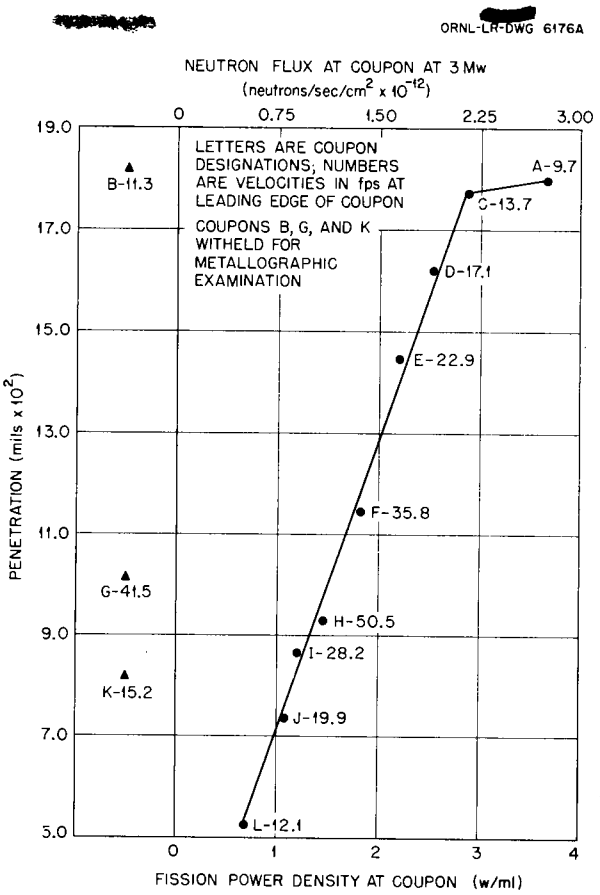

Fig. 4.19. Calculated Corrosion Penetration for Zircaloy-2 Core Sample Coupons vs Neutron Flux and Fission-Power Density at Coupon Position (FF Loop).

4.1.4.3 Status of Construction

(a) Corrosion Examination Facility. – The corrosion examination facility was completed as it was originally conceived and has been in cold-run operation. During this operation, a leak developed in a corner weld of the bottom portion of the cutting tank. This leak is now being repaired.

The manipulators, which were originally scheduled for shipment on March 15, were rescheduled for shipment on April 15.

The additional cutting bridge for this cell is now being fabricated on a completion schedule of May 10. This bridge will employ an abrasive wheel designed to operate under water.

(b) Bomb-Opening Cell. – The bomb-opening cell is being assembled in Building 4501. All parts, with the exception of the lead-glass windows, are on hand. These windows are now scheduled for delivery late in April, and the cell will be ready for use by May 1.

TABLE 4.13. WEIGHT DATA FOR ZIRCALOY-2 SAMPLE HOLDERS AND IMPACT SPECIMENS

Identification	Initial Weight (g)	Weight Change (mg)
Core Holder		
9-A	80.8213	−69.6
9-B	82.3982	−76.6
In-Line Holder		
8-A	96.1826	+350.4
8-B	94.6605	+324.0
Impact Samples		
36	17.1912	−33.6
38	17.1746	−33.3
39	17.1312	−36.4
40	17.1115	−36.4
42	17.0751	−32.5
44	17.2571	−30.1
46	17.1674	−29.0
50	16.8316	−36.1

4.1.4.4 Metallographic Examination of Specimens of HRP In-Pile Loop DD

The metallographic examination by the Remote Metallography Group of the Solid State Division of coupons and components from in-pile loop DD has been completed.[6] The details of loop DD operation and corrosion examination have been reported previously.[7]

The metallographic analysis of samples from the core cap, the pressurizer, the pressurizer heater, the piping, and representative coupons from the core and in-line arrays is summarized here. Of the samples taken from the loop components, only those from the pressurizer showed evidence of slightly increased corrosion in the grain-boundary areas. There was no evidence of a difference in attack above or below the liquid-vapor interface.

It is impossible to evaluate general surface removal because of the commercial tolerances in

[6] M. J. Feldman *et al.*, *Metallographic Examination of Coupons and Components of HRP In-Pile Loop DD*, ORNL CF-55-2-73 (Feb. 9, 1955).

[7] G. H. Jenks, H. C. Savage, *et al.*, *HRP Quar. Prog. Rep. Jan. 31, 1955*, ORNL-1853, p 88–106.

wall thickness for the materials of construction. However, a comparison of the amount of disturbed surface layer (probably due to cold work) remaining on the loop DD core cap with the disturbed layer on a cap from stock showed no measurable difference. Hence, a very low general corrosive attack of the core is indicated, even at this point, the highest flux point.

The findings on the corrosion coupons examined are summarized in Table 4.14. They confirm the difference, which was indicated by weight data[7] and visual examination, between the strong attack on the coupons in the core and the apparent lack of attack on the core walls.

4.2. LITR BOMB TESTS

G. H. Jenks

A. L. Bacarella
W. E. Clark
R. J. Davis
H. O. Day
D. N. Hess
H. A. Fisch
D. T. Jones
J. R. McWherter
M. D. Silverman
H. H. Stone
K. S. Warren
L. F. Woo

W. C. Yee

4.2.1 Introduction

During the past quarter three in-pile experiments on Zircaloy-2 bombs were completed, and the in-pile titanium experiment which was in progress at the time of the last report[8] was concluded. At present, only oxygen data are available from these bombs. Pin and solution data will be available shortly after completion of the bomb dismantling facility.

4.2.2 In-Pile Tests

4.2.2.1 Experimental

(a) Zircaloy-2. – The Zircaloy-2 stock from which the bombs were fabricated was the same as that for which an analysis was given in the last report.[8] In addition, pins of crystal-bar zirconium and of other zirconium alloys were included in certain bombs for the purpose of comparing the radiation corrosion rates of these materials with the radiation corrosion rate of Zircaloy-2. Since data from these pins are not presently available, consideration of the composition of these alloys will be covered in a future report.

Experiment Z-8, run in hole HB-6 of the LITR, was designed to test the effect of Cr(VI) on the corrosion rate of Zircaloy-2. The solution employed was 0.176 *m* in UO_2SO_4 (93% U^{235}), 0.021 *m* in $CuSO_4$, 0.046 *m* in H_2SO_4, and contained 195 ppm Cr(VI). The temperature was 250°C, and the total radiation time amounted to 1105 Mwhr. The power density was 5 w/ml. The over-all corrosion rate was 5.7 mpy, compared with 6.4 mpy for experiment H-60, which duplicated Z-8 except that no Cr(VI) was present. Chromate does not, therefore, appear to inhibit the in-pile corrosion of Zircaloy-2 appreciably, possibly because of the reduction of Cr(VI) to Cr(III) under irradiation. No loss of copper was indicated by the radiolytic gas pressure.

[8] G. H. Jenks *et al.*, *HRP Quar. Prog. Rep. Jan. 31, 1955*, ORNL-1853, p 107 ff.

TABLE 4.14. METALLOGRAPHIC ANALYSIS OF TYPE 347 STAINLESS STEEL COUPONS FROM IN-PILE LOOP DD

Identification	Weight Loss (mg)	Coupon Thickness* (mils)	Remarks
In-line position B	3.51	59.5	No attack
In-line position G	5.4	59.6	A very few shallow pits
Core position B	93.9	55.2	"Shouldered" appearance, i.e., heavy uniform removal of surfaces not protected by coupon holder; slightly accentuated attack at grain boundaries
Core position G	37.7	59.0	Many pits in the unprotected areas to 2¾ mils in depth
Core position K	6.6	59.3	A few shallow pits

*A control coupon showed a thickness variation from 59.5 to 60.0 mils.

Experiment Z-5, also run in hole HB-6, was designed to test the effect of power density on the corrosion of Zircaloy-2. The solution was 0.173 *m* in UO_2SO_4 (44% U^{235}, which gave a power density of 2.5 w/ml) and 0.021 *m* in $CuSO_4$. No free sulfuric acid was added. The temperature of exposure was 250°C for the first 1224 Mwhr, up to which time the corrosion rate was 4.5 mpy. This indicates approximate proportionality between corrosion rate and power density, since runs H-57 and H-58, which were roughly identical to Z-5 except for the employment of 93% U^{235} (which gave 5 w/ml), gave rates of 10.1 and 9.1 mpy, respectively. The increase in radiolytic gas pressure indicated a loss of 25% of the copper from the solution.

After 1224 Mwhr of irradiation, the temperature of the experiment was raised to 280°C, where the corrosion rate increased to approximately 11 mpy. The experiment was terminated after about 209 Mwhr nominally at 280°C. The last 27 Mwhr of irradiation were actually more nearly at 250°C because of failure of the furnace. As a result of the relatively short time at 280°C and the uncertainty in temperature during the period before the last point was taken, a very reliable estimate of the temperature coefficient of the corrosion rate in this experiment cannot be made.

Experiment Z-3, run in hole HB-5, employed a solution 0.171 *m* in UO_2SO_4 (20% U^{235}, which gave a power density of 2.5 w/ml), 0.019 *m* in $CuSO_4$, and 0.45 *m* in H_2SO_4. The purpose of the experiment was to test the effect of the high acid concentration upon the corrosion of Zircaloy-2 at approximately constant power density. Unfortunately, the flux in HB-5 had been considerably overestimated, so that instead of being about 2×10^{13} neutrons/cm^2/sec, or four times that in HB-6, it was somewhat less than 1×10^{13} inside the bomb. The over-all rate of 2.2 mpy which was observed is slightly less than that which would be expected for a solution similar to the one employed but only 0.04 *m* in H_2SO_4, if it is assumed that the corrosion rate is directly proportional to the power density. The experiment was terminated after 1387 Mwhr of exposure because of failure of the stainless steel capillary. Copper loss, calculated from radiolytic gas pressure decrease, amounted to 22% of the copper initially present.

(b) Titanium. – Experiment H-76, which was in progress at the time of the last report,[8] employed a bomb fabricated from titanium 75A and a solution 0.177 *m* in UO_2SO_4 (93% U^{235}, which gave a power density of 5 w/ml), 0.021 *m* in $CuSO_4$, and 0.046 *m* in H_2SO_4. The exposure temperature was 250°C, and the total radiation time was 1871 Mwhr. The over-all corrosion rate was 1.7 mpy, compared with 6.4 mpy for H-60, an experiment with Zircaloy-2 in which the same experimental conditions were utilized. Experiment H-76 was run in hole HB-6 of the LITR. No loss of copper was indicated. The corrosion rate found is in good agreement with a rate of 1.3 mpy obtained by other observers who employed a nonrocking titanium bomb in hole HB-5 of the LITR.[9]

4.2.2.2 Discussion of In-Pile Results

Data for the in-pile experiments are presented in Table 4.15 and Fig. 4.20. It should be pointed out that, in plotting these data, corrosion during times when the reactor was down was assumed to be negligible. When shutdowns are short and infrequent, this assumption appears to be valid, but when the reactor is down for two or three days, an appreciable drop in the oxygen pressure is sometimes observed. Long reactor shutdowns occurred during experiments Z-3, Z-8, and H-76 (see Fig. 4.20). It should also be mentioned that the data plotted represent those obtained by measuring the oxygen pressure at 250°C, as well as at 100°C, and also a few values taken at about 50°C. This ordinarily causes more scatter than when the data are taken at only one temperature. Where vertical lines are used to connect points, data were taken at at least two different temperatures. It is believed that the lower temperatures are generally preferable for measuring pressure because of the much smaller errors introduced into the steam pressure by small errors in temperature measurement. In the early part of Z-8, however, it was believed that lowering the temperature appreciably below 250°C would result in reduction of the Cr(VI); consequently, the data taken during the early portion of this experiment were all at 250°C.

A re-count of the cesium activity in the solutions from experiments H-60 and Z-2 resulted in the lowering of the power densities, as reported,[8] from 5.9 to 5.1 w/ml for H-60 and from 5.4 to 4.2

[9] C. H. Secoy *et al.*, *HRP Quar. Prog. Rep. Oct. 31, 1953*, ORNL-1658, p 110.

TABLE 4.15. SUMMARY OF IN-PILE BOMB CORROSION STUDIES, JANUARY 1, 1955 TO APRIL 2, 1955

Bomb No.	Bomb Material	Solution Composition (*m*)	Power Density (w/ml)	Exposure Temperature (°C)	Days Exposed*	Corrosion Rate** (mpy)	Copper Lost from Solution (%)
H-76	Titanium 75A	0.177 UO_2SO_4 (93.2% U^{235}) 0.021 $CuSO_4$ 0.046 H_2SO_4	5	250	26.0	1.7	None
Z-3	Zircaloy-2	0.171 UO_2SO_4 (19.8% U^{235}) 0.019 $CuSO_4$ 0.449 H_2SO_4	2.5	250	19.3	2.2	22
Z-8	Zircaloy-2	0.176 UO_2SO_4 (93.2% U^{235}) 0.021 $CuSO_4$ 0.046 H_2SO_4 0.0004 CrO_3 (195 ppm Cr)	2.5	250	15.4	5.7	None
Z-5	Zircaloy-2	0.173 UO_2SO_4 (44.0% U^{235}) 0.021 $CuSO_4$	5	250, 280	17.0 at 250°C 2.9 at 280°C	4.5 at 250°C 11 at 280°C	25

*LITR operating time at 3 Mw.

**Based on LITR operating time at 3 Mw.

w/ml for Z-2 as a result of the decay of 13-day Cs^{136}. Since the solution from H-59 had been discarded, no re-count was possible for this experiment, but a re-count would certainly have resulted in lowering further the reported[8] power density, which is already much lower than the value calculated from the neutron flux and the fission cross section of U^{235}. Because of the uncertainties involved in the calculation of power densities in different experiments when changes have been made in the bomb, the furnace, and the solution, the use of an internal monitor is highly desirable.

The use of a fission product such as cesium is most desirable, since it takes into account the fission cross section of U^{235}, but before such a product can be used with confidence it must be shown that the amount of cesium included in the corrosion film is negligible. It is planned to check this point by analysis of the film. The activity induced in the zirconium of the pin specimens is also being investigated as a possible internal monitor.

4.2.2.3 HB-5 Facility

The HB-5 facility was shut down as a result of the capillary failure in experiment Z-3. It is expected that this facility will be back in operation within the near future. Meanwhile, a change in design is being considered that will allow the insertion of three horizontally rocked bombs instead of the single perpendicularly rocked bomb presently employed.

4.2.3 Out-of-Pile Tests

After the failure of the stainless steel capillary in experiment Z-3, a quick comparison was made of the corrosion rates of type 347 stainless steel in solutions which were comparable to those used in Z-3 but which contained 0.04 and 0.4 *m* free sulfuric acid. For these tests, stainless steel pins in Zircaloy-2 bombs were employed, and, since the in-pile temperature of the capillary near the bomb fitting must be higher than that of the bomb as a result of gamma heating, a temperature of 300°C was employed.

Pin data indicated an over-all rate of 4.2 mpy for the low-acid experiment over the first 23-hr period and an over-all rate of 114 mpy for the high-acid experiment over the first 72-hr period. Pressure measurements for both experiments indicated a decrease in rate with time. A precipitate was observed in the bomb which contained the high-acid solution. Although solution analyses and

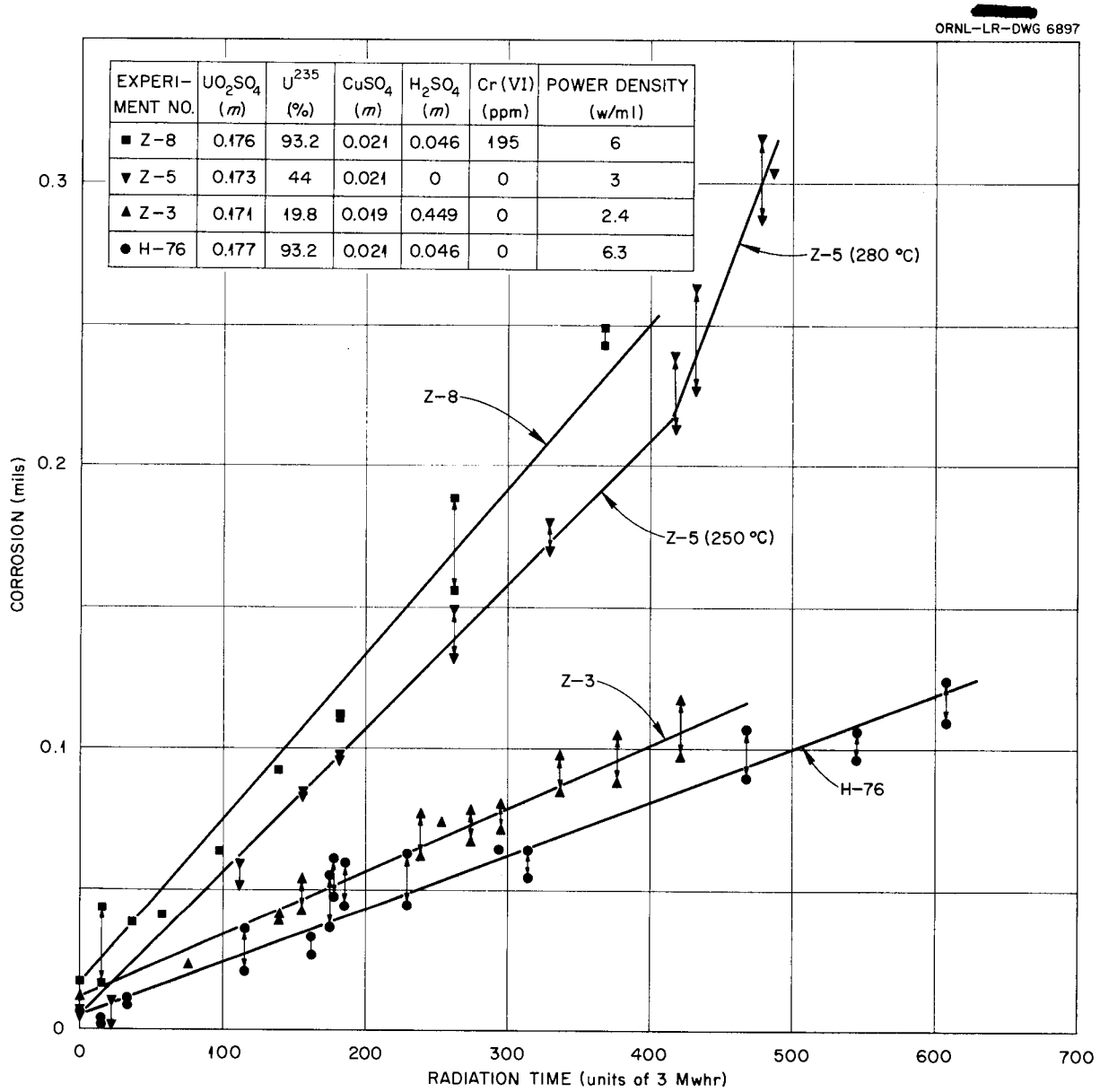

Fig. 4.20. Corrosion Data for LITR Bomb Experiments.

oxygen data are not presently available, it seems safe to assume that the initial corrosion rate in 0.4 *m* acids is at least 20 times as great as that in 0.04 *m* acid at 300°C.

Inasmuch as both loop and bomb methods employ closed systems which allow a buildup of corrosion products in solution, it is desirable to obtain out-of-pile corrosion data under conditions that will not allow this buildup to take place. A facility which will permit fresh solution to flow continuously over the corroding specimen has been designed, and the component parts are now being fabricated. It is expected that this method will yield information concerning the importance of dissolved corrosion products on the corrosion process.

4.3 MTR BOMB TESTS

G. H. Jenks
R. J. Davis J. R. McWherter
D. T. Jones H. H. Stone

The design of the MTR rocking-bomb experiment, ORNL-15, is essentially complete, and fabrication was expected to have been completed in April.

The design, in general, is the same as that reported previously.[8] The bomb and pin rack were modified to ensure that the pins are always below nominal liquid level during operation in order to prevent overheating of a pin in the high gamma flux and, consequently, the possible ignition of an explosion in the gas.

The solution to be used in the initial runs will be made up as follows: UO_2SO_4, 0.0425 *m*; $CuSO_4$, 0.05 *m*; H_2SO_4, 0.02 *m*. The high copper concentration will be employed in an attempt to minimize the radiolytic gas pressure during operation. Even with this much copper present, the radiolytic pressure at low temperature should be high, as shown in Fig. 4.21; since the vapor pressure rises with temperature, the temperature range for minimum pressure operation will be narrow.

The H_2SO_4 requirement was determined by heating solutions of 0.042 *m* UO_2SO_4 and 0.05 *m* $CuSO_4$, respectively, to 330°C with 0.01, 0.02, and 0.03 *m* H_2SO_4. Precipitation occurred in the 0.01 *m* H_2SO_4 solution; no precipitation was observed in the other solutions.

The solution for the initial runs will be irradiated at a thermal-neutron flux of approximately 1.5×10^{14} neutrons/cm^2/sec. This will give a specific power of 5 w/ml at 10% enrichment and 45 w/ml at 93.2% enrichment. The 10% enrichment experiment is tentatively scheduled for insertion in the MTR in May.

Calculations indicate that pressure and temperature fluctuations of the Baldwin cell will increase the possibility that the bomb solution will enter the water-filled stainless steel capillary which connects the bomb and the Baldwin cell. The presence of the solution in the capillary may result in corrosion of the capillary and subsequent plugging and/or possible ignition of the radiolytic gas formed in the capillary. To minimize the possibility that the solution will enter the capillary, the Baldwin cell will be filled with mercury and maintained at a constant temperature or have its temperature gradually increased throughout the experiment. The capillary will be cooled with a high-velocity air stream during operation.

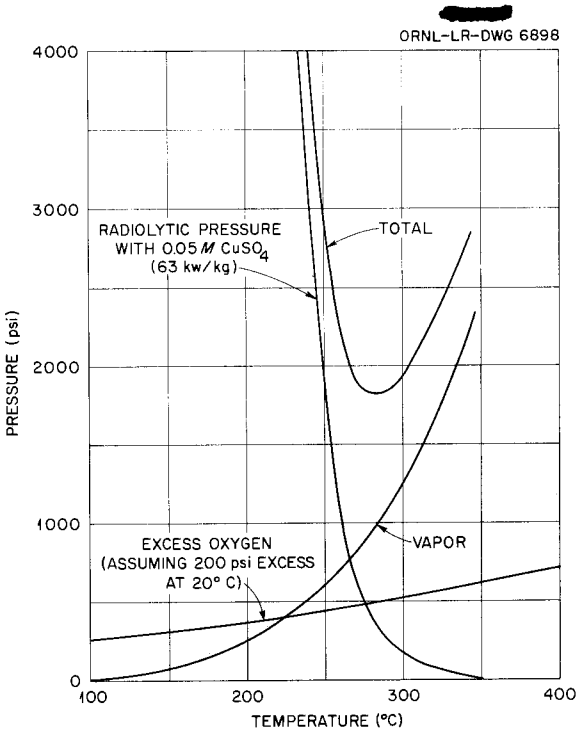

Fig. 4.21. Operating Pressure vs Temperature of MTR Rocking-Bomb Experiment.

5. LABORATORY CORROSION STUDIES

E. L. Compere
J. L. English
G. E. Moore

5.1 CORROSION OF PRECIPITATION-HARDENING STAINLESS STEELS BY SIMULATED REACTOR ENVIRONMENTS

J. L. English E. L. Compere

The precipitation-hardening stainless steels have merited consideration for various HRP applications because of their high-strength properties and their high hardness, obtained by suitable heat treatment. Type 17-4 PH stainless steel has been used as a canned-rotor-pump bearing in a few in-pile test loops and has been suggested as a bolt material for the fuel-contacting joint between the HRT core and the pressure vessel.

It has been suggested that partially hardened (heat treated 2 hr at 1000°F) type 17-4 PH would give the best combination of strength and corrosion resistance.

Type 17-4 PH stainless steel, of the heat (Armco heat 34434) purchased for fabrication into HRT core bolts, was machined into $\frac{1}{2} \times \frac{1}{16} \times 3\frac{1}{2}$ in. strips for use in twin-strip stress assemblies.[1] The strips were then heat treated for 2 hr in air at 1000°F, air cooled, pickled, and lightly polished. The hardness increased from an average Rockwell C value of 33.5 to 39.5. Several twin-strip assemblies were then stressed at room temperature to 80,000 psi. These assemblies have been tested in various media, as shown in Table 5.1.

Cracking occurred in boiling 42% magnesium chloride within 2 hr. A somewhat shorter time might have been expected at the stress of 80,000 psi, based on extrapolations of austenitic stainless steel data.[2] Thus, as suggested, although the material can be cracked by stress corrosion in very agressive media, it may be as good as the austenitic stainless steels.

Exposure to dilute acidified uranyl sulfate solution at 100, 250, and 300°C for 1000 hr or more did not produce any cracking or pitting, and undefilmed corrosion rates were quite low, less than 0.1 mpy (tests are continuing). It is interesting to note that the lowest attack appeared to occur at 300°C. Boiling 1.3 *m* uranyl sulfate solution also did not cause cracking or pitting, and currently has produced an undefilmed corrosion rate of 0.2 mpy, slowly rising.

Static-corrosion tests, described in a previous report,[3] have been continued with types 17-4 PH and 17-7 PH precipitation-hardening stainless steels. Both annealed and fully hardened wafer-type specimens of the two alloys have been exposed in simulated reactor environments at 100, 250, and 300°C for periods between 1600 and 2500 hr. The type 17-4 PH stainless steel was received in an annealed condition, hardness Rockwell C-37. The fully hardened type 17-4 PH was obtained by heat treatment for 1 hr in air at 875°F, air cooling, and pickling, with a resultant hardness of Rockwell C-44.5.

The type 17-7 PH stainless steel was received in an annealed condition, hardness Rockwell B-86. The fully hardened type 17-7 PH was obtained by a heat treatment for $1\frac{1}{2}$ hr in air at 1400°F, air cooling, heat treatment $\frac{1}{2}$ hr in air at 950°F, air cooling, and pickling, with a resultant hardness of Rockwell C-41.0. Current results from the tests, which are being continued, are summarized in Table 5.2.

The general corrosion performance of the two alloys after the extended test period remained much the same as that established by the initial exposure period. Annealed specimens appeared to be acceptable in all environments tested, whereas the specimens in the fully hardened condition exhibited erratic behavior. In boiling aerated uranyl sulfate solutions, corrosion attack on hardened specimens of both alloys was quite pronounced. Corrosion rates were observed to accelerate with increasing exposure time, and the attack, in frequent cases, was accomplished by the formation of cracks and blisters on the specimens.

At 250°C, corrosion attack by 0.17 *m* UO_2SO_4 solution appeared to be relatively mild in nature,

[1] E. L. Compere, *HRP Quar. Prog. Rep. Jan. 31, 1955*, ORNL-1853, p 123.

[2] M. A. Scheil, "Stress Corrosion Cracking in Stainless Alloys," *Corrosion Handbook* (ed. by H. H. Uhlig), p 174–182, Wiley, New York, 1948.

[3] J. L. English and E. L. Compere, *HRP Quar. Prog. Rep. Jan. 31, 1955*, ORNL-1853, p 120.

TABLE 5.1. CORROSION OF STRESSED SPECIMENS OF PARTIALLY HARDENED TYPE 17-4 PH STAINLESS STEEL BY SIMULATED HRT SOLUTIONS

Steel type: 17-4 PH
Condition: Partially hardened (2 hr at 1000°F, air cool) hardness RC-39.5
Source: Newport News Shipbuilding & Dry Dock Co. HRT core bolt stock – Armco heat 34434
Specimen type: Twin-strip stress assembly, 80,000-psi stress (room temperature)

	Test No.				
	HB 1	HB 2	HB 3	HB 4	HB 6
Temperature, °C	154	100	~100 (boil)	300	250
Solution					
UO_2SO_4	(42% $MgCl_2$)	0.04 *m*	1.3 *m*	0.04 *m*	0.04 *m*
H_2SO_4		0.006 *m*		0.006 *m*	0.006 *m*
Atmosphere	Stagnant	Air sparged	Air sparged	150-psi oxygen	150-psi oxygen
Duration, hr	2	1010	1010	1008	1008
Total attack, mg/cm^2	0.07	0.16*	0.4*	0.05*	0.2*
Average rate, mpy		0.07*	0.2*	0.02*	0.08*
Rate range, mpy		0.03–0.6	0.04–0.22	0–0.05	0.01–0.2
Rate trend	Irregular	Irregular	Slowly increasing	Irregular	Irregular
Specimen condition	Cracked and brake	Thin dark-gray film or tarnish; no cracks or pits	Thin black film on strips; no cracks or pits	Thin gray-black film; no cracks or pits	Thin black film; no cracks or pits
Solution condition		Unchanged	Unchanged	Unchanged	Unchanged

*Based on scrubbed, undefilmed weight change; test continues.

and the behavior of undefilmed specimens in the annealed condition showed no appreciable difference from the behavior of those in the fully hardened condition. However, corrosion attack was severe on hardened specimens of the alloys exposed in 1.34 *m* UO_2SO_4 solution at this temperature.

Dilute uranyl sulfate solutions at 300°C were not particularly corrosive to the two alloys, and, again, little difference was observed between the annealed and fully hardened conditions of the alloys.

In view of the observed data, the usefulness of types 17-4 PH and 17-7 PH precipitation-hardening alloys in the fully hardened condition remains questionable for exposure to these solutions.

5.2 INHIBITION OF HRT MAINTENANCE POOL WATER

E. L. Compere

Sustained and more nearly complete inhibition of corrosion by simulated HRT maintenance pool water was obtained with 300 ppm sodium chromate than with the previously tested level of 50 ppm. Although 50 ppm appeared to be adequate for several hundred hours in aerated tap water at room temperature, it was noted that, in stagnant unaerated tap water, corrosion of the more aggressive couples, such as copper-carbon steel, aluminum-carbon steel, and others, began after a few days. On the other hand, these and other metals remained bright and substantially unattacked for more than

TABLE 5.2. CORROSION OF PRECIPITATION-HARDENING STAINLESS STEELS BY SIMULATED REACTOR ENVIRONMENTS

Medium	Duration (hr)	Average Corrosion Rates[a] (mpy)			
		Annealed		Fully Hardened	
		17-4 PH[b]	17-7 PH[c]	17-4 PH[d]	17-7 PH[e]
100°C with aeration					
Distilled water	2500	0.01	+[f]	0.01	+
5% HNO_3 (not aerated)	2000	0.5	0.3	5	22[g]
0.02 *m* UO_2SO_4 + 0.005 *m* H_2SO_4	2000	+	+	11[h]	7[i]
0.17 *m* UO_2SO_4	2000	0.1		8[h]	
	2300		0.04		2[g]
1.34 *m* UO_2SO_4	2000	+		69[h]	
	2300		0.1		14[g]
250°C with 150-psi oxygen					
Distilled water	1600	+		+	+
0.17 *m* UO_2SO_4	1600	0.07	+	0.06	+
1.34 *m* UO_2SO_4	1600	0.4	0.3	10[j]	41[k]
300°C with 150-psi oxygen					
0.02 *m* UO_2SO_4 + 0.005 *m* H_2SO_4	1600	+	0.06	0	0.06
0.6 *m* UO_2SO_4 + 0.006 *m* H_2SO_4	1600			0.7	

[a]Corrosion rates for undefilmed specimens; most tests continuing.

[b]Type 17-4 PH as received, in annealed condition, hardness Rockwell C-37.

[c]Type 17-7 PH as received, in annealed condition, hardness Rockwell B-86.

[d]Type 17-4 PH nominal condition H 875; heat treated 1 hr in air at 875°F, air cooled, pickled; hardness Rockwell C-44.5.

[e]Type 17-7 PH nominal condition TH 950; heat treated 1½ hr in air at 1400°F, air cooled, then heat treated ½ hr in air at 950°F, air cooled, and pickled; hardness Rockwell C-41.

[f]Plus symbol (+) indicates weight gain on specimen.

[g]Corrosion rate increasing with time.

[h]Specimen developed cracks during test; accelerating corrosion rate; pitting.

[i]Blister formation during test; accelerating corrosion rate.

[j]Test stopped after 1100 hr.

[k]Test stopped after 200 hr.

five weeks with 300 ppm sodium chromate in stagnant tap water; no clouding of the water was observed. Visibility through a 15-ft depth of this yellow solution was checked and appeared to be very satisfactory.

5.3 BOILING NITRIC ACID SPECIFICATION TESTS

E. L. Compere J. L. English

HRP-specification boiling nitric acid tests on austenitic stainless steels for HRT use currently have been completed on 176 materials, for which the test was not made by the vendor, with 60% of the submitted specimens passing the test. This test evaluates the general quality of the metal, the adequacy of columbium stabilization when present, and the sensitivity to heat effects and welding.

5.4 HRP THORIUM OXIDE SLURRY BLANKET CORROSION STUDIES

G. E. Moore E. L. Compere

5.4.1 General

The investigation of the corrosion of type 347 stainless steel, titanium, and Zircaloy-2 by circulating aqueous thoria slurries in stainless steel toroids continued. Attention was directed to the

behavior of a number of different preparations of thorium oxide; a brief identification of these materials is given in Table 5.3. Slurries containing 500 and 1000 g of thorium per kilogram of water were circulated for approximately 150 hr at 26 fps and 250°C with about 100-psi oxygen pressure.

The corrosion rates of pin specimens inserted into the circulating slurry were based on defilmed weight losses for the type 347 stainless steel and on scrubbed weight changes for the titanium and Zircaloy-2. At a slurry concentration of 500 g of thorium per kilogram of water, rates of less than 4.5 mpy were obtained in all cases for the type 347 stainless steel and less than 2 mpy for both the titanium (75A) and the Zircaloy-2. At a concentration of 1000 g of thorium per kilogram of water, rates ranged from less than 2 mpy to 7 mpy for the stainless steel, less than 3 mpy for the Zircaloy-2, and generally less than 5 mpy for the titanium, although unduplicated values as high as 9 mpy were obtained.

5.4.2 Effect of Carbon Dioxide in Thoria Slurries

Of various possible methods of preparing thorium oxide, the thermal decomposition of an insoluble thorium salt of an organic acid has been commonly employed. Since one product of such a decomposition is carbon dioxide, it was desired to determine the effect, if any, of the presence of residual carbon dioxide on corrosion by thoria slurries. In the experiment to be described, no change in the corrosion behavior of slurries to which carbon dioxide was intentionally added was apparent, although the character of the slurry was modified.

Thorium oxide from the ORNL production batch D-17 was selected as the material for the study. Four samples of the oxide, appropriately weighed to yield two slurries each of 500 and 1000 g of thorium per kilogram of water, were heated, with occasional stirring, in Pyrex evaporating dishes at 400 to 440°C in a furnace for 5 hr. After approximately 5 min of air cooling, two samples were added directly to toroids which had first been flushed with helium to remove air. The appropriate volume of freshly boiled distilled water, through which helium was bubbled during cooling, was added to these toroids to produce slurries with a concentration of 500 and 1000 g of thorium per kilogram of water. One milliliter of 30% hydrogen peroxide, an amount calculated to produce by thermal decomposition approximately 90 psi of oxygen at 250°C, was then added to each toroid.

The other two samples were added to beakers containing the appropriate volume of freshly boiled distilled water and small pieces of solid carbon

TABLE 5.3. IDENTIFICATION OF THORIUM OXIDES USED IN CIRCULATING-SLURRY STUDIES IN TOROIDS

Material	Source	Thorium Salt Used	Maximum Calcination Temperature (°C)
Lindsay No. 7	Lindsay	Oxalate	950
Lindsay No. 8	Lindsay	Oxalate	950
Pyrohydrolyzed	ORNL	Oxalate	900
XB-1	ORNL	Oxalate	650
D-10	ORNL (Thorex)	Oxalate	650
D-17	ORNL (Thorex)	Oxalate	650
Ames	Ames Laboratory	Oxalate	650
Lindsay No. 12	Lindsay	Oxalate	650
Lindsay No. 13	Lindsay	Oxalate	650
Lindsay No. 11	Lindsay	Formate	650
Lindsay No. 16	Lindsay	Formate	650

dioxide. The slurry and carbon dioxide were kept in contact for about 15 min and then transferred to the toroids. Nominal slurry concentrations of 500 and 1000 g of thorium per kilogram of water were again used, with oxygen pressures of about 90 psi (at 250°C) from the addition of hydrogen peroxide.

These slurries were circulated for 215 hr at 26 fps and at average temperatures from 245 to 253°C in type 347 stainless steel toroids. Corrosion pin specimens of type 347 stainless steel, titanium 75A, and Zircaloy-2 were used. The corrosion data were obtained from defilmed weight losses of the type 347 stainless steel pins and from scrubbed weight changes of the titanium and Zircaloy-2. These data, together with pertinent analytical results, are summarized in Table 5.4.

Analyses at the end of the run showed that all the slurries contained some carbon. Those that were intended to be carbon-free contained considerably less carbon than the original material, which contained 1.6 mg of carbon per gram of thorium, but still analyzed about 0.17 mg of carbon per gram of thorium. Since control samples were run simultaneously in order to correct for possible carbon dioxide pickup from the air, it appears that the residual carbon is not due to contamination but is rather strongly bound in the thoria. Even after 5 hr of heating at 1000°C with stirring, the D-17 thorium oxide analyzed 0.25 mg of carbon per gram of thorium.

Those slurries to which carbon dioxide was intentionally added showed a greater carbon con-

TABLE 5.4. EFFECT OF CARBON DIOXIDE ON BEHAVIOR OF THORIUM OXIDE SLURRIES CIRCULATED IN TYPE 347 STAINLESS STEEL TOROIDS

Thorium oxide: D-17, heated at 400–440°C for 5 hr, stirred; slurry made up with boiled distilled water
Temperature: 245–253°C
Relative velocity: 26 fps
Oxygen: 90 psi (at 250°C)
Duration of test: 215 hr

Toroid	M	N	O	P
Nominal g of Th per kg of water	500	500	1000	1000
Additive		CO_2		CO_2
Average corrosion rate, mg/dm^2/day[a]				
Type 347 stainless steel, defilmed	−6.2	−9.4	−14, −11	−13, −15
Toroid, as-run	−2.8	−2.2	−6.2	−5.1
Titanium 75A, scrubbed	+0.1	−1.1	−5.3	−4.3
Zircaloy-2, scrubbed	−2.5	−4.0	−8.8	−7.4
Slurry removable by draining at 25°C, %	87	90	0	84
Slurry removed by one water wash, %	12	7	53	14
Analyses				
g of Th per kg of water	530	560		1080
mg of Fe per g of Th	2.7	2.6	3.6	3.0
mg of C per g of Th[b]	0.8	1.3	0.6	2.5
Slurry pH	7.1	5.9		5.3

[a]Conversion factors: type 347 stainless steel (mg/dm^2/day) × 0.181 = mpy; titanium (mg/dm^2/day) × 0.320 = mpy; Zircaloy-2 (mg/dm2/day) × 0.222 = mpy.

[b]Original material contained 1.6 mg of C per g of Th.

tent (1.3 and 2.5 mg of carbon per gram of thorium); this produced a negligible effect on the corrosion rates of the materials investigated, and the small differences that were observed in the data at each slurry concentration are within the ordinary statistical deviation. However, added carbon dioxide had a definite effect on the characteristics of the slurry containing 1000 g of thorium per kilogram of water; at room temperature the slurry at this concentration in the absence of carbon dioxide did not pour from the toroid after the run, whereas the slurry with carbon dioxide was readily drained. This difference in behavior of the slurries is consistent with the results which show that certain electrolytes increase the dispersion of thoria slurries[4] and decrease their viscosity.[5] The increased acidity of the carbon dioxide–containing slurry supports this view.

[4]D. E. Ferguson *et al.*, *HRP Quar. Prog. Rep. Oct. 31, 1954*, ORNL-1813, p 145.

[5]D. G. Thomas *et al.*, *HRP Quar. Prog. Rep. Oct. 31, 1954*, ORNL-1813, p 125.

In addition to these results, the data clearly show the increased corrosion rate with increased slurry concentration.

ACKNOWLEDGMENTS

The following groups contributed to the over-all program:

O. E. Menis, C. M. Boyd, R. G. Ball, R. E. Corcoran, M. L. Hubbard, I. B. Rukin, C. K. Talbott, N. M. Ferguson, W. R. Musick, T. C. Rains, *et al.* – analytical services to the dynamic loop and in-pile loop corrosion programs.

P. F. Thomason *et al.* – analytical services to the in-pile bomb test program.

U. Koskela *et al.* and S. A. Reynolds *et al.* – analytical services to the in-pile loop and bomb programs.

D. S. Toomb, J. A. Russell, *et al.* – instrumentation for loop and laboratory test programs.

J. DeLorenzo *et al.* – instrumentation for in-pile loop and bomb programs.

Part IV

ENGINEERING DEVELOPMENT

J. A. Lane

6. DEVELOPMENT OF FUEL-SYSTEM COMPONENTS

C. B. Graham

J. S. Culver
L. F. Goode
R. Goodman
J. A. Hafford
B. A. Hannaford
P. H. Harley
W. L. Ross
J. G. Smith
I. Spiewak
W. H. Stahlheber
D. S. Toomb
L. R. Weissert[1]
E. L. Youngblood

6.1 RECOMBINER DEVELOPMENT

R. Goodman P. H. Harley
I. Spiewak

The first three months of operation of the high-pressure recombiner loop were described previously.[2] During the past quarter, additional runs were carried out under the following varying conditions:

1. The platinized alumina catalyst was intentionally contaminated with UO_2SO_4. No poisoning of catalyst resulted over a two-week period of operation.
2. After a month of exposure, the performance of platinized alumina catalyst was unchanged. There was a slight platinum weight loss.
3. The life of platinized and palladium-coated stainless steel catalyst supplied by Baker Co. was less than 24 hr, although initial catalyst activity was excellent. Some further trials of stainless-based catalyst are under way.

The high-pressure recombiner loop suffered from intermittent explosions in the electrolytic cells; the cells have now been modified to dilute the H_2 and O_2 with steam before the gases leave the cells.

6.2 DUMP-VALVE TEST LOOP

J. G. Smith I. Spiewak
D. S. Toomb

Construction of the dump-valve test loop[3] is essentially complete, and the loop was subjected to a 3000-psi hydrostatic test. The installation of thermal insulation and the construction of the splash shields remain to be completed.

The first tests will be made with a prototype of the HRT dump valve whose plug is a 60-deg truncated cone with a Stellite 6 surface; the seat is type 347 stainless steel.

6.3 5000-gpm GAS SEPARATOR

J. A. Hafford I. Spiewak

The 14-in. gas separator was tested with a new set of vanes, scaled up from the HRT gas separator vanes. These vanes have only a single curvature and are therefore much easier to fabricate than the doubly curved vanes tested previously.[4] The vortex formed by the singly curved vanes was stronger than that formed by the doubly curved vanes (higher rotational velocities), but the over-all pressure drop was about the same; this indicated higher energy recovery in the exit vanes. The over-all liquid pressure drop was about 2.5 psi (two inlet velocity heads) at 5800 gpm and 125 scfm of air. The pressure drop from inlet to gas takeoff was 7 psi.

The separator was not long enough to provide 100% gas separation but did remove between 90 and 95% of the gas. Because of the short distance between the vanes on this model (5 pipe diameters), the smallest bubbles (less than approximately $\frac{1}{16}$ in. in diameter) do not have time to reach the void. Ten pipe diameters would provide sufficient time for about 99% gas removal.

The amount of liquid entrainment at the gas takeoff depended on the pressure drop between the gas void and the gas discharge line. The minimum quantity of entrainment observed was 10 gpm at an actual gas flow of 105 cfm; this was a factor of 10 below the entrainment of the doubly curved vane system.

The two-phase pressure drop in the 3-in. gas takeoff line was lower than that predicted from

[1] On loan from The Babcock & Wilcox Co.

[2] C. B. Graham *et al.*, *HRP Quar. Prog. Rep. Jan. 31, 1955*, ORNL-1853, p 135.

[3] J. G. Smith, I. Spiewak, and D. S. Toomb, Jr., *HRP Quar. Prog. Rep. Oct. 31, 1954*, ORNL-1813, p 109.

[4] C. B. Graham *et al.*, *HRP Quar. Prog. Rep. Jan. 31, 1954*, ORNL-1678, p 33.

data developed on smaller pipe. Since entrainment is so dependent on proper sizing of the takeoff, further study of two-phase pressure drop in 3- to 6-in. pipe is indicated.

6.4 SMALL REACTOR COMPONENTS

W. H. Stahleheber W. L. Ross

6.4.1 20-cfm Canned-Rotor Gas Circulator[5]

A 20-cfm gas circulator, suitable for operation in the HRT (or possibly larger scale reactors), in conjunction with a high-pressure recombination system, was ordered from Allis-Chalmers Mfg. Co. and will be delivered in about seven months. Special features of the blower include hydrostatic bearings, with the motor end running submerged in water, and provision for top maintenance. This gas circulator will be tested after delivery in a loop now being designed at ORNL.

6.4.2 ORNL Gas Circulator

A 5-gpm ORNL pump (No. 215) converted[6] to a gas circulator was returned to service after an electrical failure. It has accumulated 2200 hr of operation at 110 psi and 170°C.

6.4.3 Small Pumps

A 2000-psi, 5-gpm, canned-rotor pump[7] for chemical processing loops operated for 780 hr at 300°C with water. Operation was interrupted several times by leaks in the system, which resulted in a low liquid level. The resultant gas accumulation in the motor caused overheating.

A 1000-psi design, 5-gpm, ORNL, canned-rotor pump operated for 5300 hr. After 4850 hr at 250°C the stator was rewound with class A insulation and put back into service.

In order that stator life may be increased, one ORNL, 5-gpm pump (No. 221) was rewired[8] with the windings in series. This reduced input power to 35% (375 w), current to 25% (3.65 amp), and head to 85% (34 ft). The pump has run for 350 hr, and the test is continuing (see Fig. 6.1).

[5] C. B. Graham *et al.*, *HRP Quar. Prog. Rep. Oct. 31, 1954*, ORNL-1813, p 110.

[6] *Ibid.*, Sec. 6.3.2.

[7] P. A. Haas, *HR Processing Studies – Initial Performance of ORNL Canned Rotor Pumps of a Modified Design for 2000-psi Operation*, ORNL CF-54-11-175 (Nov. 29, 1954).

[8] C. D. Zerby, *ORNL Pump Brochure*, ORNL CF-55-1-210, Fig. 2 (Jan. 20, 1954).

6.5 DEVELOPMENT OF LARGE HEAT EXCHANGERS

L. F. Goode W. L. Ross

The initial success of the high-frequency-induced eddy current inspection method, employed on the finished ⅜-in. OD × 0.065-in.-minimum-wall HRT heat exchanger tubing and reported previously, made it desirable to explore this method more fully. Two more flaw indications, contained in the 16 rejected tubes, were subjected to x-ray and metallographic examination. Each indication pinpointed a circumferentially gouged portion of the tube through roughly one-half of the inside tube wall and ⅛ to ¼ in. along the longitudinal axis. A tool-steel chip was embedded in one of the defects. It is believed that any one of the three flaws examined to date would have caused ultimate failure had the tube been put into service.

Present plans include a re-examination of the remaining rejected tubes, with an attempt being made for calibration with a standard 0.002- to 0.004-in. inside notch. A correlation of the indications of the magnetic inspection with ultrasonic inspection will be attempted before destructive testing and inspection.

6.6 4000-gpm LOOP[9]

B. A. Hannaford D. S. Toomb
J. S. Culver

The 4000-gpm loop accumulated 700 hr of operating time, including that previously reported.[10]

The surface preparation, prior to addition of UO_2SO_4 solution, consisted of a 5% trisodium phosphate rinse for 4.5 hr at 115°C. Two clear water rinses were followed by a 3% HNO_3 rinse for 3 hr at 135°C. A series of 10 distilled water rinses, raising the pH to 6.2, was followed by a 200-hr run with water containing 100 to 200 ppm dissolved O_2 at 250°C.

A few minor modifications were made to the system to increase ease and reliability of operation. A sample bypass was added to the high-pressure loop, and a CO_2 adsorber and an O_2 flowmeter were installed in the off-gas line.

Uranyl sulfate will be added according to the following schedule, and the loop will be operated

[9] J. R. McWherter *et al.*, *HRP Quar. Prog. Rep. Nov. 15, 1951*, ORNL-1221, p 18.

[10] B. A. Hannaford *et al.*, *HRP Quar. Prog. Rep. Jan. 31, 1955*, ORNL-1853, p 137.

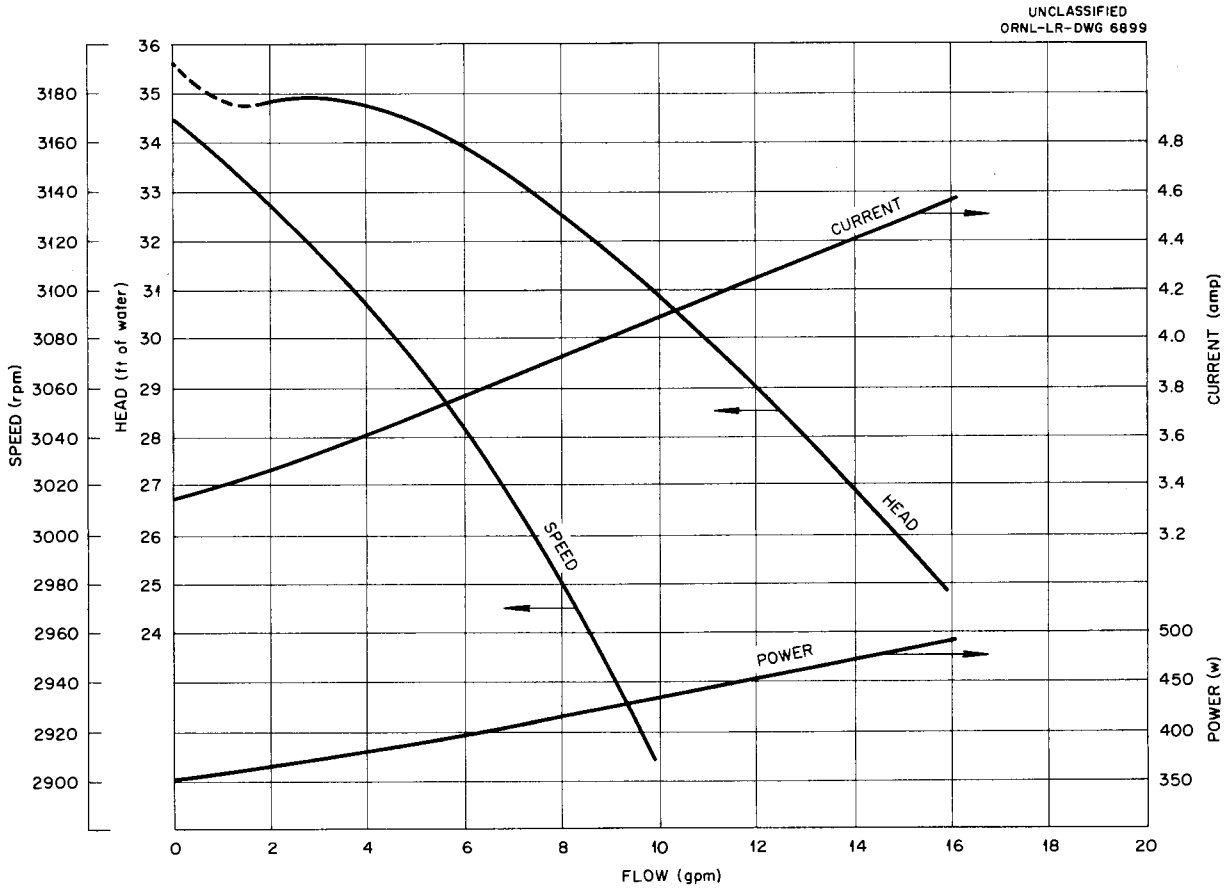

Fig. 6.1. ORNL Pump Characteristic Curves. Standard pump with alternate electrical connection.

for 200 hr at each condition:

1. a concentration of 0.0046 *m* UO_2SO_4, 0.002 *m* H_2SO_4, and 0.0005 *m* $CuSO_4$,
2. a concentration of 0.0090 *m* UO_2SO_4, 0.003 *m* H_2SO_4, and 0.001 *m* $CuSO_4$,
3. a concentration of 0.02 *m* UO_2SO_4 (10 g/liter), 0.005 *m* H_2SO_4, and 0.0025 *m* $CuSO_4$.

Following operation, the pump will be shut down and dismantled for observation of the Stellite wear rings and type 347 stainless steel cast impeller. Corrosion specimens in the sample bypass will also be removed and observed at this time.

6.7 SLURRY FEED PUMP

E. L. Youngblood J. S. Culver

During the past quarter, this unit, an HRE-type diaphragm pump, has been operated as a high-pressure source of slurry for valve tests. These tests are reported in Sec. 7.3.2.

In an effort to improve the suction characteristics of the pump, when handling the heavy slurry, a mercury leg was added between the oil pump and the diaphragm head. A preliminary test of a simple mercury leg system showed marked improvement in pumping, but the system had to be abandoned because the mercury emulsified in the oil. A new system, in which a second diaphragm head separates the oil and mercury, is now being tested.

6.8 TITANIUM PROGRAM

J. S. Culver L. R. Weissert

A titanium program with the following objectives was initiated: to acquire sufficient knowledge and experience so that a large homogeneous type of power reactor system may be confidently designed for using titanium as the containing material in

contact with the primary fuel and/or blanket solutions; to demonstrate that private industrial concerns can become experienced with titanium technology; and to show that they are capable of designing and supplying various titanium and titanium-clad components for such a reactor system.

In its present form, the program is set up to approach these objectives from two complemental directions, one by outside industry and the other by the Laboratory. Twenty-four vendors have been invited to bid on the initial phase of the program, consisting in the development and fabrication of short lengths of titanium-lined 3½- and 20-in. carbon steel pipe and a small titanium-clad heat exchanger. To date approximately half the vendors have responded to the invitation, and, of these, six indicated their interest. It is believed that the satisfactory fabrication of these components to the required test specifications will prove feasibility of the fundamental processes and will lead the way to design and fabrication of full-scale pressure vessels, heat exchangers, and piping systems. It is expected that the next program phase will include the remainder of the loop components such as pumps, valves, and fittings.

As another approach to the problem, a conceptual design and fabrication procedure is nearly completed at ORNL for the lining of 3½- and 20-in. carbon steel pipe, including circumferentially welded joints, flanged joints, and side branch attachments.

7. DEVELOPMENT OF BLANKET-SYSTEM COMPONENTS

R. N. Lyon

R. V. Bailey, A. S. Kitzes, L. F. Parsly
P. R. Crowley, B. A. Kress, J. D. Perret
D. G. Davis, C. G. Lawson, M. Richardson
R. B. Gallaher, L. E. McTaggart, D. S. Toomb
W. Q. Hullings, R. H. Nimmo, P. C. Zmola

7.1 SLURRY CIRCULATION STUDIES

A. S. Kitzes R. B. Gallaher

7.1.1 Comparison of Slurry Corrosion at 290 and 250°C in 100-gpm Loops

This quarter, for the first time, thorium oxide slurries were circulated at 290°C and 2000 psi pressure. The results were very encouraging, but they appear to indicate that the optimum conditions at 250°C are not necessarily the optimum conditions at 290°C. The tests were conducted in 100-gpm loops, which have been described previously.[1]

Data from two of the 290°C runs, S-58 and S-59, are listed in Table 7.1. For purposes of comparison, data from a 250°C run, S-54, are also listed, although they were reported in the previous progress report.[2] In addition, the iron-thorium ratio vs time is plotted for S-54, S-58, and S-59 in Fig. 7.1. As in most of the recent loop runs, these tests were conducted with oxygen in the pressurizer, from which it was brought into the circulating stream as dissolved gas in the condensate, which was bled into the motor end of the pump. In these three runs thorium oxide calcined at 650°C was used to prepare the slurry.

In runs S-54 and S-58, the circulating systems were essentially the same except for the flow restrictor, which was type 347 stainless steel in S-58 and titanium in S-54. The rod suspended along the axis of the venturi was type 347 stainless steel in both cases. The loadings in the two runs were slightly different; a higher concentration could be circulated at the higher temperature with the use of the same size of impeller. Inspection of the data in Table 7.1 reveals several interesting features:

1. The pH of the slurry in run S-54 (250°C) was higher than in run S-58 (290°C). The pH values in S-54 were always alkaline and remained above 7.6, whereas the pH values in S-58 continued to decrease from 10.1 to a value of 6.6 at the end of the run.
2. For the first 69 hr, the iron buildup in the solids, a measure of the rate of attack of type 347 stainless steel by the slurry, was slightly less at 290°C than at 250°C. The iron-thorium ratio increased from 0.25 to 1.32 mg/g in S-58 as compared with 0.07 to 2.30 mg/g in S-54.
3. The attack by the slurry on titanium was approximately the same in both runs.

In run S-59 the $\frac{3}{8}$-in. rod suspended through the throat of the venturi tube was composed of segments of three different metals – type 347 stainless steel, titanium, and zirconium. Teflon spacers isolated the various metals to minimize galvanic corrosion. The flow restrictor, a $\frac{3}{4}$-in. orifice, also contained the same metals isolated with Teflon.

Run S-63 was made in order to determine the pumping characteristics of a thorium oxide prepared by the National Lead Co. by calcining the oxalate at 750°C. It contained 2000 ppm sulfate. A slurry of 500 g of thorium per kilogram of water was circulated at 290°C for 100 hr with oxygen present. The run was stopped because the pH of the slurry dropped from 5.4 to 3.2 and because severe corrosion of the stainless steel was indicated by analysis of slurry samples. It may be concluded from these results that less than 2000 ppm sulfate is desirable in thorium oxide which is to be used in the neighborhood of 300°C.

7.1.2 Effect of Oxygen at 250°C

Three 5-gpm runs were made at 250°C with the use of oxide calcined at 900°C and less than 500 ppm sulfate with the pH lowered at room temperature from 9 to 5 by the addition of CO_2. In one run oxygen was withheld from the loop, while in the other two runs about 500 ppm oxygen was

[1] R. N. Lyon *et al.*, *HRP Quar. Prog. Rep. Oct. 31, 1953*, ORNL-1658, p 127.

[2] R. N. Lyon *et al.*, *HRP Quar. Prog. Rep. Jan. 31, 1955*, ORNL-1853, p 141–148.

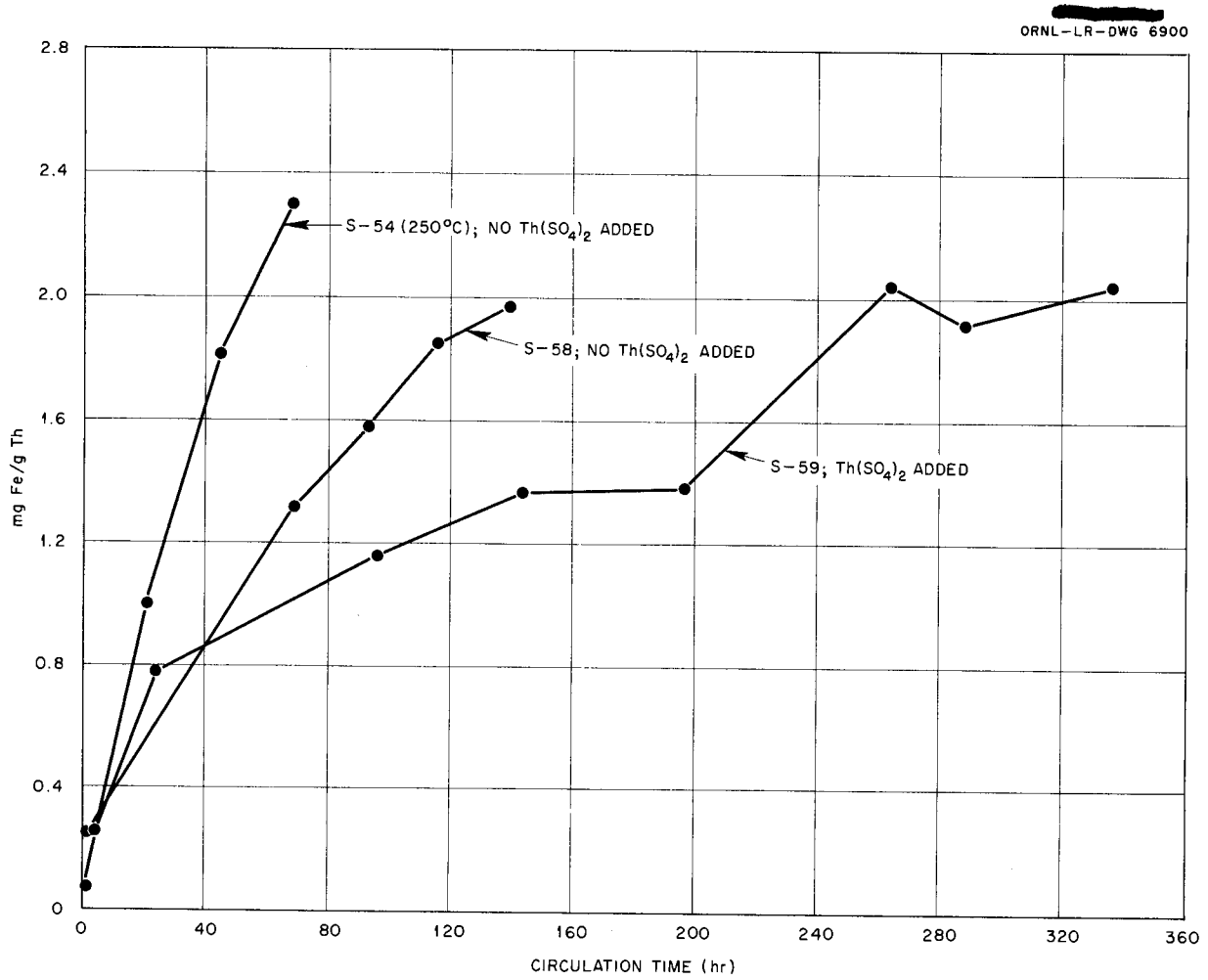

Fig. 7.1. Iron-Thorium Ratios vs Time (Runs S-58, S-59, S-54).

present. The results plotted in Fig. 7.2 indicate a beneficial effect of oxygen, at least for these short-term experiments. In run U-18, without oxygen, the pH of the slurry containing 650 g of thorium per kilogram of H_2O and 10 psi CO_2 varied between 5.4 and 6.4. In the runs with oxygen and the same thorium and CO_2 content, the pH of the slurry varied between 5 and 5.9. Inspection of the components after shutdown of runs with oxygen revealed that the stainless steel pipe walls and pump impeller were covered with a golden-brown film. There was no visible film deposited on the components after shutdown of run U-18 in which the oxygen was omitted.

7.1.3 Long-Term Attack on Stainless Steel Piping

Sections from loops S and T were cut open for examination of the interior of these pipes. Before it was dismantled, loop T had accumulated a total service time, at 250°C, of about 2000 hr with all types and concentrations of ThO_2 slurry plus about 3000 hr with $UO_3 \cdot H_2O$ slurries and water. The piping sections in Figs. 7.3 and 7.4 were defilmed with HNO_3 and HF so that the base metal could be inspected. Flow in this system was into the cap of the tee and out to the left. A small region of attack can be detected in

TABLE 7.1. DATA FOR TWO THORIUM OXIDE CIRCULATION TESTS AT 290°C AND SIMILAR DATA FOR A COMPARABLE TEST AT 250°C

Sample No.	Time (hr)	Solids (Based on Water)							Fe (mg)/Th (g)	Filtrate		Materials in System			Gas Analysis		
		Th g/kg	Fe (ppm)	Ni (ppm)	Cr (ppm)	SO_4^{--} (ppm)	Ti (ppm)	pH		pH	SO_4^{--} (ppm)	Impeller	Orifice Plate	Seal Rings	Volume (ml)	O_2 (ppm of Slurry)	H_2 (ppm of Slurry)
Run S-58 – 290°C, Cold Precipitated Oxalate Calcined at 650°C; 7.2 Liters of O_2 Added																	
0	2	324	79	8	20			10.1	0.25	10.3		Ti (tip velocity, 120 fps; wt loss, 4 g)	Type 347 stainless steel (velocity, 83 fps; wt loss, 1.911 g)	Ti	56	468	0
1	69	444	586	98	133		30	7.4	1.32	7.5					34	138	0
2	93	364	576	93	136		99	6.8	1.58	7.0							
3	116	361	667	102	154		56	6.9	1.85	7.1							
4	140	355	695	108	162		154	6.6	1.97	6.7					24	41	0
Run S-59 – 290°C, Cold Precipitated Oxalate Calcined at 650°C; 21 g of $Th(SO_4)_2$ and 7.2 Liters of O_2 Added																	
0	4	520	137	29	53	2000	<20	9.1	0.26	9.0	174	Ti (tip velocity, 120 fps; wt loss, 3 g)	Ti–Zr–type 347 stainless steel (velocity, 83 fps)	Ti	73	438	0
1	24	427	312	22	65		<20	6.8	0.78	9.2	20						
2	96	458	531	81	159	1215	<20	5.7	1.16	6.0	8				56	97	0
3	144	545	748	117	218	1285	121	5.7	1.37	6.5	9						
4	193	468	647	109	293	1125	174	5.7	1.38	6.5	15				49	34	
5	264	500	1020	132	480	1480	368	5.6	2.04	6.2	24						
6	288	558	1065	141	402	1150	402	5.5	1.91	6.5	80				124	828	
7	336	740	1515	240	544	1535	726	5.5	2.05	6.1	25				80	658	
Run S-54 – 250°C, Cold Precipitated Oxalate Calcined at 650°C; 7.2 Liters of O_2 Added																	
0	1	401	28	5	12	300	<20	9.5	0.07	8.9	<10	Ti (tip velocity, 120 fps; wt loss, 2 g)	Ti (velocity, 83 fps; wt loss, 68 mg*)	Ti	36	320	0
1	21	320	320	51	92	246	<20	9.3	1.0	6.4	<10						
2	45	318	580	89	155	281	65	7.6	1.82	7.6	<10				45	290	0
3	69	324	750	116	176	252	71	8.8	2.30	7.8	16						

*This weight loss was erroneously listed as 68 g in the last quarterly report, ORNL-1853, Table 7.1, page 143.

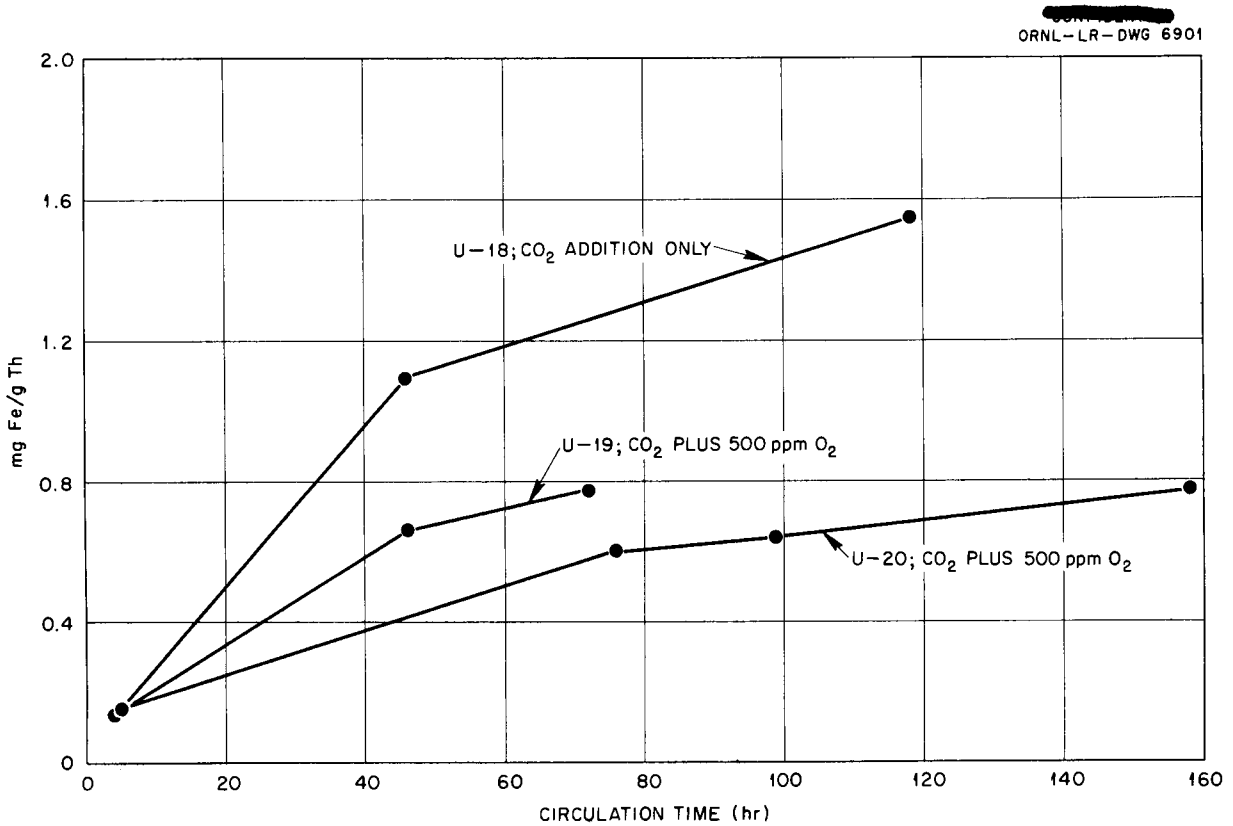

Fig. 7.2. Effect of Oxygen Addition at Constant pH.

Fig. 7.4 on the inside edge of the tee. No other region of localized attack was found in this system. The pipe, elbows, and welds showed essentially no attack; the grinding-tool marks are still visible around two of the welds.

The sections from loop S, shown in Fig. 7.5, have not been defilmed. The loop was in operation at 250°C for about 13,000 hr – 5,000 hr with ThO_2 slurries and 8,000 hr with $UO_3 \cdot H_2O$ slurries and water. Some attack was found to have occurred on the wall downstream from the orifice and at a weld downstream from the elbow. This may be seen on the upper portion of the lower section, just downstream from the flow restrictor. Since the attack is not circumferentially symmetrical, it is attributed to a period of test during which the orifice opening was intentionally eccentric and tangent to the wall. On the other hand, no attack occurred on the sampler tube which extended into the stream or on the pipe walls downstream from the sampler tube. The pipe, elbows, and walls were covered with a golden-brown oxide film except where certain areas had been attacked. The velocity in the sections of both loops was usually about 20 fps.

7.1.4 Thickening of Thorium Oxide Slurries

It is concluded from tests this quarter that when circulated in a loop at 250°C thorium oxide calcined at 800°C thickens less than at 650°C and produces no greater attack on stainless steel. On the other hand, sodium silicate will cause plugging of 5-gpm loops[3] over all practical ranges of silicate and sulfate.

The thickening of violently agitated thorium oxide slurries[4] at temperatures below about 170°C introduces low-temperature handling problems, particularly in the dump tanks and possibly in the blanket heat exchanger after shutdown. Since

[3] R. N. Lyon *et al.*, *HRP Quar. Prog. Rep. April 30, 1954*, ORNL-1753, p 164.

[4] S. A. Reed, *HRP Quar. Prog. Rep. Jan. 31, 1955*, ORNL-1853, p 83.

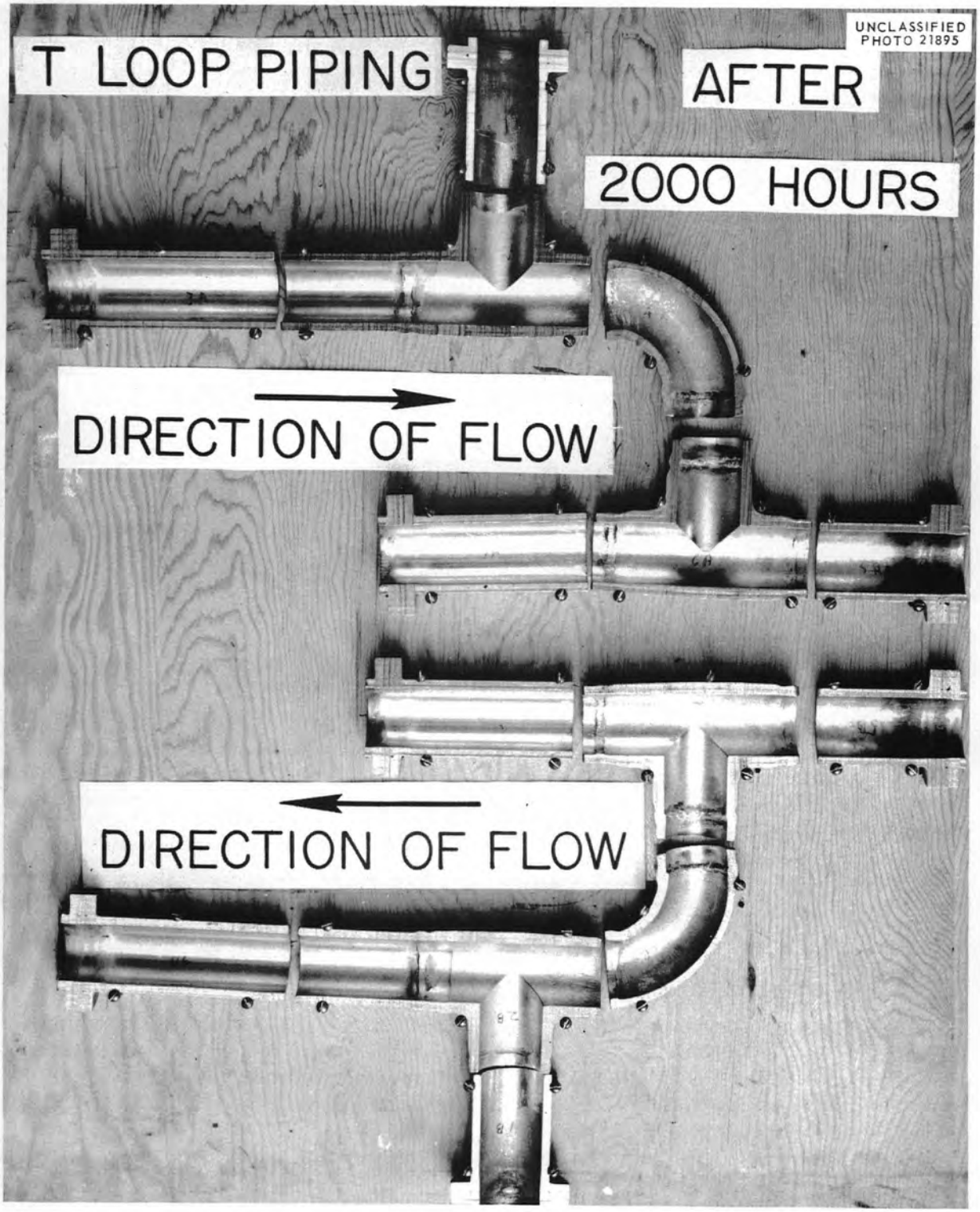

Fig. 7.3. Section of Defilmed Stainless Steel Piping from Loop T.

Fig. 7.4. Enlarged Section of T-Loop Piping Showing Welds and Grinding-Tool Marks.

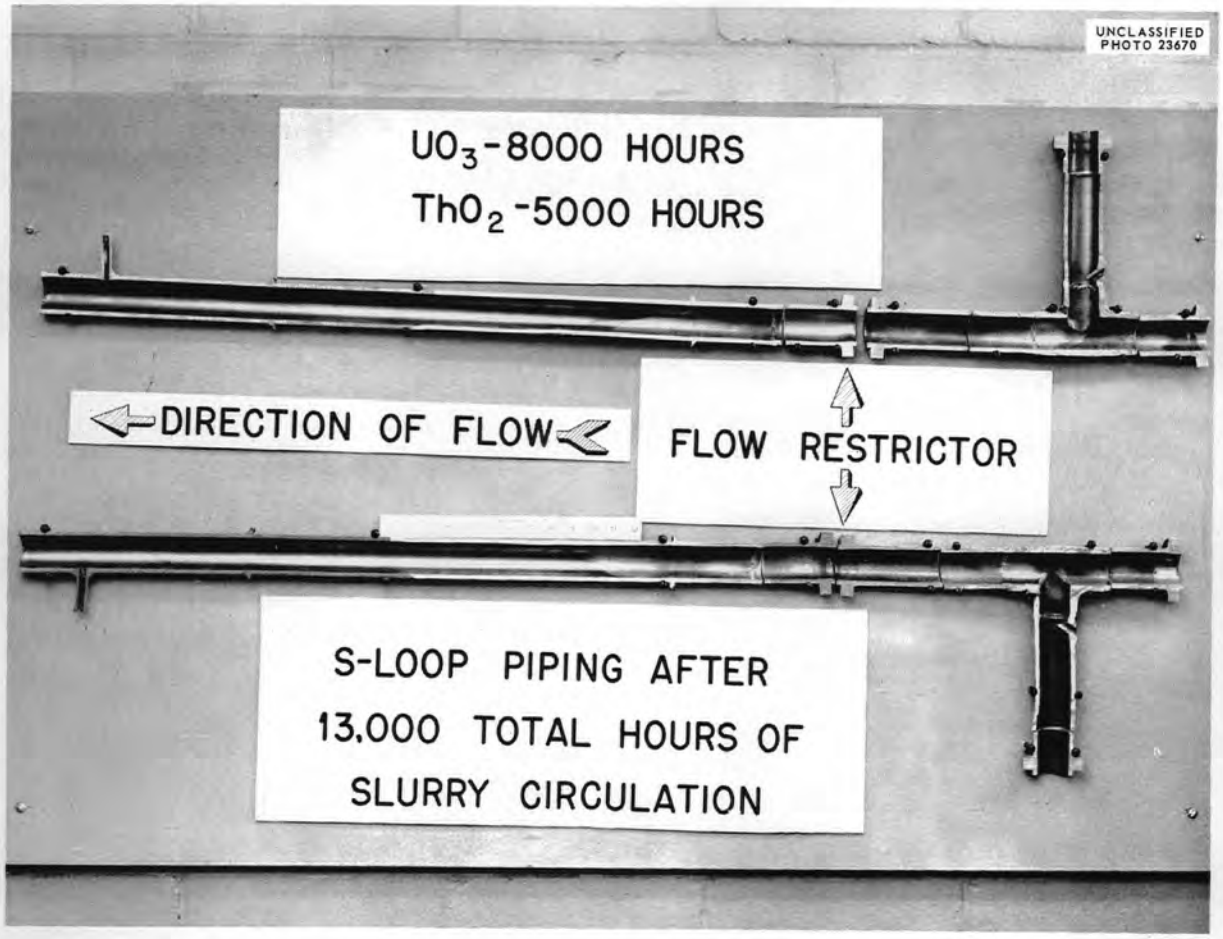

Fig. 7.5. Section of S-Loop, Not Defilmed.

previous experience has shown[5] that small amounts of sodium silicate, when added at room temperature, greatly reduce the apparent viscosity of thickened slurry and since it appeared that thorium oxide calcined at higher temperatures produces slurries which thickened less, these two approaches were used in efforts to control thickening without increasing corrosion and caking. Nine circulating loop experiments were carried out to investigate these approaches.

In the first seven 5-gpm loop runs, described in Table 7.2, which were made to test the effectiveness of sodium silicate, it will be noted that the loops became plugged in all cases. Examination of the data reveals that even at silicate concentrations as low as 0.008% sodium silicate (run X-5) and with essentially no sulfate present, the loops became plugged when cooled to room temperature. Previous experiments, as well as runs X-11 and X-12, indicate that plugging would not have occurred in these experiments had silicate not been added. Under silicate-free conditions only a sulfate concentration of 10,000 ppm is usually required to produce plugging of the loops. Chemical and microscopic examinations of the slurry plugs have not yet been completed.

In approaching the thickening problem by means of the oxide calcination temperature, it was found that 800°C was the lowest calcination temperature which produced a slurry that did not thicken in 2 hr of beating in a Waring Blendor (see Table 7.3). Since an earlier loop test with 1200°C oxide had produced drastic attack on the stainless steel

[5]R. N. Lyon *et al.*, *HRP Quar. Prog. Rep. Oct. 31, 1954*, ORNL-1813, p 125.

TABLE 7.2. EFFECT OF SILICATE ADDITIONS ON THE PUMPING CHARACTERISTICS OF ThO_2* SLURRIES AT 250°C

Run No.	Concentration (g of Th per kg of D_2O)		Additives	Circulation Time Before Shutdown (hr)	Slurry pH	Remarks
	When Loaded	During Circulation				
X-1	650	900	2 wt % $Th(SO_4)_2$ 500 ppm O_2 0.235 wt % $Na_2O(SiO_2)_{3.25}$	44	4	After 44 hr loop cooled to room temperature far silicate addition
				0		Solids had caked upon cooling and had plugged loop
X-2	650	975	2 wt % $Th(SO_4)_2$ 0.235 wt % $Na_2O(SiO_2)_{3.25}$ 500 ppm O_2	24	4.4	Circulation at 150°C was possible but loop plugged during cooling below 150°C
X-3	650	950	0.235 wt % $Na_2O(SiO_2)_{3.25}$ 500 ppm O_2	13	10.4	Loop plugged during cooling; bearing difficulty necessitated shutdown before 24 hr
X-4	650	740	0.078 wt % $Na_2O(SiO_2)_{3.25}$ 500 ppm O_2	23	10.4	Slurry could be circulated at 150°C and at room temperature; loop plugged on reheating
X-5	650	780	0.008 wt % $Na_2O(SiO_2)_{3.25}$ 500 ppm O_2	23	9.4	Slurry was recirculated at 250°C
				91	9.2	Slurry thickened and plugged loop upon second cooling to room temperature
X-6	650	620	0.009 wt % $Na_2O(SiO_2)_{3.25}$ 3000 ppm SO_4 as $Th(SO_4)_2$ 500 ppm O_2	22	7.5	Slurry recirculated at 250°C after cooling once to room temperature
				40	6.9	Plugged on reheating to 250°C after second cooling
X-7	650	620	0.1 wt % $Na_2O(SiO_2)_{3.25}$ 3000 ppm SO_4 as $Th(SO_4)_2$ 500 ppm O_2	97	5.4	Slurry was recirculated at 250°C after cooling to room temperature
				148		Venturi in loop plugged with lumps of oxide formed during second cooling ot room temperature

*Calcined at 650°C.

TABLE 7.3. EFFECT OF CALCINATION TEMPERATURE ON THE THICKENING OF THORIUM OXIDE SLURRIES DURING VIOLENT AGITATION (CALCINATION TIME, 4 hr)

Calcination Temperature (°C)	Time for Slurry* to Reach Maximum Brookfield Viscometer Reading at 60 to 70°C (min)	Concentration of Settled Bed (g of Th per kg of H_2O)
650	50	1100
750	110	1030
800	>120	1150
850	>120	1680

*Contains 800 g of thorium per kilogram of H_2O.

components, it was believed that a practical calcination-temperature limit existed. As indicated by the data plotted in Fig. 7.6, run X-12 with 800°C oxide actually produced slightly less attack than run X-11 with 650°C oxide.

In both runs X-11 and X-12, the run was stopped and started several times and there was no indication of the plugging which had been encountered in the silicate runs.

The pumped 800°C slurry was much more fluid at room temperature than was the pumped 650°C material, indicating that calcination at 800°C and perhaps at higher temperatures produces a more useful thorium oxide for use in reactor blankets than does calcination at 650°C.

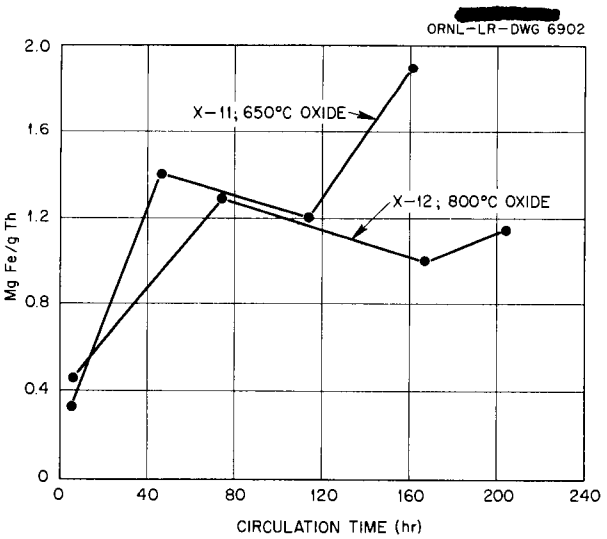

Fig. 7.6. Attack at 250°C on Type 347 Stainless Steel by ThO_2 Slurries (Containing 500 g of Th per kg of H_2O) and 500 ppm O_2.

7.2 PRESSURE DROP IN SLURRY SYSTEMS

A. S. Kitzes P. R. Crowley
C. G. Lawson

It has been reported[6] that pumped or beaten thorium oxide slurries containing 1000 g of thorium per kilogram of H_2O were either Bingham plastics or pseudoplastics at 25°C; the apparent viscosity in each case decreased as the rate of shearing strain increased. Data obtained this quarter indicate that they are Bingham plastics in the concentration range from 500 to 1570 g of thorium per kilogram of H_2O.

Shear diagrams, obtained by measuring the pressure drop required to produce a given flow rate of slurry through a length of tubing, are shown in Fig. 7.7 for a slurry prepared by beating a 650°C oxide slurry for 100 hr.

The shear diagram shown in Fig. 7.8 is for a similar slurry, which had been pumped at 300°C for 300 hr in run S-59. In both cases a finite stress was required to initiate flow.

It may also be concluded from these two tests that the thickening phenomenon associated with pumped slurries at elevated temperatures can be duplicated in the laboratory by violent agitation at lower temperatures.

[6]R. N. Lyon *et al.*, *HRP Quar. Prog. Rep. Jan. 31, 1955*, ORNL-1853, p 141–148.

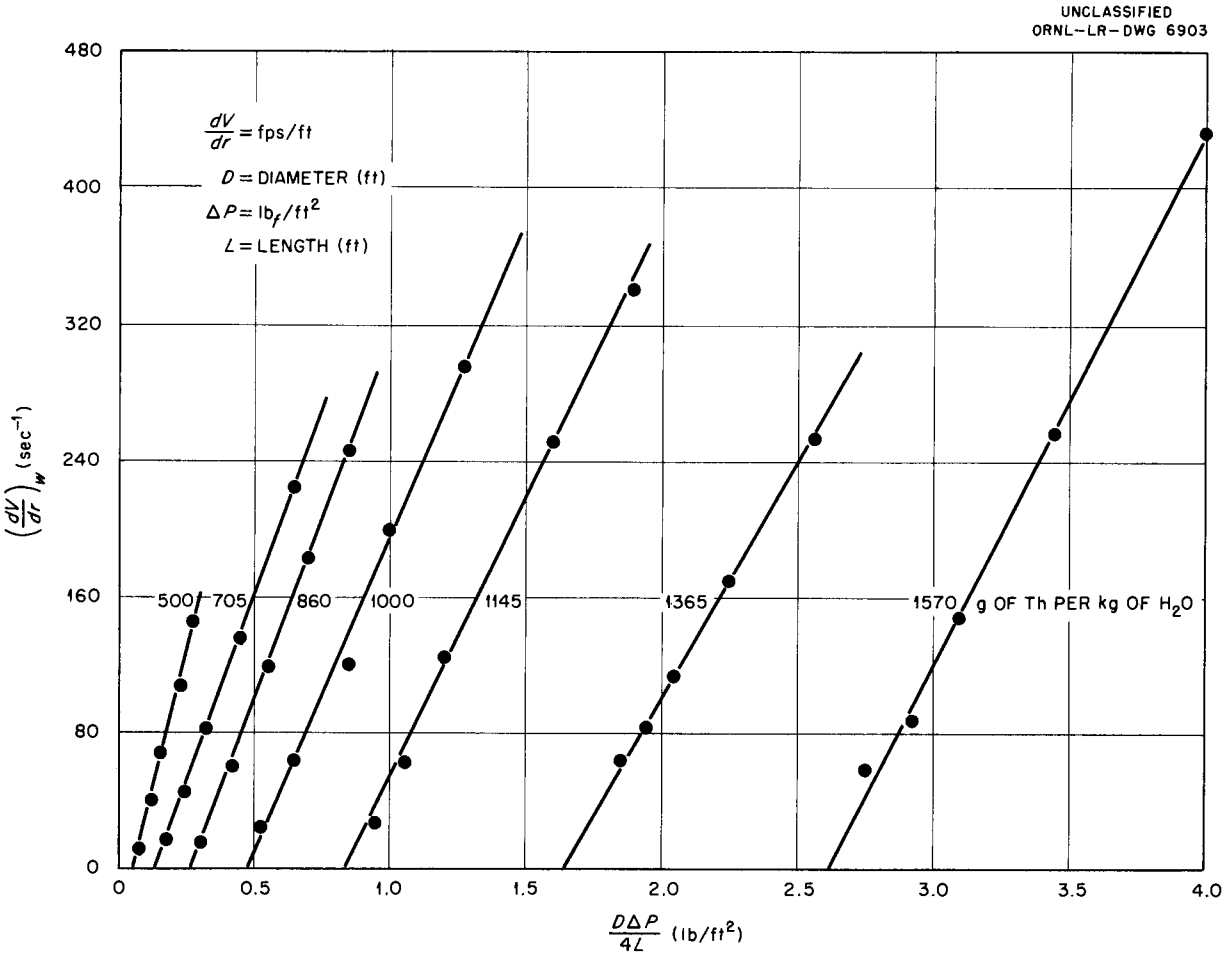

Fig. 7.7. Shear Diagrams for ThO_2 Slurry Agitated for 100 hr with Lightning Mixer.

7.3 SLURRY COMPONENT DEVELOPMENT

A. S. Kitzes

W. Q. Hullings D. S. Toomb
B. A. Kress C. G. Lawson
J. D. Perret

7.3.1 Westinghouse 200A Slurry Pump

W. Q. Hullings

Fabrication of the loop[7] to test the Westinghouse 200A slurry pump is 98% complete (Fig. 7.9). The remaining work consists in insulating the loop, checking controls, and pressure checking the system.

The Westinghouse 200A pump, designed specifically to pump slurries, is shown in Figs. 7.10 and 7.11. This pump differs from pumps that do not handle slurries in the simplicity of the volute, in the absence of pressure-balancing holes through the impeller, in the additional vanes at the back of the impeller, in the absence of rear seal rings, and in its design to handle fluids of a specific gravity of 2.

7.3.2 Valves

B. A. Kress D. S. Toomb

A program has been initiated during this quarter to test various commercial valves for use with slurries at 300°C and 2000 psi. The valves are being tested as letdown valves, on the assumption that a satisfactory letdown valve can be used as

[7] R. N. Lyon *et al.*, *HRP Quar. Prog. Rep. July 31, 1954*, ORNL-1772, p 122.

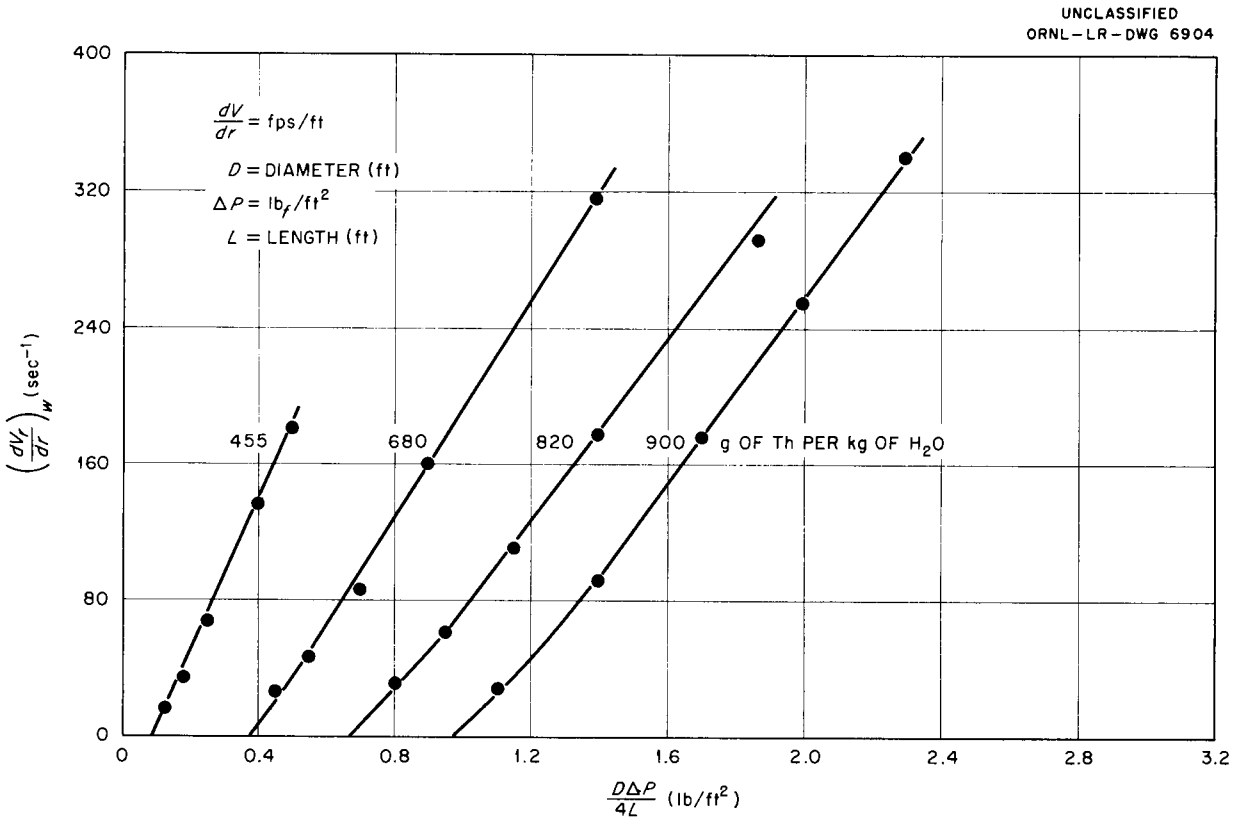

Fig. 7.8. Shear Diagrams for ThO_2 Slurry from Loop Run S-59.

a sampling valve or dump valve. The slurry injection pump loop for operation at room temperature has been modified to test valves as shown in Fig. 7.12. A diaphragm injector pump[8] is used to pump the slurry and to develop a pressure of 1000 psi, at which point the valve opens to reduce the pressure. All runs were made at about 30°C with a slurry containing 500 g of thorium oxide per kilogram of water calcined at 650°C and with a single-head pump operating at 72 rpm.

The results of the tests are summarized in Table 7.4; drawings of the valves and photographs of the valve trims after services are shown in Figs. 7.13 to 7.19.

A Pressure Products plug-type valve (Fig. 7.20) has been installed in T loop, and, to date, 30 samples of slurry at 250°C and 1000 psi have been withdrawn through the valve. The valve is still in operation.

[8] J. M. Baker, E. L. Youngblood, and D. S. Toomb, Jr., *HRP Quar. Prog. Rep. Oct. 31, 1954*, ORNL-1813, p 114.

7.3.3 Pressure-Vessel Studies

C. G. Lawson

Slurry tests in the 18-in. steel mockup of the blanket vessel, described previously,[7] were completed. Pressure drops across the blanket vessel and homogeneity of the circulating stream were determined for various flow rates. The blanket system was also dumped under a variety of conditions to determine qualitatively the settling characteristics of the slurry during dumping.

The slurry entered the pressure vessel tangentially through the two inlets and swept across the bottom of the vessel to pick up solids which had settled during a long shutdown. A takeoff annulus around the core outlet prevented settling on top of the core vessel. The temperature of the core vessel was maintained at 200°C with 225-psi steam; the temperature of the blanket fluid was varied between 25 and 170°C.

The slurry used in these tests was prepared from oxide calcined at 900 and 650°C; the shear

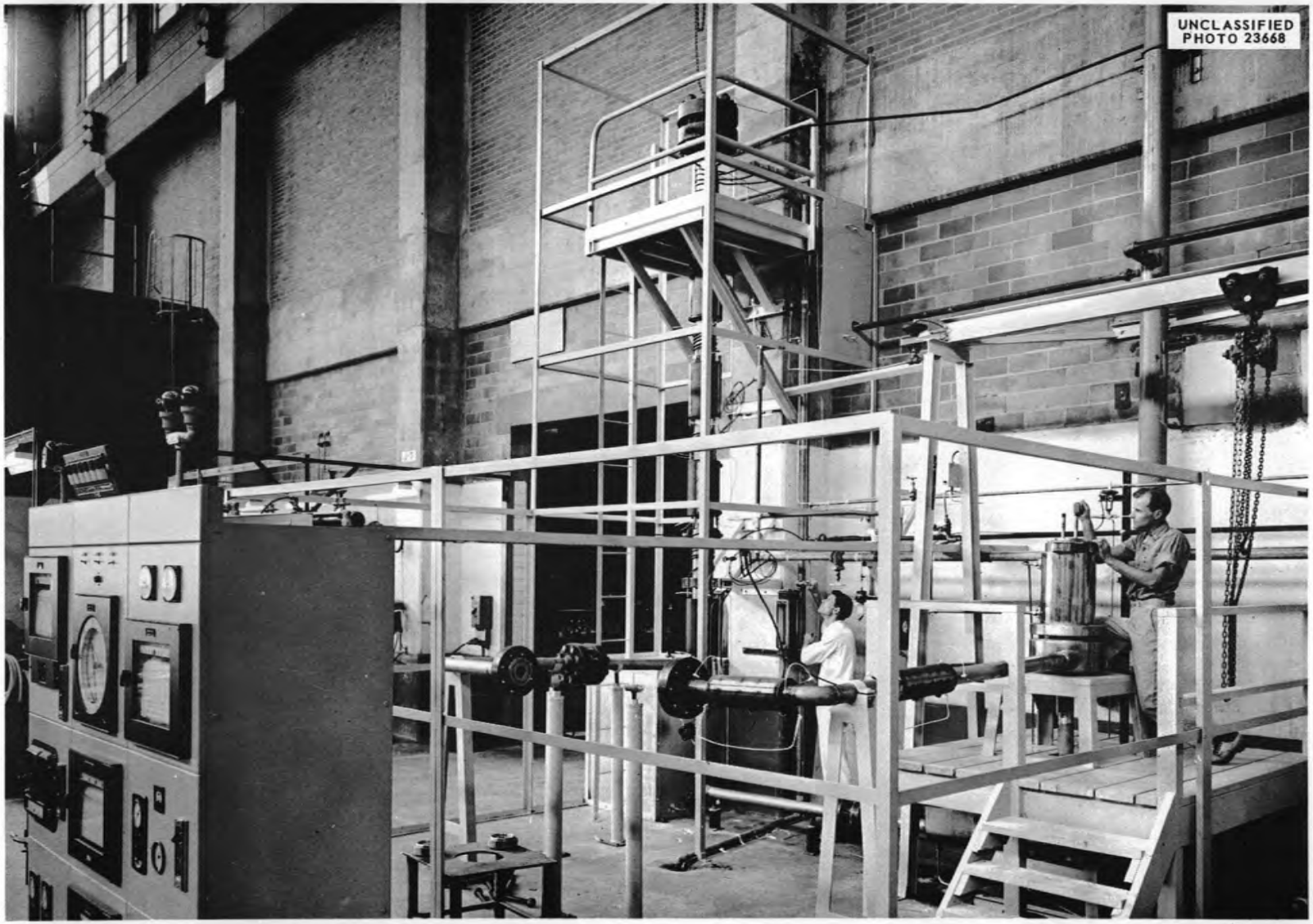

Fig. 7.9. Loop for Westinghouse 200A Slurry Pump.

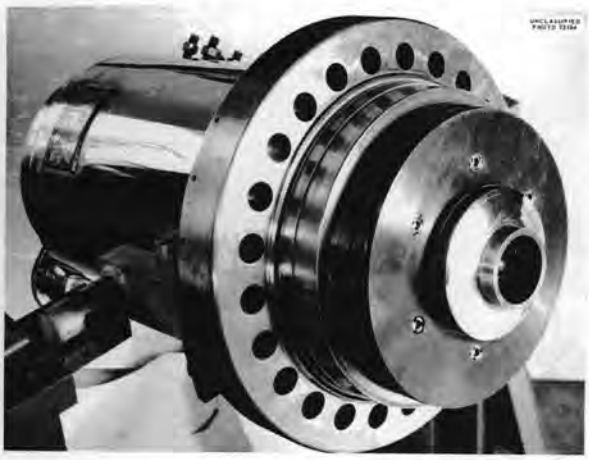

Fig. 7.10. Westinghouse 200A Slurry Pump Assembled.

diagram for the slurry was similar to the one shown in Fig. 7.7. Slurries at concentrations ranging from 250 to 1000 g of thorium per kilogram of H_2O were circulated with a Westinghouse 30A canned-rotor pump.

The following characteristics of the system were determined:

1. At a flow rate through the blanket vessel of 0.035 fps, the pressure drop across the vessel measured at various temperatures was the same as that for water. The pressure drop with water at room temperature was 17 ft, largely because of the inlet nozzles.

2. The average heat transfer coefficients with a slurry containing 1000 g of thorium per kilogram of water in the temperature range between 25 and 170°C were 25 to 30% lower than those obtained with water at the same flow rates.

3. Under steady-state conditions, the solids are homogeneously distributed throughout the pressure vessel. A mixture of thorium-uranium oxides was added to the circulating stream through the pressurizer. From the analytical data, homogeneity of solids in the circulating stream was ascertained.

4. The inlet and outlet designs are adequate to maintain homogeneity during circulation and to redisperse solids after long shutdowns. Assay of ThO_2 in samples drawn from the circulating stream before and after a 20-hr shutdown showed that the solids were uniformly dispersed within 15 min after circulation was started. In addition, lead oxide as a tracer was added to the system by artificially forming a cake on the core and pressure-vessel walls. Analytical data for the samples drawn periodically from the system after startup showed the lead oxide to be distributed uniformly throughout the slurry.

5. No solids settled on the core or adhered to the pressure-vessel walls if the system was drained while the core was kept at temperature. Under all other conditions of dumping, a slight uniform coating of thorium oxide deposited on the core and pressure-vessel walls.

7.3.4 Dump Tank–Evaporator Test

C. G. Lawson J. D. Perret

A slurry containing 100 g of thorium per kilogram of H_2O could not be circulated by boiling convection in the steel mockup of the HRT solution dump tank. The dump tank, 14 in. in diameter and 16 ft long, contains four baffles, equally spaced along the length of the tank. The baffles are welded to the tank in such a way as to form a 3-in. channel at the top of the tank for steam removal and a 3-in. channel at the bottom of the tank for the circulation of the slurry.

Inspection of the dump tank after the slurry run revealed that the solids had settled out midway between each baffle.

Modifications to the present baffling are being studied. In the meantime, a glass prototype of the dump tank has been constructed to study the effect of the arrangement of the baffles on the flow pattern through the tank.

Since the blanket dump tank is to be 24 in. in diameter, a full-diameter mockup is also being constructed.

7.3.5 Pressurizer Studies

B. A. Kress

In most of the slurry blanket systems visualized to date, steam is withdrawn from the top of the pressurizer and condensed, and the condensate is fed into the motor end of the canned-rotor pump to keep the bearings flushed free of suspended solids. The continuous removal of steam causes an upward movement of water in the pressurizer in opposition to the settling and compacting tendency of the thorium oxide. Should the solids be carried upward with the water, an accumulation would occur near the top of the pressurizer which might interfere with its effectiveness and which might even result in a solid entrainment that would

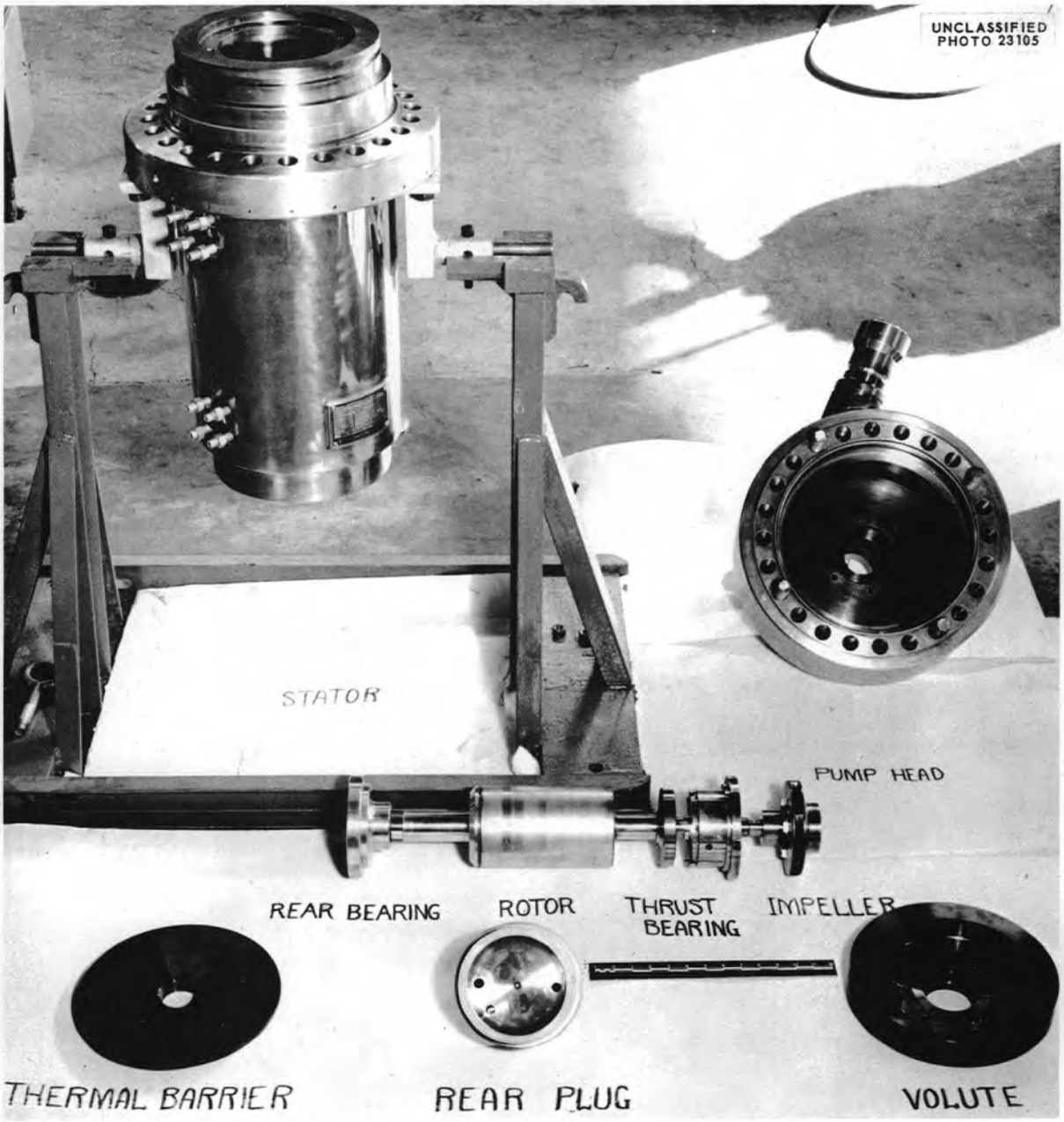

Fig. 7.11. Components of Westinghouse 200A Slurry Pump.

ultimately enter the motor end of the pump with the flushing water. It is of additional and immediate importance that interpretation of data from high-temperature loop tests is hampered by variations in the concentration by as much as a factor of 2 in the circulating part of the system because of varying accumulations in the pressurizer, which contains about one half the liquid volume.

During run T-51, data shown in Table 7.5 were taken which indicate that even though the height of the solids in the pressurizer was dependent on the steam removal rate a continuous hourly rate of about 100 lb per square foot of liquid surface did not bring an appreciable concentration of solids to the surface. At no time were solids observed in the condensate stream.

TABLE 7.4. RESULTS OF VALVE TESTS WITH ThO_2 SLURRIES PREPARED FROM OXIDE CALCINED AT 650°C

Type of Valve	Plug	Seat	Pressure Range (psi)	Number of Cycles	Remarks
Hammel-Dahl (Fig. 7.13)	Stellite 6	Zirconium	1100–300	7,465	No erosion; slight tendency to gall; seating surface completely mashed by mechanical action of plug (see Fig. 7.16)
Hammel-Dahl (Fig. 7.13)	Stellite 6	Stellite 12	900–300	4,190	Severe galling between plug and seat terminated test (see Fig. 7.16)
Modified HRE (Fig. 7.14)	Type 347 stainless steel	Type 347 stainless steel	1000–200	24,000	Stem travel decreased from $\frac{1}{8}$ to $\frac{1}{32}$ in.; lost positive shut-off near end of run; some galling occurred; seat slightly eroded but no evidence of erosion through post in plug (see Fig. 7.17)
Ball (Paul Valve Mfg. Co.) (Fig. 7.15)	Stellite 3	Type 347 stainless steel	1000–100	1,800 Valve operated for total of 54 hr but cycled for only 4 hr; balance of time valve operated in half-open position	Valve would cycle for about $\frac{1}{2}$ hr and then stick open; inspection showed guide pin bent; no wear on valve parts; ThO_2 coated ball and ball holders which could have prevented proper seating (see Fig. 7.18)
Hammel-Dahl (Fig. 7.13)	Titanium (oxidized by chemical treatment)	Titanium (oxidized by chemical treatment)	1000	Used as throttling valve operated for 188 hr	Plug and seat eroded at point of discharge; fluoride coating worn off along path of liquid (see Fig. 7.19)

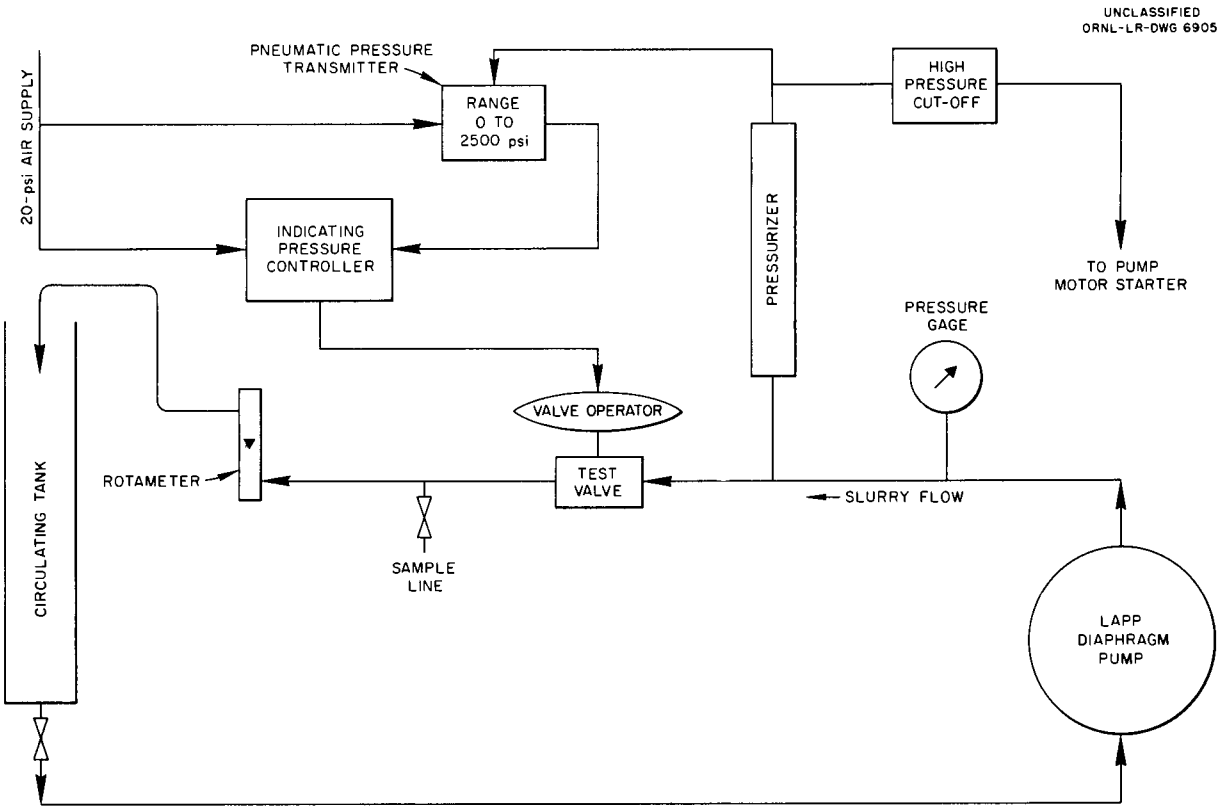

Fig. 7.12. Injection Pump Loop for Slurry Valve Tests.

TABLE 7.5. ACCUMULATIONS OF SOLIDS IN PRESSURIZER AS A FUNCTION OF THE FLOW RATE OF WATER TO THE BACK OF THE PUMP (RUN T-51)

	Water Flow Rate (liters/hr)					
	0.975	1.000	1.875	1.975	2.825	3.875
Amount of heat supplied to pressurizer to maintain flow rates						
Total kw available	5.4	7.35	7.25	7.25	7.25	7.25
Per cent time on	34	30.5	37.5	37.5	43.5	50
Average power, kw	1.8	2.2	2.7	2.7	3.2	3.6
Concentration of thorium circulated, as sampled, g of Th per kg of H_2O		585	504		446	
Volume in pressurizer containing solids, liters	4.0	4.0	5.4	5.4	6.7	8.8
Height of solids in pressurizer above circulating stream, in.	21	21	27	27	33	43
Thickness of stagnant, clear water, as measured with scintillation counter, in.	28	28	22	22	16	6
Volume of circulating stream, liters	5	5	5	5	5	5

UNCLASSIFIED
ORNL-LR-DWG 6906

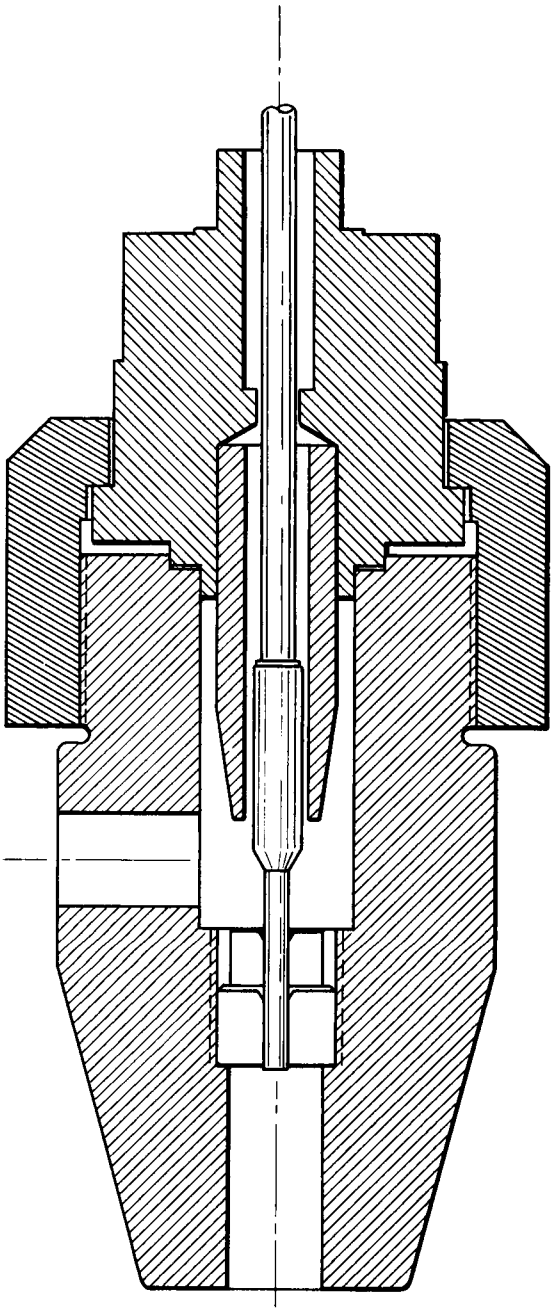

Fig. 7.13. Hammel-Dahl Bar-Stack Angle Valve.

UNCLASSIFIED
ORNL-LR-DWG 6907

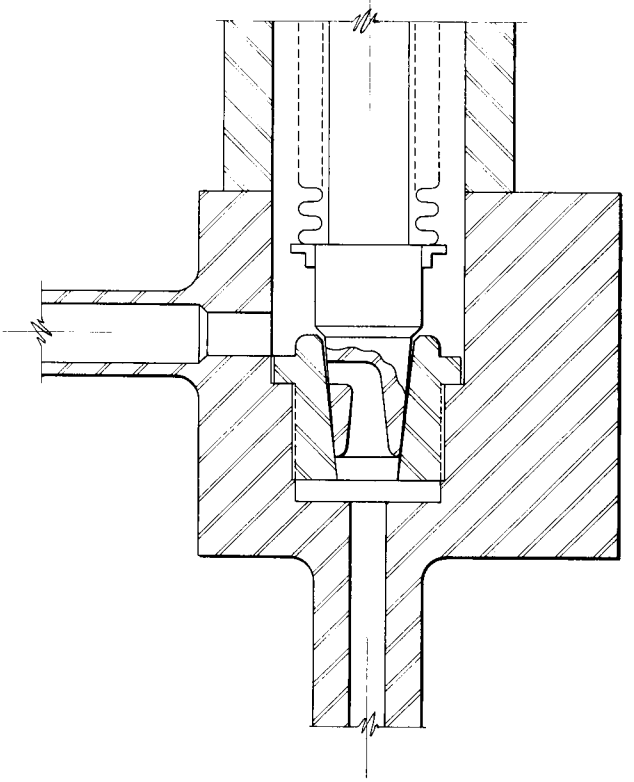

Fig. 7.14. Modified HRE Valve.

UNCLASSIFIED
ORNL-LR-DWG 6908

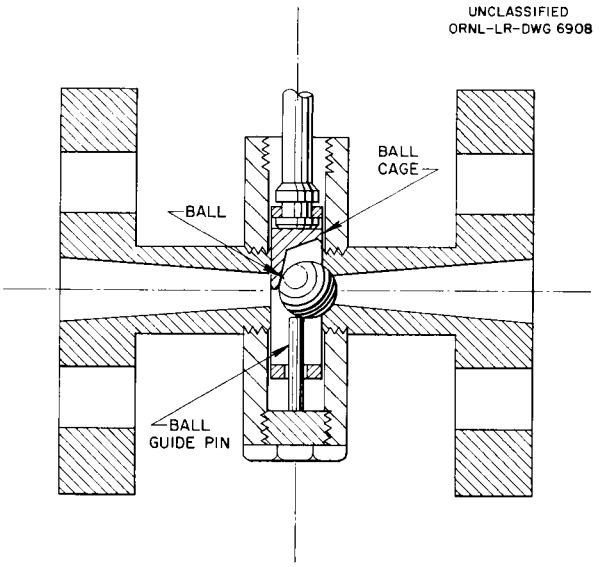

Fig. 7.15. Paul Ball-Type Valve.

Fig. 7.16. Stellite 6 Stem and Stellite 12 Seat of Hammel-Dahl Valve.

Fig. 7.18. Paul Ball Valve After Test.

Fig. 7.19. Chemically Treated Titanium Stem and Seat.

Fig. 7.17. Type 347 Stainless Steel Stem and Seat of REED Experimental Valve.

Fig. 7.20. Stem and Seat of Pressure Products Valve.

7.4 SLURRY BLANKET MOCKUP

L. F. Parsly

D. G. Davis L. E. McTaggart
R. H. Nimmo

Since further review of the radiolytic gas generation and recombination rates indicated that the quantity of gas to be removed from the high-pressure circulating loop would be only a fraction of that originally anticipated, it was decided that the in-line gas separator and the high-pressure gas-liquid separator would not be necessary for the blanket system and that sufficient steam for diluting the gases could be produced in the pressurizer. It was therefore possible to simplify the final mockup flowsheet, which is shown in Fig. 7.21. Essentially, this arrangement is a combination of two loops. With the mockup reactor (3) blanked out of the system and the bypass line (105) in place, the mockup becomes a 2000-psi, 300°C test loop and permits study of the functioning of the pump, pressurizer, and heat exchanger at design conditions. Although the basic design of the high-pressure slurry system is arranged to avoid the use of continuous slurry letdown and return, only minor design changes will be required to permit testing of that type of operation. The alternative arrangement, with line (105) removed and the mockup reactor blanket vessel (3) piped in, is limited to operation at 300 psi and 200°C by the design of the mockup pressure vessel. This arrangement permits testing of slurry flow through a full-scale mockup of the blanket system. The instrumentation is designed so that, when the loop is operating with the mockup of the reactor tied in, the blanket operating pressure will be "slaved" to the steam pressure in the core, in a manner similar to the pressure control system planned for the reactor; thus it will be possible to check the functioning of the pressure control system.

Construction of the mockup is well under way. Supporting steel for the pressure vessel and pressurizer has been erected. Fabrication of the pressurizer is approximately 85% complete, and shop fabrication of the high-pressure piping has been started. It is anticipated that the system should be ready for shakedowns by the end of the next report period.

The circulating pump to be used in the mockup is currently installed in a smaller loop for testing by the Engineering Development Section. It is expected that that test program will be completed about June 1 and that the pump will then become available for transfer to the blanket mockup.

After limited corrosion studies, it was decided to metallize the inner surface of the carbon steel mockup pressure vessel with stainless steel. It is believed that metallizing will substantially reduce the iron contamination of the slurry.

7.5 BOILING STUDIES

R. V. Bailey[9] M. Richardson
H. A. MacColl P. C. Zmola

7.5.1 Vapor Transport

A method for calculating the density distribution in a boiling system, which takes into consideration explicitly the relative velocity of the vapor and liquid, has been developed.

To summarize briefly the results presented in the last quarterly report,[10] an expression for the local vapor velocity, U_g, based on the entire cross-sectional areas of flow, is

$$(1) \qquad U_g = (U_s + U_0)\frac{f}{1-f},$$

where f is the local vapor volume fraction, U_0 is the liquid velocity based on the total cross-sectional area, and U_s is a factor which accounts for the relative velocity of the vapor to the liquid and is only a slowly varying function of geometry and fluid physical properties. For the particular case in which energy is added uniformly to the boiling mixture flowing upward through a vertical channel, the density distribution is defined by

$$(2) \qquad \frac{z}{Z_0} = \left[\frac{Z}{Z_0}\frac{h_{fg}}{v_g}\frac{A}{P}(U_s + U_0)\right]\frac{f}{1-f},$$

where z is the height measured from the point of initiation of boiling, Z is the total height over which boiling occurs, Z_0 is the total test section height, P is the total power from which vaporization results, A is the cross-sectional area of flow, v_g is the specific volume of the vapor, and h_{fg} is the latent heat.

By utilizing Eq. 1 (for uniform density systems) or Eq. 2 (for circulating systems which approach the condition of uniform heat addition) the slip

[9] Tulane University.

[10] R. N. Lyon *et al.*, *HRP Quar. Prog. Rep. Jan. 31, 1955*, ORNL-1853, p 141, esp. p 152.

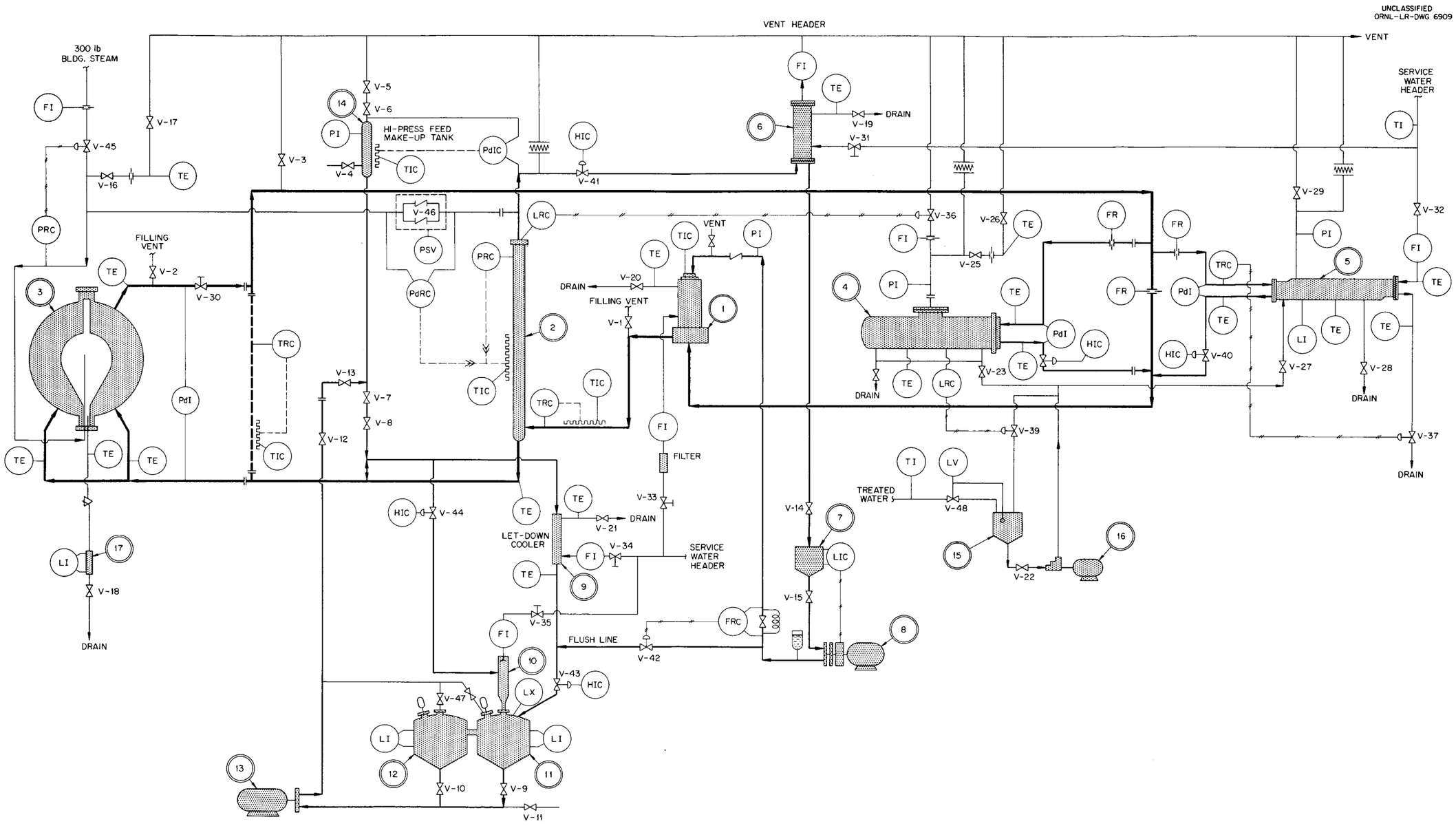

Fig. 7.21. Flowsheet of Slurry Blanket Mockup.

factor, U_s, has been calculated from various experimental data. The results are shown plotted against the specific volume of the vapor in Fig. 7.22. The Behringer data[11] were obtained from a static system (no net circulation of the boiling mixture) for which $U_0 = 0$ in Eq. 1. Both ANL and ORNL data were obtained from natural circulation apparatus. The runs at ANL were made with subcooled liquid entering the test section. The open triangles indicate the average value of U_s for five runs in which subcooling was small. The agreement of results from the various systems is rather remarkable when consideration is taken of the difference in experimental equipment from which the data were obtained. Since the slip velocity must go to zero at the critical pressure, the line representing the data has been extrapolated and passes through this point. Tentatively this line is proposed for estimating slip velocities at all pressures.

Contract work to determine vapor transport properties in natural circulation equipment at high pressures was started by the Babcock & Wilcox Co. in March 1955. The pressure range covered by the work is to be 600 to 2400 psia, for which, as indicated in Fig. 7.22, no complete data are currently available. Test sections to be run include diameters of 4 and 8 in. and heights of 5 and 10 ft. First tests will be performed by bubbling steam through the water; it is expected

[11] P. Behringer, *VDI Forschungsheft* 365 (1934).

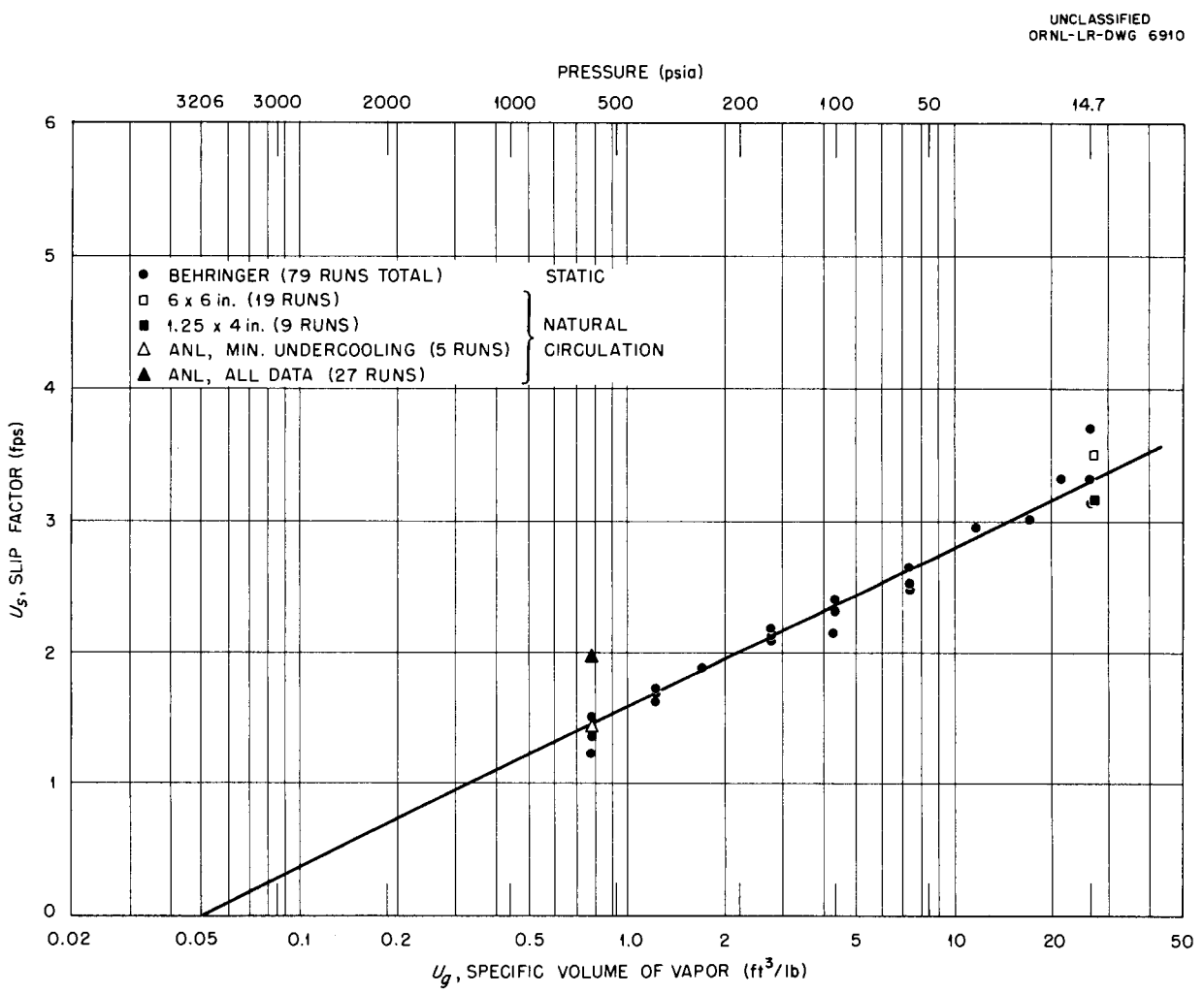

Fig. 7.22. Influence of Pressure on Slip Factor.

that the bubbling tests will substantially reduce the number of tests required of the more complicated volume-heated system.

While no extensive reactor calculations that employ the vapor transport model summarized in Eq. 1 and Fig. 7.22 have yet been made, some simple calculations have been performed that postulate natural vapor rise within a core in which heat is being uniformly generated. Representative results for operation at 2000 psia are shown in Table 7.6. The mean density of the fuel mixture depends only upon the power removal rate per unit free surface area; so the power density varies inversely with the core height in the case of natural-vapor-rise systems. There is no appreciable diameter dependence. For large units (> 10 ft in height) it appears that power densities for the same boiling-mixture density can be increased by better than a factor of 2 by employing natural circulation along with vapor separation equipment.

7.5.2 Vapor Separation

Work of determining characteristics of vapor separators suitable for boiling reactors is being done under contract by the Babcock & Wilcox Co. It is expected that this part of the program will be completed by the end of June 1955. To date, separation and flow characteristics of 11 different separators, including various modifications of each type, have been obtained. For most arrangements it has been found that the pressure drop across the separator is satisfactorily approximated by the equivalent of one velocity head of the fluid in the separator inlet.

TABLE 7.6. REPRESENTATIVE POWER DENSITIES FOR NATURAL-VAPOR-RISE BOILING SYSTEM OPERATING AT 2000 psia

Mean Density Decrease of Boiling Mixture	Power Removal per Unit Surface Area (kw/ft^2)	Power Density for Various Height Cores (kw/liter)		
		5 ft	10 ft	20 ft
0.24	1440	10.7	5.4	2.7
0.31	2160	16	8.0	4.0
0.39	3140	23	11.5	5.8

8. METALLURGY

E. C. Miller

R. G. Berggren
G. E. Elder
J. I. Federer
W. J. Fretague
W. O. Harms
W. J. Leonard
G. B. Wadsworth
J. C. Wilson

8.1 METALLURGY OF CORROSION

W. O. Harms J. I. Federer
G. B. Wadsworth

8.1.1 Stress-Corrosion Cracking of Austenitic Stainless Steels

An experimental program for studying the effects of composition, stress, and environment on the transgranular stress-corrosion cracking of austenitic stainless steels was described in a previous report.[1] The direct-loading type of apparatus, in which 0.050-in.-dia specimens are used, was modified in order to eliminate breakage of glassware at specimen failure and to facilitate removal of broken specimens. The modification consisted in replacing the spherical flask with a thicker, cylindrical one and in using a heater capable of vertical adjustment, for controlling the size of the plug of magnesium chloride at the base of the flask and for dissolving this plug during removal of the broken specimen.

Stress-strain relationships and chemical analyses were obtained for types 309 SCb, 304L, 310, 316L, 321, and 347 stainless steel. Based on an empirical formula developed by Eichelman and Hull,[2] these alloys represent a large range of martensite-forming susceptibilities, and results of the tests should indicate any relation between this tendency and the resistance to transgranular stress-corrosion cracking. The M_d temperatures for these steels were determined by adding 600°F to the M_s temperatures given by the Eichelman and Hull equation. (The M_d temperatures are defined as those above which martensite will not form from austenite as the result of plastic deformation. The M_s temperatures are defined as those above which austenite will not transform spontaneously into martensite.) The calculated M_d temperatures are as follows:

AISI Type of Stainless Steel	M_d (°F)
304L	369
347	181
321	141
316L	−17
309 SCb	< −452
310	< −452

If transgranular stress cracks propagate along martensite plates during local yielding under applied stress, it would be expected that the type 304L stainless steel would be the least resistant to this type of stress corrosion. It should be emphasized that the chemical compositions of some of the steels are somewhat different from those used in the derivation of the equation, and therefore the M_d temperatures are approximations, at best, and are to be regarded only as a relative measure of the martensite-forming tendencies of the steels being investigated.

After being swaged to size, the specimens were annealed at 1950°F with the ends supported in a horizontal tube furnace. Since distortion due to sagging during the heat treatment complicated the stress distribution on the specimens when they were ultimately loaded in the stress-cracking test apparatus, the technique of packing several specimens in small-bore quartz tubing was subsequently adopted to prevent this distortion.

Preliminary tests showed that stock type 347 stainless steel wire, which had been annealed, failed in from 10 to 16 hr at stresses slightly greater than the handbook yield stress for this material. In the as-received (apparently not fully annealed) condition, this wire broke consistently after only 1 to 2 hr of exposure at the same stress level. The results of testing the six austenitic stainless steels in boiling 42 wt % magnesium chloride solution at somewhat lower stress levels are given in Table 8.1, where it is observed that there was a rather wide range of end points for the type 304L stainless steel and that the type 316L

[1] W. O. Harms *et al.*, *HRP Quar. Prog. Rep. Jan. 31, 1955*, ORNL-1853, p 155–158.

[2] G. H. Eichelman, Jr. and F. C. Hull, *Trans. Am. Soc. Metals* 45, 77 (1953).

TABLE 8.1. RESULTS OF STRESS-CORROSION CRACKING TESTS OF ANNEALED STAINLESS STEEL SPECIMENS IN BOILING 42 wt % MAGNESIUM CHLORIDE

Specimen No.	AISI Type of Stainless Steel	Stress (psi)	Time to Failure (hr)
1	304L	20,000	4
2	304L	20,000	4
3	304L	19,000	22.5
4	304L	19,000	20.5
5	304L	20,000	3.5
6	304L	20,000	9.5
7	309 SCb	21,000	Did not fail after 100 hr*
8	309 SCb	21,000	Did not fail after 40 hr*
9	310	21,500	Did not fail after 150 hr
10	310	20,500	Did not fail after 160 hr
11	316L	20,000	9.5
12	316L	20,000	10
13	316L	28,000	14.5
14	316L	28,000	14.5
15	316L	28,000	13.5
16	316L	28,000	22
17	321	21,000	20.5
18	321	20,500	16
19	347	20,000	15.5
20	347	20,000	23.5

*Run terminated because of equipment breakdown.

stainless steel lasted longer at 28,000 psi than at 20,000 psi. The reasons for these discrepancies may be associated with the annealing method discussed above. All the specimens except Nos. 15, 16, 19, and 20 were annealed in this manner; these four were annealed after insertion into the small-bore quartz tubes.

As predicted by the theory, types 309 SCb and 310 were much less susceptible to stress-corrosion cracking than the other steels tested. Examination of specimens after failure revealed in all cases many transgranular-type circumferential cracks and only slight general corrosion.

8.1.2 Dynamic-Corrosion Study Factors Associated with Grain Size and Sigma Phase in Wrought Austenitic Stainless Steels

The effect of grain size on the corrosion of types 304L and 347 stainless steels in uranyl sulfate solutions is being studied by testing specimens having a range of ASTM grain sizes from 2 to 8. During this quarter, data were obtained to establish the time required to grow various grain sizes in these steels. The annealing temperature of 1950°F was used, since it was found to be difficult to grow large grains in the type 347 steel at lower temperatures. Lower temperatures may have to be used for type 304L, however, since grains of ASTM size

4 to 5 were found after less than 5 min exposure to 1950°F.

Type 304L was prepared in ASTM grain sizes 2–3, 3, 3–4, 5, and 6–7, the smallest size being the result of only a 2-min exposure. Grain sizes of 3–4, 4, 4–5, 5–6, 6, 7–8, and 8 were produced in type 347; the largest size was obtained after 308 hr at temperature. Efforts to overcome the inherent fine-grain tendencies of type 347 stainless steel are now under way. These include attempts to grow grains at temperatures up to 2500°F, which should put columbium carbides into solution so that they will not obstruct the growth of grains.

Dynamic-corrosion pins were machined from iron-chromium and iron-chromium-nickel alloys having compositions corresponding to the composition of the brittle sigma phase; the alloys were prepared from high-purity materials by arc melting under a purified argon atmosphere. The metastable ferritic structures in both alloys were transformed by heat treating at temperatures just below those at which the sigma phase is thermodynamically stable according to the equilibrium phase diagrams for these systems. The transformations were studied by means of metallography, changes in magnetism (sigma phase is nonmagnetic), and hardness. The chemical compositions of the alloys and the results of heat treatments are listed in Table 8.2. The iron-chromium alloy is being heat-treated at 650°C, since the persistence of ferrite suggests that at 700°C some ferrite is still stable in this alloy. Indications are that this may require an additional 50 or 100 hr at temperature.

8.1.3 Effect of Hydrogen on Properties of Zirconium and Its Alloys

A sketch of the apparatus, described in the previous report,[3] for admitting known quantities of gases to metal specimens at a given temperature, is shown in Fig. 8.1. Furnace No. 1, controlled at 700°C, contains titanium turnings and zirconium powder as a "getter" for nitrogen and oxygen, which are the principal impurities in hydrogen. Furnace No. 2 contains titanium turnings which absorb hydrogen at 400°C and give off high-purity hydrogen on heating to 700°C. Furnace No. 3, whose temperature is accurately controlled, serves as the heating jacket for the specimen reaction tube.

8.1.4 Role of Oxide Films on Rate of Hydrogen Absorption by Zirconium and Its Alloys

A description of experiments, designed to evaluate the behavior of zirconium and its alloys under simulated exposure to radiolytic gas, was given in the previous report.[3] During the past quarter, several multiple-break subsize impact specimens of Zircaloy-2 were cathodically treated at 30°C, and an electrolysis run at 250°C was initiated. Results of these experiments are described below.

The electrolyte used in the cathodic treatments was 1 *N* sulfuric acid, and its concentration was checked periodically by titration with standard sodium hydroxide solution. The specimens were

[3] W. O. Harms *et al.*, *HRP Quar. Prog. Rep. Jan. 31, 1955*, ORNL-1853, p 155–158.

TABLE 8.2. COMPOSITIONS OF SIGMA-PHASE ALLOYS AND EFFECT OF TIME ON TRANSFORMATION FROM FERRITE TO SIGMA

Alloy	Composition (wt %)			Heat-Treating Temperature (°C)	Time at Temperature (hr)	DPH* Value	Ferrite (%)
	Fe	Cr	Ni				
Fe-Cr	55.7	43.7		700	1	222	30
					8	222	30
					16	455	8.5 – 10.5
					32		8.5 – 10.5
Fe-Cr-Ni	50.6	43.7	4.94	800	1	690	
					8	698	
					15	894	0

*Diamond pyramid hardness.

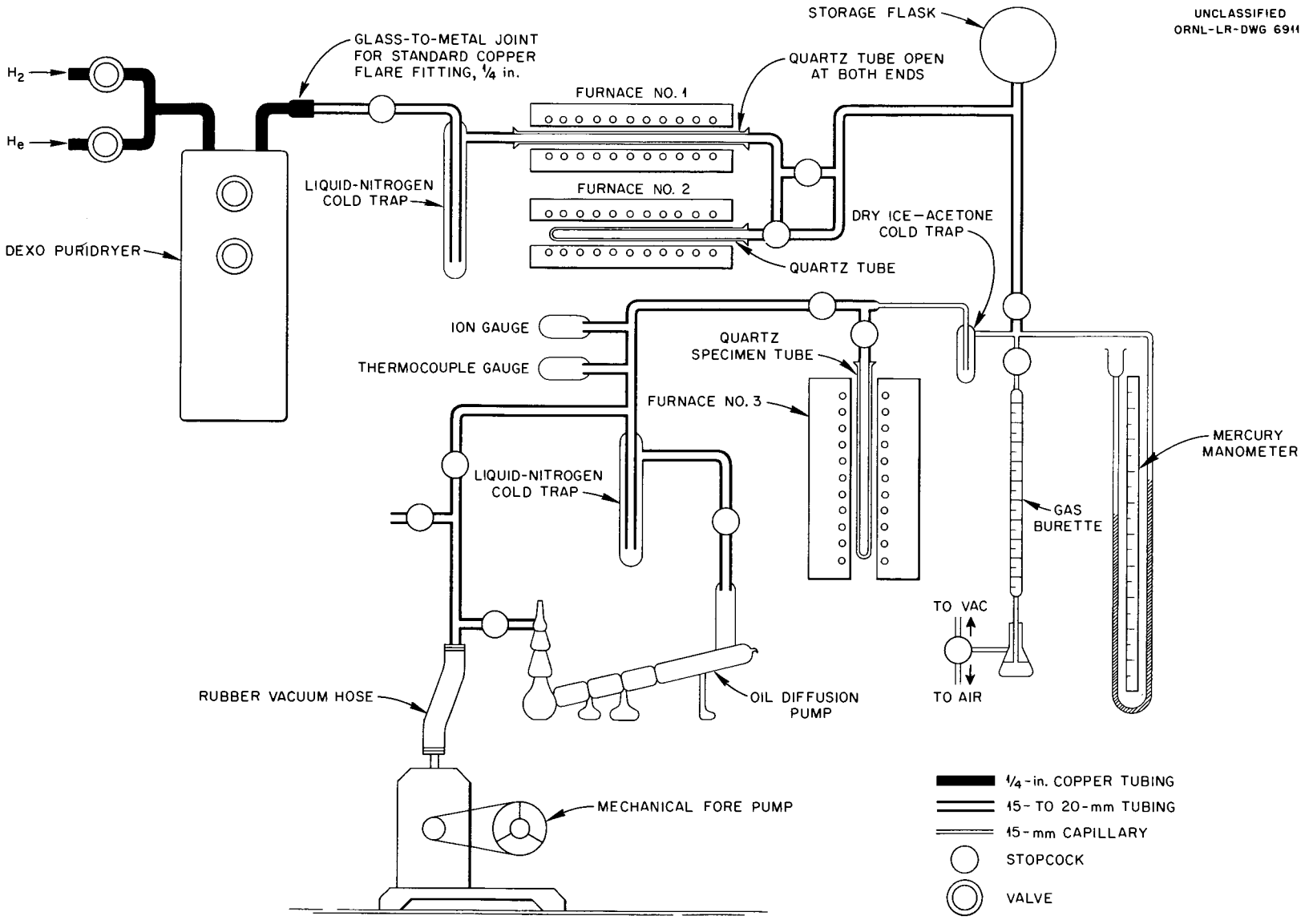

Fig. 8.1. Gas Absorption Apparatus.

swaged, machined, cleaned (by abrasion with No. 360 grit alumina powder followed by chemical polishing in 46-46-8 water–nitric acid–hydrofluoric acid solution), and, finally, vacuum annealed at 750°C.

The first run was performed with a gold anode at a current density of 10^{-8} amp/cm^2 at 30°C in pyrex glassware. After 120 hr of operation the specimen was covered with a dark-gray film which, by x-ray diffraction, was found to contain gold and a trace of zirconium nitride. Gold, but not zirconium, was found by spectrographic analysis of this film.

A second specimen, run at 10^{-6} amp/cm^2 at 30°C for 120 hr, was very heavily covered with what appeared to be the same kind of film that was observed earlier. The presence of gold suggested that perhaps some ion such as chloride ion might be forming a complex with gold with ultimate deposition on the cathode. To test this possibility, the electrolyte for the next run was prepared with demineralized water containing less than 0.5 ppm of chloride, and, after filtering through a fritted glass filter, the acid was electrolyzed at a current of 1 amp with the use of two gold electrodes. The third electrolysis was performed at 30°C at a current density of 10 ma/cm^2, which was just enough to produce a vigorous bubbling around the cathode. After 100 hr the surface was covered with a thick, smooth, yellow-brown film, which was found to be almost pure gold by spectrographic and x-ray diffraction analyses. A subsequent run, in which a porous alumina cup was used between the anode and cathode, resulted in the deposition and impregnation of a similar film on the cup, while the cathade remained bright. It was then clear that a different anode material would be required; platinum was chosen and proved to be satisfactory for this purpose. The results of hydrogen analyses by vacuum fusion were not available at the time of this writing.

The modified autoclave shown in Fig. 8.2 was used for electrolysis at 250°C in 1 *N* sulfuric acid with a platinum anode. The reactor vessel is a zirconium-lined type 347 stainless steel autoclave. A coil of platinum wire in the vapor phase is provided to catalyze the recombination of the electrolytic gas. During the first 100-hr run at 250°C, this coil was independently heated to 300°C to prevent condensation and possible poisoning of the catalyst. Upon removal of the current, no increase in cell

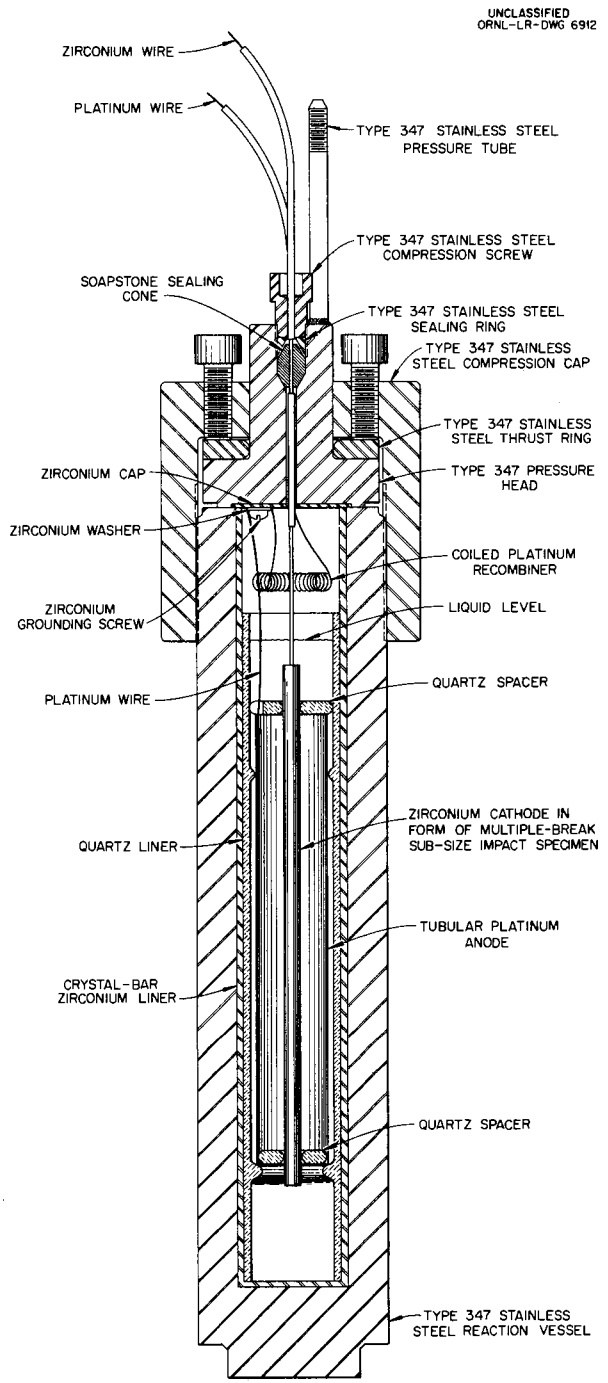

Fig. 8.2. Electrolytic Cell for Hydrogen Embrittlement Studies.

pressure was noted, indicating that the catalyst functioned satisfactorily in a 250°C environment without extra heating. The catalyst temperature may have remained above 250°C because of the heat liberated in recombination of the electrolytic gas.

A subsize Tinius Olsen impact tester was obtained and is being modified for transition-temperature studies by arranging for direct heating and cooling in the vise of the tester.

8.2 PHYSICAL METALLURGY OF TITANIUM AND ZIRCONIUM ALLOYS

W. J. Fretague

8.2.1 Commercial Titanium

Metallurgical investigations to determine the cause of embrittlement of commercial titanium, described in a previous report,[4] were continued during this quarter. Laue and Debye films obtained with specimens prepared from the exposed corrosion-specimen holder exhibited extraneous reflections which could not be attributed to any of the known compounds of titanium. No such reflections appeared in control samples. Metallographic examination indicated an as-yet-unidentified microconstituent. Examination under polarized light did not reveal the strong birefringence associated with the hydride phase. Vacuum-fusion analysis for hydrogen did not reveal any increase in hydrogen content in the exposed specimen.

Specimens of the unexposed stock (RC 70 REED item No. 11) were heated in an argon atmosphere at 250°C for periods of 500, 1000, and 2000 hr in order to determine whether the impact embrittlement, observed in the exposed specimen-holder material, was due to the temperature of exposure alone or whether the corrosive environment might be a factor. Figures 8.3, 8.4, and 8.5 illustrate typical microstructures from these specimens.

[4] W. J. Fretague, *Met. Semiann. Prog. Rep. Oct. 10, 1954*, ORNL-1875 (to be published).

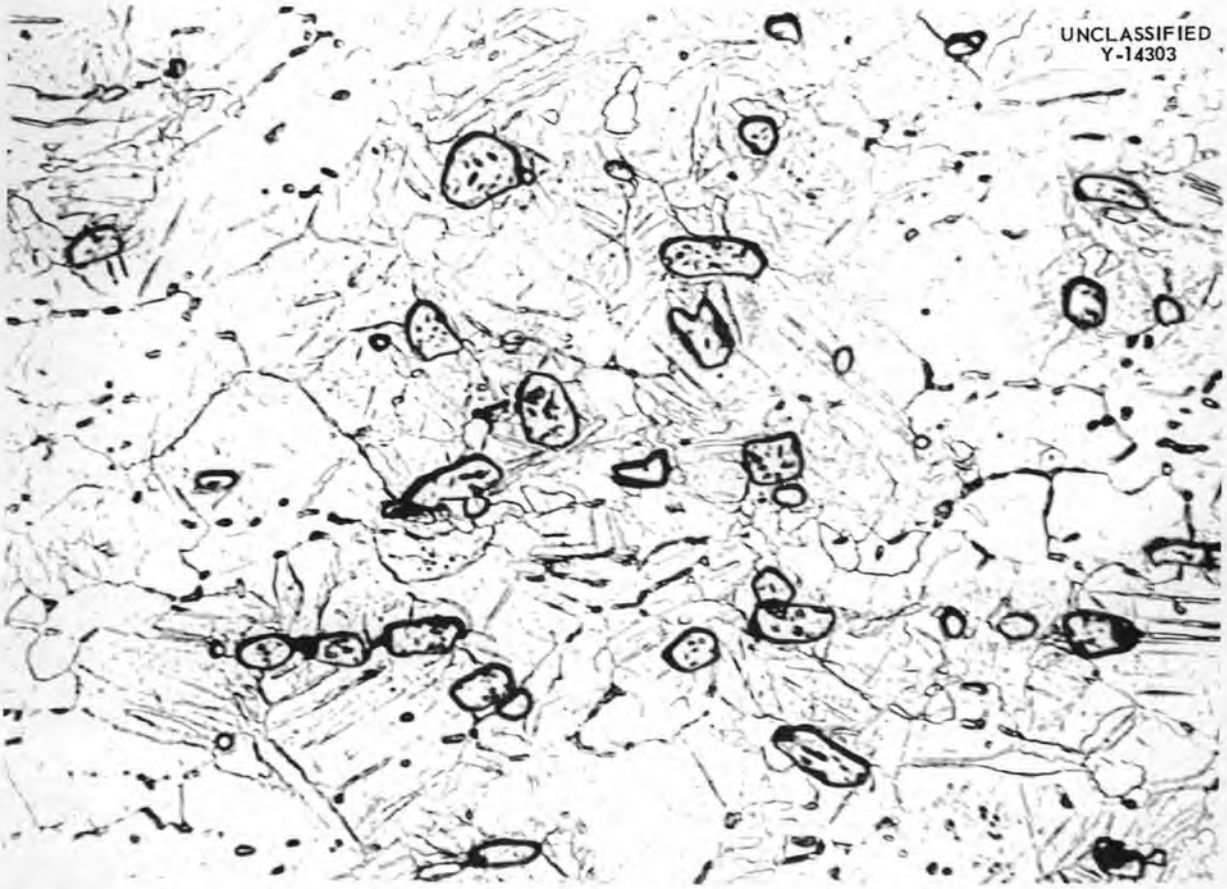

Fig. 8.3. Unalloyed Titanium Machined from Corrosion Specimen Holder Previously Exposed to HRP Loop Environments for Approximately 2000 hr. Etchant: 3 parts HF, 8 parts HNO_3, 8 parts H_2O. 500X.

Fig. 8.4. Unalloyed Titanium Bar Stock as Received. Etchant: 3 parts HF, 8 parts HNO_3, 8 parts H_2O. 500X.

The unidentified microconstituent was present in all the thermally treated specimens, as well as in the sample from the exposed specimen holders, but not in the unexposed as-received stock, indicating that exposure to temperature alone, in the absence of corrosive environment, can cause the appearance of the microconstituent.

8.2.2 Zirconium Alloys (Zircaloy-2)

Zircaloy-2 multiple-break impact specimens from the second in-pile loop (run FF) were tested over the temperature range from −196 to 300°C. Data are presented in graphical form in Fig. 8.6, together with the data obtained previously from samples irradiated in an HRP environment (loop run DD), samples exposed in the HRP in-pile mockup (loop run CC), and control samples tested in the vacuum-annealed condition.

It appears that the higher flux and longer exposure time for specimens in run FF, together with the higher acid content of the loop solution, have not caused a change in the transition temperature of the material (with the energy absorbed to break the specimens being used as a criterion). The values recorded in the high-temperature or ductile region of the curve, for specimens from loop run FF, are generally lower than those obtained on previous samples, but, since the specimens did not break completely, the data do not represent true impact-energy values. The transition temperature (brittle to ductile fracture) did not seem to be affected by the in-pile conditions to which the specimens were exposed.

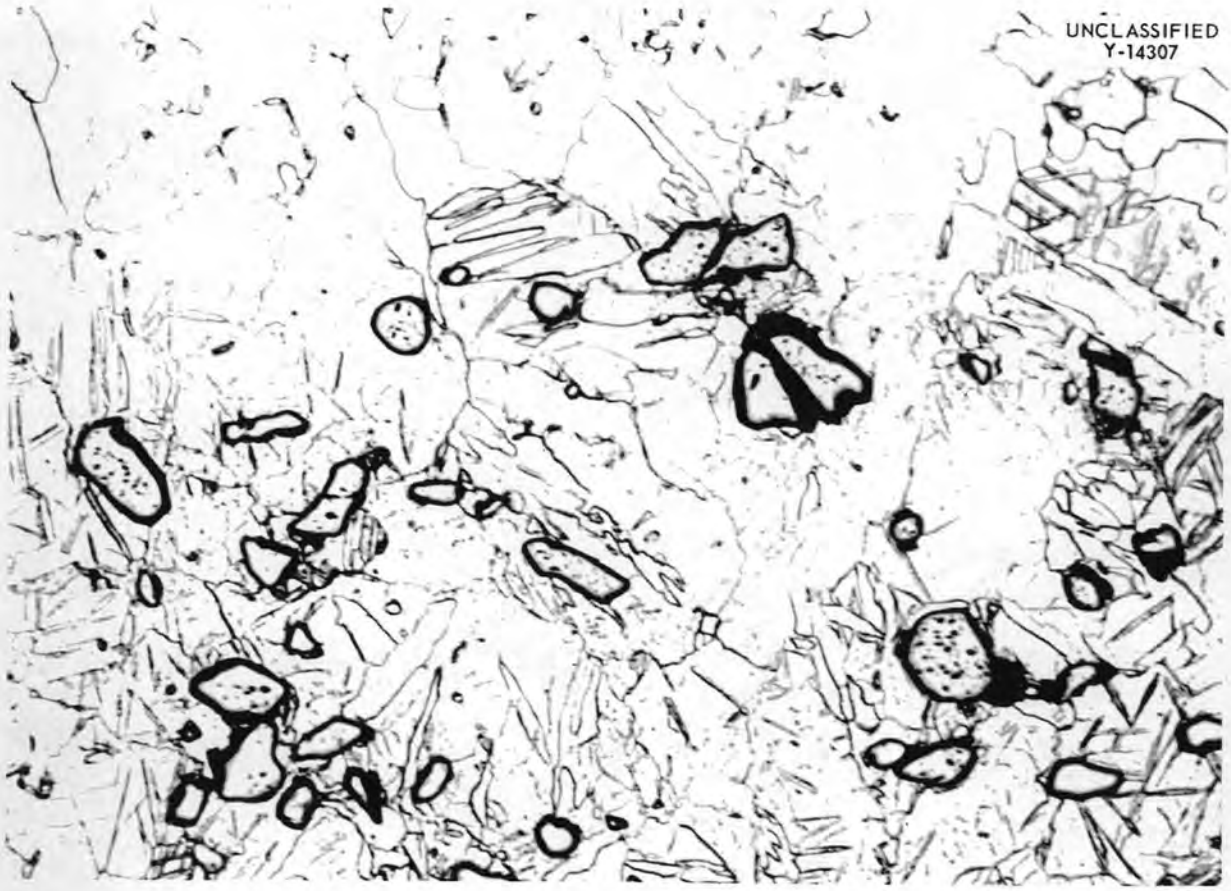

Fig. 8.5. Unalloyed Titanium (RC 70 REED Item No. 11) Heated in Purified Argon at 250°C for 2000 hr. Etchant: 3 parts HF, 8 parts HNO_3, 8 parts H_2O. 500X.

8.3 EFFECTS OF RADIATION ON STRUCTURAL METALS AND ALLOYS

R. G. Berggren J. C. Wilson

The irradiations listed previously[5] have now been completed. One additional irradiation has been completed in the HB-3 facility of the LITR; tensile and impact specimens of pressure-vessel carbon steels and USS T-1 steel were irradiated at both 60 and 300°C. Samples from the weld qualification test for the HRT pressure vessels are being prepared for irradiation, as are welded Zircaloy-2 plates duplicating HRT core-tank practice.

Tensile tests were made on austenitic stainless steels, irradiated in position L-49 of the MTR for 2443 Mwd, in contact with the reactor cooling water, at a temperature probably less than 50°C (Table 8.3). These tests confirmed the presence of a yielding phenomena in some irradiated metals and a strain-rate dependence of the yield stress in type 347 stainless steel. The presence of yield points in irradiated face-centered cubic metals was first noted by Blewitt[6] in high-purity copper, and later a similar effect was noted in 2S aluminum and type 347 stainless steel.[7]

During testing, an effort was made to study the features of the yield-point phenomenon previously reported and to ascertain the effect of testing speed on the yield point. Tests were run at two cross-head speeds that differed by a factor of 5 (0.01 and 0.05 in./min). At the lower testing speed, no

[5] R. G. Berggren and J. C. Wilson, *HRP Quar. Prog. Rep. Jan. 31, 1955*, ORNL-1853, p 162.

[6] T. H. Blewitt, ORNL, unpublished data.

[7] R. W. Hall and J. C. Wilson, *Solid State Quar. Prog. Rep. Aug. 30, 1954*, ORNL-1762, p 9.

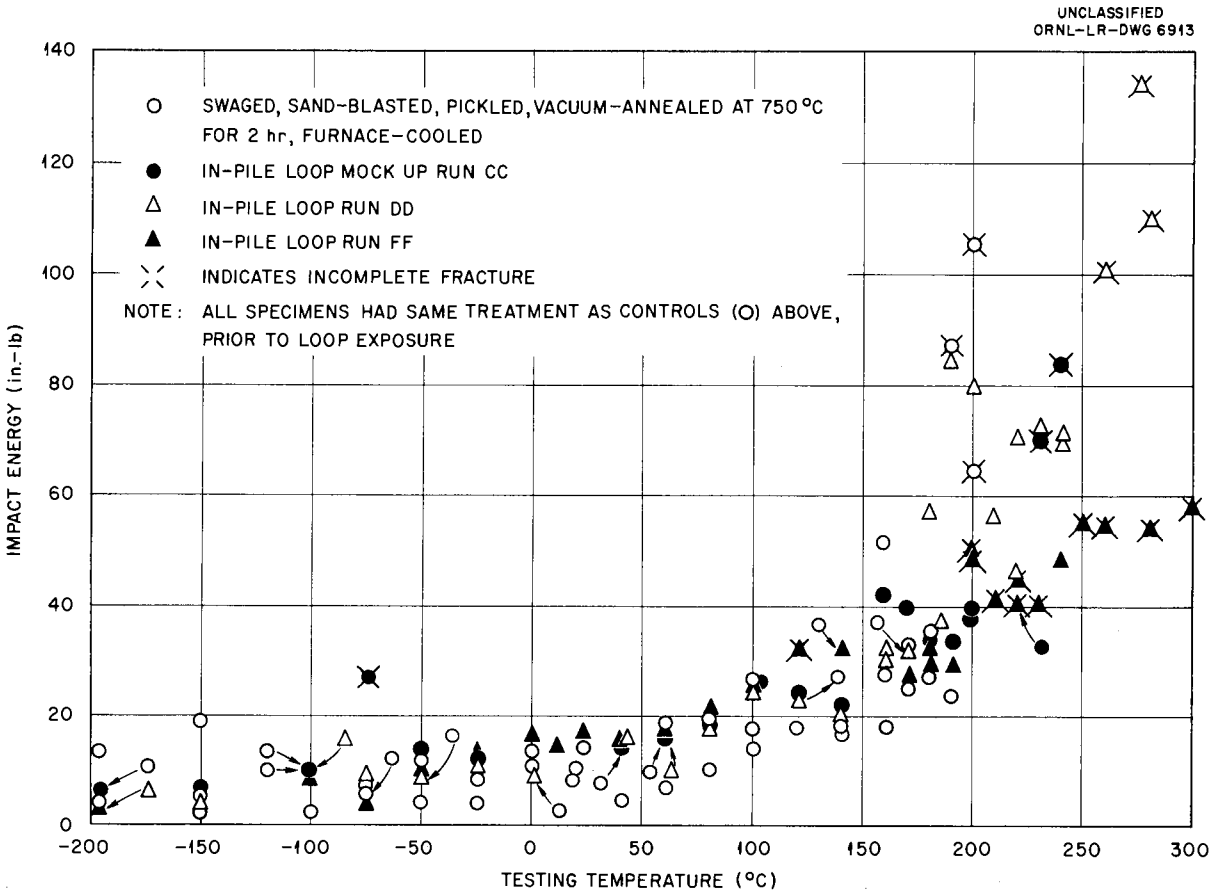

Fig. 8.6. Impact Energy vs Testing Temperature for Zircaloy-2.

drop in load occurred for the irradiated type 347 steel, although the stress-strain curve showed a point of inflection near the 0.2% offset stress. At the higher testing speed, a drop in load corresponding to a stress of 600 psi was observed. When the stresses at 0.2% offset are compared for these two tests, they differ by only 3%, but the shapes of the stress-strain curves bear out the belief that the difference is a true strain-rate effect.

Type 304 ELC stainless steel was tested only at 0.05 in./min but showed a drop in stress of about 800 psi at yielding. Type 301 stainless steel was tested at the same two speeds as the type 347 stainless steel; the sample pulled at the highest testing speed with the highest irradiation showed evidence of irregularities in the stress-strain curve, indicating that a yield point might be observed at still higher testing speeds.

Notch-bar impact tests with a subsize Izod bar[8] were begun on the same alloys as those in the tensile test. At liquid-nitrogen temperature (−196°C) the unirradiated test bars bent but did not fracture in the test. The irradiated specimens did not break cleanly, but, in all cases, greater than 50% fracture was observed. Recently, Felbeck and Orowan[9] concluded that the velocity effect (elevation of yield stress by higher strain rates) may be of greater importance in brittle fracture of carbon steels than triaxial stress conditions below the

[8]R. G. Berggren, N. E. Hinkle, and J. C. Wilson, *Solid State Quar. Prog. Rep. Aug. 31, 1953*, ORNL-1606, p 10.

[9]D. K. Felbeck and E. Orowan, *Experiments on Brittle Fracture of Steel Plates*, Mechanical Engineering Department Massachusetts Institute of Technology Technical Report No. 1, ONR Contract No. N5ori-07870.

TABLE 8.3. OFFSET AND ULTIMATE STRENGTH OF ANNEALED AUSTENITIC STAINLESS STEELS IRRADIATED AT LESS THAN 50°C IN MTR COOLING WATER

Stainless Steel Alloy	Stress at 0.2% Offset (psi)	Ultimate Tensile Stress (psi)	Cross-Head Speed (in./min)	Integrated Flux (Fast) (10^{19} nvt)
301	36,000	96,600	0.01	Unexposed
301	81,700	112,300	0.01	3.9
301	38,400	98,700	0.05	Unexposed
301	87,000	113,200	0.05	3.9
301	87,800	118,800	0.05	7.8
347	37,400	98,000	0.01	Unexposed
347	95,400	112,900	0.01	7.8
347	37,000	97,600	0.05	Unexposed
347	96,500	114,800	0.05	3.9
347	98,400	112,700	0.05	7.8
304 ELC	24,350	86,300	0.05	Unexposed
304 ELC	75,500	103,800	0.05	7.8

root of the notch. Further work may establish whether this hypothesis is applicable to irradiated face-centered cubic metals.

On the basis of the limited data above, it appears that the usefulness of the austenitic stainless steel is not greatly reduced by irradiation. The observed changes in behavior indicate, however, that further study of these steels is necessary.

Part V

CHEMICAL ENGINEERING DEVELOPMENT

F. R. Bruce

9. THERMAL BREEDER FUEL REPROCESSING

D. E. Ferguson E. O. Nurmi W. E. Unger

W. L. Carter R. W. Horton S. Peterson H. O. Weeren
J. L. Engel R. B. Lindauer J. T. Roberts M. E. Whatley
G. W. Gray F. C. McCullough A. M. Rom H. E. Williamson
C. E. Guthrie R. A. McNees W. E. Tomlin R. H. Winget
P. A. Haas

9.1 FISSION-PRODUCT CHEMISTRY

9.1.1 Neodymium Precipitation

R. W. Horton R. A. McNees
W. E. Tomlin

The results of further[1] experiments with simulated fuel solutions containing neodymium sulfate indicated that the precipitation behavior of this salt with respect to hot metal surfaces and, possibly, the solubility are influenced by the metals in the system. Experiments with saturated solutions in a rocking autoclave equipped with a stainless steel container and a stainless steel finger gave 0.1% deposition of neodymium sulfate when the finger was colder than the solution, and 8 to 10% deposition when the finger was about 25°C hotter than the solution (see Table 9.1). With a Zircaloy-2 finger and a stainless steel container, 3 to 8% deposition was observed when the finger was 25°C hotter than the solution. However, with a platinum container, the deposition of neodymium sulfate on a hot Zircaloy-2 finger

[1]For previous indications, see D. E. Ferguson *et al.*, *HRP Quar. Prog. Rep. Jan. 31, 1955*, ORNL-1853, p 183.

TABLE 9.1. DEPOSITION OF NEODYMIUM SULFATE ON METAL SURFACES IN AUTOCLAVE SYSTEM

Solution: 0.02 *m* UO_2SO_4–0.005 *m* H_2SO_4 containing traced $Nd_2(SO_4)_3$

Temperature of liquid: ~280°C

$Nd_2(SO_4)_3$ in Solution (mg per kg of H_2O)	Vessel[a] Metal	Finger[b] Metal	Temperature of Finger Relative to Solution (°C)	$Nd_2(SO_4)_3$ Deposited on Finger (%)
200	Stainless steel	Stainless steel	5–10 colder	0.1[c]
200	Stainless steel	Stainless steel	6 hotter	8.0
200	Stainless steel	Stainless steel	20–25 hotter	10.0
200	Stainless steel	Zircaloy-2	5–10 colder	0.1[c]
200	Stainless steel	Zircaloy-2	20–25 hotter	2.8
10	Platinum	Zircaloy-2	20–25 hotter	0.3[c]
1000[d]	Platinum	Zircaloy-2	20–25 hotter	0.4
1000[d]	Platinum	Zircaloy-2	20–25 hotter[e]	0.5
1000[d]	Stainless steel	Zircaloy-2	20–25 hotter	4.0
1000[d]	Stainless steel	Zircaloy-2	20–25 hotter	8.0

[a]Area of vessel in contact with liquid was 45 in.^{2}.

[b]Area of finger in contact with liquid was 7 in.^{2}.

[c]These values are based on counting rates not significantly different from background.

[d]The last four results were obtained with purified tracer (see Sec. 9.1.3).

[e]A few small crystals of rare-earth sulfates were observed on the finger. These dissolved instantly when contacted with water.

was only 0.4 to 0.5% (see Table 9.1), indicating that the presence of stainless steel corrosion products, which collect on the hot Zircaloy-2 surface, promotes the deposition of the rare-earth sulfate. This is particularly significant, since, under reactor conditions, Zircaloy-2 may possibly remain free of stainless steel corrosion products.

No deposition of rare-earth sulfate was observed on a hot metal surface in contact with a solution containing neodymium sulfate at a concentration below the solubility limit.

In circulating-loop tests, 82% of the neodymium sulfate injected into the loop deposited on and adhered to the hot (above 310°C) metal surface of the pressurizer-preheater section. This represents essentially all the neodymium sulfate precipitated in the loop (see Table 9.2).

In the autoclave tests, 500 ml of a simulated fuel solution (0.02 *m* uranyl sulfate, 0.005 *m* sulfuric acid) was heated to about 280°C in a 1-liter pressure vessel equipped with a metal finger that could be made hotter or colder than the liquid. After the system had reached temperature equilibrium, similar solution containing traced neodymium sulfate was added. After 30 min at temperature, the liquid was transferred, still at the elevated temperature, to another vessel and allowed to cool. The distribution of activity was determined, and the percentage of initial activity that appeared on the finger, whether hot or cold, was noted.

The circulating-loop tests were carried out in test loop A after the 1000-psi pump had been replaced with a 2000-psi pump, which permitted operation at pressures up to 2000 psi and temperatures up to 315°C. Into the system, containing 2 liters of 0.05 *m* uranyl sulfate–0.005 *m* sulfuric acid, an additional 6850 ml of solution containing 2568 mg of traced neodymium sulfate was pumped at a rate of 50 ml/hr over a period of 138 hr. Samples were taken hourly in sufficient volume to maintain a constant volume in the loop. The scale on the metal surfaces was dissolved in 0.8 *M* nitric acid and analyzed for neodymium. The results of radiation surveys made during the experiment verified the accumulation of Nd^{147} tracer in the upper half of the preheater portion of the loop. The temperatures of the metal surfaces in the loop could not be measured directly, but calculations indicated the wall temperature to be at least 12°C higher than the solution temperature.

9.1.2 Neodymium Solubility

R. W. Horton R. A. McNees

The solubility of neodymium sulfate in uranyl sulfate–sulfuric acid, in an all-platinum autoclave system, was 65 to 85 mg per kg of H_2O at 285°C and 40 to 50 mg per kg of H_2O at 310°C. This is somewhat higher than the value reported previously,[2] 20 to 30 mg per kg of H_2O at 285°C, which was determined in an all-stainless-steel system. However, the tracer used in the previous work contained Ir^{192} as an impurity (see Sec. 9.1.3),

[2] *Ibid.*, p 179.

TABLE 9.2. DEPOSITION OF NEODYMIUM SULFATE ON METAL SURFACES IN CIRCULATING LOOP SYSTEM

Solution: 0.05 *m* UO_2SO_4–0.005 *m* H_2SO_4; 375 mg of $Nd_2(SO_4)_3$ per kg of H_2O; total of 2568 mg of $Nd_2(SO_4)_3$

Material of loop: Type 347 stainless steel

Section of Loop	Diameter (in.)	Liquid Flow (fps)	Temperature of Solution* (°C)	$Nd_2(SO_4)_3$ Deposited (mg)
Preheater	1/8	1.8	310	2091**
Main	1/2	6.8	295	29

*Heat input to preheater section = 1.14 kw, which is equivalent to a flux of 10.4 kw/ft^2 for the 0.11-ft^2 area. Heat input to main portion of loop = 1.1 kw, which is equivalent to a flux of 1.6 kw/ft^2 for the 0.71-ft^2 area.

**Bulk found on upper half, 0.05-ft^2 area.

and a direct comparison of these results is not possible. In an all-stainless-steel circulating-loop test, the solubility was 20 to 30 mg per kg of H_2O, which, for the TBR, is equivalent to a neutron poisoning effect of 0.2 to 0.3% from neodymium in solution. This value was obtained with pure Nd^{147} tracer.

The solubility of $Nd_2(SO_4)_3$ in 0.02 *m* UO_2SO_4–0.003 *m* H_2SO_4 was determined in a platinum-lined autoclave fitted with a filter, so that solids remained in the vessel when the liquid was drained for analysis. Solubility values were also obtained in small bombs that contained 3.5 to 5.0 ml of solution and that were fitted with platinum filter disks for separating the precipitated solids from the solution. Precipitation and re-solution of neodymium sulfate in simulated fuel solution were visually observed in 6-mm-ID quartz tubes as a function of concentration and temperature; solubilities somewhat higher than those obtained by filtration methods were found (see Fig. 9.1). The solubility in 0.05 *m* UO_2SO_4–0.005 *m* H_2SO_4 in the circulating loop was determined by analysis of the flowing-stream samples taken from test loop A during the precipitation studies described in Sec. 9.1.1.

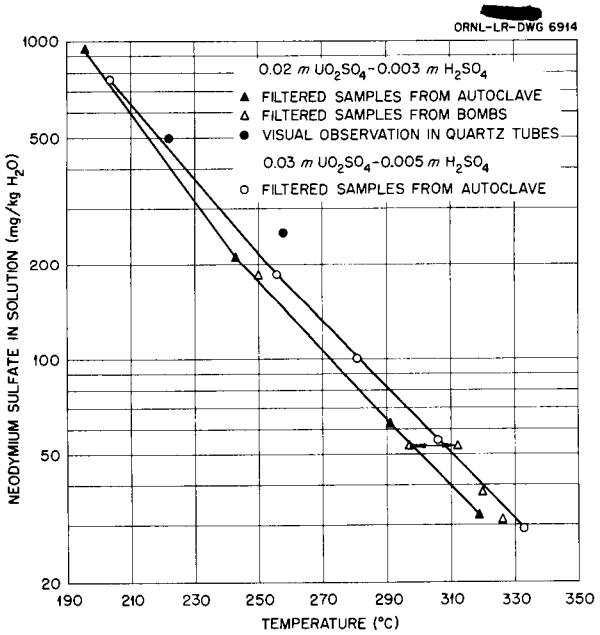

Fig. 9.1. Solubility of Neodymium Sulfate in Uranyl Sulfate–Sulfuric Acid Solutions Under Static Conditions.

9.1.3 Purification of Neodymium Tracer

R. A. McNees J. T. Roberts

As a result of decay studies, radiochemical analyses, and gamma-energy-spectrum determinations, the presence of radioactive Ir^{192} in the neodymium tracer was indicated. The material was therefore purified as follows: Lindsay Chemical Co. neodymium oxide (99%) was dissolved in dilute sulfuric acid, and the trace of thorium present was removed by coprecipitation with ferric hydroxide at a pH of 5. Neodymium was recovered from solution by precipitation as the oxalate and by ignition to the oxide at 800°C. Approximately 1 g of this oxide was sealed in a quartz ampoule and irradiated in the high-flux region of the LITR for two weeks. After ten days of cooling, the oxide was dissolved in dilute sulfuric acid, and the cations were sorbed onto a 100-ml column of Dowex 50 resin in the ammonium form. The column was eluted with 0.17 *m* citric acid–0.07 *m* diammonium citrate.

A small amount of radioactive material was eluted from the column ahead of the neodymium and at the place expected for elements 68 to 70. Gamma energy data and decay studies indicate that this was a mixture of heavy rare earths. The major part of the radioactive material, the second cut, was shown by radiochemical analysis and by gamma energy spectrum and decay studies to be pure Nd^{147}. The third cut adhered tightly to the top few centimeters of the column after the ammonium citrate elution and was only partially removed with 12 *m* hydrochloric acid. All evidence so far obtained indicates that the tightly sorbed activity was Ir^{192}. Experiments are now being performed to determine the source of the iridium and whether or not it can be completely removed from the neodymium before irradiation.

9.1.4 Iodine Removal

R. A. McNees J. T. Roberts
S. Peterson

The results of a completed in-pile experiment show that under reactor conditions iodine can be removed from fuel solution by placing metallic silver in the vapor phase. When a silvered Alundum pellet was present in the vapor phase, 90% of the iodine found after the irradiation was in the pellet. The remaining 10% was found in the solution and in washings taken from the bomb. When

only plain Alundum pellets were present in the gas phase, 90% of the iodine found was in the fuel solution.

In these experiments, 25 mg of enriched uranium (93.14% U^{235}, as $UO_3 \cdot H_2O$) was dissolved in 2.5 ml of 25 mole % excess sulfuric acid. This solution, 0.04 *m* in uranyl sulfate and 0.01 *m* in sulfuric acid, was made 0.04 *m* in copper sulfate and was placed in an irradiation bomb that had a perforated container attached to the top closure. In this container were placed either five plain pellets or one silver-impregnated Alundum pellet and four plain pellets. The silvered pellet contained 1.4 mg of silver.

The bomb containing the uranyl sulfate solution and the pellets was placed in hole 11 in the ORNL Graphite Reactor, and the controls were set so that the temperature of the gas phase was 10 to 15°C above the temperature of the liquid. The gas phase temperature was 275 to 285°C. After one week of irradiation, the reactor was shut down. The bomb was held at operating temperature for 6 hr and then was cooled and removed. After a two-week cooling period, the bomb was opened, and the liquid and the pellets were removed for analysis. The distribution of I^{131} activity 18 days after irradiation stopped is shown in Table 9.3.

Although the cause is not necessarily apparent, corrosion was much more pronounced in the experiment where no silver was used. Also, no silver could be found in the fuel from the experiment with the silvered pellet. Examination of the gamma spectrum of the silvered pellet after extraction with 1 *M* KI showed only silver and iodine activity present to any marked extent, but a very small amount of some unidentified activity was also present.

9.2 HYDROCLONE DEVELOPMENT

J. R. Engel P. A. Haas
M. E. Whatley

The necessity for metering or handling a hydroclone underflow stream was eliminated by making the hydroclone underflow port to open directly into the underflow pot. This arrangement, called the "induced underflow pot system," allows the flow pattern within the hydroclone to generate a continuous concentric countercurrent flow between the hydroclone and the pot. When the system is connected to a reactor loop, the solids distribute themselves between the pot and the loop. A steady-state ratio of the concentration of solids in the pot to the concentration in the core loop of the order of 100 would be adequate for TBR core-solution processing. In tests with a dilute suspension of ThO_2 in water (a system considered similar to the core system with respect to solids separation), steady-state concentration ratios of about 35 were obtained with 1-μ particles, and ratios of over 2000 were obtained with 4-μ particles.

The performance of a hydroclone operating in this fashion is described by the rate of flow into the pot and by two efficiencies, one expressing the probability that particles entering with the feed stream are carried to the pot, and one giving the probability that particles entering the underflow port from the pot are returned to the pot. For a simple system including a feed tank, a hydroclone, an induced underflow pot, and necessary pumps, the steady-state distribution of particles between the tank and the pot (assuming complete mixing in the pot and the tank) is given by the expression

$$\frac{C_p}{C_k} = \frac{E_1}{R}(1 - E_2) ,$$

where

C_p is the pot solids concentration,
C_k is the tank solids concentration,
E_1 is the feed-to-pot efficiency,
E_2 is the pot-to-pot efficiency,
R is the underflow ratio, or the fraction of the feed rate circulating through the pot.

9.2.1 Hydroclone Underflow Ratio

With the induced underflow pot system, underflow ratios from 0.01 to 0.04 can be obtained by varying the diameter of the underflow port and the length of the cone (see Table 9.4). Designs with higher underflow ratios have so far had efficiencies too low to be practical. A confining connecting pipe or channel between the hydroclone and the pot decreased the underflow ratio and the efficiencies. The underflow ratio increased slightly with feed rate, but only at very low rates was this effect significant.

The underflow pot size or design does not affect the underflow ratio, provided that the pot is large compared with the hydroclone size. For 0.25-in.-dia hydroclones, this criterion is met with pots of

TABLE 9.3. DISTRIBUTION OF I^{131} FROM IN-PILE EXPERIMENTS

Substance Analyzed	I^{131} Activity (d/min) After 18 Days of Cooling	
	With Silvered Pellet	With Plain Pellet
Fuel and washings	4.8×10^6	2.6×10^7
Silvered pellet	$4.9 \times 10^{7*}$	No pellet
One plain pellet	4.0×10^6	2.5×10^6

*Corrected for 90% extraction of iodine from silvered pellets by 1 *M* KI solution.

TABLE 9.4. UNDERFLOW RATIOS OF INDUCED-UNDERFLOW POT SYSTEMS

Hydroclone dimensions:	
Nominal diameter	0.25 in.
Feed inlet area	0.063 × 0.033 in.
Vortex finder, ID	0.053 in.
Line connecting hydroclone to pot, ID	0.25 in.
Operating conditions:	
Feed pressure	35 psi
Feed flow rate	0.20 gpm

Underflow Port Diameter (in.)	Cone Length (in.)	Cone-to-Pot Connection Length (in.)	Underflow Ratio
0.075	1.5	0	0.015
0.100	1.5	0	0.028
0.100	1.3	0	0.042
0.100	1.3	0.71	0.019
0.100	1.3	2.71	0.008

only 20 ml in volume. Studies on this system were made with pots of 60- and 70-ml volumes, machined from Lucite and agitated by a magnetic stirrer. The underflow ratios were determined by putting a soluble salt in the underflow pot, feeding demineralized water, and following the rate at which the salt was carried into the overflow stream.

A plot, on semilog paper, of the salt concentration of the overflow samples against Ft/V_p gave a straight line (see Fig. 9.2), which complies with the theoretical relation

$$\frac{RFt}{V_p} = -\ln\left(\frac{C}{C_0}\right), \tag{1}$$

where

F is the feed rate,

t is the time,

V_p is the pot volume,

C is the salt concentration,

C_0 is the initial salt concentration.

The underflow ratio is given by the slope of the line (see Fig. 9.3). The ratios reported in Table 9.4 were determined by this method.

9.2.2 Hydroclone Performance in an Induced-Underflow Pot System

Tests of the performance of the induced-underflow pot system with the described hydroclone were conducted with water suspensions of ThO_2 of various sizes to determine the feed-to-pot efficiency, the pot-to-pot efficiency, and the steady-state pot-to-feed-tank concentration ratio. The feed-to-pot efficiency at 35 psi feed pressure varied from 26% for about 1-μ particles to 90% for

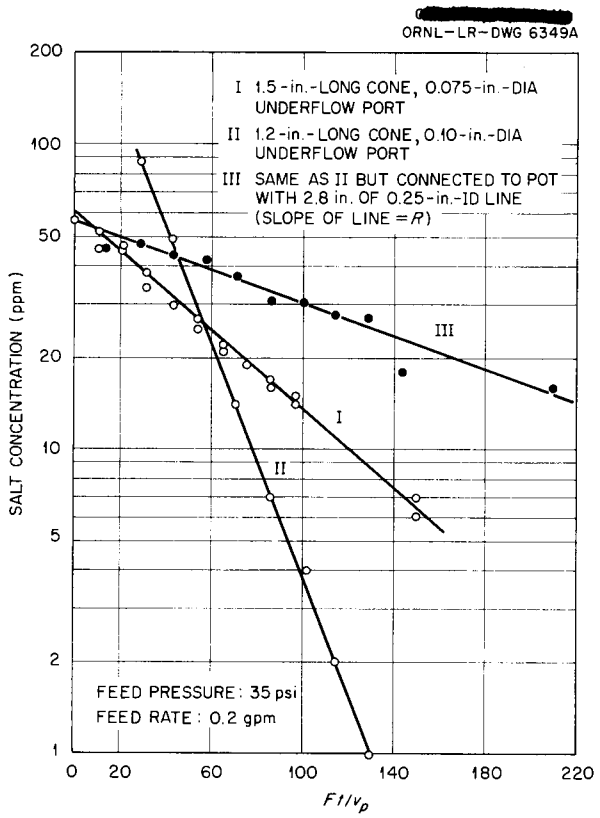

Fig. 9.2. Typical Results of Hydroclone Underflow Ratio Determinations by the Salt Dilution Technique.

about 4-μ particles (see Table 9.5). The pot-to-pot efficiencies were fairly close to the feed-to-pot efficiencies. Experimentally determined steady-state concentration ratios ranged from 35 for the finest feed material to 2400 for the coarse material. (The particle-size distribution of the ThO_2 used is given in Table 9.6.) These ratios were higher by almost a factor of 2 than the values

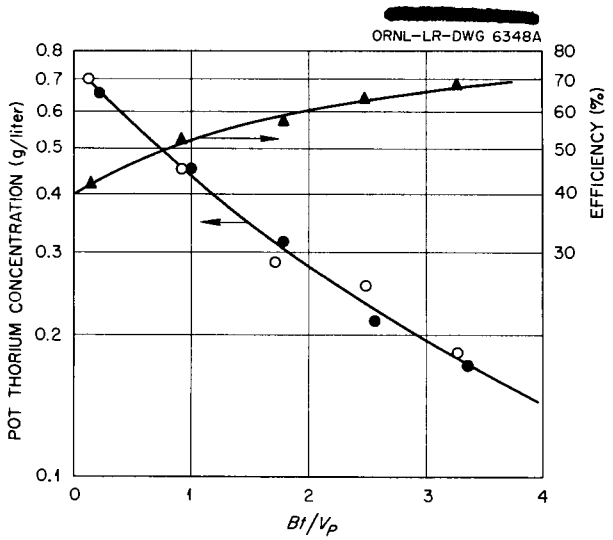

Fig. 9.3. Determination of Pot-to-Pot Efficiency for Described Hydroclone Operating with Material.

TABLE 9.5. HYDROCLONE PERFORMANCE IN THE INDUCED-UNDERFLOW POT SYSTEM

Hydroclone dimensions:		Operating conditions:	
Nominal diameter	0.25 in.	Feed pressure	35 psi
Feed inlet area	0.063 × 0.033 in.	Feed flow rate	0.20 gpm
Vortex finder ID	0.053 in.	Underflow ratio	0.0145
Underflow port ID	0.075 in.		
Cone length	1.5 in.		

Solid Material*	E_1 (%)	E_2 (%)		C_p/C_k	
		By Dilution	Direct	Calculated**	Experimental
A	26	40	30	26 (lowest)	35.6
	29			34 (highest)	37.5
B	35		34	36 (lowest)	78
	50		37	55 (highest)	93
C	96	86	90	490 (lowest)	2300
	97	94	92	1132 (highest)	2420

*See Table 9.6 for size distribution.

**$C_p/C_k = (E_1/R)(1 - E_2)$.

TABLE 9.6. PARTICLE-SIZE ANALYSES OF ThO_2 USED IN HYDROCLONE RUNS

Feed Designation	Particle Size (μ)	Amount of Feed Less Than Particle Size (wt %)	Settling Rate (in./hr)
A	3.66	100	9.65
	1.96	99	2.75
	1.50	79	1.62
	1.15	57	0.95
	0.91	44	0.59
	0.70	25	0.35
	0.60	14	0.26
B	7.1	94	35.0
	4.2	82	12.7
	2.6	65	4.85
	2.0	55	2.86
	1.3	33	1.22
	1.0	21	0.73
	0.8	11	0.46
	0.6	4	0.26
C	16.1	100	175
	9.6	91	66.0
	7.1	86	36.0
	5.1	71	18.8
	4.1	50	12.1
	3.5	29	8.80
	3.0	16	6.50
	2.0	4	2.86
	1.0	1.7	0.73

calculated from the individual efficiencies and from Eq. 1.

The feed-to-pot efficiencies were determined by injecting a small charge of slurry into the feed stream of the hydroclone and collecting the overflow stream until the hydroclone was free of the initial charge. The flow was then stopped, and the total pot volume was taken for the sample, so that all the injected particles were recovered; the percentage reporting to the pot could thus be calculated.

The method devised to obtain pot-to-pot efficiencies was to inject a charge of slurry directly into the pot while the hydroclone was being fed with clear water and to periodically sample the overflow stream and the pot contents. From the pot-sample solids concentrations, the efficiencies were calculated by the equation

$$(2) \qquad (1 - E_2)\frac{RFt}{V_p} = -\ln\left(\frac{C}{C_0}\right).$$

Unfortunately, E_2 was not constant during the test but increased because of the selective elimination of fines. The data plot (see Fig. 9.3) was therefore curved, and the original particle-size distribution had to be obtained by determining the slope at several points and extrapolating to zero time.

The pot-to-pot efficiencies were calculated directly by the equation

$$(1 - E_2) = \frac{C_f}{RC_p},$$

where C_f is the overflow solids concentration. The major disadvantage of this method was that

the concentration in the overflow was generally too low for good analytical accuracy and involved an extrapolation to zero time.

The reported steady-state distributions of solids were determined in a small system (see Fig. 9.4) consisting of the hydroclone, a 73-ml magnetically agitated underflow pot, a 2-gal agitated feed tank, a turbine pump driven by a variable-speed drive, and less than 3 ft of connecting line, which was ¼-in.-dia stainless steel tubing. The system was charged with 5 liters of water and about 0.5 g of ThO_2 and was operated for 45 min before being sampled. Agitation of the pot was necessary in experimental work to get reproducible values for the parameters involved. If settling were allowed, the apparent value of E_2 would be increased, which increases the effectiveness of the hydroclone.

The advantages of the induced-underflow pot system over a system using a recycle from the pot to the feed of the hydroclone are as follows: (1) a controlled underflow stream is not necessary; (2) particles trapped in the underflow system are not subjected to attrition by being passed through a pump; (3) the smaller effective underflow ratio provides a greater concentration of solids (practical operating considerations limit a recycle stream to about 6% of the feed rate).

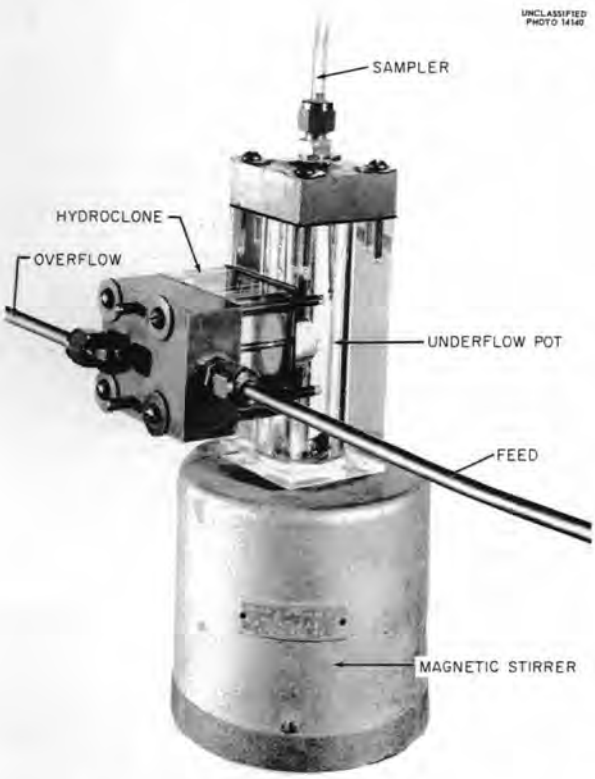

Fig. 9.4. Small Hydroclone System.

The disadvantages include two items: (1) the feed-to-pot efficiency is generally lower because of the lower underflow ratio, making the rate of solids removal per hydroclone lower; (2) for reliable operation it appears that a separate pot must be used with each hydroclone.

9.2.3 Hydroclone Corrosion

Two 0.4-in.-dia stainless steel models of the Dorr TM hydroclone were operated with 0.05 *m* uranyl sulfate–0.005 *m* sulfuric acid for 200 hr to evaluate their corrosion resistance. Results indicate that a more resistant material than stainless steel would be desirable. The corrosion was most severe in the lower part of the cone and on the inner surface of the vortex finder, being at least 0.2 in./year for one of the hydroclones, with no indication of the existence of a protective oxide film.

Because of plugging of the underflow lines, the surfaces of the hydroclones were exposed to a considerably higher concentration of solids than would be expected in normal reactor operation. The abrasive action of these solids removed the oxide film at an accelerated rate and was responsible for the rapid corrosion. The lower concentrations of solids which will exist in the reactor system might be expected to result in somewhat lower corrosion rates.

The experiments were carried out in one of the high-pressure corrosion test loops with enough pressure differential to give an initial flow rate of 1 gpm. An orifice plate was placed in the return line from one of the hydroclones to restrict its flow to 0.6 gpm. Orifice plates were also placed in the underflow lines of both hydroclones to give about 6% underflow. A bypass filter was used in an attempt to keep the loop scale from plugging the underflow orifices. The total pressure was 1000 psi and the temperature at the hydroclone inlet was 250°C.

When the hydroclones were removed from the loop, the orifices in both underflow lines were plugged. Solids had filled the lines, upstream from the orifices, and had built up to a depth of ¾ in. in the conical section of the hydroclone

operating at 0.6 gpm, and to $\frac{3}{8}$ in. in the 1-gpm hydroclone. The record of the underflow temperatures indicates that plugging occurred about 0.5 hr after startup. The orifice in the return line was not plugged at any time. The initial diameters of the plugged orifices were 0.038 and 0.033 in., and the diameter of the orifice in the return line was 0.060 in.

The hydroclones were cleaned out, and the feed pressure was measured as a function of flow rate. Comparison of these figures with similar data taken before the test shows that pressure requirements increased 20 to 40%. A similar effect was noted in the hydroclone which has been in operation with loop B. The data for one of the hydroclones are plotted in Fig. 9.5.

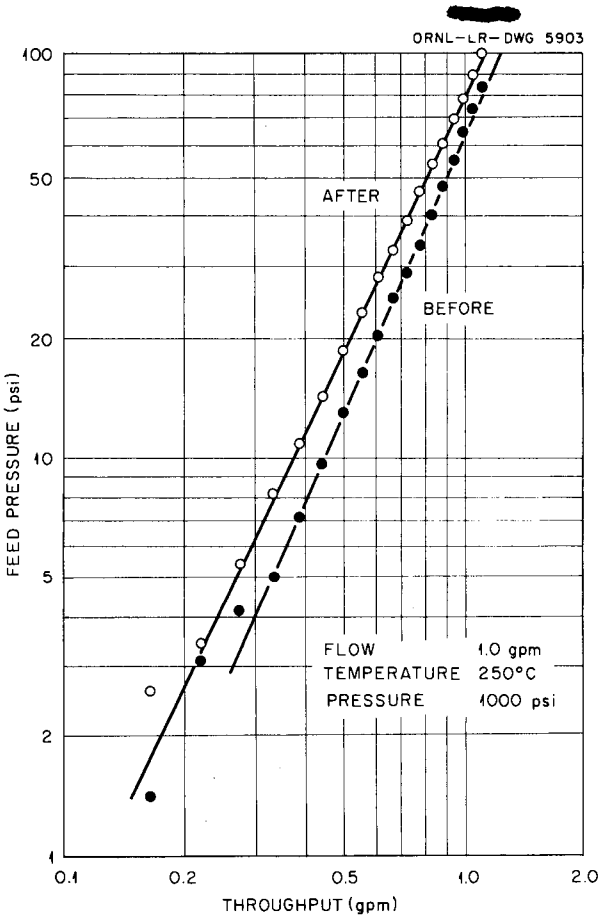

Fig. 9.5. Effect of 200-hr Operation of 0.4-in.-dia Hydroclone with 0.05 *m* Uranyl Sulfate–0.005 *m* Sulfuric Acid on Capacity.

The efficiency of the 1-gpm hydroclone decreased somewhat as a result of the corrosion. This was shown by comparison of the separation efficiencies of the corroded hydroclones with those of a new hydroclone of the same size (see Table 9.7). The tests were made with ThO_2 particles suspended in water, at a feed pressure of 35 psi with 6% underflow.

TABLE 9.7. SEPARATION EFFICIENCIES OF NEW AND CORRODED HYDROCLONES

Original hydroclone diameter: 0.4 in.

Hydroclone History	Feed Rate (gpm)	Gross Efficiency (%)
New	0.72	28
Operated 200 hr at 0.6 gpm	0.70	27
Operated 200 hr at 1 gpm	0.72	24

The 1-gpm hydroclone was sectioned along the vertical axis to show the areas of greatest wear (see Fig. 9.6). The protective oxide film was almost completely absent in the lower third of the cone and in the lower part of the vortex finder. The inside diameters were measured at the underflow port and vortex finder. These dimensions are known to have been within the tolerances (±0.005 in.) allowed in fabrication. From these figures (see Table 9.8) a minimum corrosion rate was determined. The actual corrosion rate could be as much as a factor of 2 greater than the reported values. A 0.4-in.-dia titanium-lined hydroclone with a flow rate of 1 gpm is being tested under the same conditions.

TABLE 9.8. CORROSION DATA FOR 0.4-in.-dia HYDROCLONE

Section	Vortex Finder	Underflow Port
Maximum diameter before test, in.	0.105	0.105
Diameter after test, in.	0.117	0.115
Minimum metal loss, in.	0.006	0.005
Minimum corrosion rate, in./year	0.26	0.22

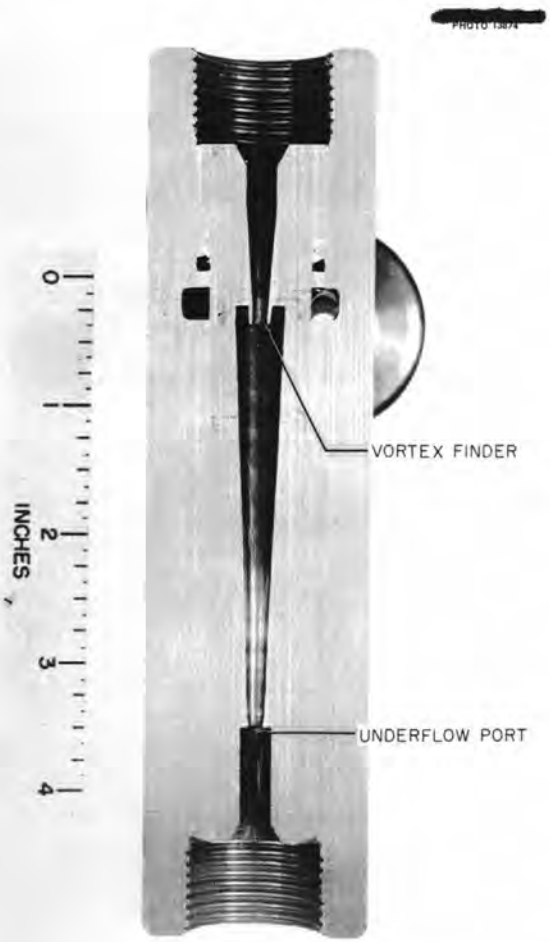

Fig. 9.6. Vertical Section of 1-gpm Hydroclone After 200-hr Operation with 0.05 *m* UO_2SO_4–0.005 *m* H_2SO_4.

9.2.4 Hydroclone Test on Loop B

Installation of test loop B was completed, and tests with the 1-cm-dia hydroclone as a part of the system were begun. The hydroclone removed precipitated neodymium sulfate from 0.04 *m* UO_2SO_4–0.0025 *m* H_2SO_4, as indicated by a 10% increase in the neodymium concentration in the underflow. The neodymium concentrations in the feed and overflow were essentially those due to solubility. Iron oxide that precipitated when ferric sulfate solution was pumped into the circulating fuel solution at 300°C was separated with an efficiency approaching 100%.

9.3 HRT CHEMICAL PROCESSING PLANT

W. L. Carter
H. O. Weeren
H. E. Williamson
F. C. McCullough
R. H. Winget
R. B. Lindauer
G. W. Gray
A. M. Rom
C. E. Guthrie

The insoluble fission products from the HRT will be centrifuged from a slip stream, bypassed around the heat exchanger, and collected in a retention tank, through which the underflow of the hydroclones will be recycled to the hydroclone feed line. The solids will accumulate to a concentration of approximately 1 g/liter and, being radioactive, will contribute materially to the heat generated in the underflow retention tank. The temperature of this tank must be controlled between 300 and 330°C. If it rises above this range, the uranium solution may separate into two phases; if it drops below, some solids will redissolve and be returned to the reactor.

The underflow retention tank temperature will be controlled by dissipating the generated heat to an air stream pumped past the surface of the tank. The air stream will be circulated by a blower and cooled by losses to the cell air. The amount of heat dissipated will be varied by changing the air temperature and circulation rate. Resistance heaters in the air stream will also be provided, so that the underflow retention tank can be heated at startup to bring its initial charge up to operating temperature before the side stream from the reactor circulating system is admitted.

9.3.1 Status of Plant

The excavation for the chemical processing area is complete. The cell floor and wall footings have been poured, and the cell linings are in the process of fabrication in the Birmingham shops of the Chicago Bridge & Iron Co.

Wherever possible, the policy of adapting previous design has been followed, not only to take advantage of previous reactor experience but to maintain a consistency of design throughout the project as well. Preliminary detailed design has been completed for the cold traps, recombiner condensers, condensate overflow tank, underflow retention tank, feed line heater, evaporator, D_2O receiver, and transfer tank. The cold trap and recombiner condensers are adaptations of designs for the HRT.

Remotely operated high- and low-pressure valves have been placed on order as extensions of existing purchase orders placed earlier for the HRT. Quotations have been received and are being reviewed for the high-pressure canned-rotor pumps required in the chemical processing area.

9.3.2 Instrumentation[3]

An HRT-design two-sampler unit will be located in the roof plugs of cell B, and the sampler lines will be connected to cell C through portholes in the walls separating the two cells. One sampler will be in series with the transfer tank and the evaporator and can sample any solutions during transfer from the tank to the evaporator. The other sampler will be connected as a bypass between the hydroclone overflow return line and the reactor dump tank, so that samples of the overflow may be taken while the plant is in operation.

The feed line from the reactor loop must be insulated to prevent heat loss to the surrounding concrete. It is planned to insulate the line with a $\frac{3}{4}$-in.-thick blanket of Santocel opacified with silicon (to minimize radiant heat transmission). The temperature drop to the concrete wall, under operating conditions, is calculated to be 3°C.

In general, the instrumentation designed for the HRT chemical processing plant will be similar to that found satisfactory in previous homogeneous reactor work. However, some instruments are being devised for special purposes. A probe, consisting of a heated stainless steel rod with thermocouples embedded in its surface at small intervals of its length, is being evaluated for the detection of tank liquid levels. The loss of heat from the immersed surface will be greater than that from the surface above the liquid. The location of the liquid level will be inferred from the location of the offset in the recorded temperatures.

Another scheme being investigated for determining the liquid level in a tank, which will also determine the total mass of liquid, consists of weighing, with load cells, both ends of a tank inclined from the horizontal. The total of the indicated weights will represent the total mass of liquid in the tank, and, from a comparison of the individual weights, the location of the center of gravity of the liquid in the tank (and therefore the position of the liquid level) can be computed.

The progressive increase in the concentration of insoluble fission products in the underflow retention tank can be sensed by the heat load on the cooling system and by the relative radioactivity of the tank. The latter will be sensed by an ionization chamber located outside the shielding opposite a collimating beam hole formed by a 1-in. stainless steel pipe embedded in lead shot and in alignment with the underflow retention tank.

The progress of evaporation of the underflow receiver contents to recover heavy water will be determined by the corresponding increase in the uranium concentration of the evaporator bottoms. Unfortunately, there is only a slight variation in the boiling point with wide variation in uranium concentration, but the electrical conductivity of the solution varies by a factor of 50 over the uranium concentration range 0.05 to 1.5 *m*. The device proposed for sensing the electrical conductivity consists of two coaxial toroidal coils spaced approximately 1 in. apart, magnetically independent of each other but linked by the conductivity of the solution separating them axially. The influence of one coil on the other is proportional to the conductivity of the solution and is accurately detected by standard instruments. The toroids must be individually enclosed in nonconductive sheaths which must be immune to corrosion and radiation damage. A search for suitable material has been initiated.

Null-balance transmitters to be used for pressure measurement would be more practical if their successful operation did not rely on the bleed air stream through small orifices and nozzles. A null-balance unit is being fitted with electrical contacts, which will control a commercial electrical transducer, and it, in turn, will supply pressure to the balance bellows. This arrangement is being evaluated by the Instrumentation and Controls Division.

Sheathing thermocouple wire in $\frac{1}{8}$-in. stainless steel tubing that can be connected to thermocouple wells with standard Swagelok fittings is being considered as an inexpensive and effective method of protecting thermocouple leads from shielding water and mechanical damage.

[3] Instrumentation developed under the direction of C. A. Mossman and R. K. Adams, Instrumentation and Controls Division.

9.4 EQUIPMENT DEVELOPMENT

P. A. Haas

Tests are being made on the applicability of frozen plugs of fuel solution for line closures in the HRT chemical processing plant. Plugs of frozen water and 0.04 *m* uranyl sulfate solution, 1¼ in. long, in ⅛-in. sched 80 pipe repeatedly held 8000-psi pressure differences. The freezing was accomplished by circulating Freon-12 through copper tubing wound and soldered along a 1-in. length of the pipe. The pipe was submerged in a water bath. Test pressures were applied by means of oil from a hydraulic jack. When the flow of refrigerant was stopped, the plugs failed in 25 to 35 sec.

10. PLUTONIUM-PRODUCER BLANKET PROCESSING

D. E. Ferguson

R. E. Leuze R. H. Rainey

The primary objective of processing the uranyl sulfate solution blanket of the plutonium producer is to remove plutonium and neptunium as rapidly as possible in order to minimize Pu^{240} buildup. The study of plutonium chemistry under simulated reactor conditions has included plutonium adsorption on metals, the rate of PuO_2 precipitation, and separation of PuO_2 with a hydroclone.

10.1 ADSORPTION OF PLUTONIUM ON STAINLESS STEEL, TITANIUM, AND ZIRCONIUM

Two of the vessels used to study adsorption of plutonium[1] from 1.7 *m* UO_2SO_4 at 250°C were descaled, and the scale solutions were analyzed for plutonium. The amount of plutonium adsorbed on the titanium vessel was 0.93 mg/cm^2, based on a material-balance calculation from the amounts in the initial and final solutions; based on analysis of the descaling solution, the amount was 0.98 mg/cm^2. The amount of plutonium adsorbed on the type 347 stainless steel vessel was 0.70 mg/cm^2 by material-balance calculations but only 0.44 mg/cm^2 by descaling-solution analysis.

An autoradiograph of the zirconium vessel, on which the amount of plutonium was 0.05 mg/cm^2, showed that the plutonium was not uniformly distributed over the surface. The exposed film showed small spots about 5 μ in diameter. Furthermore, these spots were lined up in a pattern (see Fig. 10.1) resembling the strain lines formed in the tubing when it was fabricated. This distribution suggests that the plutonium crystallizes out preferentially on surface imperfections. Autoradiographs of the type 347 stainless steel and titanium vessels are not yet available.

So that adsorption of plutonium on metals from a flowing stream can be studied, equipment is being constructed and is about 90% complete.

10.2 SEPARATION OF PuO_2 BY A HYDROCLONE

In preliminary tests, efficiencies of 15 to 70% were obtained for the separation of PuO_2 from water with a ¼-in. hydroclone. These tests were made in a laboratory setup, and material balances were poor. However, it is encouraging that concentration was obtained in all tests and that the same separation efficiency for PuO_2 was obtained by recycling the hydroclone overflow as many as four times. With proper adjustment, the hydroclone should be a useful analytical tool in determining the optimum conditions for PuO_2 particle growth.

The laboratory-scale equipment for these studies is quite simple. It consists of a 500-ml stainless

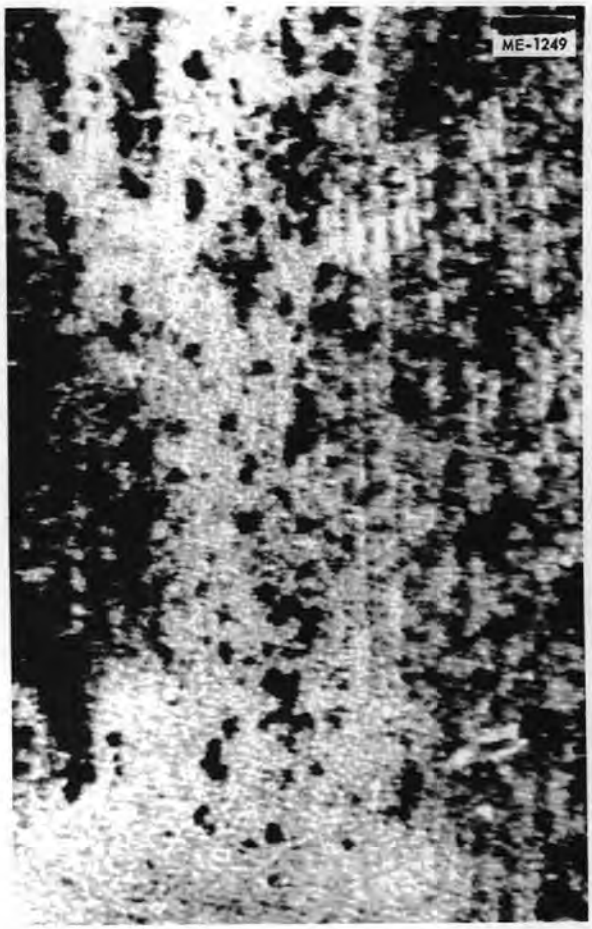

Fig. 10.1. Autoradiograph of Zirconium Vessel on Which Plutonium Was Deposited, 0.05 mg/cm^2. 60X. Reduced 16%.

[1] D. E. Ferguson *et al.*, *HRP Quar. Prog. Rep. Jan. 31, 1955*, ORNL-1853, p 192.

steel vessel to hold the feed and of a brass ¼-in. hydroclone. Feed for the hydroclone was prepared by precipitating PuO_2 from 1.25 *m* UO_2SO_4 at 250°C, centrifuging, washing with water, and reslurrying in water. Nitrogen pressure was used to force the PuO_2 slurry through the hydroclone, and the exit streams were collected in open beakers or graduated cylinders. This equipment is limited to operation at room temperature, at atmospheric pressure, and with noncorrosive solutions.

10.3 PRECIPITATION RATE OF PLUTONIUM DIOXIDE

The equilibrium solubility and the time required for plutonium to precipitate after being formed determine the amount of dissolved plutonium in the plutonium-producer blanket. Previously reported data,[1] obtained in titanium equipment under simulated reactor conditions, but with no neutron flux, indicated that supersaturation of plutonium would be less than 0.3 mg per kilogram of D_2O. Additional experiments gave the same precipitation rate when 100 mg of iron, nickel, or copper per kilogram of H_2O was added. The addition of 20 mg of chromium per kilogram of H_2O resulted in 50% more plutonium remaining in solution at the end of 30 min, and the addition of 100 mg of chromium per kilogram of H_2O gave 2.5 times as much plutonium in solution after 30 min (see Fig. 10.2). Precipitation studies made in a stainless steel vessel gave results which corresponded approximately to the PuO_2 precipitation rate in the presence of 20 mg of chromium per kilogram of H_2O. In the presence of oxygen and in the absence of radiation, the chromium in the above tests was present as chromate. However, since chromate may be reduced by radiation in a reactor, the effect of chromium on plutonium behavior may be eliminated in the reactor blanket.

Temperature has a marked effect on the rate of plutonium precipitation and on the solubility of plutonium. From the results of the precipitation-rate studies at various temperatures, the energy of activation was estimated to be of the order of 7 kcal/mole. The experiments from which the precipitation-rate data plotted in Fig. 10.3 were obtained were not carried to completion; however, if the curves are extrapolated, the following approximate solubilities (in milligrams per kilogram of H_2O) are obtained: 1.5 at 250°C, 2 at 200°C, 6 at 150°C, and 20 at 125°C.

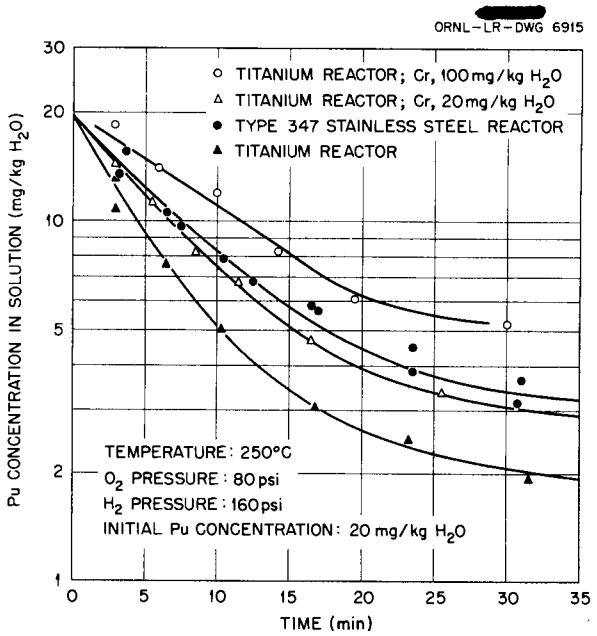

Fig. 10.2. Precipitation in Titanium and Type 347 Stainless Steel Vessels of PuO_2 from 1.25 *m* UO_2SO_4 Containing Chromium.

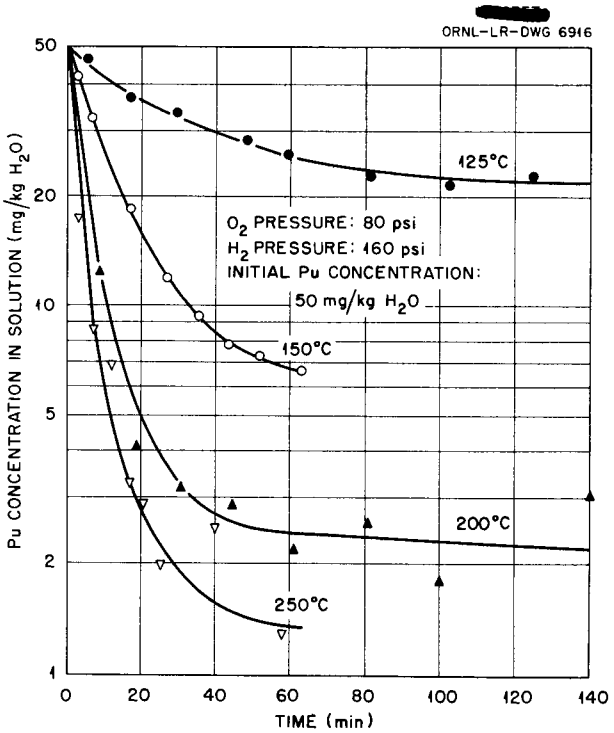

Fig. 10.3. Precipitation in Titanium Vessel of PuO_2 from 1.25 *m* UO_2SO_4 at Various Temperatures.

These precipitation-rate studies were made by injecting 15 ml of 1.25 *m* UO_2SO_4 containing Pu(IV) into an autoclave loaded with 35 ml of 1.25 *m* UO_2SO_4 under an atmosphere of 80 psi of O_2 and 160 psi of H_2 at elevated temperature. The solutions were mixed and then sampled at short intervals in order to determine the amount of plutonium remaining in solution.

11. THERMAL-BREEDER BLANKET PROCESSING

D. E. Ferguson

R. E. Leuze W. E. Tomlin

At the present time, the most obvious method for processing the thermal-breeder thorium dioxide blanket is recovery of the heavy water by evaporation, dissolution of the thorium dioxide in nitric acid and light water, and recovery of U^{233} and thorium by the Thorex process. Removal of protactinium and uranium from the ThO_2 by leaching is being investigated as the basis for an alternate processing method.

11.1 LEACHING OF THORIUM DIOXIDE

It was previously reported that 70% of the Pa^{233} was leached when irradiated thorium dioxide was refluxed in 12 *N* H_2SO_4 for 4 hr and that only 0.2% of the thorium was dissolved by this treatment.[1] X-ray diffraction analysis of the residue showed that both ThO_2 and $Th(SO_4)_2$ were present. The residue contained 32% sulfate, compared with the theoretical value of 45.3% for $Th(SO_4)_2$. The leaching of 70% of the protactinium and the conversion of 70% of the ThO_2 to $Th(SO_4)_2$ suggest that the protactinium is bound within the ThO_2 particle and that complete dissolution or metathesis of ThO_2 may be necessary for removal of the protactinium to be achieved. Essentially none of the sulfate was removed when the residue was heated at 650°C for 24 hr.

[1] D. E. Ferguson, R. E. Leuze, and W. E. Tomlin, *HRP Quar. Prog. Rep. Jan. 31, 1955*, ORNL-1853, p 196.

11.2 CORROSION OF ZIRCALOY-2 IN ThO_2-ThF_4 SLURRIES

In static autoclave tests a slurry of ThF_4 at 250°C under 200 psi of O_2 corroded Zircaloy-2 at a rate of 440 mpy. As ThO_2 was added to the ThF_4, the corrosion rate decreased as follows:

ThO_2 (wt %)	Corrosion (mpy)
10	420
25	220
40	280

In a slurry of $ThOF_2$ at 250°C under 200 psi of O_2, the Zircaloy-2 corrosion rate was 180 mpy. Control tests showed corrosion rates of less than 0.1 mpy in a ThO_2 slurry containing no fluoride.

Test pieces of polished Zircaloy-2 were heated for 24 hr in slurries at 250°C under 200 psi of O_2. The metal had been defilmed in hot concentrated sodium hydroxide solutions. The mixed ThO_2-ThF_4 slurries were prepared by heating the mixtures in water at 250°C for 24 hr, filtering, washing with water, and reslurrying. The $ThOF_2$ was prepared by dissolving thorium hydroxide in ammonium carbonate and precipitating with a stoichiometric amount of HF. The resulting $ThOF_2$ was washed with water, dried at 105°C for 6 hr, and calcined at 500°C for 7 hr.

12. SUMMARY OF WORK OF VITRO LABORATORY[1]

Encouraging results were obtained in further batch experiments on iodine removal from simulated core solution by metallic silver in contact with equilibrium vapor at elevated temperature. Rate studies with solutions of initial concentrations of 6×10^{-4} and 6×10^{-6} gram-atom of iodine per kilogram led to the following conclusions regarding the probable behavior of fission-product iodine:

1. Heptavalent iodine is reduced almost instantaneously to the pentavalent form at 250°C in oxygenated UO_2SO_4 solution.
2. The concentration of pentavalent iodine in such a solution decreases rapidly (half-period approximately 2 min) when the amount of molecular iodine in solution is negligible.
3. The rate of removal of pentavalent iodine becomes much slower when the concentration of elemental iodine reaches the same order of magnitude as that of the pentavalent, indicating a reversible equilibrium between the two forms.
4. The rate of total iodine removal from solution after the two forms reached equilibrium corresponded to a half-period of 20 to 30 min when metallic silver was exposed to the vapor above a 3.3-cm^2 liquid-gas interface; no agitation or gas sweep was used. Interpretation of these data suggests that the elemental-iodine removal was diffusion-controlled and probably could be speeded up by a sweep gas.

Future work calls for investigation of rates of removal of molecular iodine from solutions through which oxygen or inert gas is being passed; the off-vapors will be contacted with metallic silver for fixation of the iodine stripped from solution.

Loop operations provided data on the precipitation of rare earths and corrosion products in an externally heated stainless steel circulating system. Rare-earth sulfates dissolved in cold 0.02 *m* UO_2SO_4 solution were fed to the 300°C loop in five- to tenfold excess of the saturation concentration. A 5-μ filter in the 300°C exit stream collected less than 1% of the precipitated material, and analysis of the filtrate indicated no more than the expected solubility of the rare-earth tracers. It was concluded that almost all the precipitated material was deposited on the walls of the loop. About 20% of the activity remained in the system after it had been cooled and drained. This activity probably was due to Ir^{192} impurity in the tracer used (see Sec. 9.1.3). The solubility of neodymium sulfate in this system was calculated to be 0.032 g/kg at 300°C; this is consistent with ORNL observations.

An inorganic ion exchanger (zirconium phosphate) adsorbed 35 mg of cesium per gram of exchanger from simulated fuel solution at 95°C before saturation. This was half the loading obtained at room temperature. Tests are planned at slightly higher temperatures, since cooling of reactor fuel below 100°C would probably result in peroxide formation and consequent uranium precipitation. The exchanger was found to have little or no capacity for nickel and manganese ions at 95°C but did remove some copper from the fuel.

[1] W. A. Bain, *HR Fuel Reprocessing Quar. Prog. Rep. March 31, 1955*, KLX-10000.

Part VI

SUPPORTING CHEMICAL RESEARCH

E. H. Taylor

13. AQUEOUS SYSTEMS AT ELEVATED TEMPERATURES

C. H. Secoy

F. E. Clark
J. S. Gill
G. M. Hebert
F. J. Loprest
W. L. Marshall
D. M. Richardson
D. W. Sherwood
R. Slusher

13.1 DIRECT SAMPLING AS A METHOD FOR INVESTIGATING THE SYSTEM UO_3-SO_3-H_2O ABOVE 300°C

D. M. Richardson

Equipment has been developed and tested for investigating the UO_3-SO_3-H_2O system in the two-liquid-phase region by direct sampling. The material balance equations which apply in this method of analyzing the system have been reported previously.[1]

The device consists of a titanium pressure vessel of measured volume (see Fig. 13.1). At the top of the vessel a tapered valve stem is operated through a gold O-ring gasket. The bottom of the vessel is a detachable container in which a liquid sample is sealed off, at temperature, by forcing the valve stem into the pressure vessel until seating occurs. A side opening is located above the valve seat so that, after cooling to room temperature, the liquid remaining above the valve seat can be rinsed out and this part of the vessel dried before the sample container is removed for weight and volume measurements.

Reproducible results were obtained for the composition and density of the heavy-liquid phase of 2.00 *m* UO_2SO_4 at 300.0°C, with the sample container 0.500 fraction filled at room temperature (see Table 13.1). The effects of small changes in fractional filling and in temperature were shown by the results of two other experiments.

The density values were low because the tip of the valve stem became wet, but are probably less than 1% in error. Material balance within 1% was obtained in all runs. Since vibration was present throughout the 20-hr equilibration period allowed in each run, complete phase separation is believed to have been attained.

Extension of these measurements to include the determination of the composition and density of the light-liquid phase by difference is feasible but is unattractive when the simplicity of capillary sampling which is possible with the light-liquid phase is considered.

[1] D. M. Richardson, *HRP Quar. Prog. Rep. April 30, 1954*, ORNL-1753, p 151–152.

13.2 THE SYSTEM UO_3-SO_3-H_2O ABOVE 300°C

D. W. Sherwood G. M. Hebert

The primary objective of this work is the determination of the volumes of the three phases present in sealed tubes of uranyl sulfate solutions at elevated temperatures in the two-liquid-phase

TABLE 13.1. COMPOSITION AND DENSITY OF THE HEAVY-LIQUID PHASE OF 2.00 *m* UO_2SO_4

Run No.	Initial Fraction Filled	Temperature (°C)	Density at Temperature (g/ml)	Mole Ratio UO_3/SO_3	Weight Per Cent		
					UO_3	SO_3	H_2O (by Difference)
4	0.500	301.5	1.876	1.055	51.4	13.6	35.0
5	0.500	300.0	1.831	1.045	50.7	13.6	35.7
6	0.500	300.0	1.838	1.038	50.8	13.7	35.5
8	0.400	299.9	1.845	1.026	50.5	13.8	35.7

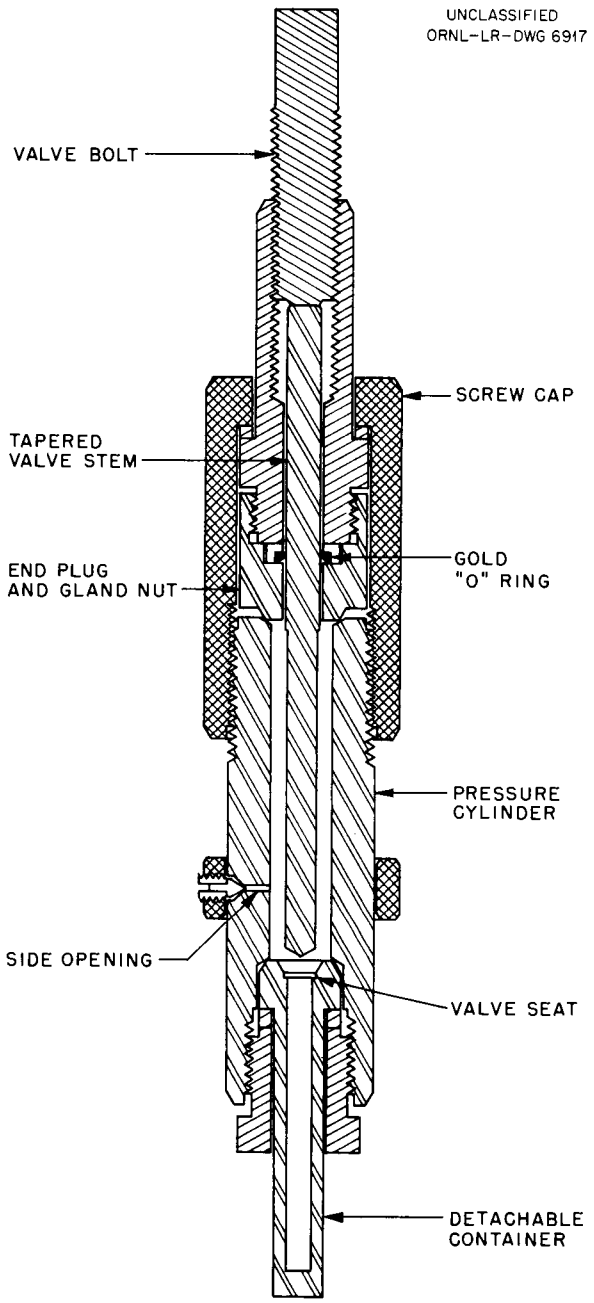

Fig. 13.1. High-Pressure Sampling Device.

region of this system. Previous reports[2,3] have discussed the techniques for measuring the positions of the interfaces in uniform-bore quartz tubes; from the positions of the interfaces the volumes of the three phases can be calculated. The very small volume of the heavy-liquid phase formed under the conditions of greatest interest (high temperature and low initial solution concentration) made it necessary to increase the length of the quartz tubes to 6 in.; this, in turn, made it more difficult to achieve uniform temperatures throughout the length of the tubes. However, with adequate temperature control it has been possible to obtain data for 2, 3, and 0.25 *m* solutions.

Additional information concerning the system can be obtained by measuring the vapor pressures of the solutions whose volumes are measured as discussed above. The Industrial Engineering Corporation of Louisville, Kentucky, is constructing, for this purpose, platinum-lined apparatus for precision pressure measurements at elevated temperatures. The specifications call for an accuracy of ±4 psi and a sensitivity of ±2 psi over the entire range of pressure (0–3200 psig) and temperature (0–375°C). Inspection and testing of the apparatus in partially completed form suggested that these specifications will be met or surpassed.

13.3 AQUEOUS SYSTEMS INVOLVING URANIUM TRIOXIDE, CARBON DIOXIDE, AND ALKALI OR ALKALINE EARTH OXIDES

F. J. Loprest W. L. Marshall

An investigation of the high-temperature phase equilibria of portions of the quaternary systems UO_3-CO_2-H_2O-MO or M_2O, where M is an alkali or alkaline earth metal, was started.

Exploratory data were obtained in the system Na_2CO_3-UO_3-CO_2-H_2O in the temperature range 150 to 290°C. Uranium solubility of 1 to 1.5 g/liter was established at 250°C for some of the mixtures. The magnesium and lithium systems will be surveyed after the present investigation has been completed.

[2] G. M. Hebert, D. W. Sherwood, and C. H. Secoy, *HRP Quar. Prog. Rep. Oct. 31, 1954*, ORNL-1813, p 164.

[3] G. M. Hebert and D. W. Sherwood, *HRP Quar. Prog. Rep. April 30, 1954*, ORNL-1753, p 150.

13.4 THE QUATERNARY SYSTEMS $NiO-UO_3-SO_3-H_2O$ AND $CuO-UO_3-SO_3-H_2O$

F. E. Clark J. S. Gill
R. Slusher

Equipment for solid-liquid equilibration studies of the $NiO-UO_3-SO_3-H_2O$ and the $CuO-UO_3-SO_3-H_2O$ systems at 100°C has been procured and is in operation. Samples have been equilibrated, but analyses are incomplete.

Equipment was designed and is now available for equilibration work at 250°C. Ten titanium bombs are agitated by turning ±15 deg from a horizontal position. Prior to sampling, the bombs are adjusted manually to a vertical position and the wet residues allowed to settle; then the supernatant liquid is sampled through a titanium or stainless steel capillary leading from the bomb. Silicone oil (DC-550) instead of fused salts is used as a bath medium because of possible explosive hazards in using titanium metal in contact with fused nitrate salts.

A series of 20 samples containing 0.04 *m* UO_2SO_4, from 0 to 0.02 *m* free H_2SO_4, and from 0 to 0.05 *m* $CuSO_4$ has been prepared. Initial experiments are in progress to determine the solubility of $Ni(OH)_2$ in these solutions at 25°C. These tests will ultimately be extended to higher temperatures.

A constant-head recording potentiometer was adapted to the analysis of dilute solutions of uranium. A fast, economical, accurate, and precise method for low concentrations of uranium in sulfuric acid is essential to adequately evaluate future data from high-temperature work in which samples are small and uranium concentrations are low.

Initial data obtained at 25°C for the four-component system $CuO-UO_3-SO_3-H_2O$ are presented in Table 13.2. Further evidence of brochantite [$3Cu(OH)_2 \cdot CuSO_4$] or antlerite [$2Cu(OH)_2 \cdot CuSO_4$] is shown in the samples that were richest in copper.

13.5 ADSORPTION OF WATER BY ThO_2

D. M. Richardson

A technique for measuring water adsorption by ThO_2 powder in unsaturated steam was tested from 160 to 360°C.

From observations of the steam pressure in a volumetric, thermostatted, pressure vessel containing measured quantities of deaerated ThO_2 and water, and from available data for the specific volume of unsaturated steam,[4] it is possible to calculate, by difference, the amount of water adsorbed.

The pressure is measured by means of a diaphragm mounted on one end of the volumetric pressure vessel. An external system, filled with mercury, is connected to the outer side of the diaphragm. When the volume of mercury in the external system is increased at a constant rate by heating, a mercury pressure vs time curve is obtained in which a

[4] J. H. Keenan and F. G. Keyes, *Thermodynamic Properties of Steam*, Wiley, New York, 1936.

TABLE 13.2. THE SYSTEM $CuO-UO_3-SO_3-H_2O$ AT 25°C (EQUILIBRATION TIME, 156 DAYS)

Sample No.	Liquid Phase			Specific Gravity	Wet Residue			Solid Phase
	CuO (wt %)	UO_3 (wt %)	SO_3 (wt %)		CuO (wt %)	UO_3 (wt %)	SO_3 (wt %)	
226	9.11	0	9.13	1.2070				
227	8.98	0.28	9.09	1.2073	12.53	0.35	9.71	Either $3Cu(OH)_2 \cdot CuSO_4$ or $2Cu(OH)_2 \cdot CuSO_4$
228	8.81	0.43	9.03	1.2097	14.93	0.10	10.65	
229	8.69	0.73	8.97	1.2104	14.81	0.54	10.12	
230	8.55	1.14	8.92	1.2103	16.96	0.61	11.10	
P-90	8.11	2.13	8.80	1.2144	45.40	0.90	18.24	
231	8.04	2.26	8.71	1.2146	18.60	1.79	11.00	
232	6.59	5.25	8.10	1.2291	22.10	3.94	12.00	
233	5.09	4.44	6.37	1.1731	16.40	24.40	13.00	Unidentified
234	1.74	2.53	2.44	1.0652	11.60	30.20	11.10	Unidentified
P-95	0.30	3.82	1.14	1.0471	6.48	47.20	13.26	Unidentified

pressure halt or plateau occurs. At this pressure the external and internal systems are balanced.

In preliminary tests of this equipment the pressures of saturated steam were measured at 160 and at 360°C with deaerated water. The observed pressures were in error by approximately 0.5%. More precise measurements are anticipated as the result of improvements in diaphragm design.

14. ADSORPTION ON INORGANIC MATERIALS

K. A. Kraus
T. A. Carlson J. S. Johnson
H. O. Phillips

14.1 ZIRCONIUM PHOSPHATE

The adsorptive properties of zirconium phosphate for certain cations were determined both by the column technique and by the equilibration technique. The zirconium phosphate was prepared from recrystallized $ZrOCl_2 \cdot 8H_2O$ by precipitation with excess H_3PO_4 or Na_2HPO_4. The precipitate was centrifuged, washed, and dried at various temperatures. The adsorptive properties of both preparations were approximately the same. The materials dried at room temperature adsorbed 0.3 to 0.5 mole of Ce(III) per kilogram of adsorbent from 0.01 *M* $CeCl_3$ solutions.

The drying temperature greatly affects the apparent adsorptive capacity of zirconium phosphate; it is still about 0.5 mole Ce(III) per kilogram of solid when dried at 120°C but essentially zero when dried at 200 or 400°C.

The materials seem to have high capacity for the adsorption of a number of ions other than Ce(III), such as Ba(II), Co(II), and U(VI). For example, about 1 ml of 0.1 *M* solutions of these salts could be passed through 1 ml of adsorbent before breakthrough occurred. Adsorption is reversible, and increased acidity leads to removal of the ions, apparently by an ion-exchange mechanism. For the ions listed, 90 to 95% of the adsorbed material could be removed readily with 1 *M* HCl.

The zirconium phosphate may be converted from a cation adsorber or exchanger to an anion exchanger by treatment with excess Zr(IV). The anion adsorptive properties were studied by following adsorption of CrO_4^{--} ion. Approximately 2 to 3 ml of 10^{-2} *M* CrO_4^{--} was adsorbed per milliliter of column bed. The CrO_4^{--} ion is readily displaced from the column by OH^- ions or by high concentration (1–2 *M*) of HCl or H_2SO_4. Dilute solutions of H_3PO_4 (0.01 *M*) remove most of the adsorbed CrO_4^{--} and reconvert the material to a cation exchanger.

14.2 ZIRCONIUM HYDROXIDE

In the previous quarterly report[1] it had been pointed out that zirconium hydroxide is essentially ineffectual as a cation exchanger in acidic solutions. However, it has now been demonstrated that zirconium hydroxide acts as an anion exchanger in acidic solutions and as a cation exchanger in basic solutions.

Zirconium hydroxide was precipitated from recrystallized $ZrOCl_2 \cdot 8H_2O$ with ammonia. After being dried at 120°C, the material showed adsorptive properties for negative ions such as Cl^-, OH^-, SO_4^{--} and CrO_4^{--}; CrO_4^{--} was particularly strongly adsorbed, and its removal could be achieved effectively only with base. The adsorptive capacity of the hydroxide seemed to be relatively insensitive to the drying temperature. Thus, material dried overnight at 120°C adsorbed 1.3 moles of CrO_4^{--} per kilogram of adsorbent from 1 *M* K_2CrO_4 solution, while the material dried overnight at 300°C adsorbed 1.1 moles per kilogram. In another preparation, material dried at 25°C overnight adsorbed 1.1 moles CrO_4^{--} per kilogram, and the material dried at 200°C adsorbed 0.8 mole per kilogram.

Further characterization of the "hydroxide" dried at 200°C was undertaken; the effects of acid concentration, type of acid, negative ion concentration, and time of equilibration were studied. Some of the results are listed in Table 14.1.

It may be noticed from this table that in many cases there appeared to be difficulty in achieving equilibrium. At high acidities, distribution coefficients tended to decrease with time, suggesting attack on the exchanger (depolymerization ?) by the acid.

To check reproducibility further and to obtain some information regarding the ideality of the exchange, adsorption of bromide tracer from HCl and LiCl solutions was studied. Some of the results are shown in Fig. 14.1. In the dilute acid region the distribution coefficients were essentially independent of time, while at higher acidities they increased with time. The arrows in Fig. 14.1 indicate a drift over a period of two to four days. Little drift with time was found in the experiments with lithium chloride. In the region 0.02 to 0.08 *M* Cl^-, log *D* varies approximately linearly with log (Cl^-), and the slope of the line is not far from unity,

[1] T. A. Carlson *et al.*, *HRP Quar. Prog. Rep. Jan. 31, 1955*, ORNL-1853, p 203.

TABLE 14.1. EFFECT OF EQUILIBRATION TIME AND MEDIUM ON THE DISTRIBUTION COEFFICIENT (*D*) OF TRACER CrO_4^{--} ON ZIRCONIUM HYDROXIDE DRIED AT 200°C

Medium	Molarity	Time (hr)	*D*
HCl	0.01	3	8,000
		21	10,000
	0.1	3	2,000
	0.5	1/12	105
		1	445
		3	680
		5	815
		22	525
		49 1/2	310
		70	240
		143	160
		166	150
	1.0	1/4	20
		1	64
		17 1/2	35
		45	25
H_2SO_4	0.001	1/4	295
		1	560
		7	1,660
		25	2,520
		138	3,200
	0.01	4	167
		24	253
	0.1	4	24
		24	35
	0.5	1 2/3	4.6
H_2SO_4	0.5	19 1/3	4.3
		23	4.0
		45	3.2
		68	2.9
	1.0	1 2/3	1.0
		19 1/3	0.8
		23	0.7
		45	0.6
		68	0.4
NaOH	0.1	3 1/2	0.5
		22	0.2
LiCl	1.0–LiCl, 0.01–HCl	1 1/2	3,200
	2.0–LiCl, 0.1–HCl	1	396
	4.0–LiCl, 0.1–HCl	1	230
	10.0–LiCl, 0.1–HCl	3	13
		66	1
Na_2SO_4	1.0	2	110
		66	223
	1.0–Na_2SO_4, 0.01–H_2SO_4	2	28
		66	58
	2.0	3/4	54
		66	136

suggesting that ion exchange is approaching ideality.

The adsorptive capacity of the material for bromide ions was reasonably high; for example, from 0.01 *M* HCl–0.1 *M* KBr solutions, about 0.5 mole of Br^- per kilogram could be adsorbed.

The exchanger as prepared apparently contains a considerable amount of chloride ion. Thus, on treating it with 0.1 *M* NaOH, 1 g of the material was found to liberate approximately 0.6 mmole of chloride ion as determined by silver nitrate titration. When the material is immersed in various acid solutions, further uptake of chloride ion may occur at high acidities and a loss of chloride ion may occur at low acidities. Undoubtedly these experiments measure the hydroxide-chloride ion-exchange equilibrium, and further experiments along these lines are planned. As anticipated, the exchanger shows very great selectivity for hydroxide ion, and hydroxide-chloride exchange was appreciable even in 10^{-3} *M* HCl.

If, in 0.1 *M* NaOH, the base uptake is compared with the amount of chloride liberated, it is found that the two values are not equivalent. Thus 1.2 mmoles of base was adsorbed per gram of solid, while only 0.6 mmole of Cl^- was liberated. Unquestionably the material was becoming a cation exchanger. This was confirmed by following sodium uptake with sodium tracer in 0.1 *M* NaOH. Further, adsorption of Cs-tracer (Cs^{137}) from 0.1

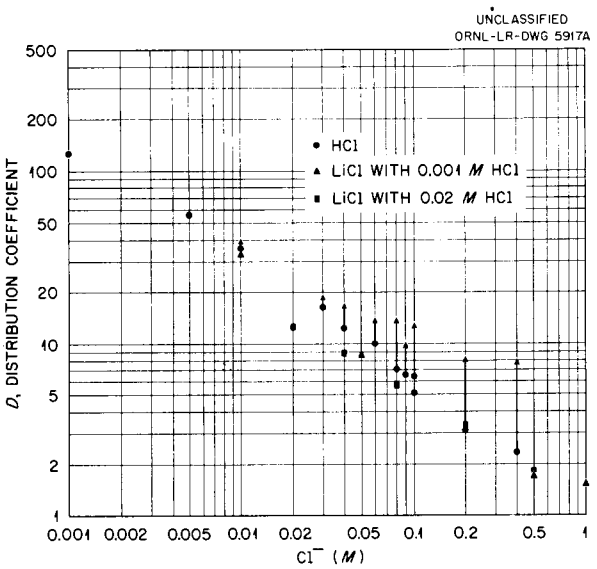

Fig. 14.1. Adsorption of Br^- by Zirconium Hydroxide.

M NaOH was found to be appreciable (*D* = about 10). As anticipated, the cation-exchange properties disappeared in acid solutions and the Cs-tracer could be removed, for example, with 0.1 *M* HCl.

14.3 THORIUM HYDROXIDE

No experiments were carried out on the anion-exchange (adsorptive) properties of thorium hydroxide aside from demonstrating with chromate that such anion-exchange properties exist. However, as a sideline to this work, it was found that when precipitated thorium hydroxide was dried at 300°C overnight the material dispersed readily in water to give an opalescent solution. Thorium under these conditions showed a very high "solubility." Thus, in one example, up to 2.8 g of the dried "hydroxide" could be dispersed in 1 g of water. Dispersions containing 1 to 2 g of hydroxide per gram of water did not precipitate in at least a week at room temperature. However, the material precipitated when the "solutions" were heated to high temperatures. After heating overnight, some of these precipitates redispersed on cooling. Thus, a dispersion containing 1.2 g of thorium hydroxide per gram of water was heated overnight at 130°C. It precipitated, but redispersed on cooling. A dispersion containing 0.6 g of thorium hydroxide per gram of water did not precipitate on heating overnight at 130°C, but precipitated on heating to 240°C. This material also redispersed on cooling. It is anticipated that more prolonged heating might cause irreversible changes and that the redispersibility on cooling might be expected to disappear.

14.4 OTHER HYDROXIDES

Anion-exchange properties of the "hydroxides" of Fe(III), Cr(III), mixtures of Cr(III) and Fe(III), Ti(IV), Mo(VI), and W(VI) were studied with chromate tracer. All of these, except Mo(VI) and W(VI), showed strong adsorption of chromate, similar to the hydroxides of Zr(IV) and Th(IV). The chromate adsorption in all these cases apparently can be described in terms of anion-exchange terminology. The "hydroxides" of Mo(VI) and W(VI) (molybdic and tungstic acids) showed cation-exchange properties (see also Sec. 14.5).

14.5 ZIRCONIUM TUNGSTATE PRECIPITATES

It was found that zirconium tungstate precipitates show cation-exchange properties. In a typical preparation, aqueous solutions of Na_2WO_4 and of $ZrOCl_2$ were separately adjusted to a pH of about 1 and then mixed in quantities to give a 5:1 ratio of tungsten to zirconium. The precipitate, after centrifugation and without washing, was dried at room temperature overnight. The material had reasonable ion-exchange capacity, since it could adsorb 0.12 mole of Ce(III) per kilogram from 0.05 *M* HCl. Some of the adsorptive properties for various tracers are given in Table 14.2.

Adsorption of the tracers was rapid (90% complete in 5 min) and appeared to be reversible, although desorption occurred more slowly. In equilibration experiments in HCl media it was found that adsorption decreased slowly over several days. This

TABLE 14.2. ADSORPTION OF CATIONS ON ZIRCONIUM TUNGSTATE PRECIPITATE

Tracer	HCl (*M*)	Distribution Coefficient
Ce(III)	0.1	>1000
Ce(III)	1.0	~5
Co(II)	0.1	~40
Cs	1.0	~200

decrease was not observed in KCl solutions, suggesting that, as in the case of zirconium hydroxide, attack on the solid (depolymerization ?) by the acid occurred.

Preparations of zirconium molybdate, thorium tungstate, hafnium tungstate, and titanium tungstate also showed cation adsorption. However, not until the variables in the preparation and drying of these adsorbers are investigated more fully can quantitative comparison be made.

The adsorptive properties of zirconium tungstate were investigated as a function of drying temperature. The distribution coefficients were found to decrease with temperature up to about 600°C and then to rise abruptly when drying was extended to 800°C. Thus, the distribution coefficients for Co(II) tracer in 0.03 *M* HCl were 360, 16, 2, and 430 after drying overnight to 120, 150, 600, and 800°C, respectively. The capacity of the material dried to 800°C was very much lower [0.005 mole of Ce(III) adsorbed per kilogram from 0.05 *M* HCl] than that of the material dried at low temperatures.

Several preparations of zirconium tungstate gave somewhat different values of *D* (distribution coefficient) and apparent capacity. However, they showed qualitatively the same effect of drying temperature and maintained the same relative specificity for various tracers.

Tungstic acid, precipitated in the white form, also showed cation-exchange properties. Its capacity was about twice that of the material brought down with zirconium, and its distribution coefficients for Ce(III) and Co(II) tracers were much higher. Large and incompletely understood variations occur among preparations, however, and peptization in low concentrations of electrolyte precludes definite statements at this time about the properties of this material. Adsorption on tungstic acid did not seem to decrease so sharply with temperature as it did on zirconium tungstate, and the sharp rise in adsorbability on drying at 800°C was not observed.

15. ANALYTICAL CHEMISTRY

O. Menis
R. G. Ball
C. M. Boyd
R. E. Corcoran
A. D. Horton
P. F. Thomason
M. L. Hubbard
F. J. Miller
W. R. Musick
I. B. Rubin

15.1 ELECTRODEPOSITION OF COPPER FROM SOLUTIONS OF URANYL SULFATE AT A CONTROLLED CATHODE POTENTIAL

The deposition of copper from solutions of uranyl sulfate by means of a controlled cathode potential was investigated. The cathode potential was controlled[1] at −0.2 v vs S.C.E.; this yielded optimum conditions from the standpoints of adherent deposits of copper and maximum rate of deposition.[2] In solutions of uranyl sulfate (40 mg/ml), copper in the range of 12 to 61 mg was determined with a precision of 0.3%. The constant for the rate of deposition of copper was estimated to be 0.04 min^{-1}.

15.2 ELECTRODEPOSITION OF NICKEL FROM SOLUTIONS OF URANYL SULFATE AT A CONTROLLED CATHODE POTENTIAL

A study of electrolytic methods for the deposition of nickel from solutions of uranyl sulfate was initiated. In an initial study, about 7% of the nickel in solution was deposited at a controlled cathode potential after the copper had been removed and the uranyl ions had been precipitated with pyridine. This quantity of nickel will be sufficient for the determination of nickel by a combination of a proposed isotopic dilution and mass-spectrometric methods.

15.3 CONDUCTIVITY AND pH MEASUREMENTS OF AQUEOUS SLURRIES OF THORIUM COMPOUNDS

A study to evaluate the use of conductivity measurements for the estimation of impurities in slurries of thorium oxide or for the characterization of the properties of thorium oxide from various sources was continued.[3] Experiments to estimate the effect of small amounts of thorium sulfate on the conductivity of aqueous slurries of thorium oxide are being made. The conductivity and pH values under equilibrium conditions for slurries of thorium oxide, thorium sulfate, and thorium oxide to which thorium sulfate was added have been determined. The hydrolysis products of thorium sulfate were adsorbed on the oxide. The conductivity measurements permit the estimation of hydronium ions and other ions present in solutions only after adsorption equilibrium has been attained.

15.4 POLAROGRAPHIC DETERMINATION OF BARIUM

A polarographic method was investigated for the determination of microgram quantities of barium[4] in thorium oxide. A linear relation between the diffusion current and the concentration of barium was established. The precision was found to be 1% for barium chloride in the range of 0.5 to 1.5×10^{-3} *M*. A diffusion current for barium was not obtained when 2-thenoyltrifluoroacetone was used for the extraction of thorium from solutions of thorium oxide that contained barium.

15.5 DISSOLUTION OF REFRACTORY MIXTURES OF THORIUM AND TITANIUM OXIDES

In the analysis of slurries of thorium oxide which contained a relatively high percentage of titanium, it was found that the usual methods used to dissolve the materials were not successful.[5] Of the several methods tried – prolonged boiling with a mixture of hydrofluoric and perchloric acids, fusion with sodium hydroxide in gold crucibles, and heating in an autoclave at 250°C with hydrochloric acid in sealed tubes – the last method was most effective. The reaction of the

[1] R. W. Lamphere and L. B. Rogers, *Anal. Chem.* **22**, 463 (1950).

[2] J. J. Lingane, *Electroanalytical Chemistry*, p 272, Interscience, New York, 1953.

[3] C. M. Boyd, *Anal. Chem. Semiann. Prog. Rep. Oct. 20, 1954*, ORNL-1788, p 41.

[4] I. M. Kolthoff and H. P. Gregor, *Anal. Chem.* **20**, 541 (1948).

[5] C. K. Talbott, *Anal. Chem. Semiann. Prog. Rep. April 20, 1953*, ORNL-1547, p 19.

[redacted]

oxide mixture with hydrochloric acid in a sealed tube at 250°C resulted in complete dissolution of the oxide.

15.6 DISSOLUTION OF ALUMINUM OXIDE AND DETERMINATION OF PLATINUM

Methods were investigated for dissolving pellets of aluminum oxide, which are very refractory, prior to the estimation of the platinum content. Treatment with aqua regia and fusion with sodium hydroxide, in nickel or gold crucibles, either failed to dissolve the sample completely or led to a loss of platinum. The aluminum oxide was dissolved successfully by treating with hydrochloric acid at 250°C in a sealed quartz tube. The platinum residue was dissolved in aqua regia, and the platinum was then estimated as the platinum–stannous chloride complex according to the procedure of Ayers and Meyer.[6] The precision for the estimation of platinum was better than 1%.

15.7 FLAME PHOTOMETRY OF SILVER

The flame photometry of silver was explored in order to develop a rapid and sensitive method for the estimation of silver in slurries of thorium oxide and solutions of uranyl sulfate. The optimum conditions for the gas pressure, slit width, voltage of the photomultiplier tube, sensitivity, and solvent medium were established. For concentrations of silver in the range of 0 to 40 ppm, the slope of the calibration curve was 1.00 relative emissivity unit per ppm silver, with a precision of 1%.

15.8 SPECTROPHOTOMETRIC DETERMINATION OF ETHYLENEDIAMINETETRAACETIC ACID AS THE COPPER COMPLEX

A method for the determination of ethylenediaminetetraacetic acid (EDTA) as described in an industrial bulletin[7] was investigated. The following conditions were studied: wave length of maximum absorbancy, effect of buffer, selection of reference solution, sensitivity, and stability. Maximum absorption was found to occur at 262 mμ. At this wave length, in 0.2 *M* buffer, the molar absorbancy index is 9700. The sensitivity was found to increase as the concentration of buffer was increased, but a decrease in the precision was noted under these conditions. For concentrations of EDTA in the range of 20 to 60 μg per milliliter of final volume, the precision was about 5%. Errors, due to slight deviations from Beers Law, were reduced by a factor of 5 when a calibration curve was used.

15.9 POLAROGRAPHIC DETERMINATION OF CHROMIUM(VI) AND TOTAL CHROMIUM IN HOMOGENEOUS REACTOR FUELS

Chromium(VI) may be separated from homogeneous reactor fuel solutions by ion exchange in a Dowex 50 anion resin column. The effluent, which contains Cr(VI) as the chromate ion, is made 0.75 *M* in sodium hydroxide, and the resulting solution is analyzed polarographically for Cr(VI).

Chromate ion gives a well-defined wave at $E_{1/2}$ of −0.85 v vs the S.C.E. Concentrations of Cr(VI) of the order of 0.5 ppm can be determined by this method.

To determine total chromium in the fuel, the lower valence states are oxidized to Cr(VI) by adding a slight excess of potassium permanganate. This solution is passed through the column, and Cr(VI) is determined as before. Although permanganate ion also passes through the column, it does not interfere in the polarographic determination of chromate ion.

The relative standard deviation for a concentration of 2 μg of Cr(VI) per milliliter is 2%.

15.10 PHOTOMETRIC TITRATION OF SULFATE IN HOMOGENEOUS REACTOR FUELS

Milligram quantities of SO_4^{--} were titrated with barium perchlorate in an alcoholic medium with Thoron used as an indicator, according to a procedure outlined by Fritz and Yamamura.[8] Uncertainty as to the end-point location was eliminated by use of an automatic, photometric titration with either a Welch Densichron and glass filters or a single phototube (RCA No. 929) load-resistor arrangement. Aliquots containing of the order of 0.1 mg of SO_4^{--} can be titrated to 1% precision in this way.

[6] G. H. Ayers and A. S. Meyer, Jr., *Anal. Chem.* 23, 299–304 (1951).

[7] *The Versenes*, Technical Bulletin No. 2, Bersworth Chemical Co., Framingham, Mass., 1954.

[8] J. S. Fritz and S. S. Yamamura, *Rapid Microtitration of Sulfate*, ISC-540 (Nov. 12, 1954).

[redacted]